Shear Assessment and Strengthening of Reinforced Concrete T-beams with Externally Bonded CFRP Sheets

Brindley, Monika

Award date:
2018

Awarding institution:
University of Bath

SHEAR ASSESSMENT AND STRENGTHENING OF REINFORCED CONCRETE T-BEAMS WITH EXTERNALLY BONDED CFRP SHEETS

Monika Brindley

A Thesis Submitted for the Degree of Doctor of Philosophy

Department of Architecture and Civil Engineering

University of Bath

October 2017

CONTENTS

ACKNOWLEDGMENTS

First and foremost, I would like to thank my lead supervisor Professor Tim Ibell for his support, encouragement, friendship and most of all patience throughout the course of my PhD study. I would also like to thank my co-supervisors, Dr Antony Darby and Dr Mark Evernden for their help and fruitful discussions leading to the culmination of this Thesis.

I would like to acknowledge the financial support obtained from the Engineering and Physical Research Council (EPSRC) and the University of Bath, grant number EP/I018921/1. The project was carried out jointly with the University of Cambridge and thanks must go to the research team led by Professor Janet Lees. I would also like to thank the project sponsors and partners, namely Parsons Brinckerhoff, Tony GEE Consultants, Ove Arup and Partners Ltd, LG Mouchel and Partners, Highways Agency, Concrete Repairs Ltd, The Concrete Society for their support and invaluable comments on the research work undertaken. I would like to thank Hughes Brothers for supplying their products for research purposes, and Fyfe S.A. and Fibrwrap UK for their help and support with sourcing and application of their products. I would further like to thank Ebor Concrete for their diligent work on the T-beam test specimens, especially Paul Whitham for his invaluable comments regarding specimen fabrication. I would also like to thank the development team of ATENA, Cervenka Consulting s.r.o., and Professor Milan Jirasek and Dr Petr Havlasek of CTU in Prague who provided support and practical advice on numerical modelling during my stay at CTU. Special thanks must also go to Professor Pascal Lava of KU Leuven for his support and advice regarding the use of the Digital Image Correlation software MatchID. I would also like to thank my colleagues from Network Rail, who frequently challenge my way of research application in real life situations, and for their on-going support of my research interests.

This work would not be possible without the help of the laboratory technicians of the University of Bath, particularly William Bazeley, Neil Price, David Williams and David Ariño Montoya, who went above and beyond their roles to deliver the ambitious experimental programme. Their help, guidance and friendship during my stay at Bath were greatly appreciated.

And most of all, I would like to thank my family and friends for their unwavering support and patience.

ABSTRACT

Existing reinforced concrete bridges may be deemed inadequate to carry the ever-increasing traffic loads according to the current codes and standards before they reach the end of their design life. It may therefore be required to either strengthen or replace these structures, which can be costly and causes disruptions to the infrastructure. This work investigates experimentally the possibilities to extend the useful life of existing reinforced concrete slab-on-beam structures deficient in shear by means of structural strengthening with fibre-reinforced polymers (FRP). The experimental campaign involved mechanical testing of ten full-scale T-beam specimens, representative of typical existing slab-on-beam bridges. Two sizes of test specimen were used to investigate the effect of size on the ultimate shear capacity of the beams. The investigated shear-strengthening configurations included externally bonded carbon fibre reinforced polymer (CFRP) sheets in a U-wrap configuration with and without end-anchorage and deep embedded CFRP bars. Unstrengthened control specimens were also tested to provide baseline for comparison. The results from the experimental programme revealed that while the deep embedment strengthening solution provides an increase in shear capacity of up to 50%, the strengthening with CFRP U-wraps results in reduced capacity compared with the underlying control beam. This presents a major implication in terms of safe design predictions of shear capacity of reinforced concrete T-beams strengthened with CFRP sheets as this is the most commonly used shear-strengthening scheme in practice. The study also demonstrated that greater contribution from the externally bonded CFRP U-wraps can be achieved using end-anchorage systems, which delay the debonding of the CFRP. The applicability of current codes of standards and guidelines was studied as well as appropriateness of using advanced numerical methods for assessment of existing reinforced concrete structures. It was found that while the standards used for assessment greatly under-predict the shear capacity, the guidelines for FRP-strengthened beams either under- or over-predict the shear capacity of the tested beams. More accurate predictions are possible using advanced fracture mechanics-based methods for both the unstrengthened as well as the strengthened beams.

1 INTRODUCTION

1.1 Background

Extending the useful life of our ageing reinforced concrete infrastructure through repair and strengthening, rather than costly removal and replacement, is a priority for infrastructure owners and managers worldwide. Apart from physical intervention due to deterioration, higher volumes of traffic on the infrastructure often require increase in the structure's capacity, which can only be achieved through strengthening. For over 30 years, fibre-reinforced polymer (FRP) materials have been used as additional reinforcement to increase, or reinstate, the strength capacity of existing reinforced concrete structures. These materials with their high strength-weight ratio, durability and relative ease of application offer numerous advantages over traditional strengthening materials, such as steel. The cost of physical intervention on an infrastructure asset is greatly affected by the costs associated with road closures and diversions. Therefore, the use of FRP materials has the potential to offer tangible economic benefits in terms of saving resources and minimizing disruption while also reducing the impact on the environment long term.

To date, resin-bonded carbon FRP fabric strengthening systems have been the most commonly used, where typical applications include flexural, shear and column strengthening. Despite these advanced materials being used more frequently in the past few decades, our understanding of the behaviour of these FRP-strengthened structures has not kept pace with the increase in applications. In particular, there is a lack of practical knowledge where brittle shear failures of large reinforced concrete structures are considered. The complex nature of shear failures and the inability to accurately predict the precursors prior to failure were demonstrated by the catastrophic collapse of the de la Concorde Overpass in 2006 in Canada. Therefore, an accurate assessment of the existing structures prior to strengthening is crucial in determining whether increase in shear capacity may be required, and indeed possible.

The current design guidelines for strengthening of reinforced concrete structures with FRP materials are TR55 (2012), ACI-440 (2008) and *fib* Bulletin No. 14 (*fib* TG9.3, 2001). The basis of these documents was drawn upon the results of specific studies, typically conducted on small-scale rectangular beams (Denton et al., 2004; Collins et al., 2008).

Recent studies have highlighted the limitations in current design guidelines for FRP shear strengthening of reinforced concrete beams with complex geometries. A study on FRP-strengthened T-beams in a U-wrap configuration (bonded on three sides) conducted at the University of Cambridge (Dirar et al., 2007) has demonstrated that the TR55 greatly over-predicts the shear contribution of the FRP. An independent pilot study conducted at the University of Bath (Wen, 2009) on large-scale (750 mm deep) FRP sheet-strengthened rectangular beams has shown that the TR55 greatly under-predicts the shear capacity. The issue of geometry and size clearly requires further investigation, considering that 54% of the structures identified in a technical report published by Highways England (Highways Agency, 2003) are slab-on-beam structures.

This apparent contradiction in experimental results in direct comparison with TR55 predictions for large structures with complex geometries presents a real concern to designers and infrastructure managers alike. In order to instill confidence in the use of FRP materials on existing reinforced concrete structures, it is required to provide an insight and understanding of the fundamental relationship between the size and the geometry of the structure and its behaviour. This is only achievable through targeted experimental testing of large-scale T-beams, whose size and geometry reflects the characteristics of typical slab-on-beam structures.

1.2 Research hypothesis and objectives

The targeted experimental and numerical programme detailed in the presented work aims to deliver guidance for strengthening of existing reinforced concrete T-beams in shear using FRP materials. The primary objective is to investigate the limitations of shear strengthening with externally bonded FRP sheets and the potential of deep embedded FRP bars as an alternative to fabric-bonded systems. The deliverables of this project will have a significant and timely impact in the construction sector, providing practical, safe and durable strengthening solutions to meet the growing demands on our ageing reinforced concrete infrastructure.

The core research objectives of this research are threefold:

- To address the influence of the specimen size;
- To determine the effective FRP contribution and debonding effects; and

- To develop a numerical method which could be used to deliver robust, mechanics-based design code formulations for industry and governmental bodies for FRP shear-strengthened reinforced concrete structures.

Size effect in strengthened beams

The majority of laboratory tests available in the literature have been conducted on small-scale rectangular specimens, generally with their depths ranging from 100 to 300 mm. Due to the limitations of these tests, the applicability of the insight gained from these tests is questionable when considering large-scale, non-rectangular structures. According to a recent study of shear tests conducted over the past 60 years on beams without shear reinforcement highlighted that fewer than 8% of the total of 1850 tests considered had a depth greater than 560 mm (Collins et al., 2008).

However, existing reinforced concrete structures may have complex geometries and depths typically ranging from 600 to 1000 mm. Therefore, it is necessary to consider realistically sized and shaped T-beams, which are more representative of existing reinforced concrete slab-on-beam structures than rectangular beams. Such an approach has the potential to model the behaviour of FRP-strengthened beams with complex geometry while overcoming the practical constraints of testing full slab-on-beam decks. A recent preliminary study at the University of Bath conducted on large rectangular fabric-strengthened beams showed that size effect not only affects the capacity of the beam but also the failure mode (Wen, 2009). It can therefore be expected that the effect of size on the capacity and the behaviour of flanged beams will be considerable and must be addressed. Further investigation of the effect of size in combination with the strengthening solution used is therefore necessary and of practical interest to practitioners and infrastructure managers alike.

Effective FRP contribution and debonding in fabric-strengthened beams

Apart from the effect of size on the behaviour and failure mode of reinforced concrete beams in shear, there remain significant gaps in our understanding about the local crack and debonding behaviour in beams strengthened with FRP sheets. Recent studies have shown that the bonded FRP sheet being stretched at an oblique angle, in literature referred to as non-principal stretching, may influence the debonding behaviour (Dirar et al., 2007; Ibell et al., 2007; Teng et al., 2009). This issue is neglected in the current design guidelines, such as TR55 (2012), whose approach is based on an anchorage model

(Neubauer and Rostasy, 1997). Another variable identified as having influence on the shear behaviour of T-beams strengthened with continuous FRP sheets in a U-wrap configuration is the end anchorage in combination with the beam depth. The determination of the effective contribution of the anchored FRP is therefore imperative in cases where the additional FRP reinforcement does not penetrate the flange of the T-beam. A recent study at the University of Cambridge (Dirar et al., 2007) highlighted the possibility that the thickness of the FRP laminate as well as its effective width may not contribute to the overall shear capacity of the beam in a linear fashion.

Design formulations for FRP-strengthened slab-on-beam structures

Current design approaches for shear strengthening of reinforced concrete beams with FRP materials assume that the total shear capacity is equal to the sum of the individual capacities of the concrete, steel reinforcement (where present) and the FRP. However, even without the additional FRP reinforcement, reinforced concrete beams in shear were shown to be prone to size effect (Kani, 1966, 1967; Bazant, 1968; Bazant et al., 1984, 1991). The reduction in the concrete contribution caused by the formation of a shear discontinuity and subsequent shear sliding is therefore of particular concern. It was demonstrated in a pilot study conducted at the University of Bath that the contribution of the FRP strengthening to the overall capacity of the beam is indeed influenced by size effect (Wen, 2009). Furthermore, the extent to which the bonded FRP sheets stretch over the shear discontinuity in concrete was found to be dependent on the type of end anchorage (Ortega et al., 2009; Mofidi et al., 2012; Grelle and Sneed, 2013; Bae and Belarbi, 2013). It is therefore required to observe experimentally the behaviour of full-scale reinforced concrete T-beams strengthened with externally bonded FRP sheets and to incorporate the findings within appropriate design approaches. Furthermore, investigation of the applicability of the use of the variable truss analogy in EC2 (BSI EN 1992-1-1, 2004) in combination with the current FRP design guidelines is also required, as currently no guidance exists to address this issue.

1.3 Research programme and methodology

A synergistic experimental, analytical and numerical approach was developed to deliver the research objectives. Experimentation was to be conducted independently at the University of Bath and the University of Cambridge, in a synchronized manned to ensure consistency across the tested specimens. The University of Cambridge was to further

investigate the effect of size on fabric-strengthened T-beams analytically, whereas the numerical investigation was conducted at the University of Bath. The work at the University of Bath, both experimental and numerical, also included the investigation of specimens strengthened with deep embedded CFRP bars as an alternative to the fabric-bonded systems.

Three intrinsically linked work packages were developed and shared between the two universities. In work package 1 (WP1), the local concrete-FRP behaviour was investigated and debonding models formulated. In WP2, the primary focus was on the global T-beam behaviour with emphasis on size effect. In the final work package, WP3, robust mechanics-based design guidelines were delivered. The theoretical science-based analysis was conducted in tandem with the experimental programme and in a synergistic manner at both universities. The particulars of the work packages relevant to the work conducted at the University of Bath and presented in this work are further discussed in detail in Chapter 3 of this Thesis.

2 LITERATURE REVIEW

2.1 Introduction

This Chapter presents a brief review of the shear behaviour of reinforced concrete beams with and without shear reinforcement, and outlines the key factors affecting the shear capacity of a structure. The applicability of the current design and assessment codes widely accepted for determining the shear capacity of existing slab-on-beam reinforced concrete structures is critically examined altogether with their assumptions and limitations. Furthermore, alternative methods of determining the shear capacity of reinforced concrete structures are presented and their advantages over conventional code approaches discussed. Strengthening techniques using FRP materials are discussed altogether with their suitability for shear strengthening of structures with complex geometries. The current design guidelines for such strengthening are reviewed and their applicability compared with findings available from existing research. Furthermore, the appropriateness of the simplistic additive nature of the codified approaches, where the overall shear capacity of FRP-strengthened reinforced concrete beams is determined as a sum of the individual contributions of the internal steel, concrete and the additional FRP for bridge structures is examined and evaluated.

2.2 Behaviour of reinforced concrete beams in shear

To fully understand and appreciate the complexity of reinforced concrete beam behaviour in shear and shear failures, it is imperative to consider the shear transfer actions and mechanisms as well as key parameters influencing the beam behaviour. This section offers a brief overview of shear-related effects typically exhibited by reinforced concrete beams with and without transverse shear reinforcement.

2.2.1 Shear transfer actions and mechanisms

Shear in reinforced concrete beams represents a complex issue due to the nature of co-existing shear transfer mechanisms that could develop. According to ASCE-ACI Committee 426 (1973) and ASCE-ACI Committee 445 (1998), there are five main shear transfer actions and mechanisms that could develop in a beam with transverse shear

reinforcement. These include shear transfer in the uncracked compression zone above the neutral axis, aggregate interlock, residual tensile stresses, dowel action and tension in the transverse shear reinforcement. The components contributing to the shear capacity of a reinforced concrete beam are shown in Figure 2.1 and briefly described below.

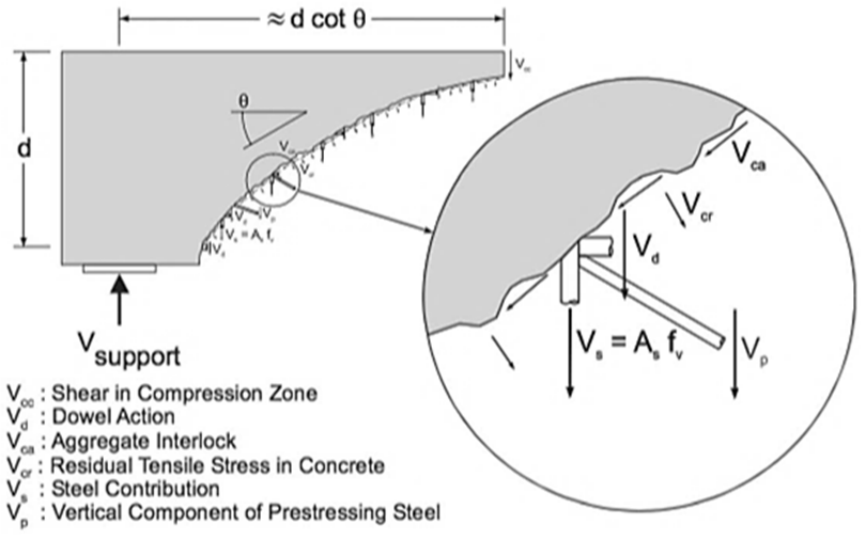

Figure 2.1 – Components contributing to shear resistance of a steel reinforced concrete beam.

Shear in the uncracked zone: Shear forces in a beam may be transferred in the uncracked concrete compressive zone above the neutral axis. The cracks follow the compression force path, meaning that the shear cracks propagate in a direction normal to the principal tensile stress.

Beam and arch action: In deep and short span beams arch action is dominant. This is because the applied force is transferred directly into the support via the diagonal strut action (Pillai and Menon, 2003). Shear forces in slender beams however are transferred through beam action. In beams with transverse shear reinforcement multiple shear cracks occur in the web prior to failure. In beams without transverse shear reinforcement, depending on the amount of longitudinal reinforcement, a single shear crack may develop propagating from the support to the applied load.

Aggregate interlock: When concrete cracks, shear transfer occurs through shearing of two rough surfaces against each other. In beams with higher concrete compressive strength the shearing plane is smoother because the crack propagates through the aggregate rather than around it, as is the case in lower strength concrete, see Figure 2.2. For crack widths, greater

than 1 mm it is assumed that the integrity of the material is lost and failure along the shear plane occurs.

(a) (b)

Figure 2.2 – Aggregate interlock in (a) gravel concrete (intermediate and low strength) and (b) lightweight concrete (Walraven, 1980).

Dowel action: In beams without transverse shear reinforcement shear forces may be transferred through dowel action provided by the bond between the longitudinal reinforcement and the surrounding concrete. With increasing amount of longitudinal reinforcement, the shear capacity also increases, provided the flexural capacity of the beam is not overcome.

Shear reinforcement: In beams with transverse shear reinforcement a truss action may develop, depending on the amount and spacing of the shear links. The shear forces are then transferred via this truss through concrete compressive struts and the yielding shear links that act as ties.

These shear transfer mechanisms are difficult to isolate and therefore it is not possible to quantify their individual contribution to the overall shear capacity of a beam. It is unclear as to which of these actions and mechanisms contribute the most to the overall shear capacity and which should be ignored for practical and safe shear capacity predictions.

2.2.2 Factors affecting beam behaviour

Research into the behaviour of reinforced concrete structures has uncovered certain factors that may influence the beam behaviour and may therefore reduce the overall shear capacity of the structure. For beams without transverse shear reinforcement these were identified as concrete strength, beam size and geometry, shear span to effective depth ratio, longitudinal reinforcement ratio and axial force. Other significant parameters influencing the beam behaviour include co-existing high shear force and high bending moment, dominant in

continuous beams, and loading regime. The latter is of importance in beams supported on the bottom and loaded on the bottom or supported on the top and loaded on the top. In these cases, the applied forces cannot be transmitted directly through the inclined struts, as is the case in beams supported on the bottom and loaded from the top, and the beam may fail at lower ultimate loads.

For beams with transverse shear reinforcement, the main factor influencing the beam behaviour is the amount of shear reinforcement crossing the shear crack. Other significant parameters include axial compression and concrete strength. Size effect was not identified as a major parameter influencing the shear capacity, since the shear cracking is largely controlled by the shear reinforcement (ASCE-ACI Committee 426, 1973; ASCE-ACI Committee 445, 1998).

These parameters are discussed further in more detail. It should be noted that beams with less than minimum recommended shear reinforcement would be considered as beams without shear reinforcement if the shear reinforcement ratio falls outside the scope of the design or assessment code. It is therefore imperative to consider all the above-mentioned parameters influencing shear capacity of beams with and without shear reinforcement.

Concrete strength: With increasing concrete strength, the shear capacity of a beam also increases. Previous research findings did not clearly define whether the shear capacity of a beam is dependent on the compressive concrete strength or the tensile concrete strength (Moody et al., 1954). However, the majority of current design and assessment codes, based on most recent research findings, accept the compressive concrete strength as the key parameter in shear predictions (BSI EN 1992-1-1, 2004; ACI-318, 2014; BS 5400-4, 1990; BD 44/15, 2015). Furthermore, it was demonstrated experimentally that concrete strength has greater influence on the overall shear capacity of a beam without transverse shear reinforcement (Mphonde and Frantz, 1984). In beams with large amount of transverse shear reinforcement the concrete strength was not the primary factor influencing the beam behaviour in shear (Elzanaty et al., 1986).

Shear span to depth ratio: A major factor influencing the behaviour of reinforced concrete beams regardless of their size, shape, concrete strength and reinforcement is the shear span to depth ratio (*a/d*). The transition point between failure modes was found experimentally to be at *a/d* approximately equal to 2.5 for rectangular reinforced concrete beams (Kani, 1964, 1966), see Figure 2.3.

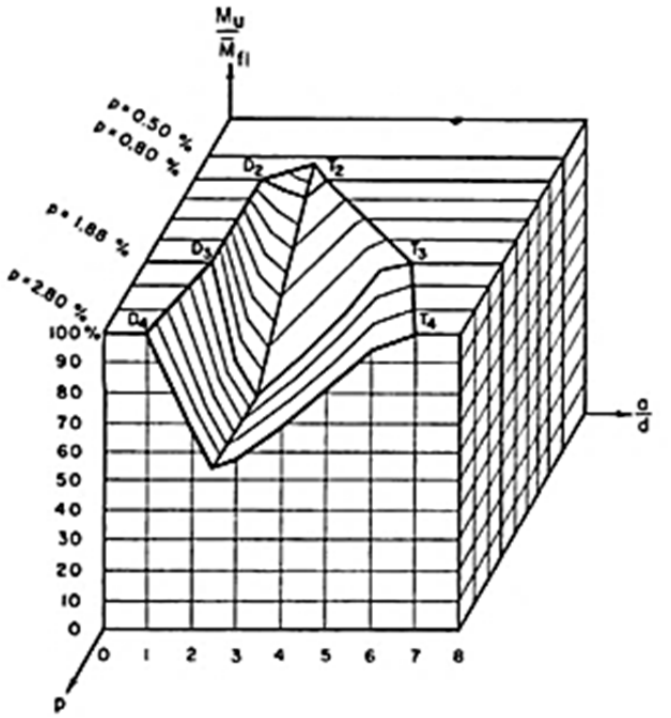

Figure 2.3 – Kani's shear valley – relative beam strength versus shear span to depth ratio *a/d* and longitudinal reinforcement ratio ρ (Kani, 1966).

Below this threshold however the beams develop an arching action, which in turn results in an increased shear capacity (Ahmad et al., 1986; Mphonde and Frantz, 1984). For beams with *a/d* greater than 2.5, the failure is sudden, brittle and in diagonal tension. It was demonstrated experimentally that this type of failure is dominant in beams with higher reinforcement ratios and almost non-existent in beams with lower longitudinal steel reinforcement ratios (Kani, 1964; Zsutty, 1971).

The type of loading in combination with the *a/d* ratio may also present another major parameter affecting the shear capacity of reinforced concrete beams under concentrated loads as demonstrated by Brown et al. (2006). Such type of loading is typical on highway bridges in terms of single wheel or axle loads and the influence of loading regime on shear behaviour is therefore of importance to designers and infrastructure managers.

Structure size and geometry: Reinforced concrete beams have been demonstrated to be prone to exhibit size effect – a phenomenon, where smaller beams require a greater amount of supplied force to fail compared with larger beams of the same geometry (Kani, 1966, 1967). The effect of size on the shear capacity of reinforced concrete beams appears to be more prominent in beams with no to low amount of transverse shear reinforcement and/or

low amount of longitudinal reinforcement (Bazant et al., 1984, 1991). Size effect in beams with higher amounts of reinforcement and beams with complex geometry is difficult to capture and so to quantify due to the potential of co-existing shear failure mechanisms (Bazant, 1968). The loading and the geometry of the structure may also influence the beam behaviour due to several load-carrying mechanisms that could develop and co-exist (Fernandez and Ruiz et al., 2009). However, the width of the beam was not found to have a significant effect on the shear strength capacity (Kani et al., 1979). Therefore, the size effect in beams is primarily dependent on the beam depth. In flanged sections, the slab dimensions may be critical in determining the shear failure mode and shear capacity. It was proved experimentally that for flanged beams with a/d ratio greater than 2.5 the shear resistance of beams is provided by the flange and not, as widely assumed, the web (Kotsovos et al., 1987). Reinforced concrete beams with large amounts of longitudinal steel reinforcement may develop web shear cracks rather than flexural shear cracks and behave similarly to deep and pre-stressed beams (Whitehead, 2002). The difference between web shear crack and flexural shear crack is illustrated in Figure 2.4.

Longitudinal reinforcement: The amount of longitudinal reinforcement has a direct impact on the shear capacity of a beam as well as its behaviour. With increasing ratio of longitudinal reinforcement, the shear capacity also increases. Conversely, with decreasing ratio of longitudinal reinforcement, the dowel action decreases. Historically, where the longitudinal reinforcing bars were bent up in the region close to support, the bent reinforcement provided resistance against shearing forces that may occur in that region. In modern reinforced concrete structures, where the longitudinal reinforcing bars are bent up behind the support to provide additional anchorage length, the shear capacity increases due to the enhancement from supports (BD 44/15, 2015). Beams with distributed longitudinal reinforcing bars over the depth of the beam were proved to achieve greater shear capacity while maintaining small sizes of shear cracks (Collins and Kuchma, 1991).

Axial force: In reinforced concrete members subject to axial tension the shear strength decreases, as the shear crack angle is steeper over almost the full depth of the member. Appropriate amount of top and bottom longitudinal reinforcement may ensure the beam fails in a relatively ductile manner. Axial compression on the other hand increases the shear capacity of a member as axial compression increases the depth of the uncracked compression zone and decreases the width of the shear cracks (Mattock and Hofbeck, 1962).

Shear reinforcement: In beams with transverse shear reinforcement the shear links yield when the concrete cracks and thus increase the shear capacity of the beam. With increasing amount of shear reinforcement, the shear capacity of a beam also increases.

2.2.3 Shear failures of reinforced concrete beams without shear reinforcement

Shear failures of beams without shear reinforcement are dependent on many factors as previously discussed in this section. Shear failures are initiated by inclined shear cracks and these cracks are typically divided into two types – web shear cracks and flexural shear cracks, shown in Figure 2.4.

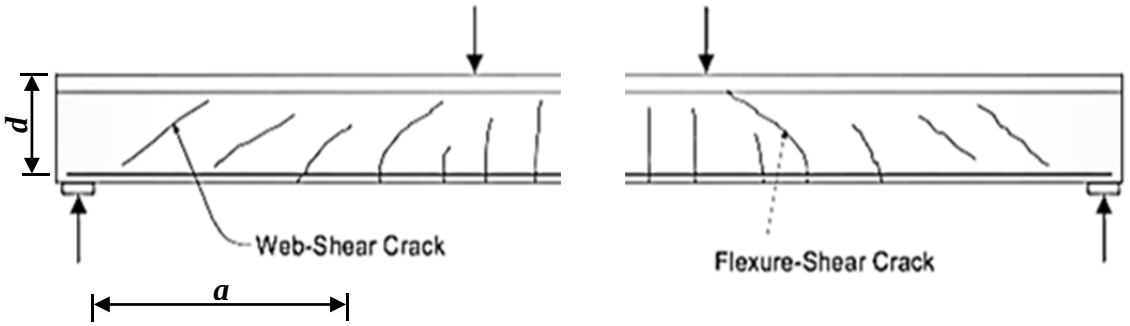

(a) (b)

Figure 2.4 – Typical crack patterns in reinforced concrete beams in shear: (a) web shear crack, (b) flexure-shear crack.

The failure modes of beams without shear reinforcement are most commonly classified according to their *a*/*d* ratios (ASCE-ACI Committee 426, 1973) as follows:

Very slender beams (a/d > 6): These members will most likely fail in flexure prior to the formation of inclined cracks, as they are not shear critical.

Slender beams (2.5 > a/d > 6): Beams that fall within the limits for slender beams may develop some flexure-shear cracks from the flexural cracks. The propagation of these cracks will cause yielding of the tension steel. The beams will fail in *diagonal tension*, where the beam is split into two segments.

Short beams (1 < a/d < 2.5): In short beams, two possible failure modes can occur – *shear-tension* and *shear-compression*. In cases where a diagonal crack may propagate along the longitudinal steel reinforcement causing splitting of the concrete from the

reinforcement, the beam fails in shear-tension. The diagonal crack may also propagate toward the top of the beam, resulting in crushing failure in the compression zone, referred to as shear-compression.

Very short beams (a/d < 1): In very short beams, inclined cracks develop between the applied load and the support point. Therefore, most of the shear force is carried directly by arch action. Several failure modes may occur: anchorage failure, bearing failure, flexural failure and tension failure of the arch rib. Compression failure of the strut is also possible.

Figure 2.5 shows the generally accepted failure mode compared with that postulated by Kotsovos (1984) for beams with *a/d* values between 1 and 2.5.

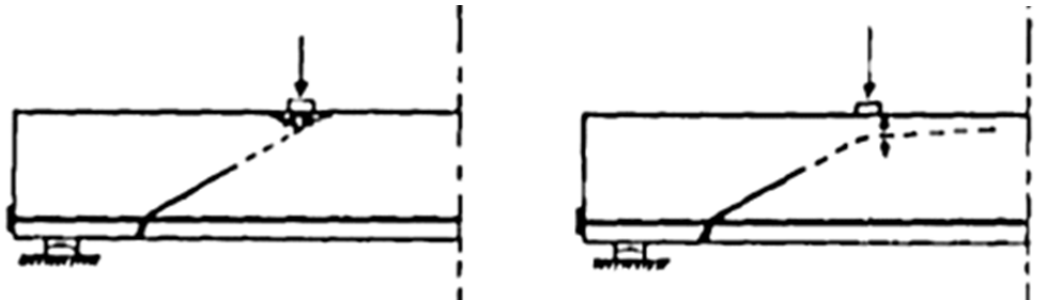

(a) (b)

Figure 2.5 – Failure modes of reinforced concrete beams: (a) generally accepted failure mode, (b) failure mode of concrete beams with values of *a/d* between 1 and 2.5 (Kotsovos, 1984).

2.2.4 Shear failures of reinforced concrete beams with shear reinforcement

In beams with transverse shear reinforcement, the shear transfer and therefore the failure modes are different to those observed in beams without shear reinforcement discussed previously. Shear cracking in these beams is controlled by the amount of shear reinforcement and the shear capacity depends on the yielding of the links crossing the shear crack. In beams with nominal amount of shear reinforcement, a flatter shear crack may develop causing increase in shear capacity after the steel links have yielded due to shear transfer along the friction interface of the shear crack.

On the other hand, beams with large amounts of shear reinforcement may fail due to web crushing, where the concrete in the inclined struts fails. This failure mode, however, is more likely to occur in beams with thin webs, such as I-beams, due to higher stresses in the web. Multiple inclined shear cracks in the web may appear, forming a truss, through which

the shear forces are being transferred between the load point and the support point. This is discussed further in detail in the following section.

2.3 Shear capacity predictions for reinforced concrete beams

It is widely accepted that the overall shear capacity of a beam with transverse shear reinforcement, V, may be expressed as the sum of the capacity of the underlying concrete beam, V_c, and that of the steel links, V_s. The expression then reads

$$V = V_c + V_s \tag{2.1}$$

This section presents an overview of the current standards and codes of practice with provision of shear capacity calculations altogether with the theory on which they were formulated. Numerical methods and their suitability for shear capacity predictions of reinforced concrete beams are also discussed here.

2.3.1 ACI-318

The shear capacity of concrete sections without transverse shear reinforcement can be calculated according to ACI-318 (2014) as follows

$$V_c = 0.17\sqrt{f_c'}\,b_w d \qquad \text{[N, mm]} \tag{2.2}$$

where V_c is the shear force resisted by the concrete section, f_c' is the concrete compressive strength, b_w is the width of the beam and d the effective beam depth. This equation may be used in lieu of a more complicated equation (2.3), provided that $\sqrt{f_c'} \leq \sqrt{69}$.

$$V_c = \left(0.16\sqrt{f_c'} + 17\rho_w \frac{V_u}{M_u} d\right) b_w d \qquad \text{[N, mm]} \tag{2.3}$$

The contribution of the transverse steel reinforcement, V_s, can be calculated as

$$V_s = \frac{f_{yt} d}{s} A_v(\sin\alpha + \cos\alpha) \qquad \text{[N, mm]} \tag{2.4}$$

where f_{yt} is the tensile strength at yield, s is the spacing of the steel links, A_v is the area of the steel links at a cross-section and α the angle between the steel link and the horizontal.

The design equations for predicting shear in concrete beams are based on the shear causing significant diagonal cracking. The ACI-ASCE Committee 326 (1962) concluded that any increase in shear capacity beyond the shear which caused the significant diagonal cracking must be ignored for beams without transverse reinforcement. This was due to the large variation in failure mechanisms observed in experimental investigations beyond the point of first cracking. This assumption was criticized by leading researchers and Bazant et al. (1984, 1987, 1991, 2007) pointed out that the diagonal cracking is not proportional to the ultimate load and therefore a uniform factor of safety against failure is not provided. Another major drawback of the approach outlined in the ACI Code is that it does not recognize size effect. The ACI Code shear design equations for non-prestressed concrete beams were derived from tests on relatively small (340 mm) and heavily reinforced (2.2%) beams carried out in 1962. Therefore, the applicability of these equations to reinforced concrete beams with greater depth than that tested is questionable.

2.3.2 BS 8110 and BD 44/15

The UK design codes BS 8110 (1997, now retracted) and BS 5400-4 (1990) use the following equation to calculate the nominal shear stress in a concrete beam in the form

$$v = \frac{V}{bd} \tag{2.5}$$

where τ was replaced by v and $b_w z$ with bd. Previously, in CP114 (1969), the expression was used to obtain the shear-cracking load by replacing v with the empirically determined tensile strength of concrete (Mörsch, 1909).

The design shear equations in BS 8110 and BS 5400 are based on the 45° truss model with the addition of a concrete term. From BS 8110, the expression to predict a diagonal cracking shear, V_c, in a concrete beam is given as

$$V_c = 0.79 \left(\frac{400}{d}\right)^{\frac{1}{4}} \left(\frac{100 A_s}{bd}\right)^{\frac{1}{3}} bd \left(\frac{f_{cu}}{25}\right)^{\frac{1}{3}} \tag{2.6}$$

where A_s is the area of the longitudinal steel and f_{cu} the cube compressive strength of concrete. It should be noted that in this approach the concrete contribution is evaluated separately to that of longitudinal steel, and thus ignores the advantage of having both shear

and longitudinal reinforcement evaluated as acting together.

The above equation is known to produce relatively conservative shear capacity predictions (Valerio, 2009), and therefore an assessment code, BD 44/95 (1995, now superseded by BD 44/15, 2015), was developed by the Highways Agency (now Highways England). This document essentially modifies the design code equations and removes conservatism by relaxation of some of the assumptions made for design. Practically this means that the shear assessment expression in BD 44/95 was obtained by modification of the BS 5400 shear design equation by adopting a lower bound rather than a mean best fit to test data. There is also a provision for the use of a reduced partial safety factor for the concrete strength if the worst credible strength of concrete is determined. The expression to evaluate diagonal cracking shear in concrete, as given by BD 44/95, reads

$$V_c = 0.24\left(\frac{500}{d}\right)^{\frac{1}{4}}\left(\frac{100A_s}{bd}\right)^{\frac{1}{3}} f_{cu}^{\frac{1}{3}}\, bd \tag{2.7}$$

The new version of BD 44/15 offers provisions to calculate shear capacity for beams with and without effective shear reinforcement. The ultimate shear resistance, V_u, of a section without effective shear reinforcement is given by the following equation

$$V_u = \Gamma\kappa\xi_s\nu_c b_w d \tag{2.8}$$

Where effective vertical links are present, the ultimate shear capacity V_u of a section shall be calculated according to the following equation

$$V_u = \Gamma\left(\kappa\xi_s\nu_c b_w d + \frac{f_{yv}}{\gamma_{ms}}\frac{d}{s_v}A_{sv}\right) \tag{2.9}$$

In both equations, Γ is a reduction factor to allow for inadequate anchorage of the longitudinal reinforcement, which is calculated from the following equations

$$\Gamma = \sqrt{\frac{\alpha_s F_{ub}}{F_{ub,max}}} \leq 1.0 \tag{2.10}$$

where

$$\alpha_s = 1.0 + \frac{1.6\sigma}{0.3 f_{cu}} \leq 2.6 \tag{2.11}$$

where α_s is a factor to account for increased bond due to transverse pressure in the support region and where σ is the transverse pressure on the reinforcement due to ultimate loads. The parameter F_{ub} represents the total ultimate anchorage force in the tension reinforcement at the front face of the support, similarly to cl. 5.8.6.3 of BD 44/95 but $\alpha_s F_{ub}$ should not be taken as greater than $A_s\, f_y/\gamma_{ms}$

and

$$F_{ub,max} = 6\xi_s \nu_c b_w d \tag{2.12}$$

In the above expressions

$$\xi_s = \left(\frac{500}{d}\right)^{\frac{1}{4}} \geq 0.7 \tag{2.13}$$

The parameter ν_c is the ultimate shear stress in concrete and is calculated from the following equation

$$\nu_c = \frac{0.24}{\gamma_{mv}} \left(\frac{100 A_s}{b_w d}\right)^{\frac{1}{3}} f_{cu}^{\frac{1}{3}} \tag{2.14}$$

The factor κ is to take account of shear enhancement near supports and allows for shear strength increase for sections within a distance $a_v < 3d$ from the face of the support. The enhancement then takes the form of an increase in the allowable concrete shear stress $\xi_s \nu_c$ by a factor $\kappa = 3d/a_v$, with limitations on total shear stress as per cl. 5.3.3.3 of BD 44/15.

2.3.3 Eurocode 2

The EN 1992-1-1 (2004) gives the following equation for the calculation of shear force, $V_{Rd,c}$, of sections without transverse reinforcement

$$V_{Rd,c} = b_w d \left[\frac{0.18}{\gamma_c} k (100 \rho_l f_{ck})^{\frac{1}{3}} + 0.15 \sigma_{cp}\right] \tag{2.15}$$

where the term $0.18/\gamma_c$ and the constant 0.15 are nationally determined parameters with γ_c equal to 1.5 for persistent and transient actions and 1.2 for accidental actions, ρ_l is the ratio of the longitudinal reinforcement, f_{ck} the characteristic concrete compressive strength and σ_{cp} the average longitudinal stress (positive for compression, negative for tension).

$V_{Rd,c}$ should not be taken as less than

$$b_w d \left(0.035 k^{\frac{3}{2}} f_{ck}^{\frac{1}{2}} + 0.15 \sigma_{cp}\right) \tag{2.16}$$

and where

$$k = 1 + \sqrt{\frac{200}{d}} \leq 2.0$$

is the size effect factor where d is in mm and

$$\sigma_l = \frac{A_{sl}}{b_w d} \leq 0.02$$

where A_{sl} is the area of the longitudinal steel.

The code articulates that even members without shear reinforcement have some shear strength and this is considered by the provision of the minimum requirement for $V_{Rd,c}$.

The code adopts a widely accepted truss model for the predictions of the effects of shear reinforcement. The equation for calculating the shear force due to the shear reinforcement, $V_{Rd,s}$, follows from equilibrium

$$V_{Rd,s} = \frac{A_{sw}}{s} z f_{ywd} \cot\theta \tag{2.17}$$

where A_{sw} is the area of the vertical shear reinforcement, s the spacing of the shear links, z the lever arm, f_{ywd} the design yield strength of the shear links, and θ the truss angle. The code postulates that the term $\cot\theta$ takes value of 1, corresponding to the truss angle value of 45°. The assumption that the truss forms at 45° to the longitudinal axis of the beam gives grossly underestimated predictions of shear capacity for beams with shear reinforcement. One way of rectifying this is to include the capacity of the concrete calculated from (2.15), and the shear response is therefore considered plastic. In this respect, such an approach is equivalent to that of the BS 8110 and the ACI code.

EN 1992-1-1 on the other hand adopts a variable truss approach, where the shear reinforcement is assumed to carry all the shear force, and therefore the truss angle, θ, can take any value between $\cot^{-1} 0.7$ and $\cot^{-1} 2.5$. In certain cases, the shear strength may also be limited by the crushing strength of the strut.

The strength of the strut that provides an absolute upper limit to the shear force, $V_{Rd,max}$, that can be supported by the section can be calculated as

$$V_{Rd,max} = \frac{\sigma_c b_w z}{\cot\theta + \tan\theta} \tag{2.18}$$

The equation assumes that the strut will crush at the ultimate load and that the average stress in the strut, σ_c, can be expected to be proportional to the concrete compressive strength. The limiting value of σ_c is defined as νf_{cd} where ν is an empirical efficiency factor that takes into consideration the actual distribution of stress across the section and the effects of crushing at failure. The equation then reads

$$V_{Rd,max} = \frac{b_w z \alpha_{cw} \nu_1 f_{cd}}{\cot\theta + \tan\theta} \tag{2.19}$$

where $z \cong 0.9d$ and α_{cw} is a coefficient considering any applied compression force. The recommended value for ν_1 is ν defined as

$$\nu = 0.6\left(1 - \frac{f_{ck}}{250}\right) \tag{2.20}$$

The above equations are appropriate for concrete members with vertical shear reinforcement.

2.3.4 *fib* Model Code 2010

The equation of shear behaviour according to *fib* MC 2010 reads as follows

$$V_{Ed} \leq V_{Rd} = V_{Rd,c} + V_{Rd,s} \leq V_{Rd,max} \tag{2.21}$$

where V_{Ed} is the design shear force and the rest of the terms as defined previously.

The components $V_{Rd,c}$ and $V_{Rd,s}$ of the state equation can be obtained from the following equations

$$V_{Rd,c} = 0.9k_v \frac{\sqrt{f_{ck}}}{\gamma_c} b_w d \tag{2.22}$$

$$V_{Rd,s} = 0.9 \frac{A_{sw}}{s_w} f_{ywd} d(\cot\theta + \cot\alpha)\sin\alpha \tag{2.23}$$

It is apparent from the above equations that the *fib* Model Code assumes that the concrete contribution to the design shear resistance depends on the concrete compressive strength, f_{ck}, the web width, b_w, and the effective depth d. The partial safety factor of the concrete, γ_c, depends on the design situation and the selection of parameter k_v depends on the level of approximation. The latter considers the ability of the web to resist aggregate interlock stresses, which provides increase in the shear strength due to the concrete contribution. The code recognizes that a limiting value of the shear force that a concrete section can withstand cannot exceed the crushing capacity of the concrete. This limiting shear force is calculated from

$$V_{Rd,max} = 0.9k_c \frac{f_{ck}}{\gamma_c} b_w d \frac{\cot\theta + \cot\alpha}{1 + (\cot\theta)^2} \tag{2.24}$$

where θ is defined by the level of approximation and indicates the angle of principal compressive stress in the web. The angle α is the angle of the stirrups or bent bars taken from the horizontal axis of the beam. The term k_c is a concrete strength reduction factor, which considers the effect of cracked concrete.

There are four levels of approximation (LoA), where the first three are the most applicable to everyday engineering problems. Level IV on the other hand offers a more comprehensive means of analysis using finite element methods or stress field analysis. The shear capacity of a reinforced concrete cross-section with shear reinforcement according to the LoA III can be calculated as follows

$$V_{Rd} = V_{Rd,c} + V_{Rd,s} \leq V_{Rd,max}(\theta_{min}) \tag{2.25}$$

where

$$V_{Rd,c} = 0.9k_v \frac{\sqrt{f_{ck}}}{\gamma_c} b_w d \approx \frac{0.36}{1 + 1500\varepsilon_x} \left(1 - \frac{V_{Ed}}{V_{Rd,max}(\theta_{min})}\right) \frac{\sqrt{f_{ck}}}{\gamma_c} b_w d \qquad (2.26)$$

and in combination with equation (2.23) for $V_{Rd,s}$ the equation for $V_{Rd,max}$ reads

$$V_{Rd,max} = 0.9k_c \frac{f_{ck}}{\gamma_c} b_w d \frac{\cot\theta + \cot\alpha}{1 + (\cot\theta)^2} \approx \frac{2.80}{1.2 + 55\varepsilon_1} \frac{f_{ck}^{\frac{2}{3}}}{\gamma_c} b_w d \frac{\cot\theta_{min} + \cot\alpha}{1 + (\cot\theta)^2} \qquad (2.27)$$

It is evident from the above equations that the *fib* Model Code (2010) is striving to balance the accuracy and complexity of analysis to suit the different levels of approximation for both design and assessment. Increasing the level of approximation also increases the level of accuracy of shear capacity predictions.

2.3.5 Numerical methods for predicting shear capacity

The shear capacity of a reinforced concrete structure may also be obtained by numerical methods. Due to the complex behaviour of reinforced concrete structures, most finite element (FE) methods are only applicable within the linear range until concrete starts to crack. To accurately model the behaviour of concrete, a combination of FE methods with fracture mechanics is therefore required (Belletti et al., 2013).

Non-linear fracture mechanics-based FE software ATENA (Advanced Tool for Engineering Non-linear Analysis) is a commercial package that was purposely developed to model and analyze reinforced concrete structures. It is possible to model the behaviour of reinforced concrete structures in 2D and 3D, which offers a great flexibility and versatility for analysis. It was demonstrated that in the case of reinforced concrete beams, a simple 2D model may sufficiently simulate the structural behaviour, and therefore proceeding to a more complex 3D model may not be necessary (Dadvar, 2014).

Furthermore, analysis of cracking in ATENA is possible, which means that the location of cracks at their initiation and at failure can be analyzed. This presents a great advantage over the codified approaches, which only predict the ultimate capacity of the beams. The effect of size on the beam behaviour is therefore considered by the software, using the laws of fracture mechanics to predict cracking. ATENA was demonstrated to predict the ultimate capacity as well as structural behaviour of beams with a great accuracy compared with experimental data (Sucharda and Brozovsky, 2014).

2.4 Repair and strengthening of reinforced concrete structures

When the capacity of a bridge is deemed insufficient, the consideration is given to whether to repair or strengthen. The aim of structural repairs is to bring the structure back to its original as-built capacity, whereas strengthening aims at increasing the live loading capability of the structure beyond its design capacity. The repair of reinforced concrete structures typically consists of replacement of defected concrete sections; treatment of corroded reinforcement and/or replacement of corroded steel sections in joints for example. Strengthening generally involves a more intrusive intervention with additional structural elements designed to enhance the capacity applied to the structure. The modern alternative to steel plates and strips are FRP fibres in combination with epoxy resin applied onto the concrete surface. These advanced materials offer significant advantages over steel for their low weight, high strength, impact resistance, stiffness, flexibility, ease of application and durability.

2.4.1 FRP materials for structural strengthening

The materials most frequently used for strengthening of reinforced concrete structures are presented in Table 2.1 with their typical material properties.

Table 2.1 – Material properties of typical shear-strengthening materials.

Material	Tensile strength [MPa]	Modulus of elasticity [GPa]	Density [kg/m^3]
Carbon fibres	2200 – 5600	240 – 830	1800 – 2200
Aramid fibres	2400 – 3600	130 – 160	1400 – 1500
Glass fibres	3400 – 4800	70 – 90	2200 – 2500
Epoxy adhesive	50 – 90	3 – 5	1100 – 1400
CFRP composite	1500 – 3700	160 – 540	1400 – 1700
Steel bars and plates	280 – 1900	190 – 210	7900

The density of the FRP composites is approximately four times less than that of steel, offering significant weight and material savings. The overall strength and stiffness of the

resulting FRP composite are considerably lower than those of the fibres alone and greatly affected by the matrix used. The maximum elongation of the epoxy resins is in the range of 2% to 8%, depending on the material used. Furthermore, FRP materials do not yield before reaching their ultimate tensile capacity and exhibit a linear elastic stress-strain relationship until failure (TR55, 2012).

The composites can be engineered to have different properties in different directions depending on the orientation of the fibre reinforcement within the resin matrix. Uni-directional elements such as woven fabrics, strips, plates and bars take advantage of the high tensile strength in the principal fibre direction. The tensile strength in the cross-fibre direction is generally very low due to the brittle matrix being prone to splitting and separation of the strands of fibres. For this very reason, multi-directional FRP materials are readily available to provide additional strength in the non-principal fibre directions, for instance bi- or multi-directional woven fabrics and sheets.

2.4.2 Strengthening of concrete structures using FRP

FRP materials are versatile in their application due to the fact they come in many shapes and forms, and for their light weight and durability. It is therefore possible to achieve the most suitable strengthening solution for a given structure, including those where access may be limited. Strengthening of reinforced concrete structures may be divided into three categories, according to the type of strengthening required as flexural, shear and confinement.

Flexural strengthening: Horizontal load-bearing members, such as slabs and beams, may be strengthened with strips, plates and sheets to provide additional flexural capacity. These additional FRP elements are either bonded using an epoxy adhesive or mechanically fastened to the bottom soffit of the element. In some cases, further increase in flexural capacity may be achieved through application of the FRP strips or bars into pre-cut groves, referred to as near surface mounted reinforcement. Externally applied pre-stressing tendons may also be used.

Shear strengthening: There are various options to increase the shear capacity of a reinforced concrete beam. There are three main types of shear strengthening divided according to their application – externally bonded reinforcement (EBR), near surface mounted (NSM) and deep embedment (DE). These types are further discussed in detail in

Section 2.4.3.

Confinement: Additional capacity for vertical load-bearing elements, such as columns, may be provided using FRP strips and sheets. The application of FRP fabrics in this instance offers many advantages due to the versatility of the fabrics and its ability to be wrapped around any shape to provide additional confinement.

2.4.3 Shear strengthening of beams using FRP

Externally bonded FRP: To achieve the most suitable strengthening solution, the FRP materials can be applied to the existing beam in several ways. Undoubtedly the most preferred strengthening solution offers the externally bonded FRP due to its relative ease of application. FRP sheets, strips and plates are bonded to the free sides of the beam using epoxy adhesive. In most practical applications, the deck or floor slab obstructs the topside of a beam, and therefore only bonding on the unobstructed sides is possible. In cases where full wrapping of the beam is not possible, the FRP is either bonded to the sides and the bottom soffit, referred to as a U-wrap configuration, or to the sides only, referred to as side bonding.

Typical strengthening solutions using externally bonded FRP sheets and strips are shown in Figure 2.6.

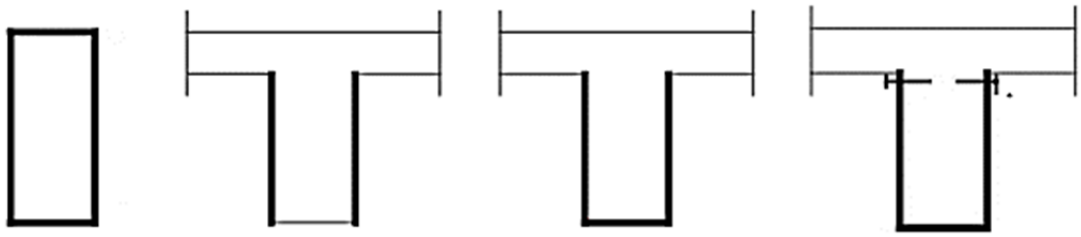

(a) (b) (c) (d)

Figure 2.6 – Typical configurations for externally bonded FRP sheet and strip strengthening: (a) fully wrapped, (b) side bonded, (c) U-wrap, (d) U-wrap with end anchorage.

Even though the exact contribution of the FRP bonded to the bottom soffit on the overall shear capacity is difficult to quantify, side bonding is the least effective of the externally bonded strengthening systems. This is due to the limited anchorage length of the FRP material at the bottom soffit of the beam, where a shear crack is expected to initiate, and therefore more prone to debonding from both free ends of the FRP reinforcement.

To prevent premature debonding of the externally bonded FRP, the sheets and strips can be anchored either into the web or the compression zone. Localized (spike anchors, fan anchors) and continuous (bar-in-slot) anchorage devices may be used to prevent the premature debonding of the FRP sheets and plates. Furthermore, in cases where only a full wrap would provide the required shear increase it is possible to drill through the slab and anchor the FRP on the topside of the beam. This technique connects the top and the bottom chords of the beam and was successfully used on large-scale strengthening schemes in the UK and globally (REF3b, 2014).

Near surface mounted FRP: Another externally applied shear-strengthening method is the near surface mounted FRP, which requires a more intrusive surface preparation compared with the surface bonded sheets and strips. Typically grooves and slots are cut into the surface concrete for bonding of strips and bars. The main advantage of this technique over the externally bonded FRP described earlier is that the FRP material is embedded into the surface concrete while maximizing the contact of the FRP with the surrounding concrete. Such an approach enhances the bond between the FRP element and the surface concrete, decreasing the likelihood of premature debonding due to insufficient bond area. While FRP bars can only be bonded from two sides of the beam using this method, strips can be bonded on three sides in a U-wrap configuration.

Deep embedded FRP bars: The deep embedment technique, developed at the University of Bath, is relatively new and was first used in the UK to increase the load carrying capacity of a coffered floor slab in a data storage centre in London in 2012. In this case the deep embedment technique, using steel bars rather than FRP, was the only feasible method to carry out strengthening (REF3b, 2014). In this strengthening system holes are drilled through the top or bottom soffit of the beam and FRP bars inserted as additional shear reinforcement. This technique offers a greater increase in shear capacity compared to that achievable through both the externally bonded and the near surface mounted FRP systems due to the superior FRP-concrete bond that can be achieved (Valerio, 2009; Mofidi, 2012). The major advantage of the deep embedment is that the FRP bars inherently connect the top and the bottom chords of the beam and therefore act in a similar manner to traditional internal steel shear links.

However, due to the more invasive nature of the application of deep embedded FRP bars as well as the near surface mounted FRP reinforcement there is a possibility of damage to the existing steel reinforcement during application and subsequent corrosion. These issues

should be addressed at the design stage and the suitability of both strengthening solutions considered on a case by case basis.

2.5 Design of shear-strengthening schemes using FRP

The concept of shear capacity predictions, where the individual contributions of the components are added together as in the case of reinforced concrete beams, is also widely accepted to predict the shear capacity of FRP-strengthened reinforced concrete beams. The overall shear capacity of the beam, V, may be expressed as the sum of the shear capacity of the concrete, V_c, steel, V_s, and the additional FRP, V_f.

The expression then reads

$$V = V_c + V_s + V_f \tag{2.28}$$

This section presents a review of currently used design codes for shear capacity predictions of reinforced concrete beams strengthened with FRP materials, altogether with the theory on which they were formulated. Numerical methods and their suitability to determine the shear capacity of FRP-strengthened reinforced concrete beams are also discussed here.

2.5.1 ACI-440

The American ACI-440 provides guidance for strengthening of concrete beams in shear with externally bonded FRP sheets. The contribution of the FRP strengthening, V_f, according to ACI-440 (2008) is given by

$$V_f = \frac{A_{fv} E_f \varepsilon_{fe} d_f}{s_f} (\sin\alpha + \cos\alpha) \tag{2.29}$$

where A_{fv} is the total area of the FRP sheet reinforcement bonded, d_f is the effective depth of the sheets (defined as the total depth of the sheet less the cover to the tension steel), s_f is the spacing of the sheets, α is the inclination of the sheets to the longitudinal axis of the beam, E_f is the effective Young's Modulus and ε_{fe} is the effective strain of the FRP sheets that can be achieved at the ultimate limit state. The code recognizes that the sheets can be applied in a full wrap, U-wrap or side-bonded configurations, and this is considered using

a reduction coefficient ψ_f as a multiplier of the FRP contribution V_f. The reduction coefficient for a full wrap is 0.95 and for a U-wrap or side-bonding configurations 0.85.

The value used for the effective strain, ε_{fe}, depends on the strengthening system used. For the fully wrapped case this value is determined as the lesser of 0.004 and $0.75\varepsilon_{fu}$; for the U-wrap and side bonding the value equals the lesser of 0.004 and $k_v\varepsilon_{fu}$. The reduction factor, k_v, is calculated from

$$\kappa_v = \frac{\kappa_1\kappa_2 L_e d_f}{11900\varepsilon_{fu}} \leq 0.75 \tag{2.30}$$

where ε_{fu} is the ultimate strain of the FRP sheet.

The effective bond length of the sheets, L_e, over, which the effective strains develop, can be obtained from

$$L_e = \frac{23300}{\left(t_f E_f\right)^{0.58}} \tag{2.31}$$

and the reduction factors, κ_1 and κ_2 can be determined using the following equations

$$\kappa_1 = \left(\frac{f_c'}{27}\right)^{\frac{2}{3}} \tag{2.32}$$

$$\kappa_2 = \frac{d_f - L_e}{d_f} \quad \text{(U-wrap)} \tag{2.33}$$

$$\kappa_2 = \frac{d_f - 2L_e}{d_f} \quad \text{(side bonding)} \tag{2.34}$$

According to ACI-440, the spacing of the FRP sheets should comply with the limits for the spacing of internal steel links as outlined in ACI-318 (2008). Furthermore, the total shear reinforcement, $V_s + V_f$, should not be greater than $0.66\sqrt{f_c'}b_w d$.

2.5.2 TR55

According to TR55 (2012), the contribution of the FRP to the shear capacity is given by

$$V_f = \frac{E_{fd}\varepsilon_{fse}A_{fs}\left(d_f - \frac{n}{3}l_{t,max}\right)(\cos\beta + \sin\beta)}{s_f} \quad (2.35)$$

where E_{fd} is the design Young's Modulus of the FRP composite, ε_{fse} is the effective strain that can be achieved at the ultimate limit state by the FRP sheets, A_{fs} is the total area of the FRP sheet wrapped or bonded, d_f is the effective depth of the sheets (defined as the total depth of the sheet less the cover to the tension steel), β is the inclination of the sheets to the horizontal axis of the beam. The effective strain, ε_{fse}, is taken as the lesser of 0.004, $\varepsilon_{fd}/2$ and $\sqrt{f_{ctm}/E_{fd}t_f}$.

The coefficient n considers the strengthening solution used, with $n = 0$ for fully wrapped beams, $n = 1$ for U-wrapped configuration and $n = 2$ for side bonding. The anchorage length required to develop full anchorage capacity, $l_{t,max}$, is obtained from

$$l_{l,max} = 0.75\sqrt{\frac{E_{fd}t_f}{f_{ctm}}} \quad (2.36)$$

If the strengthening system utilizes strips, the spacing between the strips should not exceed the least of $0.8d_f$, $d_f - (n/3)l_{t,max}$ and $b_f + d_f/4$. The ultimate shear strength of a section, V_u, is limited by the shear stress leading to diagonal compression failure in the concrete, regardless of the amount of FRP reinforcement. In the UK, this value equals to the lesser of $0.75\sqrt{f_{cu}}$ and 4.75 MPa, according to the bridge design code BS 5400-4 (1990). As the final step in the process, the ultimate bending capacity should also be checked, assuming reduction in the area of the tensile longitudinal reinforcement due to the additional demand in shear caused by the shear strengthening.

TR55 as the only design code for strengthening using FRP provides guidance on deep embedded bars as additional shear reinforcement. The approach, investigated by Valerio et al. (2009), assumes that the FRP bars embedded in the concrete section act in the same manner as internal steel reinforcement, assuming truss analogy. Adjustments are made to consider the equivalent strain in the FRP bars, ε_{fse}, which is conservatively set equal to 0.004, regardless of the type of FRP used.

Similarly to the surface bonded FRP reinforcement, there is an anchorage length beyond

which no increase in capacity can be achieved. This anchorage length can be calculated from

$$l_{b,max} = \frac{\varepsilon_{fse} E_{fd} A_f}{\left(\pi d_b \frac{\tau_b}{\gamma_A}\right)} \tag{2.37}$$

where A_f is the bar cross-sectional area, d_b is the diameter of the deep embedded bar, τ_b is the average bond stress over the length of the anchor, which can be conservatively taken as 15 MPa based on experimental evidence in lieu of actual test values, γ_A is the partial safety for adhesive.

A contribution from the deep embedded bars, based upon a 45° truss analogy, can be added to the contribution from the steel shear links, calculated in accordance with BS EN 1992, based upon the variable angle truss. The total shear capacity can therefore be calculated as

$$V_{Rd,s,f} = V_s + V_f = \frac{A_{sw}}{s} z f_{ywd} \cot\theta + \frac{\varepsilon_{fe} E_{fd} A_f}{s_b} w_{eff} \tag{2.38}$$

where s_b is the spacing of the deep embedded bars and w_{eff} is the effective width over which the deep embedment bars will act.

This width should be taken as

$$w_{eff} = h - 2l_{b,max} \tag{2.39}$$

where h is the strengthened depth of the structure and $l_{b,max}$ calculated according to equation (2.37).

2.5.3 *fib* Bulletin No. 14

The design model in the ultimate limit state, according to *fib* Bulletin No. 14 (*fib* TG9.3, 2001), is applicable to members of rectangular, T and double-T cross-section. This code builds on the model of Triantafillou (1998) and Taljsten (1999) and assumes that the external FRP reinforcement may be treated in analogy to the internal steel. Therefore, the FRP is assumed to carry only the normal stresses in the principal fibre direction. The effective strain in the FRP is assumed to develop in the principal material direction at the ultimate limit state (concrete diagonal tension), and in general is less than the tensile

failure strain. The shear capacity of a strengthened concrete member may be calculated according to the EC2 format as follows

$$V_{Rd} = min\left(V_{cd} + V_{wd} + V_{fd}, V_{Rd,2}\right) \tag{2.40}$$

The FRP contribution to the overall shear capacity, V_{fd}, can be determined from

$$V_{fd} = 0.9\varepsilon_{fd,e}E_{fu}\rho_f b_w d(\cot\theta + \cot\alpha)\sin\alpha \tag{2.41}$$

where $\varepsilon_{fd,e}$ is the design value of effective FRP strain, E_{fu} is the elastic modulus of FRP in the principal fibre orientation, ρ_f is the FRP reinforcement ratio equal to $2t_f \sin\alpha / b_w$ for continuously bonded shear reinforcement of thickness t_f or $\left(2t_f/b_w\right)\left(b_f/s_f\right)$ for bonded strips or sheets with width of b_f at spacing of s_f, d is the effective depth of a member, b_w is the minimum width of the cross-section over the effective depth, θ is the angle of the diagonal crack with respect to the member axis (assumed equal to 45°) and α is the angle between the principal fibre orientation and the longitudinal axis of the member.

The effective strain, $\varepsilon_{f,e}$, for a fully wrapped (or properly anchored) CFRP where FRP fracture governs can be calculated as

$$\varepsilon_{f,e} = 0.17\left(\frac{f_{cm}^{\frac{2}{3}}}{E_{fu}\rho_f}\right)^{0.30}\varepsilon_{fu} \tag{2.42}$$

For CFRP sheets side-bonded or in a U-wrap configuration the effective strain is determined as

$$\varepsilon_{f,e} = min\left[0.65\left(\frac{f_{cm}^{\frac{2}{3}}}{E_{fu}\rho_f}\right)^{0.56} \times 10^{-3}, 0.17\left(\frac{f_{cm}^{\frac{2}{3}}}{E_{fu}\rho_f}\right)^{0.30}\varepsilon_{fu}\right] \tag{2.43}$$

where the first expression refers to failures governed by the peeling-off the CFRP sheets and the second expression to those governed by fracture of the CFRP sheets.

For fully wrapped AFRP members, where FRP fracture governs, the effective strain is calculated as

$$\varepsilon_{f,e} = 0.048\left(\frac{f_{cm}^{\frac{2}{3}}}{E_{fu}\rho_f}\right)^{0.47} \varepsilon_{fu} \quad (2.44)$$

In all equations f_{cm} is in MPa and E_{fu} in GPa. The effective FRP strains give values that are above the yield strain of internal stirrups. Should this not be the case then the FRP strains should also be used for the calculation of the contribution of the internal steel.

2.5.4 Numerical methods for predicting shear capacity of FRP strengthening

Numerical methods may be used to analyze the behaviour and obtain the shear capacity of FRP-strengthened reinforced concrete beams. The purpose-built non-linear finite element fracture mechanics-based software ATENA, discussed in detail in Section 2.3.5, is also capable of analyzing large reinforced concrete structures additionally reinforced with FRP materials (Kotes and Kotula, 2007).

The software is suitable to model unstrengthened and strengthened beams in 2D as well as 3D, depending on the complexity of the problem and the desired accuracy of the solution. Modelling strengthening of reinforced concrete structures strengthened with FRP bars can be achieved in ATENA 2D similarly to the methods of modelling steel reinforcement by either using discrete bars or smeared reinforcement. Modelling of sheets and strips within the 2D environment requires that the FRP material is modelled as equivalent discrete bars of material properties such as diameter and perimeter defined by the user based on the material density. Spacing of these discrete bars must also be very fine to simulate the continuous nature of the FRP sheets. The interface between the FRP and the concrete can be modelled using a bond material model and the bond law specified by the user. Specific material parameters, such as fracture energy and crack opening law can be defined in these models (ATENA Strengthening, 2016; ATENA Theory, 2016; ATENA Troubleshooting, 2015).

ATENA 3D in combination with GiD modelling interface was specifically developed to provide the possibility to model and analyze reinforced concrete structures strengthened with FRP. It is a very flexible and universal simulation programme where several approaches to model the strengthening can be utilized for the different types of FRP strengthening. The methods suitable for modelling of different strengthening solutions depend on the type of utilized material model for the FRP strengthening material and the

interface between the FRP and the surface concrete as well as modelling complexity. Each material model can be defined by different material parameters. The FRP material can be modelled as 1D reinforcement for discrete bars. For strengthening with FRP fabric, utilizing 2D membrane elements with a composite material for reinforced concrete is recommended to capture the orthotropy of the material by smeared reinforcement and to create a computationally efficient model. This can further be modified for 2D and 3D shell elements, however the 2D modification model for reinforced concrete is possible only in ATENA Science. In ATENA Engineering, methods employing 3D shell elements must be used, however, the model is computationally demanding (ATENA Strengthening, 2016). ATENA 3D was demonstrated to be able to accurately predict the ultimate load-carrying capacity of the beam as well as the local and global structural behaviour compared with experimental data (Al-Bayati and Al-Mahaidi, 2014; Khene et al., 2016; Sabol and Priganc, 2013).

2.6 Current state of research on FRP-strengthened beams

Extensive research has been undertaken in recent years in the shear strengthening of reinforced concrete beams with FRP materials (Triantafillou,1998; Khalifa and Nanni 2000, 2002; Chen and Teng 2003a, b; Bousselham and Chaallal 2004, 2006, 2008; Carolin and Taljsten 2005; Zhang et al., 2005; Jayaprakash et al., 2007; Grande et al., 2007; Bukhari et al., 2010).

However, this Section is focused on the current state of research into reinforced concrete full-scale T-beams in shear strengthened with FRP composites. The behaviour of the underlying reinforced concrete beam is typically included for comparison in the selected literature. Therefore, only the most relevant recent research findings that formed the basis for the experimental and analytical work presented in this Thesis are discussed in the following sections. It should be noted that most published work prior to 2012 formed the basis of the codified approaches presented and discussed in detail in Section 2.3 and Section 2.5 and it is therefore not required to review in detail here.

2.6.1 Failures of FRP-strengthened reinforced concrete T-beams in shear

Two main failure mechanisms can be distinguished for reinforced concrete beams strengthened in shear with FRP materials – debonding from the concrete surface or rupture. Rupture of the externally bonded FRP sheets and strips is predominantly the

failure mode in beams of rectangular geometry where full wrap configuration is possible and unlikely to occur for deep embedded bars (Belarbi and Acun, 2013; Valerio et al., 2009; Barros and Dias, 2005). Debonding of externally bonded FRP sheets and strips was identified as the predominant failure mode for side bonded and U-wrap configurations (Chen and Teng, 2003b; Chen and Teng, 2003a; Teng et al., 2009; Belarbi and Acun, 2013). Beams strengthened with near-surface mounted strips and bars as well as deep embedded bars primarily fail due to the failure of the bond between the FRP material and the surrounding concrete (Valerio et al., 2009; Mofidi et al., 2012; Chaallal et al., 2011; Qin et al., 2014).

According to an extensive review of the failure modes carried out by Belarbi and Acun (2013) on a diverse set of experimental data provided by NCHRP Report 678 (2011), no debonding failures occurred in fully wrapped beams for the reviewed database. On the other hand, 83% of failures reported on were due to debonding for beams strengthened in the U-wrap configuration and 92% of failures were due to debonding in the case of side bonded FRP.

In beams strengthened with externally bonded FRP sheets and strips where the debonding of the sheets is prevented using an effective end-anchorage system, the failure mode of the beam is controlled by the failure of the anchorage system. This can either be through debonding of anchorage strips and bars or because of pulling out of the concrete, as is the case for spike anchors and through-anchorage systems (Smith and Kim, 2008; Mofidi et al., 2012; Bae and Belarbi, 2013; Koutas and Triantafillou, 2013).

2.6.2 Debonding of externally bonded FRP sheets

FRP debonding is a premature failure mechanism of beams strengthened with externally bonded FRP sheets and strips in U-wrapped and side bonded configurations. This is caused by the limited anchorage length provided, compared with fully wrapped beams. The failure is characterized by peeling off the surface layer of the concrete to which the FRP is bonded at the onset of shear crack formation in the underlying reinforced concrete beam (Chen and Teng, 2003a; Sas et al., 2008; Lu et al., 2009; Mofidi and Chaallal et al., 2011; Chen et al., 2012). Once the tensile strength of the concrete is reached, a localized bond failure occurs between the concrete and the FRP sheets (Teng and Chen, 2009; Colalillo and Sheikh, 2014). The FRP sheets are inactive before a shear crack develops in the beam, which

initiates a progressive debonding process until the free edge of the FRP sheets is reached and the beam fails.

The FRP sheets can debond within the FRP-epoxy interface or at the concrete/epoxy interface. It was proved experimentally that the majority of debonding failures commonly occur within the surface layer of concrete at a small distance from the FRP-epoxy interface (Chen and Teng, 2003a; Lopez-Gonzales et al. 2012). A thin layer of concrete can therefore be observed attached to the FRP sheet after debonding occurred at the crack location. This is caused by the much lower bond strength of the concrete layer compared with that of the epoxy. There are several factors that can affect the bond performance and thus the overall shear capacity of the strengthened beam – concrete strength, surface preparation, axial rigidity of the FRP, provided bond length, thickness of the FRP laminate and the material properties of the epoxy resin used.

According to an experimental study carried out by Lopez-Gonzales et al. (2012), for lower concrete strength the debonding failure occurred in the concrete and was not found dependent on the adhesive thickness. Contrary to this, a thicker adhesive layer in combination with higher strength concrete resulted in a delayed debonding failure.

2.6.3 Effectiveness of FRP strengthening for T-beams in shear

By 2004, the U-wrap configuration was identified as the most effective strengthening solution for T-beams, which was evidenced by experimental results (Bousselham and Chaallal, 2004). Generally, the U-wrap configuration was demonstrated to be more effective in terms of enhancing the shear capacity of a reinforced concrete beam than the side bonded configuration, regardless of its geometry (Grande et al., 2007; Belarbi and Acun, 2013). Further increase in shear strength is achievable with end-anchorage devices, which was researched extensively and evidenced experimentally (Khalifa and Nanni, 2000; Jinno et al., 2001; Ortega et al., 2009; Deifalla and Ghobarah, 2010; Al-Mahaidi and Kalfat, 2011; Mofidi et al., 2012; Koutas and Triantafillou, 2013; Bae and Belarbi, 2013; Grelle and Sneed, 2013). End-anchorage systems for the externally applied FRP sheets and strips prevent and/or delay the debonding of the FRP sheets and therefore promote a more efficient use of the FRP material.

Furthermore, it was demonstrated experimentally that the debonding of FRP U-wraps can be controlled using bi-directional CFRP sheets (Jayaprakash et al., 2007; Bousselham and

Chaallal, 2008). In both studies, none of the T-beams failed due to debonding of the CFRP U-wraps. Bousselham and Chaallal (2008) conducted a review of experiments on 17 full scale T-beams of depth 350 mm and 175 mm strengthened with continuous bi-directional sheets in a U-wrap configuration. The authors found that doubling the amount of FRP did not lead to increase in shear strength for the 350 mm deep specimens with no internal shear reinforcement. It was also found that increasing the amount of the internal shear reinforcement by decreasing the spacing of the steel links leads to a lower contribution of the FRP to the overall shear capacity of the strengthened beam. Size effect was also observed in this study for beams without shear reinforcement. The specimen of depth 175 mm with 1 layer of FRP sheets achieved an increase in shear strength of 65% due to the application of the FRP. However, the increase in the specimen of 350 mm depth with the same properties was only 48%. This finding demonstrated that the beam depth as well as the arrangement of the internal shear reinforcement has a great influence on the effective contribution of externally applied FRP sheets to the shear capacity of the beam.

Contrary to this, Foster et al. (2016) in their experimental campaign on full-scale T-beams strengthened with externally applied uni-directional CFRP sheets in a U-wrap configuration showed that only marginal increase in shear strength was achieved for typical bridge beams. This was regardless of the FRP thickness used as well as the size of the beam, as three directly scaled beam sizes were tested.

Greater shear capacity of T-beams strengthened with externally applied FRP U-wraps can be achieved using an end-anchorage system by as much as 70%. Mechanical anchor systems as well as those relying on the chemical bond between the FRP and the concrete can be used (Ortega et al., 2009; Mofidi et al., 2012; Grelle and Sneed, 2013; Bae and Belarbi, 2013). Horizontal continuous FRP strips can also be used to prevent the debonding of FRP U-wraps, however, the experimental results from various studies on their effectiveness are contradictory (Schnerch, 2001; Mahaidi and Kalfat, 2011; Bae and Belarbi, 2013).

Using internally applied FRP bars rather than externally bonded FRP sheets and strips can further increase shear capacity of a reinforced concrete beam of a rectangular as well as T-beam cross-section (Valerio et al., 2009; Mofidi et al., 2012; Chaallal et al., 2011; Barros et al., 2013; Qin et al., 2014, Raicic, 2016). Increase in shear strength of up to 96% was observed in experimentally tested beams strengthened with GFRP bars (Jemaa et al.,

2015). These findings are suggesting that the deep embedment strengthening technique may offer a suitable alternative to strengthening with externally bonded FRP sheets.

2.6.4 Development of FRP shear resistance models

It was demonstrated in the previous section that attempts were made to quantify experimentally the contribution of the FRP to the overall shear capacity of an FRP-strengthened reinforced concrete T-beam. However, these assumed that the FRP contribution is simply the difference between the capacity of the strengthened beam and the underlying control specimen. It was discussed in Section 2.5 that this additive approach is widely accepted in the most frequently used design guidelines for FRP-strengthened reinforced concrete beams. However, the applicability of this approach is questionable, since the strengthened beam behaves like an FRP-reinforced concrete composite and the sharing of the load between the components may be altered due to the FRP application.

Several researchers developed FRP shear resistance models based on their experimental findings and compared with existing guidelines for strengthening of reinforced concrete beams with FRP composites (Sas et al., 2009; Mofidi and Chaallal, 2011; Chen et al., 2013, Colalillo and Sheikh, 2014). These models were compared with large amounts of experimental data from literature. Discrepancies and a large scatter of data were reported on for beams failing due to debonding, highlighting the issue of being able to accurately predict the shear capacity of a FRP-strengthened beam in shear based on empirical models.

Comparison of shear strength predictions to ACI-440 (2008), CNR-DT 200/2004 (2004) carried out by Chen et al. (2013) reported on predicted shear strength versus the experimental shear strength coefficient of 0.563 for the ACI-440, 0.267 for the CNR-DT 200/2004 and 0.798 for Chen et al. (2013). Similarly, comparison of 119 shear strengthened beams to the same standards as well as Chen and Teng (2003a) by Colalillo and Sheikh (2014) reported on average experimental to predicted shear strength ratio of 1.23 for the Chen and Teng (2003a) model, and 1.33 and 1.13 for the ACI and the CNR standard, respectively. Further 200 tests on rectangular beams and T-beams were compared by Sas et al. (2009) using the Chen and Teng (2003a) model. The model provided safe predictions for T-beams, however, a large scatter was observed for the rectangular beams where the capacity in several cases was either greatly over- or under-estimated. Mofidi and Chaallal (2011) compared their model with predictions from ACI-440 and CNR-DT 200/2004 with a database of 75 reinforced concrete beams. The ratio of the predicted to

actual shear capacity was 0.61 for the Mofidi and Chaallal (2011) model, 0.37 and 0.42 for the ACI and CNR standard, respectively. Foster et al. (2016) compared experimentally obtained shear capacities for full-scale T-beams strengthened with externally bonded FRP sheets with ACI-440 (2008), *fib* Bulletin No. 14 (2001) and TR55 (2012), demonstrating a large scatter of predicted versus actual shear capacity ratios. It is therefore evident that none of the models, whether theoretical or accepted in guidelines, can accurately determine the shear capacity of a reinforced concrete beam strengthened with externally bonded FRP. Unsafe design predictions may therefore be obtained in cases where the models over-predict the contribution of the FRP to the overall shear capacity of the strengthened reinforced concrete beam.

The design guidelines proposed by Valerio et al. (2009) and subsequently accepted in TR55 (2012) provide safe predictions of shear capacity for beams strengthened with deep embedded bars. This is due to the conservative assumption of maximum allowable strains for the FRP bars at 0.4%. Quapo et al. (2016) compared TR55 (2012) predictions with published experimental results as well as a numerical FE model developed by the authors. The TR55 predicted versus experimental shear strength ratio was 1.57 with a standard deviation of 0.54, whereas for the numerical predictions the ratio was 1.08. The study also indicated that further increase in shear strength can be achieved by using inclined deep embedded bars and the increase in concrete compressive strength. However, it was found that the shear strength decreased with the increase in shear span to depth ratio and internal stirrup to FRP bar ratio. The predicted increase in shear strength was not found to be dependent on the size of the beam.

2.7 Concluding remarks

The interaction of various shear mechanisms due to the non-homogeneity of the material and varying loading arrangements in FRP-strengthened reinforced concrete beams results in a complex, non-linear problem with many variables. The key parameters greatly influencing the shear behaviour of an unstrengthened reinforced concrete beam were identified as the shear span to depth ratio, the reinforcement ratio, the concrete strength, and the size and geometry of the structure. The critical review of the current design and assessment codes and their applicability to assess the shear capacity of existing structures revealed that the most conservative codes are those based on the truss analogy. The more advanced plasticity-based approaches that use the strut-and-tie models offer a greater

accuracy in predicting the ultimate shear capacity. However, the *fib* Model Code (2010), which is the most evolved of the currently available codes, presents a greater flexibility in terms of different levels of assessment applicable to different assessment scenarios. The code employs fracture mechanics to account for size effect in combination with probable failure modes and consequently offers a greater accuracy of shear predictions.

It is therefore critical to apply the most appropriate code and hence level of analysis depending on the assessment criteria. For design, understandably, the conservative nature of simple truss models is appropriate to ensure adequate provision against shear failures. However, for assessment of existing structures, reduction or removal of such conservatism may result in overly optimistic shear capacity predictions and ultimately lead to unexpected catastrophic failures.

Furthermore, accurate shear capacity predictions of existing reinforced concrete bridges are crucial to determine the degree to which to repair or strengthen the structure. Without accurate predictions of the cracking and the ultimate load for shear-critical elements, the design of strengthening schemes using similarly simplistic additive approaches to obtain the overall shear capacity may lead to serious consequences. All the design guidelines for shear strengthening using FRP fabrics assume that the only active component is in the vertical direction and do not consider the non-principal stretching of the sheets.

Currently, there is lack of research on stretching of the FRP sheets in the non-principal direction, which is invariably the case in shear-strengthening practice. Furthermore, there is lack of research on full-scale T-beams, typical of existing slab-on-beam bridge structures, which would demonstrate the applicability of the codified approaches for assessment and design of FRP strengthening for realistic flanged sections. Investigations of the suitability of deep embedded bars as an alternative to externally bonded FRP sheets conducted on beams with geometries representative of existing bridge structures are also scarce.

Therefore, based on the literature review presented in this Chapter, experimental testing was required to determine the effect of size and shape of FRP-strengthened reinforced concrete T-beams on the overall shear capacity and mechanical behaviour.

Further analytical investigation was required to determine the suitability of current design guidelines for predictions of shear strength of flanged beams strengthened with FRP sheets and deep embedded FRP bars.

3 METHODOLOGY

3.1 Introduction

This Chapter details the planning and execution of the experimental component of the research programme and the subsequent analytical work. The entire experimental programme was carried out in collaboration with the University of Cambridge and the contribution of both universities is acknowledged accordingly within the text. Decisions made regarding the test setup, materials used, construction methods as well as the strengthening schemes selected for investigations are discussed. Sequencing of interlinked work packages and their individual and combined contributions to the development of the theoretical concepts are also presented here.

3.2 Research rationale

The three key objectives of the presented research programme were to:

1. Investigate size effect in FRP-strengthened T-beams;
2. Determine effective FRP contribution in FRP-strengthened T-beams; and
3. Provide design formulations for FRP-strengthened slab-on-beam structures.

3.2.1 Effect of structure size and geometry on shear behaviour

Comparison of typical lab-scale specimen and real scale beams as part of an existing structure is shown in Figure 3.1.

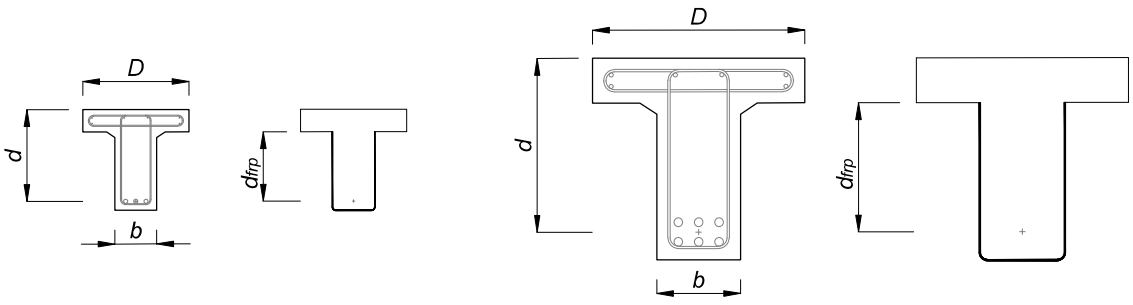

(a) (b)

Figure 3.1 – Slab-on-beam structures: (a) typical lab-scale specimen size, (b) real-life structure.

Even though researchers as well as practicing engineers consider T-beams to be representative of typical slab-on-beam concrete structures, most previous research was conducted on small-scale rectangular specimens. Tests on such beams shear-strengthened with FRP materials exhibit inconsistencies in behaviour as well as performance and this has been predominantly attributed to size effect. Beams with complex geometries are known to behave differently to simple rectangular beams, which is a further cause for concern regarding discrepancies in experimental findings. Early theories that formed the basis of most current design guidelines were tested on rectangular beams where externally bonded FRP materials were bonded to all four sides either in strips or continuous sheets. Such an approach is practically impossible for most of existing structures where the slab obstructs the top of the beam. The only feasible option then in most cases is bonding on three sides only, referred to as U-wrap. Sufficient overlap of the FRP material on the top of the rectangular beam provides further additional benefits in terms of preventing the FRP from debonding. U-wrap configurations inevitably result in reduced anchorage length and are therefore susceptible to premature debonding failures. With the FRP often terminating at the neutral axis level, further concerns arise in cases where there is no link between the tension and compression zones. These major issues raise important questions if it is safe and economically viable to strengthen large concrete structures in shear using externally bonded FRP materials.

3.2.2 Effective FRP contribution in FRP-strengthened beams

Ideally, in strengthening situations where external shear reinforcement, such as FRP sheets and strips, is additionally added to enhance the capacity of a beam, the reinforcement should be fully anchored in the compression zone to prevent premature debonding. In cases where the beam is integral with the slab, holes must be drilled through the flange to accommodate the shear reinforcement, taking care to avoid cutting any existing steel. However, this approach might not be viable for strengthening bridges, where the surface of the bridge deck remains in place or the strengthening is to be carried out under service loads. In such cases, a continuous bar-in-slot anchorage system offers a possible alternative. The bars anchoring the sheets into the compression zone are typically embedded into the bottom soffit of the slab. This, however, might not be possible for cast-in-place bridge beams with haunches, where the sheets would have to be applied over the haunch and anchored into the slab. The presence of the haunch detail further reduces the

anchorage length of the sheets and the only viable option is anchoring into the beam web underneath the haunch, as indicated in Figure 3.2 (b). Anchoring into the haunch itself is not advisable, since cutting a groove along the beam would be difficult to achieve.

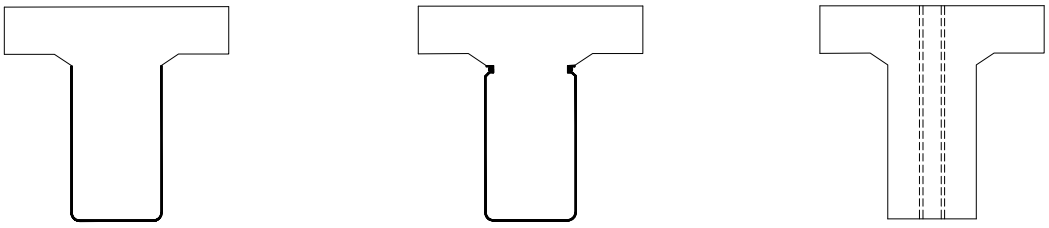

(a) (b) (c)

Figure 3.2 – Investigated strengthening solutions: (a) U-wrap without end-anchorage system, (b) U-wrap with end-anchorage system, (c) deep embedment.

In cases where the web of the beam is not accessible, the possibility exists to strengthen the beam internally with reinforcing deep embedded bars in concrete as additional shear reinforcement (Valerio, 2009), see Figure 3.2 (c). This strengthening technique presents a viable alternative to externally bonded FRP reinforcement. This technique also offers significant advantages over the fabric strengthening systems in terms of material savings and its potential suitability for application under full service load.

3.2.3 Design formulations for FRP-strengthened slab-on-beam structures

Research conducted on FRP-strengthened reinforced concrete beams highlighted that in situations where FRP materials bridge a crack, load sharing between steel and FRP at the crack location becomes complicated (Mofidi et al., 2016). The contribution of concrete in shear-strengthened beams is largely neglected or underestimated in current design guidelines, which in turn leads to inaccurate shear capacity predictions. Furthermore, these predictions are predominantly based on lower-bound plasticity solutions, where the ultimate shear capacity, V_u, of an unstrengthened reinforced concrete beam is expressed as a single collective term

$$V_u = V_s + V_c \tag{3.1}$$

where V_s is the shear contribution of transverse steel reinforcement and V_c is the shear

contribution of concrete.

For strengthened beams, this expression is further extended by the contribution of the FRP, V_f, and leading to a formulation of the ultimate shear capacity being expressed as the sum of the individual components

$$V_u = V_s + V_c + V_f \tag{3.2}$$

This additive approach is generally adequate for design situations of new reinforced concrete structures, where the lower-bound solution assumes that the beam fails when all shear reinforcement yields simultaneously. Practically, such an approach may greatly underestimate the shear capacity of a reinforced concrete beam and therefore the suitability of the addition of individual shear capacities for accurate assessment of existing reinforced concrete structures is questionable. On the other hand, the contribution of any additional FRP reinforcement is calculated based on strains reached in the FRP at debonding. Current experimental research revealed that these predictions are very optimistic, especially in cases of externally bonded FRP sheets without end anchorage (Mofidi et al., 2012). Furthermore, the contribution of the concrete, the steel and the FRP will occur at different stages of loading and therefore a design process based on the addition of the individual shear capacities for externally bonded FRP sheet strengthening is fundamentally flawed and inappropriate.

The increase in shear capacity due to the application of FRP sheets, V_f, depends on the anchorage length, $l_{l,max}$, calculated according to TR55 as

$$l_{l,max} = 0.75 \sqrt{\frac{E_{fd} t_f}{f_{ctm}}} \tag{3.3}$$

and is therefore a function of the Young's modulus, E_{fd}, the thickness of the FRP laminate, t_f, and the concrete tensile strength, f_{ctm}.

Premature debonding of continuous FRP sheets can alter the load transfer between the steel, concrete and FRP and it is therefore crucial to identify their individual contributions (Mofidi, 2012; Lees, 2001). Even though there is a significant amount of research on FRP debonding parallel to the principal fibre direction (Grande et al., 2007; Mofidi et al., 2012;

Belarbi and Acun, 2013), there is still a lack of research that considers debonding in the non-principal direction, which is invariably the case in shear-strengthening practice. Furthermore, local debonding effects may lead to catastrophic global failure events, especially in cases where insufficient anchorage length is provided to transfer the required loads. To this end, it is imperative to observe and understand the local debonding processes in isolation as well as global in beam behaviour. Based on thorough understanding of the underlying debonding mechanisms, robust, mechanics-based approaches to predict the effectiveness and performance of FRP-strengthened reinforced concrete systems are necessary and will indeed be possible. For practical purposes, it is of paramount importance to clearly identify when strengthening is necessary, that is accurately determining the residual shear capacity of an existing reinforced concrete structure. Furthermore, it is crucial to be able to accurately predict the performance of the unstrengthened and strengthened structure under load, and to determine what type of strengthening is the most suitable for a given situation. Such practical limits for strengthening will ultimately lead to progressive improvement in shear-strengthening practice for reinforced concrete structures in terms of assessment as well as management of structurally deficient structures.

3.3 Research methodology

To deliver the research objectives outlined in Section 3.2 and to provide industry-relevant data, a targeted research programme focused on full-scale slab-on-beam structures was developed. The experimental investigations and analytical work were carried out simultaneously, in a synergistic manner, and the research objectives delivered in three intrinsically linked work packages (WP) as follows

WP1: Investigation of local and debonding behaviour;
WP2: Investigation of scale in T-beam structures; and
WP3: Development of design guidelines.

The scope of the above work packages is described in detail in the following sections.

3.3.1 Investigation of local and debonding behaviour

The purpose of this work package was threefold:

1. To investigate debonding processes and non-principal stretching of the externally

bonded FRP fabric;

2. To determine the load-sharing contributions made by the concrete, internal steel and the FRP; and
3. To contribute to the development of debonding models for FRP-strengthened systems.

To investigate load-sharing interactions in FRP-strengthened systems successfully, it is critical to separate out the contributions of steel, concrete and FRP. The ability to predict where a shear crack will originate and how it will further propagate is extremely important for the observation and subsequent analysis of the stretching and debonding behaviour of externally bonded FRP sheets. Therefore, experiments on uncracked asymmetric push-off specimens with a known shear plane were proposed to isolate the mechanics of the steel, concrete and FRP interactions to precede the main beam series.

This type of test was originally used by Hofbeck and Mattock (1962) to create a pure shear plane and to isolate various shear effects. The modified specimen size geometry is shown in Figure 3.3.

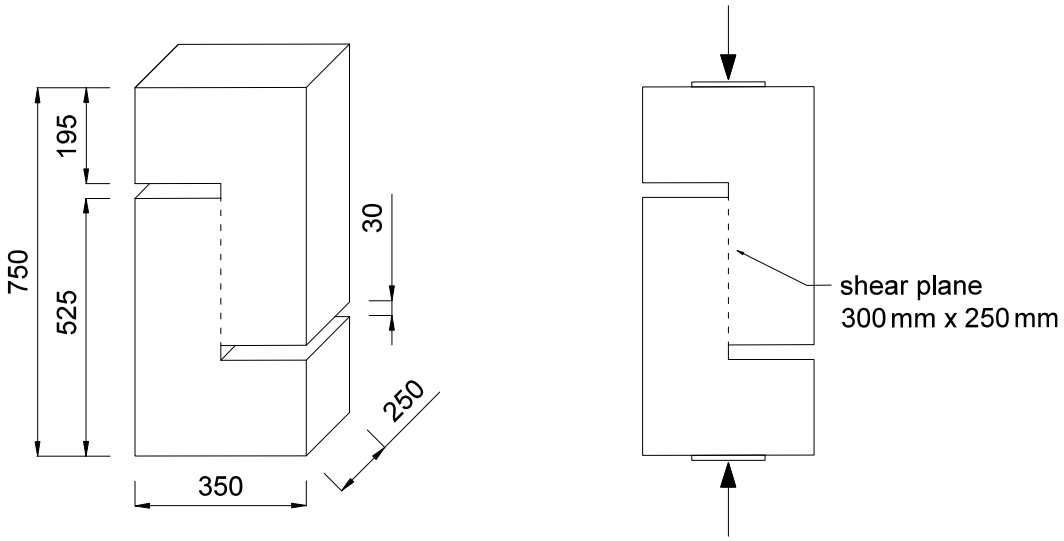

Figure 3.3 – Modified shear-friction push-off specimens – overall geometry and loading [mm].

The original *Hofbeck* specimens with a 0° shear crack inclination were designed to derive the equation for the shear-friction capacity of reinforced concrete sections with internal steel links in pure shear and in shear with tension acting across the shear plane. More recently, these types of specimen were used to observe the interaction of concrete sections

in shear without internal steel reinforcement but with externally bonded FRP reinforcement (Saenz and Pantelides, 2005). The innovation in the current work lies in testing the concrete-FRP interactions in the presence of steel stirrups crossing the shear plane. It was of interest to ascertain the critical mode of fracture within the concrete and the FRP-concrete interface in a controlled environment prior to the beam series. This experimental programme allowed for the observation of the variability of potential fracture modes of the specimens strengthened with externally bonded FRP sheets. Furthermore, for the localized tests to be relevant to the beam series, the novel component of this experimental investigation was modified geometry of the specimens to model real-life situations, with overall dimensions of 750 mm x 350 mm x 250 mm. Design and construction details are discussed in detail in Chapter 4.

Review of existing literature highlighted that discrepancies in behaviour of FRP-strengthened systems exist when experiments on uncracked and cracked specimens are compared (Jayaprakash et al., 2009). This preliminary finding led to the inclusion of additional experiments on pre-cracked push-off specimens in the experimental programme to investigate the behaviour of the FRP fabric crossing a pre-existing shear crack. To investigate the effectiveness of both the externally bonded FRP sheets and internally applied FRP bars across a known shear plane, deep embedment was also included in this study to complement the beam series. This experimental programme was carried out simultaneously with the experiments at the University of Cambridge on modified push-off specimens with inclined shear plane (Foster et al., 2016).

The main objectives of this joint study were to determine the load sharing between the materials and to observe debonding processes in the FRP-reinforced concrete systems across a known shear plane in shear-compression. The push-off specimens are uniquely suitable for controlled debonding investigation when principal stretching of the FRP sheets does not align with principal strains. Isolation of such stretching in a strengthened beam might not be possible as the inclination of the shear crack relative to the direction of stretching of the FRP across the shear crack is not known prior to testing.

The investigated parameters included the steel and FRP ratios crossing the shear plane as well as the anchorage length of the externally bonded FRP sheets. Two different percentages of internal steel were selected to represent threshold shear reinforcement ratios according to both historic and current design codes. Three wrapping schemes were considered for specimens strengthened with externally bonded FRP sheets to vary the

anchorage length from a U-wrap to a full wrap with overlaps. To investigate differences in behaviour between externally and internally applied additional shear reinforcement, deep embedment specimens with comparable amounts of FRP were also tested. In total, twelve experiments were carried out on initially uncracked specimens, including unstrengthened control specimens to serve as a baseline for comparison. The cracked unstrengthened control specimens from the main test series were retained, strengthened with externally bonded sheets in the same manner as their fully wrapped uncracked counterparts, and tested. This was to investigate the effect of a pre-existing crack on CFRP debonding and the load sharing between the steel, which had yielded, and the CFRP, neglecting the contribution of the cracked concrete. The investigated configurations are presented in Figure 3.4.

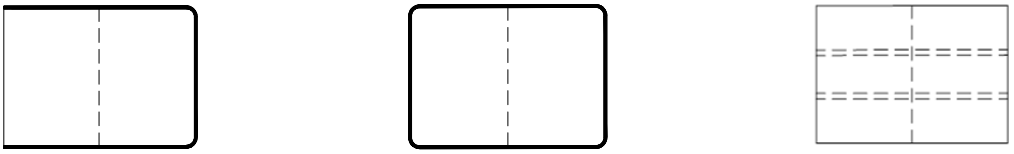

(a) (b) (c)

Figure 3.4 – Push-off specimens (top view) investigated strengthening solutions: (a) U-wrap with varying anchorage length, (b) full wrap, (c) deep embedment.

3.3.2 Investigation of scale in T-beam structures

Investigation of size effect in beams through physical testing is achieved by using appropriately scaled specimens in either two or three dimensions. Since slab-on-beam structures are by their very nature three-dimensional, scaling in three dimensions was adopted. Sizes ranging from the higher end of the laboratory scales to realistic scales of existing highway structures were identified as the most appropriate in order to obtained meaningful data from the experimental testing.

Three sizes of test specimens were designed, ranging from bridges to buildings with their geometry scaled in three dimensions. Two series on the larger side of the size spectrum were tested at the University of Bath, with the smaller beams and a selection of medium size beams being tested at the University of Cambridge to complement the series and to provide a significant overlap.

The geometry of the tested beams is shown in Figure 3.5 and Figure 3.6.

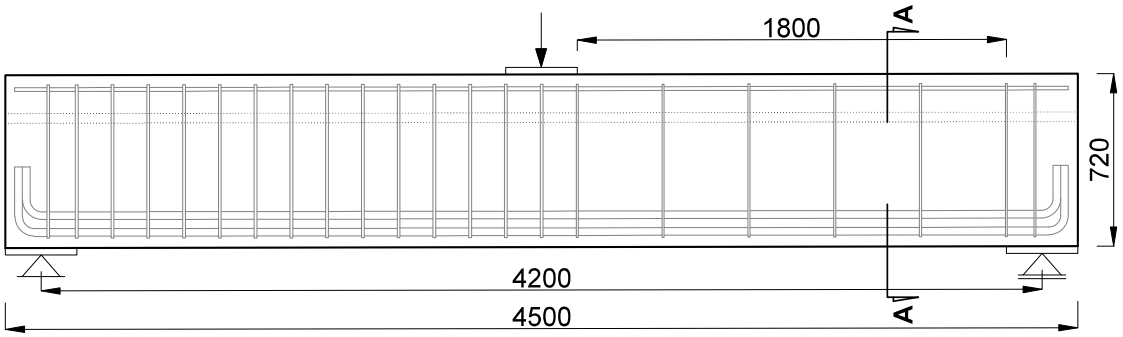

(a)

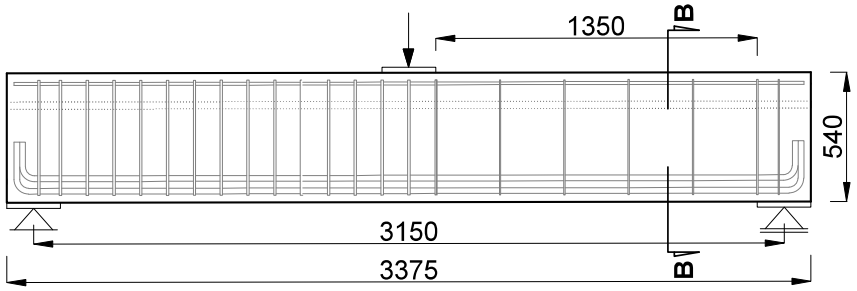

(b)

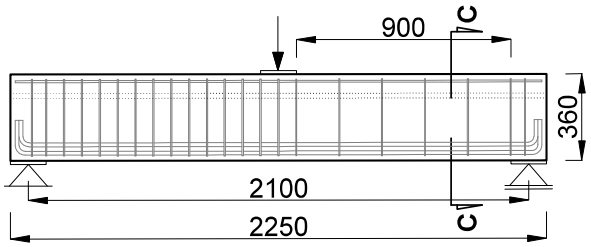

(c)

Figure 3.5 – Scaling of T-beam specimens: (a) large T-beam (Bath), (b) medium T-beam (Bath and Cambridge) and (c) small T-beam (Cambridge) [mm].

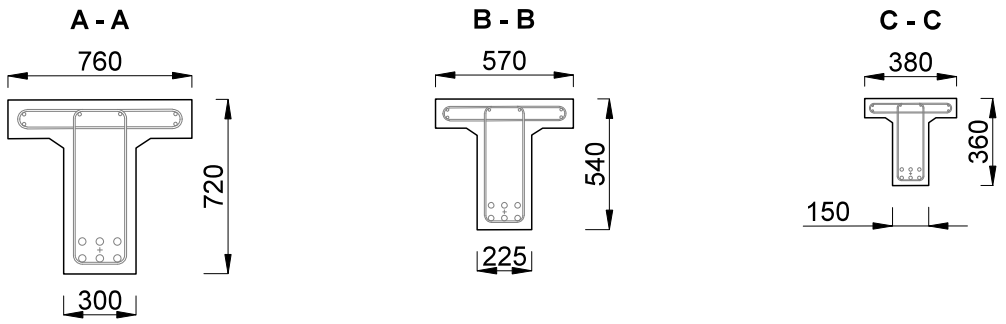

(a) (b) (c)

Figure 3.6 – Scaling of T-beam specimens – section through: (a) large T-beam (Bath), (b) medium T-beam (Bath and Cambridge) and (c) small T-beam (Cambridge) [mm].

The joined-up research between the two universities was driven by a common goal to conclusively rule out inconsistencies caused by procedural errors in testing at two independent testing facilities.

The sole variable tested on all sizes of specimens was the strengthening method used to prevent further inconsistencies caused by varying multiple interlinked parameters at once. The focus of this study was on the key aspects where the FRP strengthening ratio and the influence of end anchorage on the overall beam performance were investigated. The beams tested at the University of Cambridge were strengthened in the U-wrap configuration, whereas at Bath the investigated scenarios included U-wrap with bar-in-slot end-anchorage system and the deep embedment solution across both tested sizes. The novel component of this work package was a synergistic and collaborative approach to investigate experimentally, analytically and numerically the size effect in both the concrete and the strengthening system within one research programme at two independent testing facilities. This work package was led by the University of Bath with input from the University of Cambridge.

Materials and construction methods for the specimens were selected to closely match those used in historic concrete structures. The design of the test specimens was based on existing cast-in-place reinforced concrete bridges from the period between 1930 and 1970 in the UK. These structures are deemed insufficient in shear according to current design guidelines and are being increasingly identified as critical for repair and strengthening.

To successfully investigate size effect, it was of paramount importance for the geometrical ratios to be maintained. Therefore, not only were the specimens scaled in all three dimensions, but also the overall test setup was scaled accordingly – including the dimensions of the supporting and loading plates. The proportion of steel stirrups was deliberately designed to provide lower than the recommended values for shear reinforcement according to current design guidelines, nominally less than 0.1%. The design purposely violated both design conditions in terms of proportion as well as the maximum spacing of the reinforcing bars, according to current design codes.

To obtain meaningful test data, it was crucial to ensure that all tested beams failed in diagonal shear, regardless of the strengthening method used, and that the capacity of the machine was not reached. For the overall success of the project it was also necessary to ensure that all beam sizes failed in shear, including the small specimens, which had the potential to fail in flexure, tested independently at the University of Cambridge.

3.3.3 Development of design guidelines

Understanding of the key issues of size, FRP contribution to the overall shear capacity of a strengthened reinforced concrete beam and debonding developed in WP1 and WP2 is critical for the most accurate way to implement these effects into design formulations. The experimental programme was designed to provide a direct and measurable insight into the inter-relationships between the key parameters influencing the behaviour of shear-strengthened reinforced concrete systems.

3.4 Experimental considerations

3.4.1 Specimen design and fabrication

The geometry, size and shape of the specimens in the presented experimental programme were based on existing slab-on-beam bridge structures. The design process of the reinforced concrete beams was initiated at the large scale first and then scaled down to obtain a scaled replica of the large bridge beams. The properties of the concrete were chosen to reflect the reported actual strength of existing reinforced concrete bridges built after the 1930's. According to (Thun et al., 2006), the minimum concrete cube compressive strength required was in the range of 50 to 80 MPa with average tensile strength between 2.6 and 3.8 MPa.

The push-off specimens were fabricated in-house at both the University of Bath and the University of Cambridge, using bent reinforcing bars from a local supplier, sourced independently. The beams were prefabricated by a precast company for both universities, with large beams and medium beams for the University of Bath cast on separate occasions and the University of Cambridge beams cast independently at a later date. The same concrete mix and reinforcement supplied by the precaster were used throughout the experimental programme. Both universities supplied the shear links for the tested span sourced independently from a local supplier.

3.4.2 Specimen preparation and strengthening

The preparation of the specimens for strengthening included abrasive surface preparation for application of the externally bonded FRP sheets and drilling of holes for the application of the deep embedded FRP bars as additional shear reinforcement. The details of the specimen preparation for testing are described in Chapter 4 and Chapter 5 for the push-off specimens and the T-beams, respectively.

The fabric used for strengthening with FRP sheets was custom-weave, uni-directional reinforcing CFRP fabrics with a two-component epoxy adhesive, whose properties are further discussed in Chapter 4. Two types of unidirectional fabrics from the same manufacturer were used to vary the percentages of the CFRP material crossing the shear plane and to reflect ‘lightly’ and ‘heavily’ strengthened scenarios. Such an approach was chosen to maintain the number of applied layers across the test series to prevent inconsistencies in behaviour due to potential interlayer delamination. The fabric used to model the ‘heavy’ strengthening cases had effectively twice the amount of fibre content as that used for ‘light’ strengthening. The carbon fibres in the main fibre direction in both fabric types were oriented at 0° weaved together by carbon fibres (light) and coarsely spaced aramid fibres (heavy) at 90°. In both cases, according to the manufacturer, for design purposes these cross-fibres were assumed to provide no additional strength in the cross-fibre direction. The CFRP fabric was used with the manufacturer-approved two-component epoxy adhesive.

The CFRP bars used for deep embedment were sand-coated spirally wound Aslan 200. In the case of the push-off tests, these bars were used in combination with a manufacturer tested and recommended non-sag two-component epoxy adhesive, suitable for anchorage into concrete. For the application in the beam series, the same two-component epoxy

adhesive used for the application of the externally bonded CFRP sheets was used to ensure the bond strength between the FRP and concrete was identical.

The details of the strengthening are presented in Chapter 4 and Chapter 5 for the push-off specimens and the T-beams, respectively.

3.4.3 Instrumentation

The strains in the internal steel stirrups were measured using electrical resistance post-yield strain gauges. The strain gauges used throughout the experimental programme were 2 mm long and of type TML-YFLA-2-11 bonded with CN-Y adhesive. They were placed centrally on each leg of each stirrup, so that the variation in strain along the steel bar across the shear plane could be recorded. The positioning of the strain gauges is discussed in detail in Chapter 4 and Chapter 5 for the push-off specimens and the T-beam specimens, respectively. Strains of the concrete were not measured using physical strain gauges for the following reasons:

1. Surface strains in the proximity of a crack are not representative of the internal strain distribution. Assuming strain gauges are activated at first cracking of concrete, strain readings in the concrete itself would have had little meaning beyond the point of cracking;
2. The undeformed steel stirrups equipped with strain gauges provided an internal ‘strain probe’ to reflect the internal strain distribution. However, in reinforced concrete the strains recorded along the bars do not necessarily correspond to those of the surrounding concrete;
3. The CFRP sheets in the externally strengthened specimens obstructed the concrete surfaces and therefore application of strain gauges would have been impractical and their presence would have potentially resulted in serious issues with bond in the location of the strain gauge;
4. The use of the Digital Image Correlation (DIC) technique to obtain full-field surface displacement and strain measurements was employed in all tests and therefore surface strain gauges on concrete were deemed expensive, unnecessary and difficult to achieve due to their localization with respect to the shear crack.
5. Surface strains are not representative of through-section strains as this is a 3D variation in strain flow.

All specimens strengthened with externally bonded CFRP sheets were equipped with strain gauges after 72 hours of curing. The strain gauges used throughout the experimental programme were 45°/90° 3-element rosettes, of type TML-BFRA-2-3 for CFRP composites and applied with CN adhesive. For the deep embedment specimens, each CFRP bar was equipped with two centrally applied strain gauges to measure the strain distribution on the top and the bottom of the bar crossing the shear plane. Such an arrangement was chosen for all reinforcement crossing the shear plane after an initial pilot study on one push-off specimen with multiple strain gauges positioned along the steel stirrups. The strain gauges were 2 mm single-element foil gauges of type TML-BFLA-2-5 for CFRP composite materials and applied with CN adhesive. The positioning of the strain gauges on the CFRP materials is further discussed in Chapter 4 and Chapter 5 for the push-off specimens and the T-beams, respectively.

To provide additional displacement and strain measurements, unlimited by the number of channels available, a non-contact optical DIC technique was employed. Two high-definition off-the-shelf cameras were used to capture an image every 5 seconds. To obtain accurate measurements, positioning of the cameras for 2D imaging was critical to ensure the plane of the lens was parallel with the shear plane. The DIC setup is further discussed in detail in Chapter 4 and Chapter 5 for the push-off tests and the T-beam tests, respectively. Matt black blackboard paint was used as a primer for the reflective CFRP surfaces, on which a thick coat of matt white paint was applied. The unique DIC pattern was then applied through a randomly generated laser-cut stencil using matt black spray paint. Such an approach was adopted after a preliminary study on the push-off specimen test series to ensure a reproducible and size-adequate DIC pattern was applied to all monitored surfaces throughout the beam test series. The results from the pre-cracked push-off specimens strengthened with CFRP sheets in the full wrap configuration using this modified pattern were used to calibrate the DIC software for the beam series.

Strain distribution using the DIC technique was monitored in two dimensions for the following reasons:

1. No out-of-plane movement was detected during the initial pilot test series on CFRP-strengthened push-off specimens;
2. No out-of-plane movement was expected until the CFRP sheets were debonded from the concrete surface and therefore it was assumed that the results could be taken at face value prior to debonding;

3. 3D monitoring would require a more complex setup, pre-processing correlation and post-processing of the images, which could result in inaccurate strain readings due to potential errors;
4. Validation of strain readings in any case was only possible against two-dimensional physical strain measurements obtained from surface-applied strain gauges; and
5. The primary objective to employ the DIC technique was to observe cracking in the CFRP-strengthened specimens where the visibility of the cracks was obstructed by the externally bonded sheets.

3.5 Concluding remarks

Design of the experimental research programme was driven by two intrinsically linked work packages. In the first work package, local and debonding behaviour in CFRP shear-strengthened reinforced concrete were to be investigated. Furthermore, the interaction of steel, concrete and CFRP crossing the shear plane was to be observed and separated using asymmetric push-off specimens. These specimens were intended to adequately represent the beam portion of typical average-sized reinforced concrete slab-on-beam structures.

In the second work package, size effect on the behaviour of CFRP-strengthened reinforced concrete T-beams was to be investigated. Initially, a T-beam representative of typical slab-on-beam bridges was designed for experimental testing. This beam was then scaled down to create a medium-sized and small replica of the large bridge beam. The experimental programme from both work packages was carried out in collaboration with the University of Cambridge. The beam design work was led by the University of Bath with input from the University of Cambridge, while the design of the push-off specimens was carried out independently. The large and the medium-scale specimens were to be tested at Bath with some medium and small-scale beams to be tested at the University of Cambridge to provide sufficient overlap between the tested series. At the University of Bath, an optical DIC measurement technique was to be employed alongside physical strain measurements for the monitoring of strains in the beam test series. This method was selected to provide full-field mapping of displacements and strains to indicate the stretching of the CFRP sheets as well as the position of the shear crack behind the CFRP sheets.

4 PUSH-OFF TESTS

4.1 Introduction

This Chapter presents results and findings from the test series carried out on initially uncracked and pre-cracked asymmetric push-off specimens strengthened with CFRP materials. The test results and observations obtained from the series on uncracked push-off specimens are presented starting with unstrengthened control specimens, followed by the specimens strengthened with externally bonded sheets and finally the deep embedment specimens. The results and observations from the tests on pre-cracked push-off specimens and the bond strength tests are also presented in this Chapter. Each set of results for the push-off specimens includes the failure mode of the specimen, observed behaviour, and strain profiles from internal steel shear links and CFRP materials.

4.2 Specimen details

4.2.1 Specimen design and construction details

In all the tests, the specimens had overall rectangular dimensions 750 mm x 350 mm with width 250 mm and constant shear plane dimensions 250 mm x 300 mm. The overall geometry and reinforcement detail are shown in Figure 4.1.

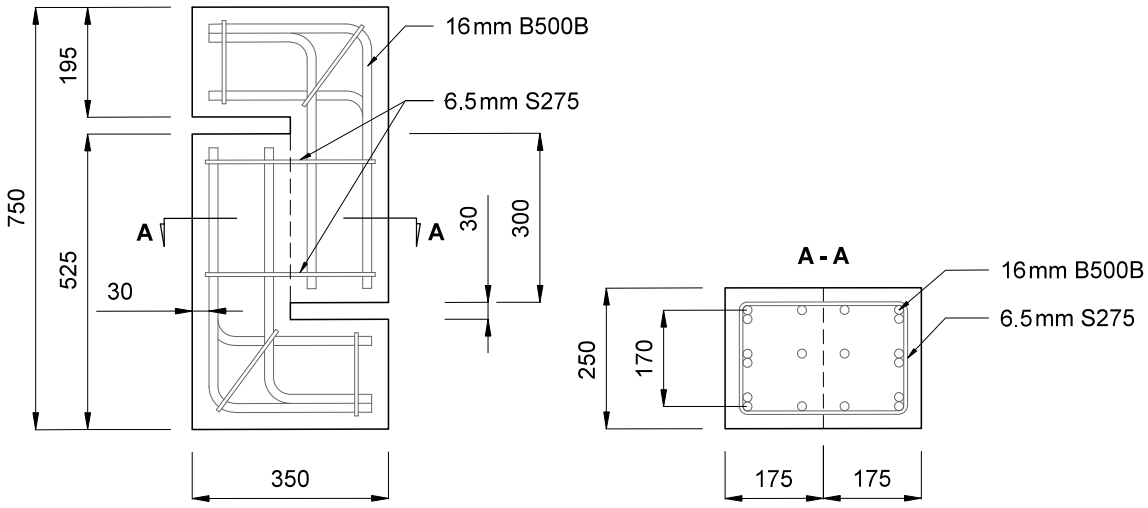

Figure 4.1 – Push-off specimen geometry and reinforcement detail: long section and through section [mm].

4.2.2 Material properties

The steel properties of the plain mild S275 grade steel used for the shear links and deformed B500B grade for main reinforcement are presented in Table 4.1.

Table 4.1 – Push-off specimen steel material properties

Designation	d_s [mm]	Grade	Bar type	f_y [MPa]	f_u [MPa]	ε_{sy} [%]
Main rebar	16	B500B	Deformed	517	631	0.27
Links	6.5	S275	Undeformed	328	435	0.16

Average values from three samples. Tested according to BS 4449:2005 and BS 4482:2005.

The concrete mix used for all specimens was design strength 50 MPa at 28 days, with maximum allowable aggregate size of diameter 16 mm. The concrete mix proportions are presented in Table 4.2.

Table 4.2 – Push-off specimen concrete mix proportions.

Material	Per m^3	Per batch	Specifications
Stone	930 kg	77 kg	10 – 5 mm crushed gravel
Sand	655 kg	55 kg	Fine 40%, coarse 60%
Cement	515 kg	44 kg	Portland CEM II/B – V 32.5 R
Water	220 l	19 l	Water to cement ratio 0.43
Plasticiser	6428 ml	540 ml	Adoflow S

The poured concrete was hand-compacted. A sufficient concrete cover of 30 mm to main reinforcement was provided. Each concrete batch produced one specimen, four standard 100 mm x 100 mm x 100 mm cubes and three 100 mm x 200 mm cylinders. The control cube specimens were tested at 7, 14 and 28 days to determine the compressive strength and the cylinder specimens at 7 and 28 days to determine the tensile splitting strength. The remaining cube and cylinder specimens from each batch were tested with their corresponding push-off specimens on the test day. The average concrete compressive strength at 28 days was 50 MPa, and the tensile splitting strength 3.2 MPa. The average concrete compressive strength at test day, age approximately 90 days, was 57.5 MPa, see Table 4.4 for details. The average tensile strength remained unchanged at 3.2 MPa.

For strengthening with externally CFRP sheets a custom-weave, unidirectional reinforcing CFRP fabric from the Tyfo® product range (Tyfo strengthening systems, 2012, 2014) with a two-component epoxy adhesive was used. The geometric ratios varied from 0.8% for 'lightly' and 1.6% for 'heavily' strengthened. Two weights of the fabric from the same manufacturer were used to vary the CFRP ratio while keeping the number of layers constant at two layers, as described in Chapter 3. For the deep embedment strengthening, 10 mm diameter sand-coated spirally wound CFRP bars were used in combination with a manufacturer recommended non-sag epoxy resin. The composite CFRP sheets were tested in uniaxial tension to obtain the ultimate tensile strength and elongation at rupture in both the principal fibre (Type A) and cross-fibre (Type B) directions. All test samples were equipped with single-direction strain gauges, positioned at the centre of both sides of the tested CFRP coupons and aligned with the principal fibre direction.

The composite coupon samples were prepared from the same batch and in the exact configuration as they were used for strengthening of the push-off and beam specimens to obtain representative material properties. Two layers of CFRP fabric with the manufacturer approved two-component epoxy adhesive and thickening agent, silica fume, were used for fabrication of the composite sheets. The average values from the CFRP coupon tests are summarized in Table 4.3.

Table 4.3 – CFRP composite material properties.

Composite Tyfo®	Specimen	f_{fu} [MPa]	ε_{fu} [%]
SCH11-UP[a]	Type A	1340	1.1
	Type B	35	0.5
SCH-41[b]	Type A	1070	1.1
	Type B	29	0.3
SCH-41/SCH11-UP[c]	Type A	1020	1.1
	Type B	17	0.3

[a] Nominal composite thickness 1.0 mm (two layers of 0.5 mm).

[b] Nominal composite thickness 2.0 mm (two layers of 1.0 mm).

[c] Nominal composite thickness 1.5 mm (one layer of 1.0 mm and one of 0.5 mm).

Type A – Average values from a minimum of three tests per composite sheet.

Type B – Average values from admissible test samples.

Tested in accordance with BS EN ISO 527-5:2009.

4.2.3 Test series

Twelve initially uncracked push-off specimens with either two or three internal shear links were tested. Eight specimens were strengthened with externally applied CFRP sheets; two with deep embedded bars and two were used as unstrengthened control specimens. The anchorage length for the externally bonded sheets varied from a short U-wrap, calculations of which were previously described in Chapter 3, to a full wrap with 250 mm overlaps on the sides of the specimen.

The tested strengthening configurations are presented in Figure 4.2 (a) through to Figure 4.2 (e). Additionally, two tests were carried out on pre-cracked push-off specimens strengthened with externally applied CFRP sheets in the fully wrapped configuration with overlaps at sides, as shown in Figure 4.2 (f).

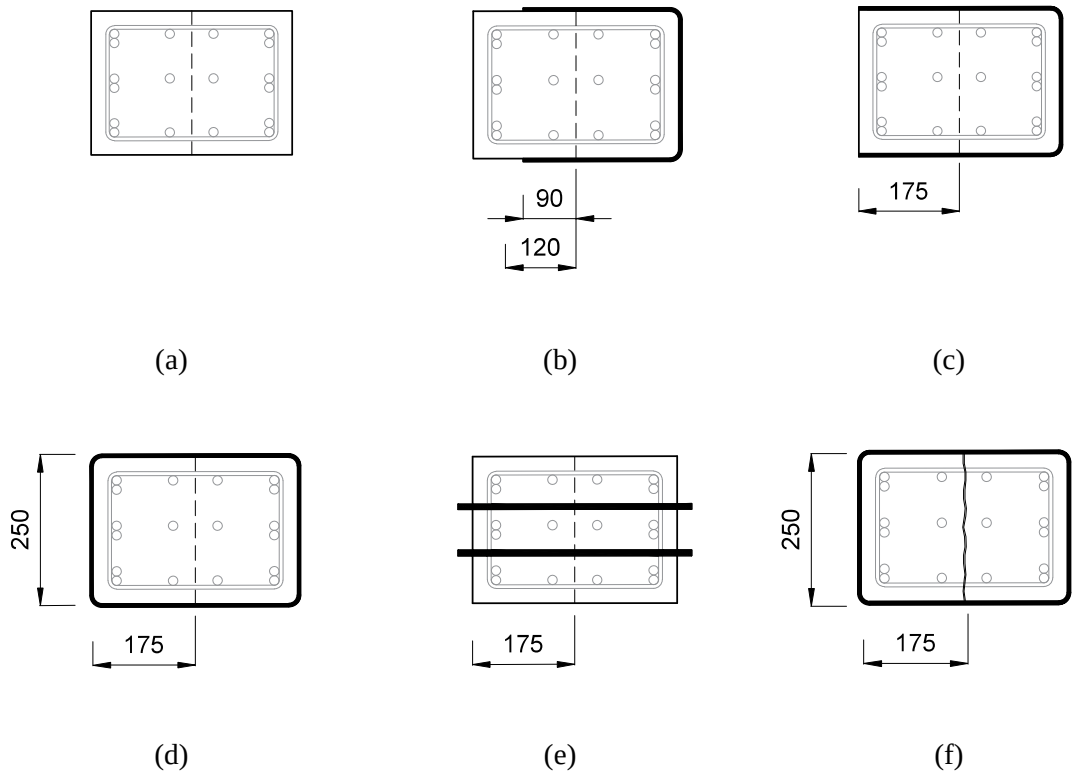

Figure 4.2 – CFRP strengthening configurations: (a) unstrengthened control specimen, (b) short U-wrap, (c) long U-wrap, (d) full wrap with 250 mm overlaps at sides, (e) deep embedment and (f) pre-cracked fully wrapped specimen with 250 mm overlaps at sides [mm].

The test matrix of the push-off specimens tested in this programme is presented in Table 4.4 alongside their details and material properties.

Table 4.4 – Push-off specimen details and reinforcement configurations.

Specimen	Steel		Concrete		CFRP		
	ρ_v [%]	$\rho_v f_y$ [MPa]	f_{cu}[a] [MPa]	f_t[b] [MPa]	ρ_f [%]	$\rho_f f_u$ [MPa]	L_t [mm]
C2	0.17	0.58	62.1	2.6	–	–	–
F1S2	0.17	0.58	53.6	2.3	0.8	7.9	90[c]
F2S2	0.17	0.58	54.3	2.5	1.6	15.8	125[c]
F1L2	0.17	0.58	60.1	3.8	0.8	7.9	175
F2L2	0.17	0.58	53.0	3.2	1.6	15.8	175
F1W2	0.17	0.58	57.6	2.8	0.8	7.9	425
F2W2	0.17	0.58	52.9	3.0	1.6	15.8	425
D1B2	0.17	0.58	60.0	3.6	0.8	17.4	175
PF2W2	0.17	0.58	–	–	1.6	15.8	425
C3	0.26	0.86	61.3	3.7	–	–	–
F1W3	0.26	0.86	56.0	3.7	0.8	7.9	425
F2W3	0.26	0.86	62.3	3.7	1.6	15.8	425
D1B3	0.26	0.86	56.7	3.2	0.8	17.4	175
PF2W3	0.26	0.86	–	–	1.6	15.8	425

[a] Concrete compressive cube strength on test day according to BS EN 12390-3:2009

[b] Concrete splitting tensile strength on test day according to BS EN 12390-6:2009.

[c] CFRP anchorage length calculated according to TR55: $L_t = L_{t,\,max.}$

For ease of orientation, the designation of the specimens is formed using letters and numbers representing the configuration of the test specimen. Unstrengthened control specimens are designated by a letter **C** followed by a number – **2** for specimens with two links (0.17% steel ratio) and **3** for specimens with three links (0.26% steel ratio). In the case of specimens with CFRP strengthening, a letter **F** indicates fabric sheets and **D** deep embedment. Following is a number indicating the CFRP material ratio – **1** for 'lightly' strengthened (0.8%) and **2** for 'heavily' strengthened (1.6%). The second letter indicates the strengthening configuration. In the case of a U-wrap configuration (bonded on three sides), a letter **S** indicates 'short' anchorage length (calculated according to TR55) and **L** 'long' anchorage length (utilizing the full available bond length beyond the shear plane). A letter **W** designates the fully wrapped specimens with overlaps on either side (utilizing the full bond length of the sides beyond the face of the specimen). For deep embedment, the

letter **B** indicates bars. The last number represents the steel shear links in the specimen. Initial letters **PF** indicate pre-cracked specimens strengthened with fabric material. For example, a pre-cracked specimen fully wrapped with 1.6% of CFRP fabric sheets with three links is designated PF2W3.

4.2.4 Specimen preparation and strengthening

The preparation of the test specimens for external sheet application consisted of wet grit blasting, removing the top layer of concrete to expose aggregate for bonding. The edges were cut and rounded to a minimum recommended diameter of 15 mm (TR55, 2012), to prevent the CFRP fabric from premature rupture. The concrete surfaces were air-dried for a minimum of 7 days and further cleaned by wire brushing and all impurities and dust removed by pressurized air. The fabrics were cut to desired lengths and saturated with thoroughly mixed epoxy using a roller brush. The concrete surfaces were primed with one layer of epoxy before applying another single layer of epoxy thickened with silica fume; see Figure 4.3 (a). The thickening agent ensured that the CFRP stayed attached to the vertical concrete surface for the time of curing. The first layer of CFRP was applied onto the prepared surface of the specimen, aligning the fibres on the sides to prevent creasing of the fabric. The fibres were oriented at 90° to the shear plane in all cases. A thin layer of thickened epoxy was applied onto the first CFRP sheet with the second CFRP sheet applied. The second sheet was straightened and finished with a thickened layer of epoxy; see Figure 4.3 (b) for detail.

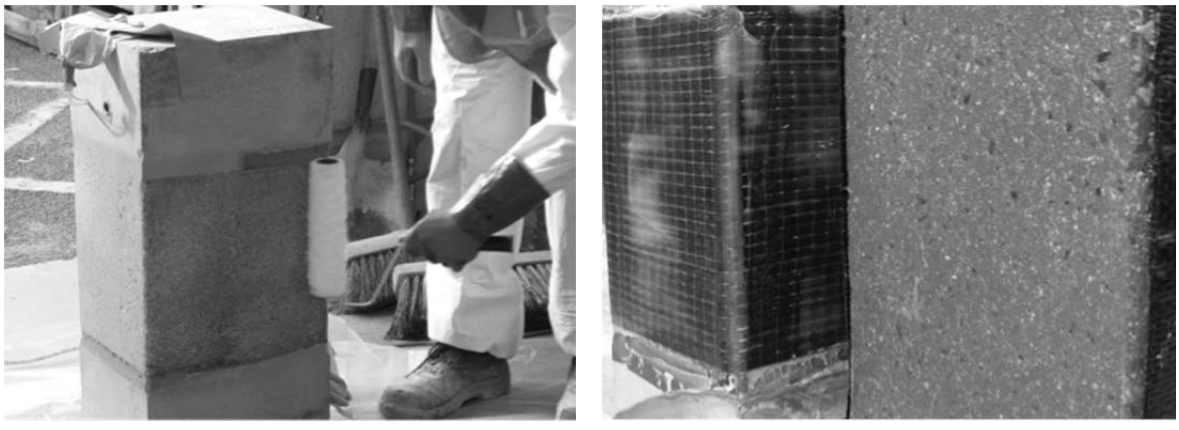

(a) (b)

Figure 4.3 – Preparation and strengthening of push-off specimens: (a) surface preparation for bonding, (b) applied CFRP sheets and close-up of prepared surface for bonding.

For the two deep embedment specimens, the preparation consisted of drilling four holes into each specimen through the concrete for bonding. Minimum 14 mm diameter holes were provided, to accommodate strain gauges and lead wires applied to the CFRP bars and to prevent their damage during application (Hughes Brothers, 2018). Standard masonry drill bit was used without the diamond tip to prevent damage if the main bars were struck. In preparation for bonding, the holes were cleaned using a round wire brush and pressurized air. The non-sag two-component epoxy was mixed in a nozzle of a handgun and injected from one end into each hole as recommended by the manufacturer and applied onto the bar surface. The bar was then slowly pushed through until the epoxy appeared from the other side of the hole, suggesting no air was trapped in the adhesive surrounding the bar. The CFRP bars were intentionally longer than the width of the specimen, with approximately 25 mm projection on either side, to visually monitor slip of the bars during debonding.

The two cracked unstrengthened control specimens after testing were removed from the test machine and their concrete surfaces prepared for bonding in the same manner as for all externally strengthened specimens. The surface preparation and the rounded corners are shown in Figure 4.4 (a). In both cases only the ‘heavy’ strengthening with 1.6% CFRP ratio in a full wrap configuration was applied, see Figure 4.4 (b). Two layers of the heavier CFRP fabric were used and the specimens prepared for testing similarly to their uncracked counterparts. The pre-existing crack was covered with epoxy; however, the full depth of the crack was not filled with adhesive.

(a) (b)

Figure 4.4 – Pre-cracked push-off specimen PF2W3: (a) specimen C3 post-test surface preparation for bonding, (b) CFRP sheet application.

4.2.5 Test setup and testing procedure

All specimens were tested under axial compression in a 2000 kN Instron machine to promote direct shear across the shear plane. The specimens were strip-loaded through rigid 15 mm thick steel plates of width 150 mm monotonically under a displacement rate of 0.2 mm/minute until failure. The centered position of the loading plates ensured axially concentric loading and minimized potential eccentricity or undesirable failure modes. The displacement was applied through the top rotary base of the test machine, which was free to rotate to level the loading. The pre-cracked specimens were tested in the same manner, with specimen PF2W3 initially loaded to approximately 300 kN, unloaded and reloaded until failure. This was to observe the behaviour of the CFRP sheets when stretched to a certain degree, relieved and then further stretched. Test setup is shown in Figure 4.5.

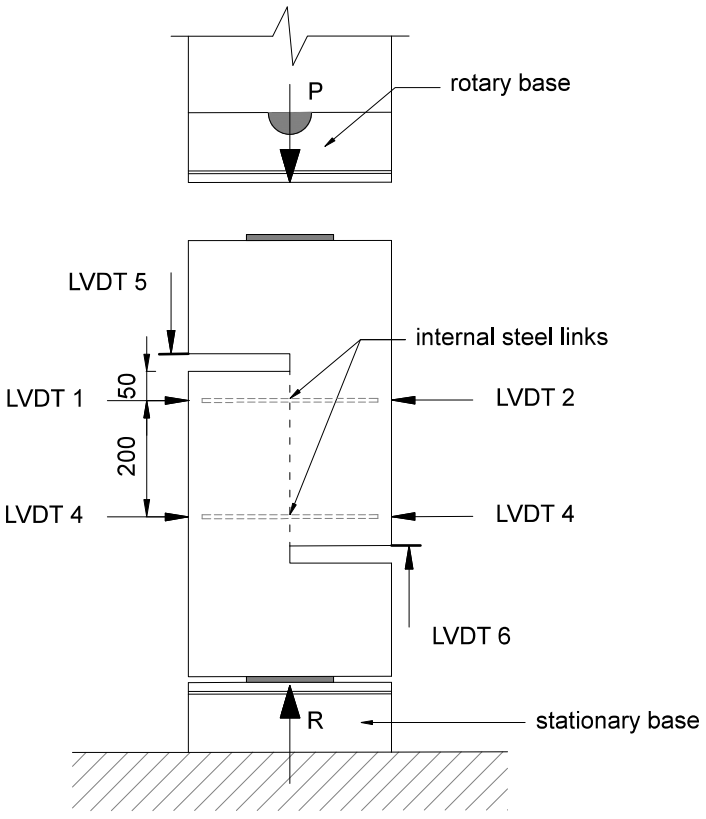

Figure 4.5 – Push-off test setup showing positioning of external LVDTs [mm].

4.2.6 Instrumentation

In all specimens, electrical resistance strain gauges were fixed to the internal steel shear links and the CFRP materials. These were single-direction post-yield for the steel and material-specific single-direction gauges and 45° strain gauge rosettes for the CFRP

materials, previously discussed in Chapter 3. Figure 4.6 shows instrumentation on internal steel and CFRP sheets and bars for all specimens.

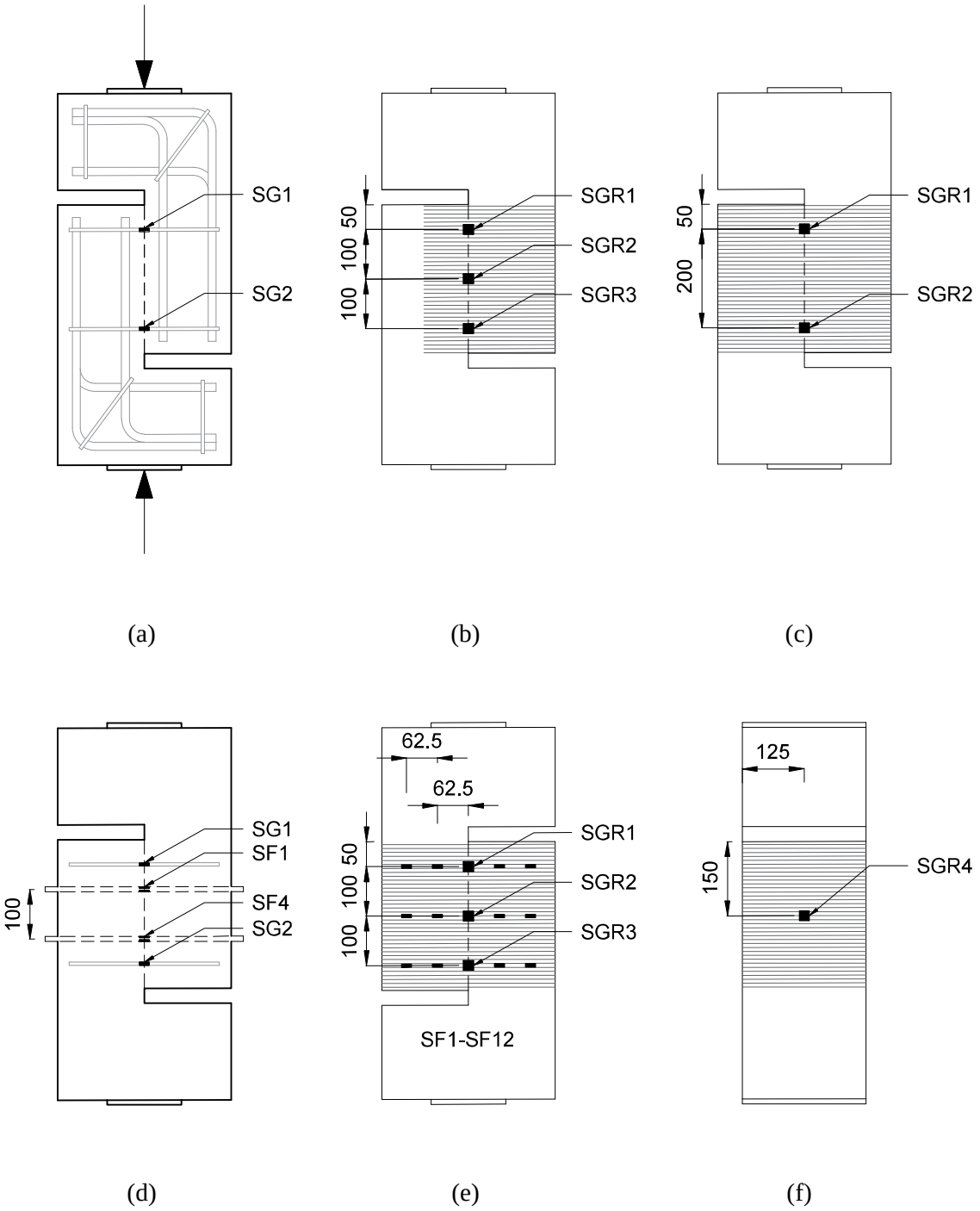

Figure 4.6 – Push-off specimen instrumentation: (a) unstrengthened control specimen C2 – long section, (b) specimens strengthened with CFRP sheets in a U-wrap configuration – front view, (c) specimens strengthened with CFRP sheets in a fully wrapped configuration – front view, (d) deep embedment specimen – long section, (e) pre-cracked specimen strengthened with CFRP sheets in a fully wrapped configuration – rear view and (f) side view [mm].

The single direction strain gauges on steel reinforcement were placed centrally on each leg of each shear link, so that the variation in strain along the steel bar across the shear plane could be recorded. The designation of the strain recording devices follows a simple pattern: the strain gauges **SG1-2** were located on the front face and **SG3-4** on the rear face of the specimens with two internal steel shear links. In the specimens with three links, strain gauges **SG1-3** were on the front face and **SG4-6** on the rear face of the specimen.

Specimens with CFRP sheets bonded in a U-wrap configuration were equipped with three 45° strain gauge rosettes on each face of the specimen and fully wrapped specimens with two strain gauges. The top and the bottom strain gauge were aligned with the position of internal steel strain gauges. Similarly to the numbering convention adopted for the unstrengthened control specimens, strain gauges **SGR1-2** and **SGR1-3** were located on the front face of the specimen and **SGR3-4** and **SGR4-6** on the rear.

The CFRP bars were also equipped with strain gauges, where each bar was fitted with two centrally positioned unidirectional strain gauges, with **SF1-4** on the front and **SF2-3** on the rear. Each location had two strain gauges positioned on the top and the bottom of the bar. The cables connecting the strain gauges to the data-logging device along the CFRP bars leading out of the specimen were in the stationary half of the specimen.

The pre-cracked push-off specimens fully wrapped with CFRP sheets were equipped with strain gauges on the rear face of the specimen. Three 45° strain gauge rosettes, **SGR1-3**, were applied along the shear crack as in the case of their uncracked counterparts. One strain gauge rosette, **SGR4**, was also positioned at mid-height on the overlap at one side of the specimen. This was to capture potential stretching and/or debonding in this region. Additional single direction strain gauges, **SF1-12**, were used to capture the debonding processes propagating from the pre-existing crack towards the anchored edges of the CFRP wrap.

A set of six linear variable differential transformers (LVDTs) was used to measure the horizontal (crack width) and vertical shear displacement. The LVDTs measuring the horizontal displacement, **LVDT 1-4**, were positioned at the location of internal steel shear links. **LVDT 5** and **LVDT 6** were monitoring the vertical displacement of the top shearing segment of the push-off specimen. These LVDTs were tracking the vertical displacement of steel brackets mounted onto the specimen. The simplified test setup with positioning of LVDTs is shown in Figure 4.5.

4.3 Summary of test results

All specimens failed in direct shear. The summary of main experimental results is presented in Table 4.5, followed by detailed discussion in subsequent Sections of this Chapter. The ultimate load capacity, P_u, of the specimens is presented with the corresponding shear stress, v_u, calculated as ultimate load divided by the shear plane area. Values of shear capacity enhancement due to the application of the CFRP, P_f, were calculated by subtracting the capacity of the unstrengthened control specimen from the capacity of the strengthened specimen.

Table 4.5 – Summary of main experimental results.

Specimen					Increase due to CFRP		Failure mode
	ρ_v [%]	ρ_f [%]	P_u [kN]	v_u [MPa]	P_f [kN]	P_f [%]	
C2	0.17	–	411	5.48	–	–	Shear –brittle
F1S2	0.17	0.8	505	6.73	94	23	Cover separation
F2S2	0.17	1.6	591	7.88	180	44	Cover separation
F1L2	0.17	0.8	687	9.16	276	67	Debonding/shear
F2L2	0.17	1.6	722	9.63	311	76	Debonding/shear
F1W2	0.17	0.8	756	10.08	345	84	Debonding/shear
F2W2	0.17	1.6	758	10.11	347	84	Debonding/shear
D1B2	0.17	0.8	705	9.40	294	72	Shear/spalling
PF2W2	0.17	1.6	510	6.80	–	–	Debonding/rupture
C3	0.26	–	637	8.49	–	–	Shear – brittle
F1W3	0.26	0.8	796	10.61	159	25	Debonding/shear
F2W3	0.26	1.6	807	10.76	170	27	Debonding/shear
D1B3	0.26	0.8	711	9.48	74	12	Shear/spalling
PF2W3	0.26	1.6	633	8.43	–	–	Debonding/rupture

The unstrengthened control specimen C3 with three links showed an increase of approximately 50% compared with the specimen C2 with two links. In all cases, strengthening with CFRP materials increased the shear capacity of the specimens. In the case of externally bonded CFRP sheets, this varied dramatically and was found to be dependent on the anchorage length provided. The specimens with a short anchorage length

showed an increase in shear strength of 23% and 44% for the lighter CFRP fabric (specimen F1S2) and the heavier fabric (specimen F2S2), respectively. The provision of a longer anchorage length further increased the shear strength for both CFRP fabric weights. The ultimate capacities recorded for both specimens, F1L2 and F2L2, were comparable with an increase of 67% and 76%, respectively. The fully wrapped cases with two steel links, specimens F1W2 and F2W2, both showed an identical increase in shear strength of 84%, regardless of the weight of the CFRP fabric used. This result suggests, when compared with the U-wrapped specimens with a long anchorage (F1L2 and F2L2), that only a negligible increase in shear strength was possible with additional anchorage through overlaps at sides.

The fully wrapped specimens with three shear links showed an increase of 25% and 27% for F1W3 and F2W3, respectively. This indicates that the underlying unstrengthened control specimen with three links was already particularly strong and the addition of CFRP sheets provided only a moderate increase in shear strength. The results from all wrapped cases showed similar values of ultimate shear strength at failure. The ultimate capacity reached in specimens with three shear links was only marginally higher than that recorded in specimens with two links. This result indicated that the concrete must have reached some limiting capacity, which was not affected by the amount of CFRP reinforcement crossing the shear plane.

The deep embedment specimens D1B2 and D1B3 reached ultimate shear capacity values close to those of the U-wrapped specimens with a long anchorage, F1L2 and F2L2. Furthermore, both D1B2 and D1B3 showed similar increase in shear strength, regardless of the amount of steel reinforcement crossing the shear plane. This also suggests that for internally applied CFRP bars as additional shear reinforcement, the concrete must have also reached some limiting capacity.

The residual capacity of the cracked control specimen C2 was 1.67 MPa (125 kN) and that of C3 was 2.12 MPa (159 kN) when the test was stopped. In both cases the steel had yielded and the shear crack was opened to 0.8 mm and 1.5 mm at the end of testing for C2 (strengthened PF2W2) and C3 (strengthened PF2W3), respectively. In the case of PF2W2 the ultimate shear capacity overcame the capacity of the uncracked unstrengthened control specimen C2. In the case of PF2W3, the ultimate capacity was identical to that reached by the unstrengthened control specimen C3. The same procedure to obtain the CFRP contribution to the overall capacity as for the uncracked specimens was followed. The

CFRP contribution was obtained by subtracting the residual control specimen strength from the ultimate strength of the strengthened specimen. Because of the large difference between the residual and the ultimate capacity of the specimens, this resulted in a major increase in shear capacity due to the CFRP by approximately 300% in both cases. Such a result demonstrated that if CFRP sheets stretch over a pre-existing discontinuity, their contribution rapidly increases until the CFRP sheet fully debonds from the concrete surface. A summary of strain readings from internal steel strain gauges and those on CFRP materials are presented in Table 4.6.

Table 4.6 – Summary of maximum strains recorded at failure.

Specimen			Steel	CFRP		
	ρ_v	ρ_f	ε_{se}	$\varepsilon_{fe,\ 0\text{-}max}$	$\varepsilon_{fe,\ 90\text{-}max}$	$\varepsilon_{fe,\ 45\text{-}max}$
	[%]	[%]	[%]	[%]	[%]	[%]
C2	0.17	–	0.66	–	–	–
F1S2	0.17	0.8	0.14	0.19	0.22	0.48
F2S2	0.17	1.6	0.11	0.16	0.22	0.35
F1L2	0.17	0.8	0.69	0.24	0.17	0.56
F2L2	0.17	1.6	1.15	0.18	0.14	0.65
F1W2	0.17	0.8	1.57	0.26	0.16	0.91
F2W2	0.17	1.6	1.21	0.21	0.09	0.57
D1B2	0.17	0.8	0.48	0.48	–	–
PF2W2	0.17	1.6	–	0.57	0.08	0.73
C3	0.26	–	0.18	–	–	–
F1W3	0.26	0.8	1.22	0.27	0.33	0.70
F2W3	0.26	1.6	0.70	0.18	0.29	0.60
D1B3	0.26	0.8	0.37	0.38	–	–
PF2W3	0.26	1.6	–	0.52	0.05	0.09

The steel strain values, ε_{se}, are the maximum strains recorded at failure. The strains in the CFRP sheets, $\varepsilon_{fe,\ max}$, are the maximum strains recorded by the 45° strain gauge rosettes at failure in 0° (principal fibre), 90° (cross-fibre) and 45° directions. The steel strains indicate, that the steel in the U-wrapped specimens with short anchorage lengths, F1S2 and F2S2, did not yield at failure (yield at 0.16% determined from standard tensile steel tests). In all other cases of strengthening with externally bonded CFRP sheets the steel had

yielded prior to failure. Significant amount of elongation is apparent from the steel readings on wrapped specimens with two steel links. In the case of the deep embedment specimens, the strains in steel links reached levels around 0.4%, with 0.48% and 0.37%, for D1B2 and D1B3, respectively, and were of the same values as the strains recorded in steel links at failure. This result indicates that the deep embedded CFRP bars behaved in a similar manner as the internal steel shear links.

The strains recorded in the principal fibre direction, $\varepsilon_{fe,\,0\text{-max}}$, in the CFRP sheets across the shear plane were consistently lower in the U-wrapped specimens when compared with the fully wrapped cases. Furthermore, the cases strengthened with the 'light' reinforcing CFRP fabric were showing greater strains at ultimate compared with their 'heavily' strengthened counterparts. The strains in the cross-fibre direction were higher than those in the principal fibre direction for the specimens with a short anchorage length, F1S2 and F2S2. In contrast, these are lower in all fully wrapped cases. The strains reached in the pre-cracked specimens were particularly high and of similar values, at 0.57% and 0.52% for PF2W2 and PF2W3, respectively. The strains in the cross-fibre direction were very low by comparison.

4.4 Unstrengthened control specimens

4.4.1 Failure modes

Failure modes of the control specimens are presented in Figure 4.7.

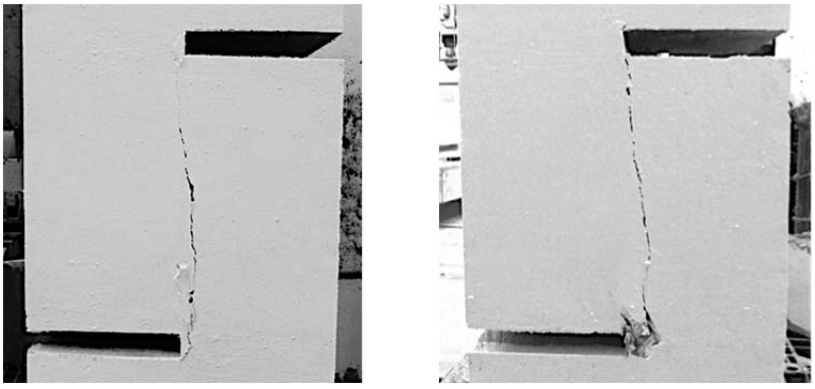

(a) (b)

Figure 4.7 – Failure modes of control specimens: (a) specimen C2, (b) specimen C3.

Both specimens failed in shear with a single vertical crack across the shear plane, as anticipated. No additional cracking was observed. The test was stopped immediately after failure to retain the specimens for further testing.

4.4.2 Observed behaviour

The shear stress versus shear displacement and crack width are presented in Figure 4.8 (a) and Figure 4.8 (b), respectively.

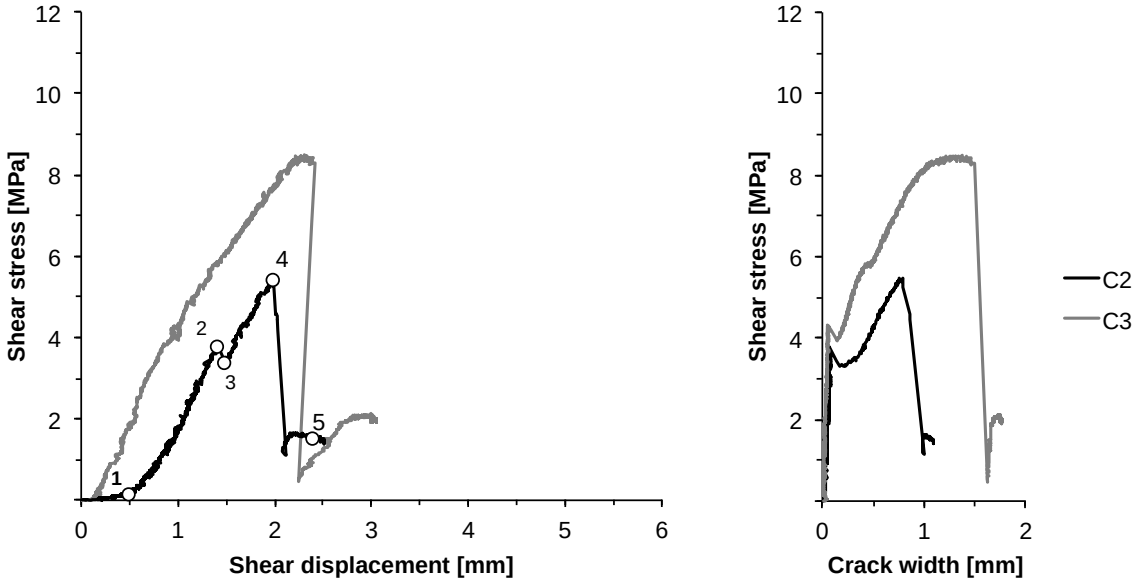

(a) (b)

Figure 4.8 – Unstrengthened control push-off specimens: (a) shear stress versus shear displacement – (1) initiation of stable contact, (2) uncracked concrete capacity reached, (3) steel yields, (4) integrity of the system is lost due to the loss of shear-friction and (5) residual capacity of the yielded steel; (b) shear stress versus crack width.

It should be noted that a certain level of bedding in was observed in the case of specimen C2 and this was rectified in the shear stress versus shear displacement graphs in the following sections for reasons of direct comparison with strengthened cases. Such behaviour was not observed in the case of the specimen C3.

The slip when concrete cracked and steel started to yield was also less pronounced in the response of the specimen C3. The corresponding crack width from the shear stress versus

crack width plot shows that the widening of the crack occurred rapidly after the first cracking of concrete.

4.4.3 Steel strain profiles

The steel profiles obtained from the internal strain gauges for specimen C2 and C3 are presented in Figure 4.9.

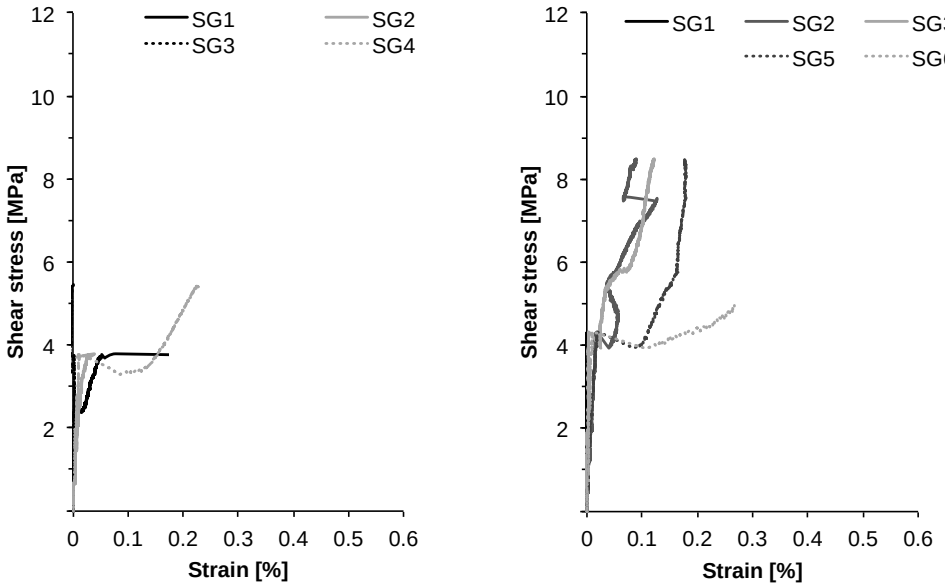

(a) (b)

Figure 4.9 – Shear stress versus steel strains – unstrengthened specimens: (a) C2 and (b) C3.

The strain readings for the specimen with two internal steel links suggested that the steel yields immediately after the concrete cracks (yield strength of steel links at 0.16% strain, as determined from material testing on steel links, presented in Section 4.2.2). It should be noted that strain gauges SG2 and SG3 behaved erratically after the first cracking in concrete occurred and appeared to have been subject to compression. Also, SG1 appeared to have failed immediately after the concrete cracked, see Figure 4.9 (a).

For specimen C3 however, the strain gauges registered yielding of the steel links prior to failure and some links did not yield. The readings of all strain gauges post-peak behaved erratically and therefore only values until peak are shown. This is due to the sudden and abrupt failure, at which point the steel links were unable to transfer the load at ultimate.

Readings from faulty strain gauges were excluded from the graphs throughout this Chapter, unless otherwise stated.

4.5 Specimens strengthened with externally bonded CFRP sheets

4.5.1 Failure modes

All tested specimens strengthened with externally bonded CFRP U-wraps failed in shear with distinct failure modes at the CFRP-concrete interface. In all cases the failure was in the concrete, either in the top surface layer or through separation of the concrete cover.

The failure mode of the specimens provided with limited (short) anchorage length, specimens F1S2 and F2S2, was the most dramatic of the series, shown in Figure 4.10.

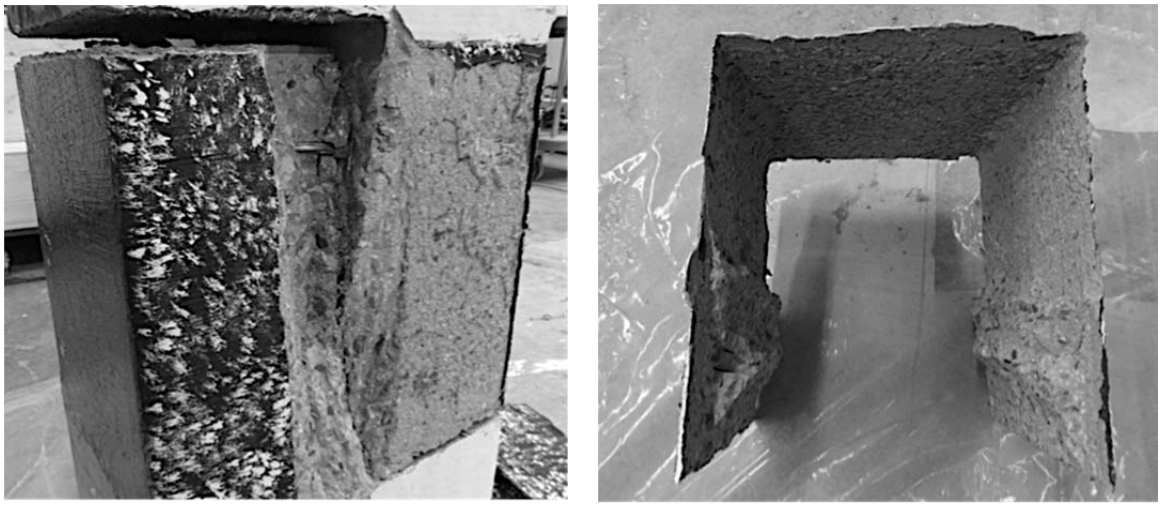

(a) (b)

Figure 4.10 – Failure modes of specimens strengthened with short U-wraps: (a) specimen F1S2, (b) removed U-wrap from specimen F2S2.

Without any warning of debonding, the specimens failed suddenly in a very energetic and abrupt manner. The failure appeared to have initiated from the shear crack location and further propagated towards the free edges of the CFRP wrap through the concrete cover layer. This was further investigated post-test by removing the CFRP sheets.

The CFRP sheets with the concrete cover attached were carefully removed in cases where this was possible due to the extent of the damage caused by separation. Figure 4.10 (b)

shows a full CFRP wrap with concrete attached at the shear plane location on both the front and the rear face of the specimen.

The specimens with long anchorage length, F1L2 and F2L2, utilizing the full available length beyond the shear crack, failed through separation of the CFRP-concrete interface. The failure was gradual, with debonding announced by tearing noises throughout the test. Figure 4.11 (a) shows specimen F1L2 post-test while the CFRP U-wrap was being removed.

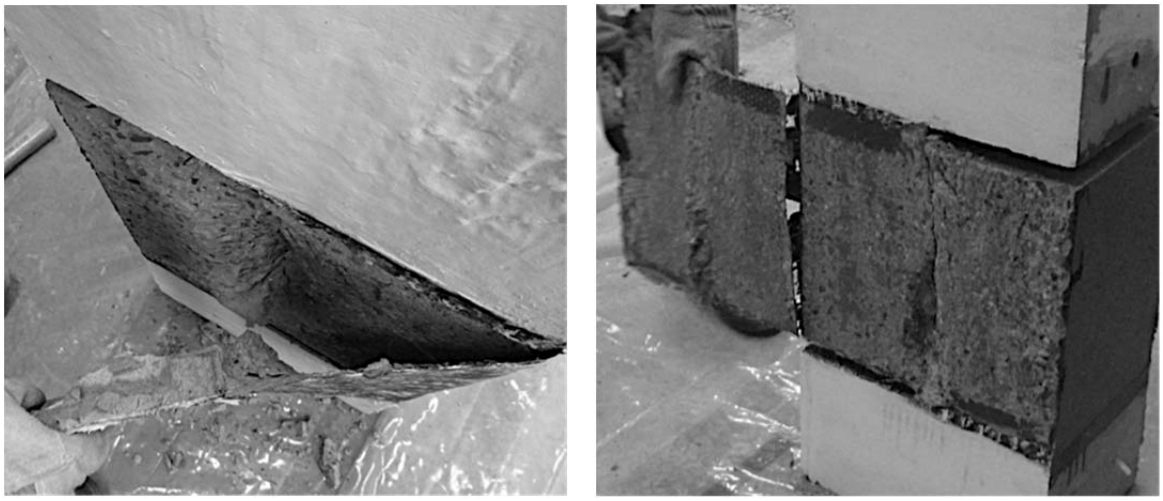

(a) (b)

Figure 4.11 – Failure mode of specimen F1L2: (a) specimen after testing, (b) specimen after removal of the CFRP U-wrap.

The damage caused by debonding of the CFRP wrap was observed to be of a lesser degree when compared with the concrete cover separation cases in specimens with short anchorage length, F1S2 and F2S2. Figure 4.11 (b) shows the extent of damage caused by the CFRP-concrete separation. It appears that the separation was initiated by the shear crack and further propagated towards both ends of the specimen, similarly to the F1S2 and F2S2 specimens. Upon reaching the free edge of the CFRP U-wrap and when the CFRP was fully separated from both faces of the specimen, the specimen failed abruptly.

Figure 4.12 shows the specimen F2L2 after testing with the CFRP U-wrap being removed. It is apparent from Figure 4.12 (a) that a larger portion of the concrete cover remained bonded to the CFRP wrap and that this occurrence was not symmetrical. This failure mode appeared to be a mixed mode between the mode observed in specimens with short

anchorage length, F1S2 and F2S2, and the specimen with long anchorage length, F1L2.

The fully wrapped specimens with overlaps either side failed in shear, through CFRP-concrete separation, as shown in Figure 4.13. This failure mode was near identical to the failure mode of specimen F1L2. However, the concrete cover remained fully attached to the specimen and only a thin layer of surface concrete was found attached to the wrap at the shear zone location.

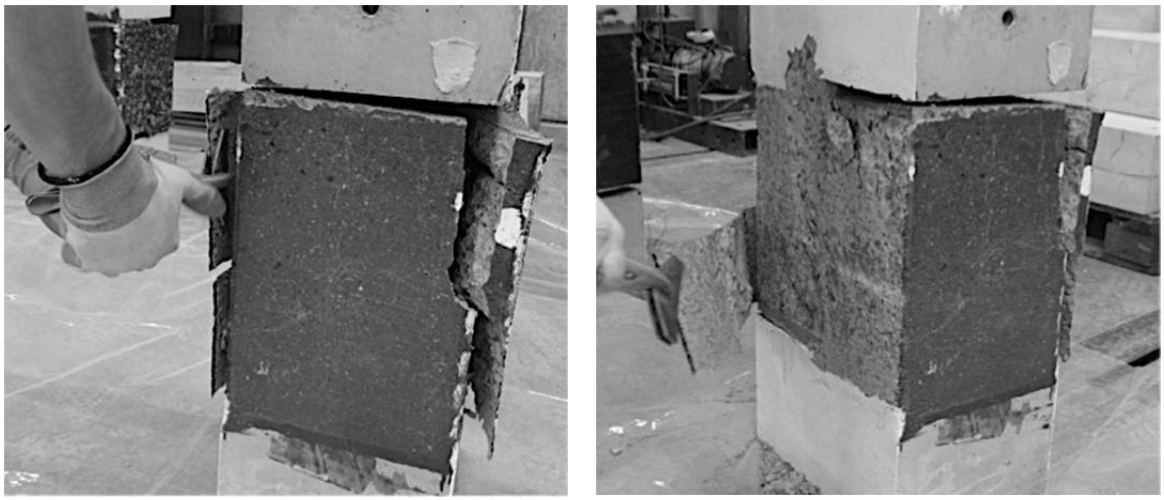

(a) (b)

Figure 4.12 – Failure mode of specimen F2L2: (a) specimen after testing, (b) specimen after removal of the CFRP U-wrap.

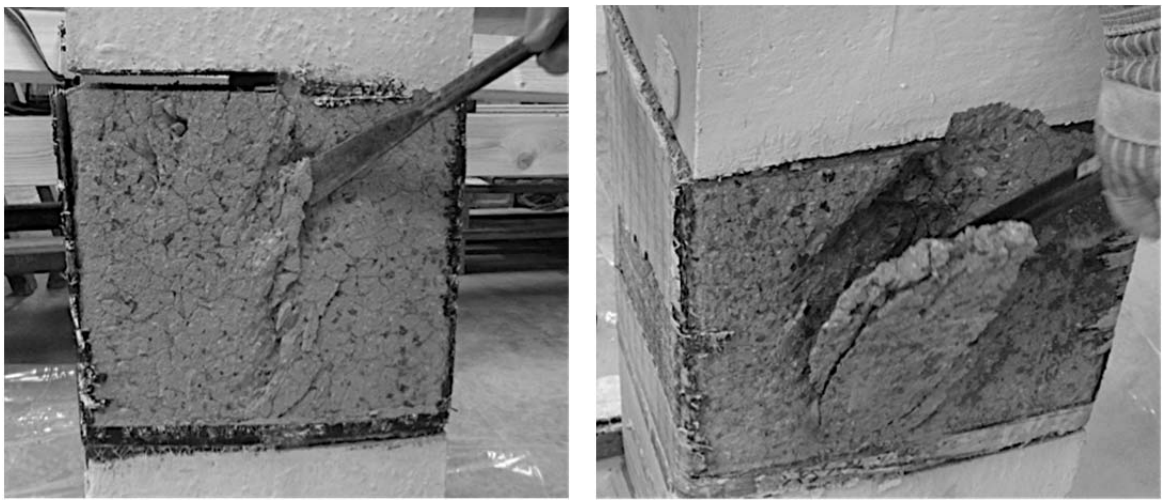

(a) (b)

Figure 4.13 – Failure modes of specimens fully wrapped with CFRP sheets: (a) specimen F1W2, (b) specimen F2W3.

4.5.2 Observed behaviour

Figure 4.14 shows the experimentally obtained shear stress versus shear displacement and crack width curves for specimens with two internal steel shear links (0.17% steel ratio) in combination with two layers of the thinner CFRP fabric (0.8% CFRP ratio). The plot directly compares the specimen with limited (short) anchorage, F1S2, specimen F1L2 with long anchorage (utilizing the entire available bond length) and the fully wrapped specimen F1W2, in contrast with the unstrengthened control specimen, C2.

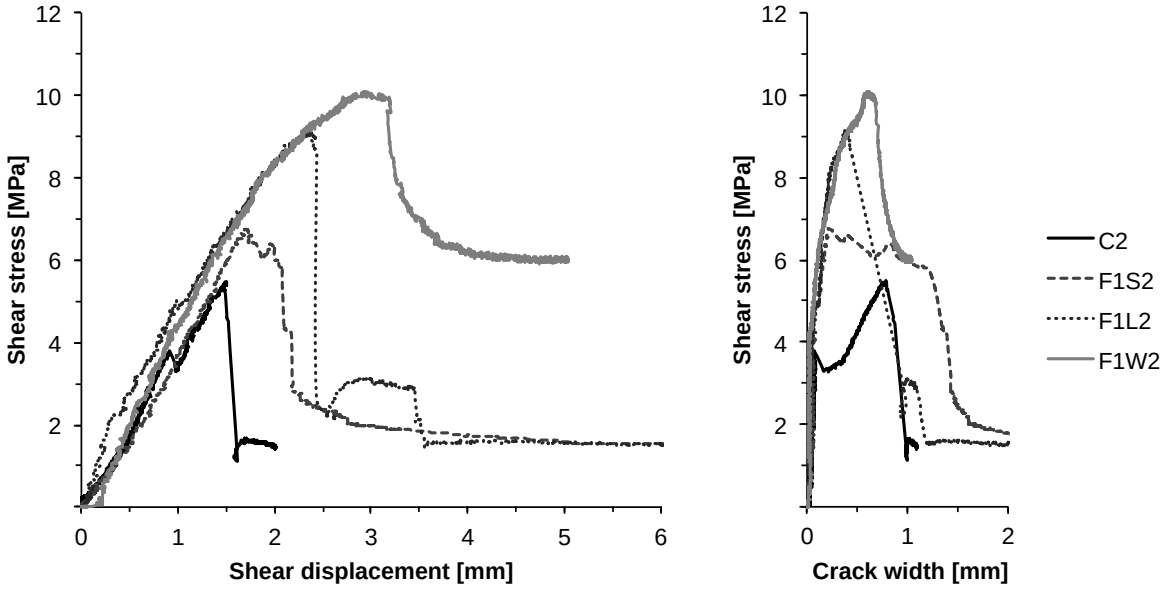

(a) (b)

Figure 4.14 – Push-off specimens with internal steel 0.17% and externally bonded CFRP sheets 0.8%: (a) shear stress versus shear displacement, (b) shear stress versus crack width.

Similarly, Figure 4.15 shows the experimentally obtained shear stress versus shear displacement and crack width curves for specimens with two internal steel shear links (0.17% steel ratio) in combination with two layers of the thicker CFRP fabric (1.6% CFRP ratio). It is apparent from the plots in Figure 4.14 and Figure 4.15 that the behaviour of the specimens with externally bonded CFRP sheets is similar regardless of the ratio of the CFRP crossing the shear plane. The specimens with the short anchorage length, F1S2 and F2S2, failed prematurely due to the debonding of the CFRP sheets. Specimens with long

anchorage length, F1L2 and F2L2, reached greater ultimate capacity, however also failed due to progressive debonding of the CFRP sheets.

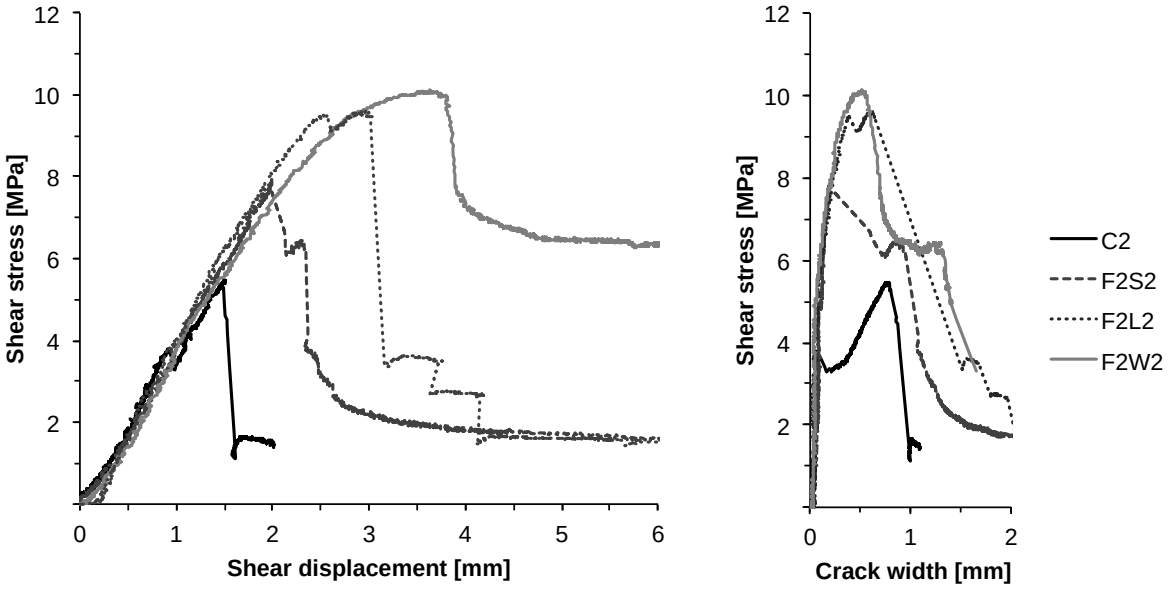

(a) (b)

Figure 4.15 – Push-off specimens with internal steel 0.17% and externally bonded CFRP sheets 1.6%: (a) shear stress versus shear displacement, (b) shear stress versus crack width.

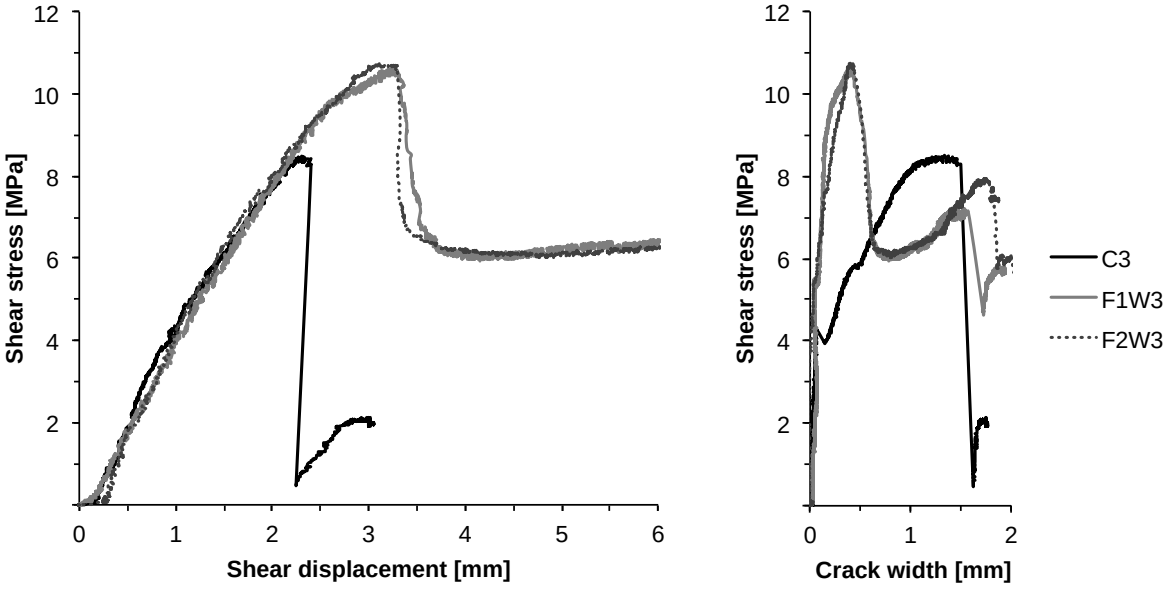

(a) (b)

Figure 4.16 – Push-off specimens with internal steel 0.26% and externally bonded CFRP sheets 0.8% and 1.6%: (a) shear stress versus shear displacement; (b) shear stress versus crack width.

Figure 4.16 shows the experimentally obtained shear stress versus shear displacement and crack width curves for specimens with three internal steel shear links (0.26% steel ratio) fully wrapped with CFRP sheets for specimen F1W3 (0.8% CFRP ratio) and specimen F2W3 (1.6% CFRP ratio).

The similarity in structural behaviour for both investigated CFRP ratios suggests that a concrete limiting shear-friction capacity must exist, which can be achieved through the interfacial bond between concrete and CFRP sheets that controls the behaviour of the system.

4.5.3 Steel strain profiles

Steel strain profiles for all specimens strengthened with externally bonded CFRP sheets are presented in Figure 4.17 through to Figure 4.20 for comparison of the behaviour of internal steel links alone. The strains obtained experimentally from the CFRP sheets will be discussed in detail later in Section 4.5.4.

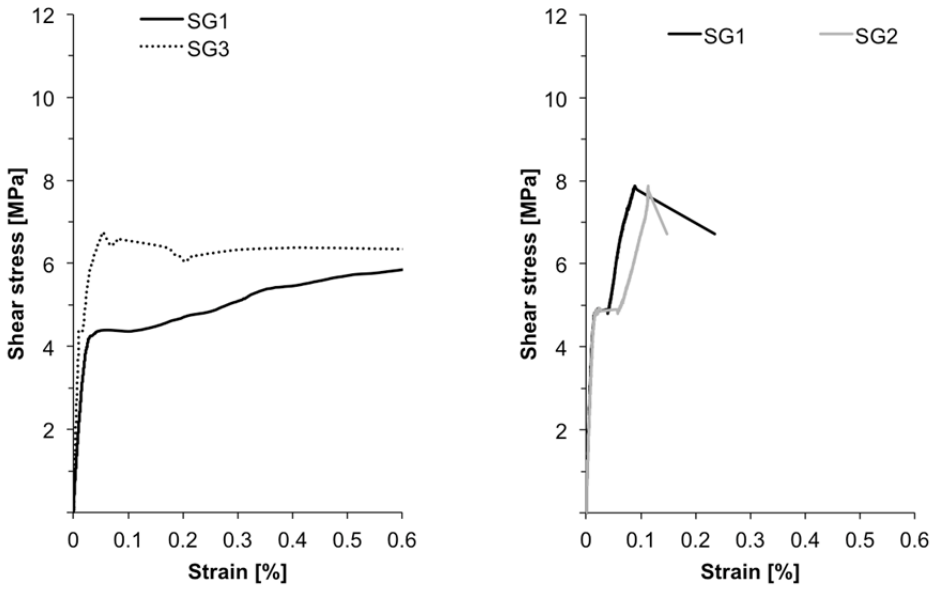

(a) (b)

Figure 4.17 – Shear stress versus steel strains – U-wrap specimens with short anchorage length: (a) F1S2 and (b) F2S2.

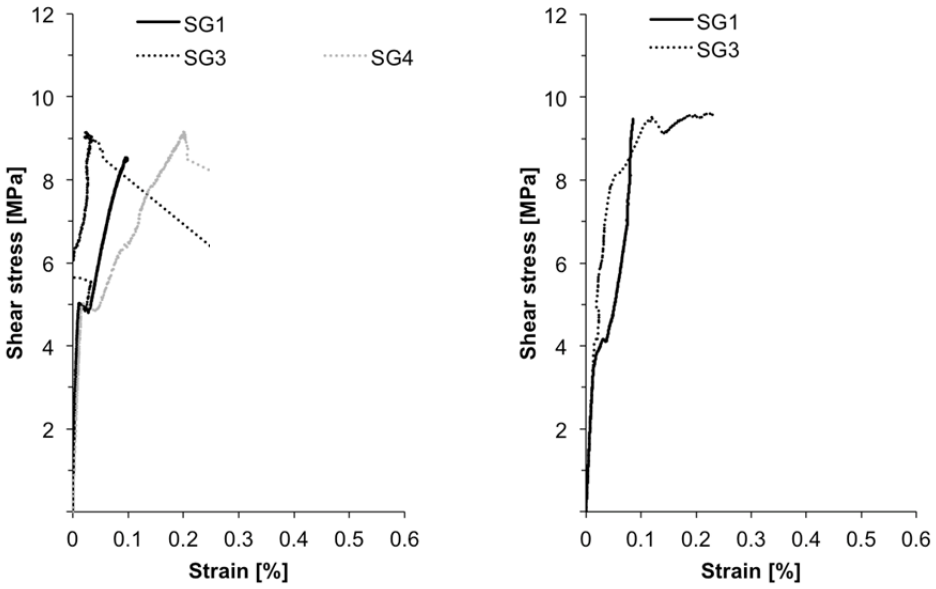

(a) (b)

Figure 4.18 – Shear stress versus steel strains – U-wrap specimens with long anchorage length: (a) F1L2 and (b) F2L2.

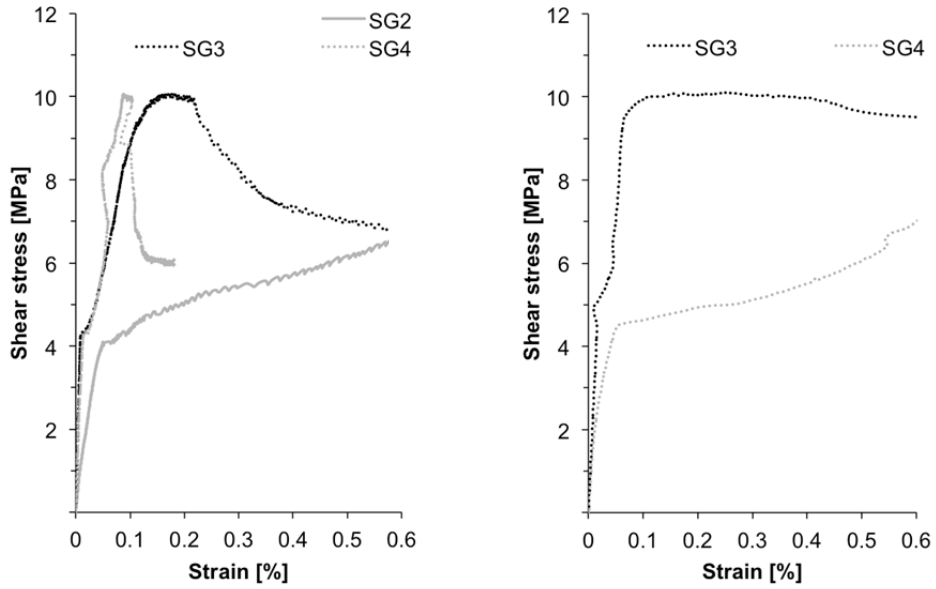

(a) (b)

Figure 4.19 – Shear stress versus steel strains – fully wrapped specimens: (a) F1W2 and (b) F2W2.

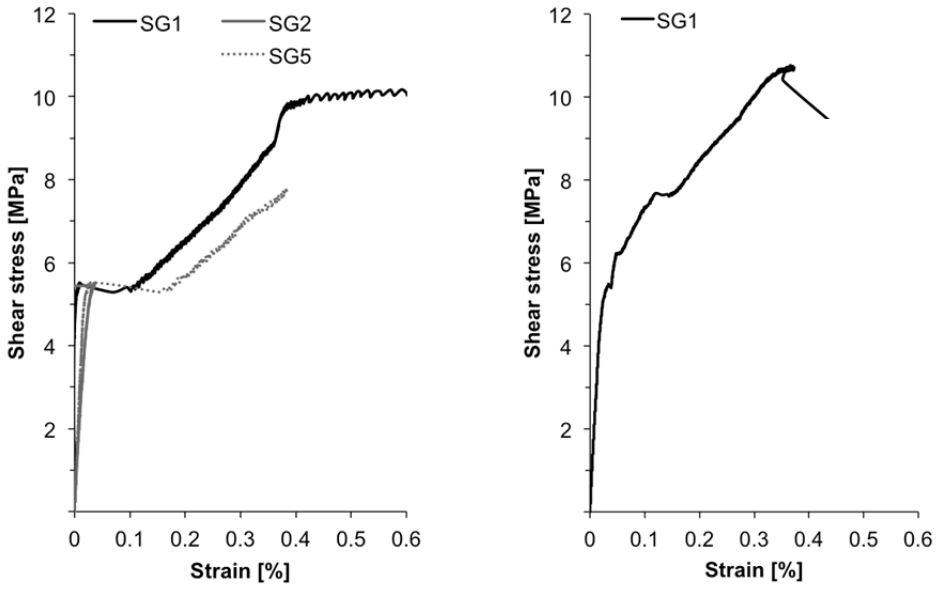

(a) (b)

Figure 4.20 – Shear stress versus steel strains – fully wrapped specimens: (a) F1W3 and (b) F2W3.

The results indicated two extremes in behaviour – while the steel has not yielded in the specimens with short anchorage, F1S2 and F2S2, prior to failure, the links in the fully wrapped specimens with three internal shear links, F1W2 and F2W3, have yielded prior to failure. The results therefore demonstrated that with increasing anchorage length, the contribution of the internal shear links to the overall shear capacity of the push-off specimen also increases as they are allowed to activate prior to full separation of the CFRP.

4.5.4 CFRP strain profiles

CFRP strain profiles for all specimens strengthened with externally bonded CFRP sheets are presented in Figure 4.21 through to Figure 4.24 for comparison of strains obtained from the CFRP sheets only. The strains obtained from the internal steel links were presented in section 4.5.3.

The results indicated that the specimens with short anchorage length, F1S2 and F2S2 shown in Figure 4.21, failed due to premature debonding of the CFRP sheets. The progressive debonding of the CFRP sheets is indicated in the plots by reversed strain

readings post peak.

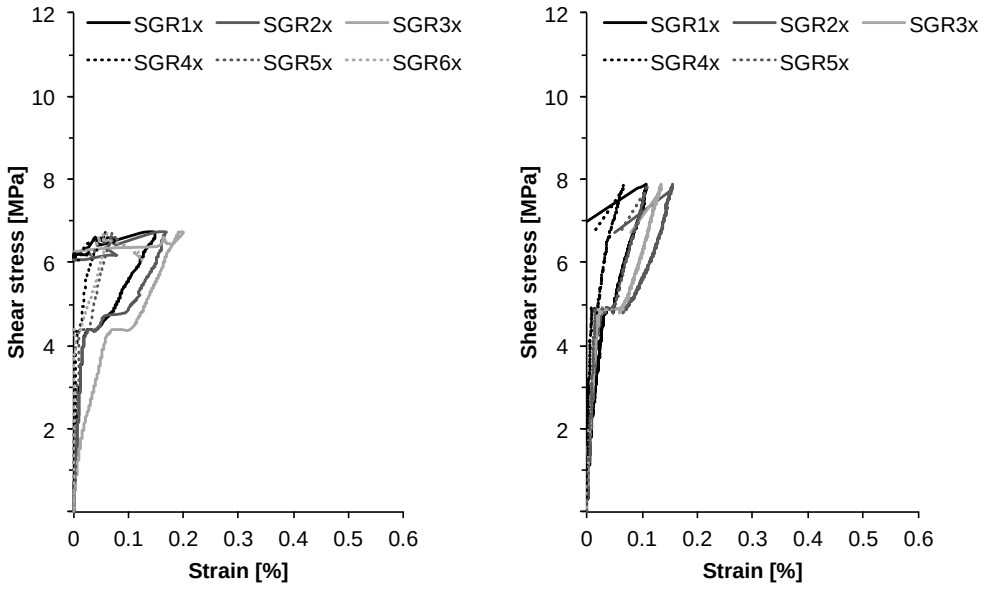

(a) (b)

Figure 4.21 – Shear stress versus CFRP strains – U-wrap specimens with short anchorage length: (a) F1S2 and (b) F2S2.

In all other tested cases presented in Figure 4.22 through to Figure 4.24, the CFRP sheets stretched over the discontinuity in the concrete with progressive debonding until failure. In the case of specimens strengthened in the U-wrap configuration with long anchorage length, F1L2 and F2L2, the sheets were stretching until the free edge of the CFRP wrap was reached and slip occurred, see Figure 4.22.

In the case of fully wrapped specimens, presented in Figure 4.23 and Figure 4.24, the debonding process and subsequent failure were delayed by the additional bond length beyond the available bond length on the sides of the specimens. However, the specimens did fail due to debonding when the CFRP wraps debonded sufficiently enough for slip in concrete to occur.

The maximum strains recorded at failure were observed to be consistent for the two thicknesses of the CFRP sheet. The thinner fabric (0.8% CFRP ratio) was stretching to a greater extent compared with the thicker fabric (1.6% CFRP ratio) and this is possibly caused by the differential stiffness of the two laminates.

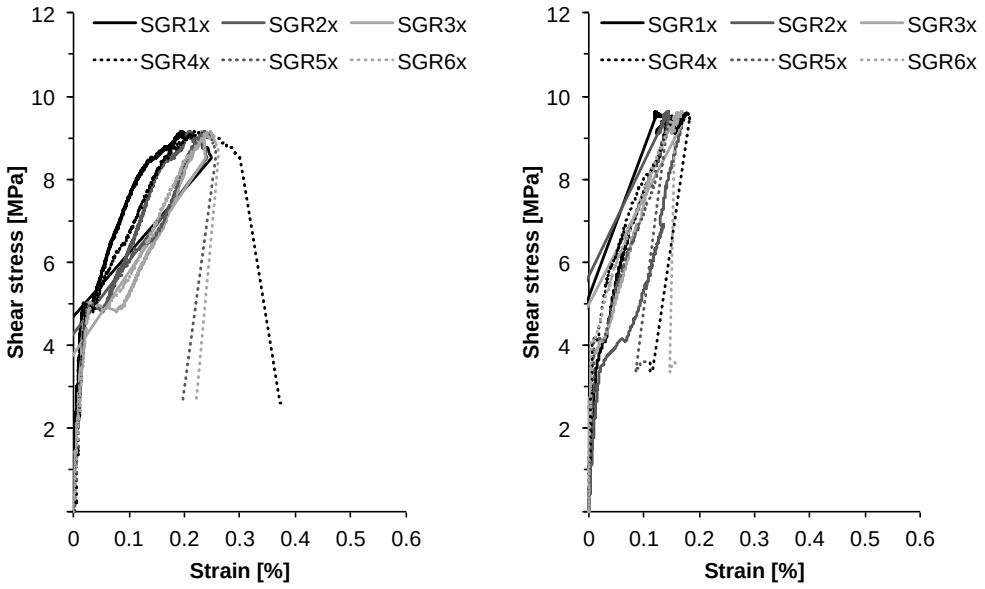

(a) (b)

Figure 4.22 – Shear stress versus CFRP strains – U-wrap specimens with long anchorage length: (a) F1L2 and (b) F2L2.

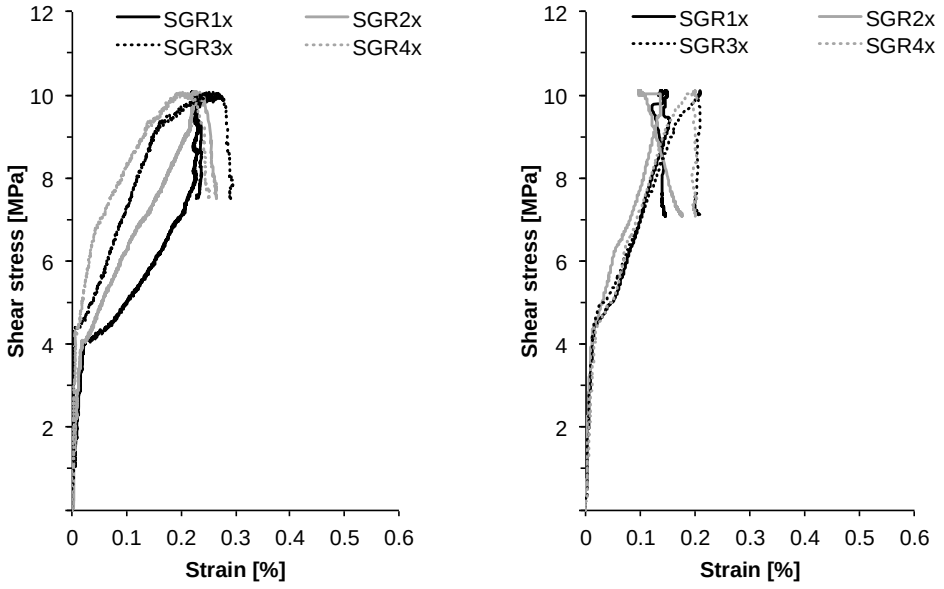

(a) (b)

Figure 4.23 – Shear stress versus CFRP strains – fully wrapped specimens: (a) F1W2 and (b) F2W2.

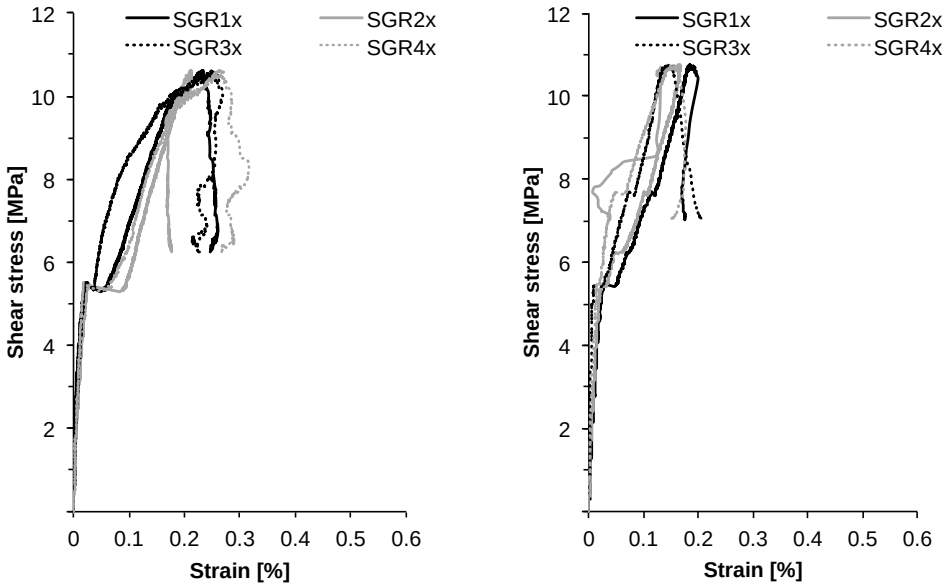

(a) (b)

Figure 4.24 – Shear stress versus CFRP strains – fully wrapped specimens: (a) F1W3 and (b) F2W3.

4.6 Deep embedment specimens

4.6.1 Failure modes

Figure 4.25 shows the failure modes of the deep embedment specimens.

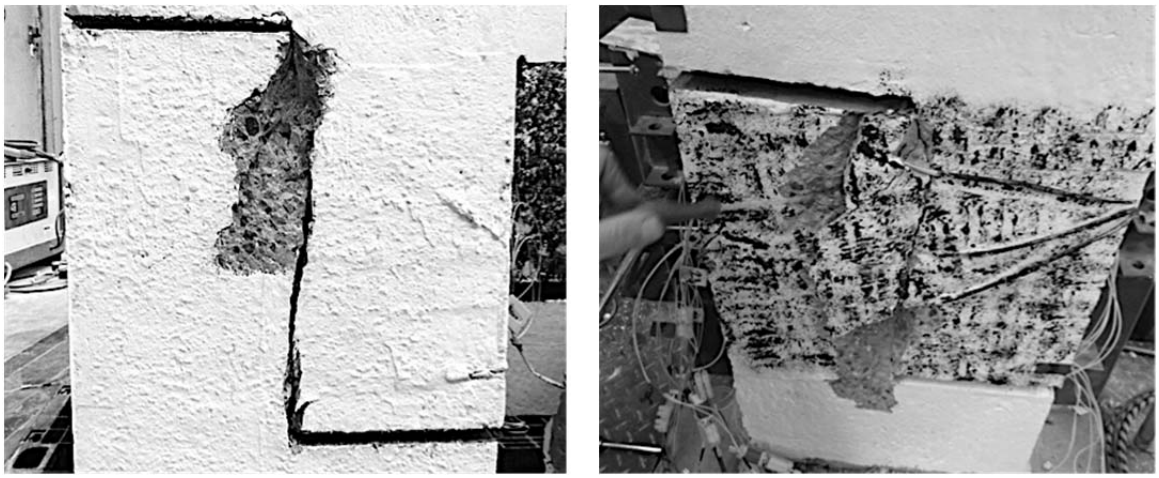

(a) (b)

Figure 4.25 – Failure modes of deep embedment push-off specimens: (a) specimen D2B2, (b) specimen D2B3.

Both specimens failed in shear with significant spalling of concrete on both faces of the specimens at the shear plane location, see Figure 4.25. The specimen was taken apart after testing to expose the deformed steel reinforcement and to extract the CFRP bars, as shown in Figure 4.26.

The CFRP bars debonded in the top moveable segment of the specimen, through separation within the adhesive-concrete interface, as is apparent from Figure 4.26 (b). The portion of the bar in the reaction segment of the specimen was fully bonded to the surrounding concrete upon extraction. This suggests that a possibility exist that the CFRP bar debonded due to the presence of cables from the internal strain gauges along the CFRP bar.

(a) (b)

Figure 4.26 – Deep embedment push-off specimen DB2W3 investigation post-test: (a) extracted CFRP bars, (b) exposed steel reinforcing cage.

4.6.2 Observed behaviour

The deep embedment specimens D1B2 and D1B3 were compared with the specimens strengthened with externally applied CFRP sheets with long anchorage F1L2 and F2L2, see Figure 4.27.

The test results showed that the deep embedment strengthening offers an equivalent increase in shear capacity for reinforced concrete specimens to the externally bonded CFRP sheets in a U-wrap configuration with sufficient end anchorage, regardless of the CFRP and steel ratios.

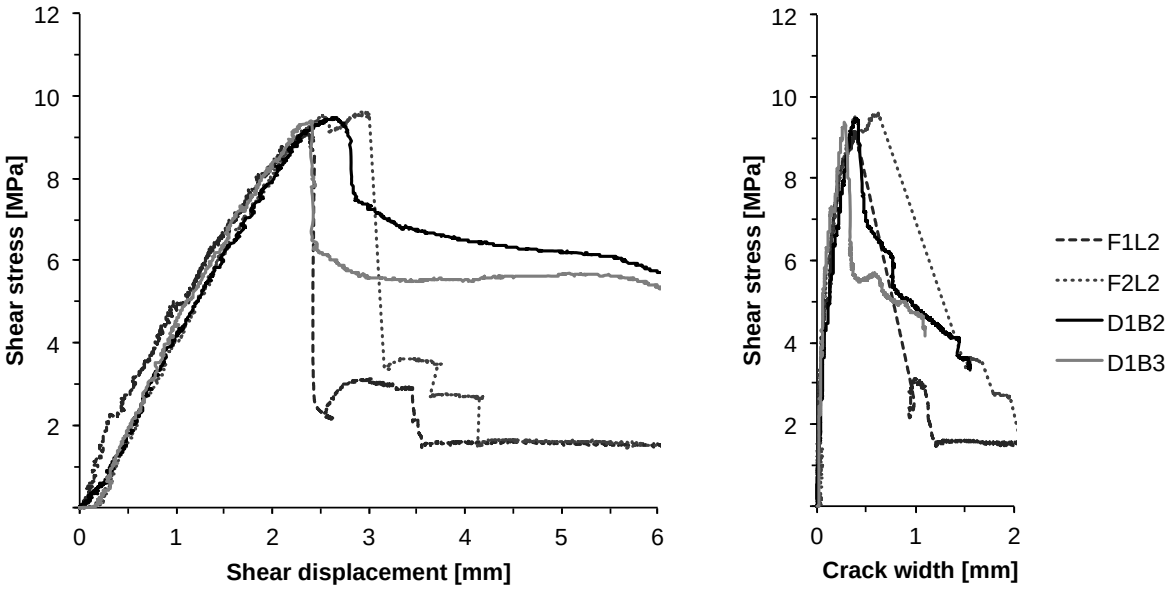

(a) (b)

Figure 4.27 – Comparison of deep embedment and externally bonded CFRP U-wrap with long anchorage: (a) shear stress versus shear displacement, (b) shear stress versus crack width.

4.6.3 Steel strain profiles

Figure 4.28 shows the shear stress versus steel strains for specimen D1B2 and D1B3.

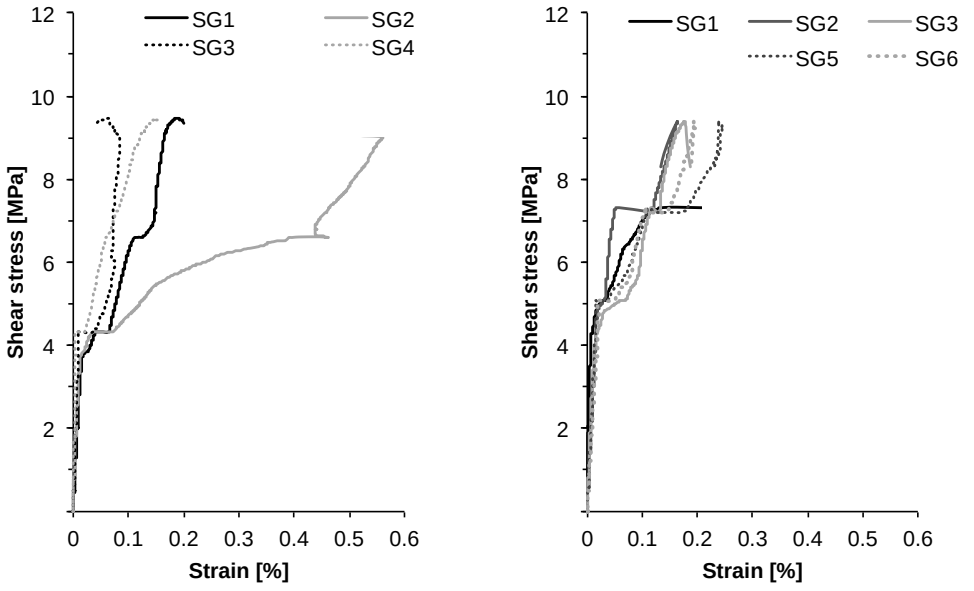

(a) (b)

Figure 4.28 – Shear stress versus steel strains – deep embedment: (a) D1B2 and (b) D1B3.

The readings suggest that the steel has yielded in specimen with three shear links, D1B3, however, only some shear links have yielded in specimen D1B2.

4.6.4 CFRP strain profiles

Figure 4.29 shows the shear stress versus CFRP strains recorded specimens D1B2 and D1B3.

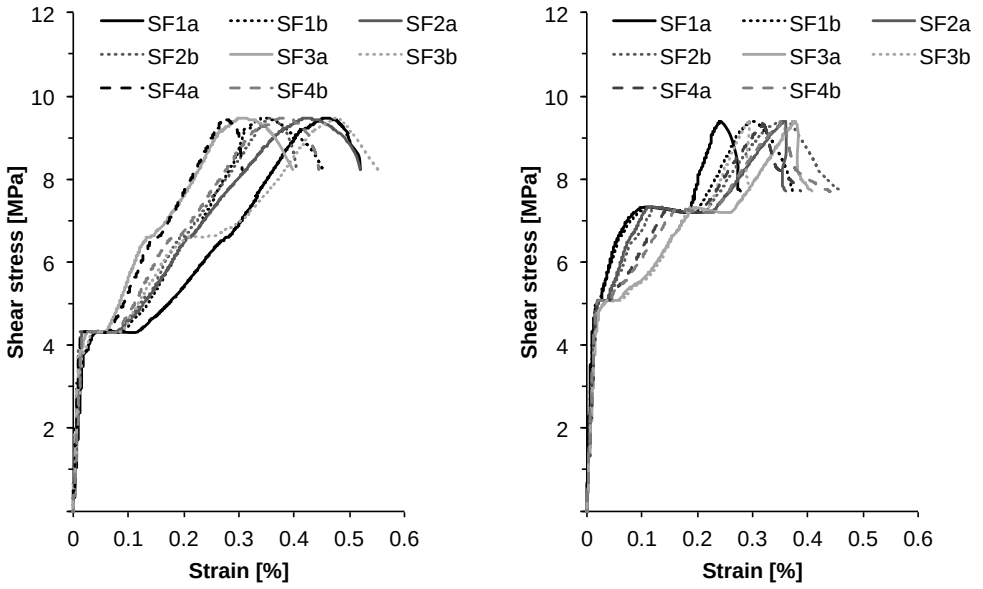

(a) (b)

Figure 4.29 – Shear stress versus CFRP strains – deep embedment: (a) D1B2 and (b) D1B3.

The strain readings on the CFRP bars from both deep embedded specimens showed that the bars are activated at first concrete cracking, much like the steel links, and contribute until failure, when the bars debond and slip occurs.

4.7 Pre-cracked push-off specimens strengthened with CFRP sheets

4.7.1 Failure modes

Both specimens PF2W2 and PF2W3 failed in shear due to separation of the CFRP wraps, as shown in Figure 4.30. The separation of the CFRP-concrete interface was gradual until failure. The specimen failed when the CFRP sheet fully debonded on both faces of the specimen and slip occurred. Only a small amount of concrete was observed attached to the

CFRP when the CFRP wrap was removed after testing. This was caused by separation of the concrete layer within the pre-existing crack, which was not fully injected by resin.

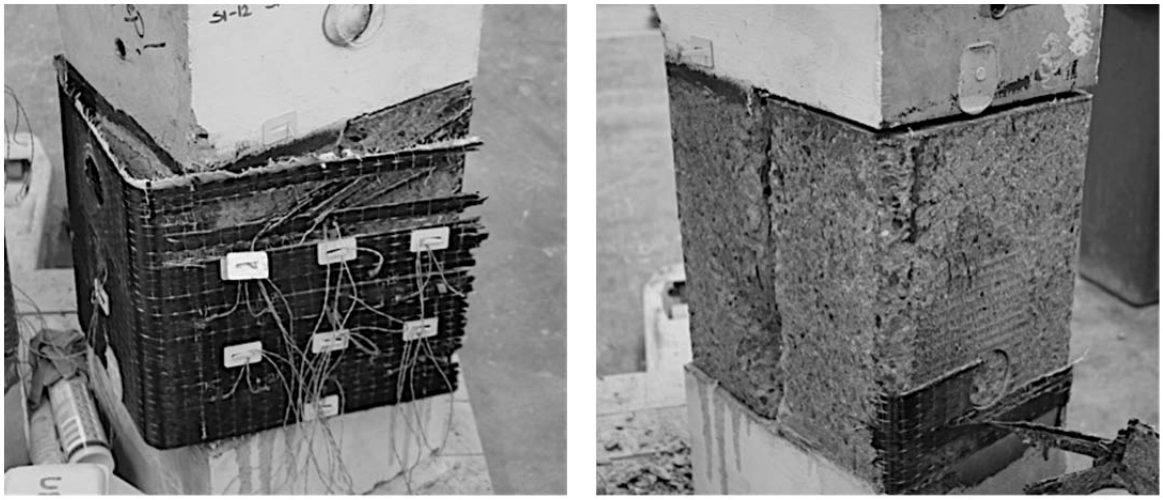

(a) (b)

Figure 4.30 – Failure modes of pre-cracked push-off specimens: (a) specimen PF2W2 after testing, (b) specimen PF2W3 after removal of the CFRP wrap.

The separation of the CFRP composite in the main fibre direction (splitting) is also evident from Figure 4.30 (a), as well as the rupture within the CFRP sheet along one of the edges. However, the splitting and subsequent rupture of the CFRP sheets occurred after the specimen reached its maximum load-carrying capacity and therefore was not the cause of failure. The CFRP wrap was removed with relative ease, suggesting the entire bond area was damaged and the CFRP fully separated.

4.7.2 Observed behaviour

Figure 4.31 shows the shear stress versus shear displacement and crack width curves for the pre-cracked specimens PF2W2 and PF2W3. To compare the behaviour of the identical cracked and uncracked cases, these curves were plotted against their uncracked counterparts, F2W2 and F2W3 rather than their control specimens.

The shear stress-displacement graph shows that the CFRP wrap enabled the specimen PF2W2 to reach large vertical displacement. The failure mode was dominated by gradual debonding of the CFRP wrap, which is also apparent from the relationship between shear stress and both displacement and crack opening. The specimen failed at a higher load than

its unstrengthened uncracked control counterpart from the previous test series, with a shear crack width of approximately 1.7 mm at failure.

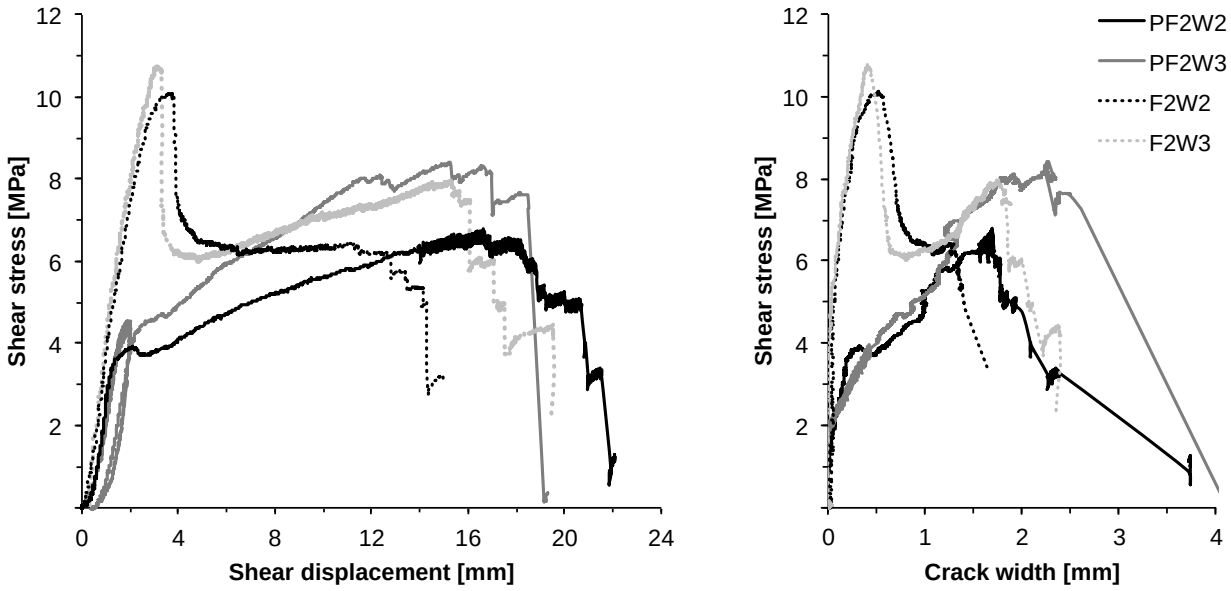

(a) (b)

Figure 4.31 – Comparison of pre-cracked push-off specimens and their uncracked counterparts: (a) shear stress versus shear displacement, (b) shear stress versus crack width.

The second pre-cracked specimen with three steel links, specimen PF2W3, exhibited similar behaviour to the specimen with two links, PF2W2, showing a large vertical displacement as well as shear crack opening at failure at approximately 2.5 mm.

4.7.3 CFRP strain profiles

Figure 4.32 shows the shear stress versus CFRP strains recorded for specimens PF2W2 and PF2W3. The sudden drop in shear stress in Figure 4.32 (b) was caused by an abrupt rupture of the CFRP sheets at the edges of the specimen and subsequent slip along the pre-existing crack in concrete.

It should be noted, however, that this slip due to the localized rupture of the CFRP sheets occurred after the specimen reached its peak capacity. This was shown in Figure 4.30.

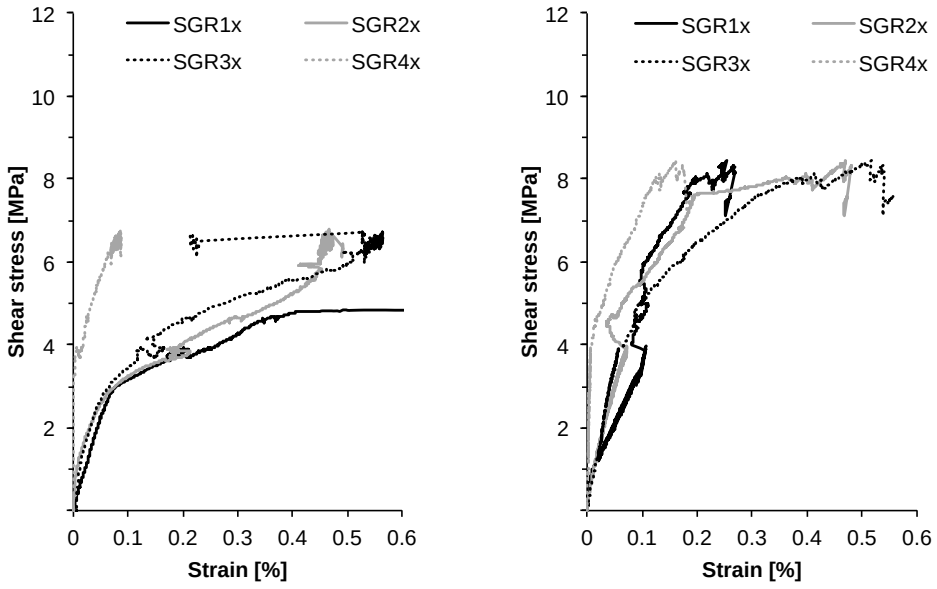

(a) (b)

Figure 4.32 – Shear stress versus CFRP strains – pre-cracked specimens: (a) PF2W2 and (b) PF2W3.

4.7.4 CFRP debonding

Figure 4.33 and Figure 4.34 show the strains recorded for specimens PF2W2 and PF2W3, respectively, relative to the position of the shear crack, indicated on the graphs as location 0. The stress values on the graphs indicate the shear stress at which the strains were reached in the CFRP wrap. The locations at which strains were measured were at 50 mm away from the edges of the specimen to obtain meaningful readings at points where the CFRP may debond, across the shear crack and in the location between these two points.

The results indicated that whilst the CFRP wrap was stretching over the pre-existing crack in the case of specimen PF2W2 to the point where the CFRP ruptured (upper region), the strain readings at the location of the crack were consistently lower for specimen PF2W3. However, the shear stress reached at failure due to the application of the CFRP was greater for the specimen PF2W3. The CFRP in this case did not rupture prior to failure.

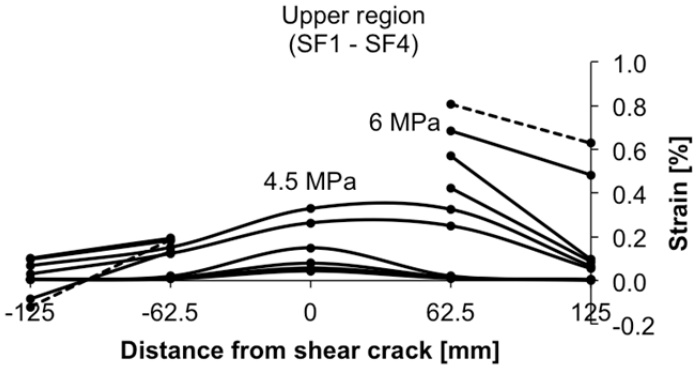

(a)

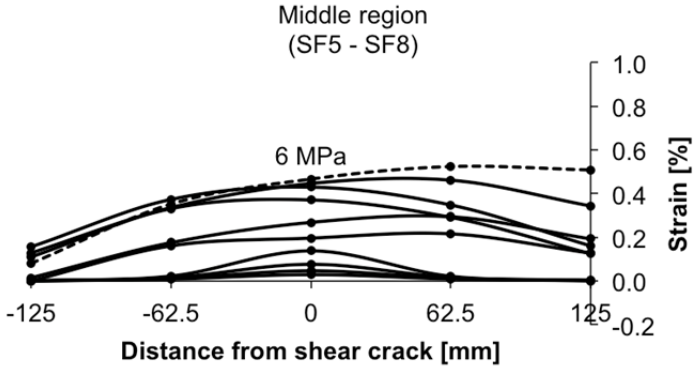

(b)

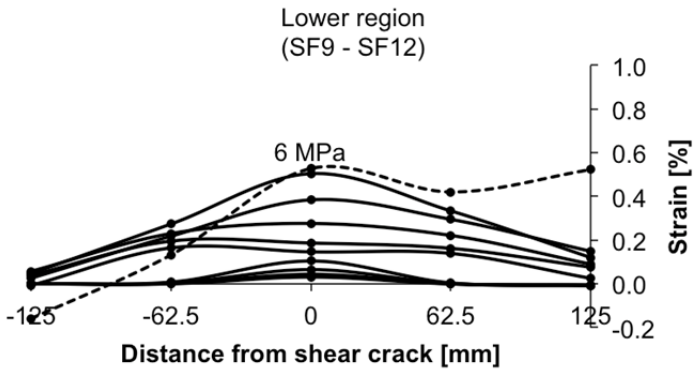

(c)

Figure 4.33 – CFRP strain profiles – pre-cracked push-off specimen PF2W2: (a) upper region, (b) middle region and (c) lower region (0 denotes shear plane position on the horizontal axis).

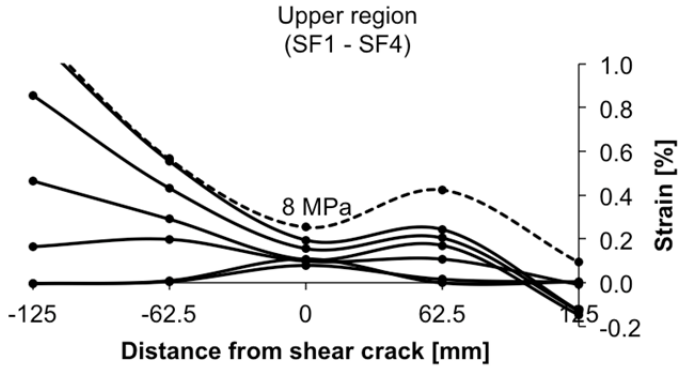

(a)

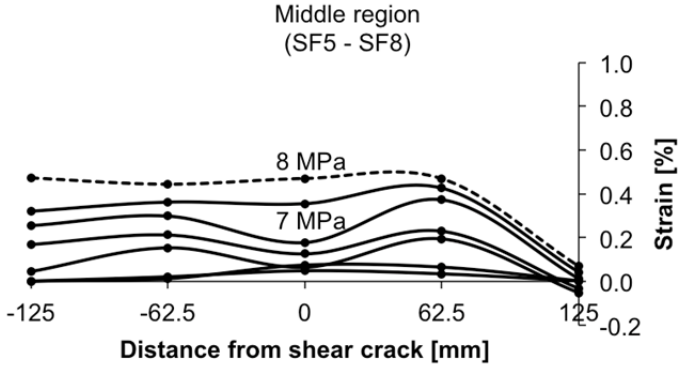

(b)

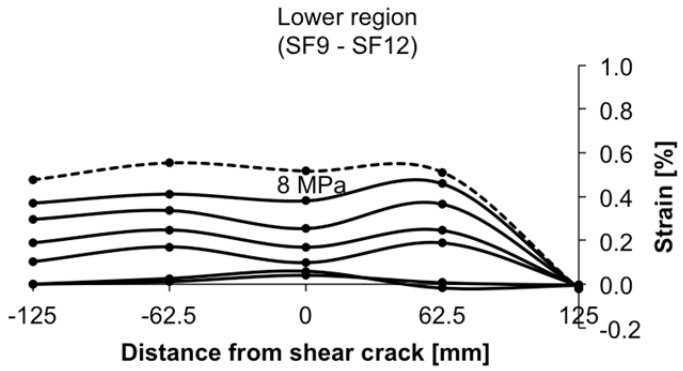

(c)

Figure 4.34 – CFRP strain profiles – pre-cracked push-off specimen PF2W3: (a) upper region, (b) middle region and (c) lower region (0 denotes shear plane position on the horizontal axis).

4.7.5 Concrete bond strength tests

The bond strength of the CFRP-concrete interface was tested following the testing of the pre-cracked push-off specimens. The tests were carried out using the standard test method for determining the pull-off strength for FRP laminate systems according to ASTM D7522. Figure 4.35 (a) shows the tested area on the push-off specimen after the tester was removed.

(a) (b)

Figure 4.35 – Bond strength test: (a) separation in the concrete substrate on the push-off specimen, (b) failure modes within the CFRP-concrete interface.

Several locations were tested on both pre-cracked specimens in the undamaged regions on the sides of the specimens for concrete only and for CFRP-concrete bond strength to obtain representative data. The mean value of bond strength of the CFRP to the concrete, f_{bf}, was 3.0 MPa with failure in the concrete substrate. In all cases of permissible failure (i.e. valid test results) these values greatly exceeded the 1.4 MPa minimum tension adhesion strength requirements of ACI-440 (2008).

Figure 4.35 (b) shows a comparison of bond quality in regions where the CFRP was fully bonded to concrete (right) with regions where CFRP was fully debonded and separation occurred in the adhesive rather than the substrate.

4.8 Behaviour of the externally bonded CFRP sheets

The non-principal stretching of the externally bonded CFRP sheets was of interest in the initially cracked specimens.

The results are presented in Table 4.7, with all values positive.

Table 4.7 – Strains in the CFRP sheets obtained for uncracked specimens.

Specimen	ε_1 [%]	ε_2 [%]	ε_3 [%]	ε_{max} [%]	ε_{min} [%]	θ [º]	γ_{max} [%]
F1S2	0.19	0.22	0.48	0.14	0.11	16	0.25
F2S2	0.16	0.22	0.35	0.13	0.12	10	0.25
F1L2	0.24	0.17	0.56	0.27	0.17	18	0.43
F2L2	0.18	0.14	0.65	0.24	0.19	25	0.43
F1W2	0.26	0.16	0.91	0.44	0.25	32	0.69
F2W2	0.21	0.09	0.57	0.32	0.16	35	0.47
F1W3	0.27	0.33	0.70	0.38	0.27	26	0.65
F2W3	0.18	0.29	0.60	0.23	0.27	21	0.50

The strains in the CFRP in all three monitored directions from strain gauge rosettes were averaged across the shear plane. The maximum principal strain ε_{max} and the minimum principal strain ε_{min} were then calculated, as well as the principal strain direction, angle θ, and the maximum engineering shearing strain, γ_{max}, according to the following equations:

$$\varepsilon_{max} = \frac{1}{2}\left[\varepsilon_1 + \varepsilon_2 + \sqrt{2\{(\varepsilon_1 - \varepsilon_3)^2 + (\varepsilon_2 - \varepsilon_3)^2\}}\right] \tag{4.1}$$

$$\varepsilon_{min} = \frac{1}{2}\left[\varepsilon_1 + \varepsilon_2 - \sqrt{2\{(\varepsilon_1 - \varepsilon_3)^2 + (\varepsilon_2 - \varepsilon_3)^2\}}\right] \tag{4.2}$$

$$\gamma_{max} = \sqrt{2\{(\varepsilon_1 - \varepsilon_3)^2 + (\varepsilon_2 - \varepsilon_3)^2\}} \tag{4.3}$$

$$\theta = \frac{1}{2} tan^{-1}\left\{\frac{2\varepsilon_3 - (\varepsilon_1 + \varepsilon_2)}{\varepsilon_1 - \varepsilon_2}\right\} \tag{4.4}$$

where ε_1 is the strain measured in the horizontal (fibre) direction, ε_2 is the strain measured in the vertical (non-principal fibre) direction and ε_3 is the strain measured in the 45° direction.

For both weights of the CFRP fabric used, the results indicated, that with decreasing bond length the principal angle also decreases. The principal angle in the case with 1.6% CFRP and short anchorage length, specimen F2S2, was only 10º. With increasing anchorage

length of the U-wrap, the principal angle also increased to 18º and 25º for specimen F1L2 and F2L2, respectively. The greatest principal angle was recorded in the fully wrapped specimens with two shear links at 32º for specimen F1W2 and 35º for specimen F2W2. In contrast, specimens with three shear links, specimen F1W3 and F2W3, showed lower values of principal angle at 26º and 21º, respectively.

Strikingly, the values of the maximum engineering shear strain, γ_{max}, were identical for F1S2 and F1S3 at 0.25%, and for F1L2 and F2L2 at 0.43%. These results suggest that the same levels of engineering shear strain can be achieved through adequate anchorage length calculated based on the thickness of the CFRP sheet. For the fully wrapped specimens, the engineering shear stain levels were comparable for specimens F1W2 and F1W3 at 0.69% and 0.65%, respectively, and 0.47% for specimen F2W2 and 0.50% for specimen F2W3. These results indicate that the levels of engineering shear strain in the fully wrapped cases depend on the thickness, and therefore relative stiffness, of the applied CFRP wrap.

4.9 Discussion of test results

4.9.1 Effectiveness of CFRP materials

To quantify the effectiveness of the investigated strengthening solutions, it is necessary to establish the quantitative and qualitative measures for comparison. The effectiveness was therefore assessed according to the influence of anchorage length and the CFRP material used on the overall performance of the system.

Figure 4.36 shows the material effectiveness of the CFRP strengthening configurations in the uncracked push-off specimens. The ultimate shear stress, v_u, was normalized by the concrete compressive strength, f_{cu}, of the individual tested specimens. To obtain comparable results in terms of to what extent the composite material was utilized at failure, the effective (maximum recorded) strain in the CFRP in the principal fibre direction was normalized by the ultimate tensile strain. Generally, the heavier CFRP fabric, series F2, utilized less than 20% of the ultimate capacity of the material prior to failure in U-wrapped specimens and 21% in the fully wrapped case.

The lighter fabric, used in series F1, showed greater variation in material utilization prior to failure and this depended on the anchorage length provided. With increasing anchorage length, the material utilization of the CFRP wrap also increased. This result indicates that

with longer anchorage length greater strains in the CFRP sheets are achievable prior to failure due to CFRP debonding.

The fully wrapped specimen with two links F1W2 utilized the material to 26% compared to 27% for the F2W2. The fully wrapped specimens with three links showed 21% and 18% material utilization at failure for F1W3 and F2W3, respectively. In comparison to the externally bonded systems, the deep embedment specimens showed that 27% and 22% of the CFRP bar ultimate capacity was utilized at failure for D1B2 and D1B3, respectively. This result demonstrated that the CFRP material is more effective in the case where fewer internal steel links cross the shear plane.

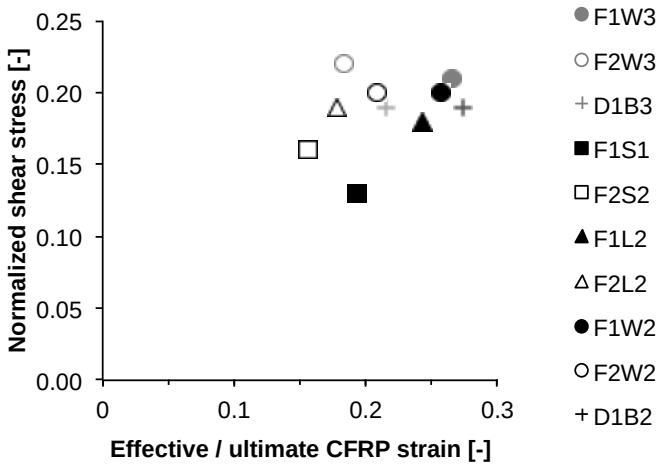

Figure 4.36 – Material effectiveness in CFRP strengthening.

The effectiveness of strengthening with fully wrapped CFRP sheets in the case of push-off specimens with a pre-existing shear crack was around 300% compared to the residual capacity of the pre-cracked control specimen. This finding points to the possibility that great increase in shear strength is possible for elements with pre-existing crack and low residual capacity when fully wrapped. In the case of the specimen with two pre-yielded steel links, PF2W2, the strengthened specimen exceeded the capacity of the underlying uncracked control specimen, C2.

4.9.2 CFRP behaviour

The investigation of the non-principal stretching of the externally bonded CFRP sheets showed that the principal angle decreases dramatically with decreasing anchorage length. The engineering shear strain also decreases with decreasing anchorage length, supporting

the hypothesis that anchorage length provided beyond the location of the shear crack has an immense impact on the ultimate shear capacity of the strengthened system. The thickness of the CFRP sheets, however, did not prove to be a major factor in achieving greater shear-friction capacity. This is because the calculation of the required anchorage length is dependent on the thickness of the CFRP sheets to ensure debonding strains can be developed over the effective length of the CFRP. This was supported by the similar values of ultimate shear stress recorded for all fully wrapped specimens regardless of the thickness of the CFRP sheets or the amount of internal steel links crossing the shear plane. This finding pointed to the possibility that a limiting shear-friction capacity of concrete must exist, which controls the ultimate shear-friction capacity of the strengthened push-off specimen.

The strain readings from the CFRP bars in the deep embedment specimens showed similar values to those recorded on the internal steel shear links. This finding demonstrated that the deep embedded CFRP bars behave in a similar manner as the internal steel links, and therefore, the entire strengthened system behaves like a reinforced concrete element.

4.9.3 CFRP-concrete interface

The CFRP in all specimens strengthened with externally bonded CFRP sheets debonded in the concrete substrate caused by opening of the shear crack. Different modes of separation were observed depending on the anchorage length provided. Specimens with short anchorage length, F1S2 and F2S2, and specimen F2L2 with long anchorage length, showed fracturing of the concrete in the full depth of the concrete cover. Specimen F1L2 and all fully wrapped specimens showed debonding in the surface concrete layer. In all cases the debonding was induced by the opening of the shear crack and the specimens failed prematurely in the cases where short anchorage length was provided. The mixed mode failure of specimen F2L2, where the CFRP U-wrap debonded in the surface concrete layer on one face of the specimen and separated through the concrete cover on the other, showed that for the heavier CFRP fabric the entire available bond length might not have been sufficient to develop debonding strains. This hypothesis is supported by the low strains recorded in the principal fibre direction, as discussed in Section 4.8 in detail.

Differential debonding of the CFRP bars was observed in the case of deep embedment after the bars were extracted from one of the specimens after testing. This was possibly

caused by the presence of the lead wires from the strain gauges, which could have had a negative effect on the local bond quality.

The observed failure modes that were described and discussed in detail in Section 4.4 through to Section 4.7 are summarized in Figure 4.37.

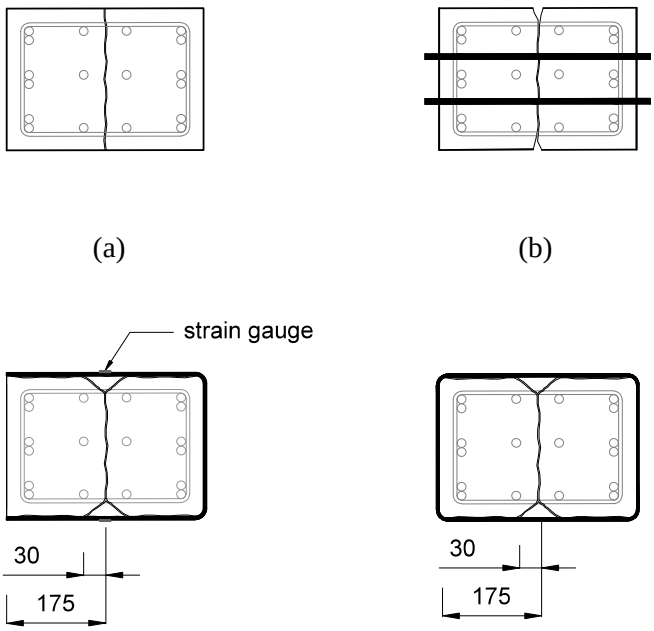

Figure 4.37 – Push-off specimens – failure modes: (a) unstrengthened control specimen, (b) deep embedment specimen, (c) specimen strengthened with CFRP wrap in a U-wrap configuration showing positioning of the strain gauges at the shear crack location and (d) in a fully wrapped configuration.

4.9.4 Comparison with theoretical predictions

A modified shear-friction theory was used to predict the shear-friction capacity of the specimens, based on the work of Mattock (2001) and extended by the work of Saenz and Pantelides (2005). Such an approach appears appropriate for push-off specimens where internal steel and externally applied reinforcement cross the shear plane.

In general, the theory assumes the specimens fail in two successive stages: 1) the shear stress is controlled by the concrete alone until the concrete tensile strength is reached and 2) the additional imposed shear stress is resisted by the steel-concrete and the CFRP-concrete interaction. The latter assumes that the steel and the CFRP act as a clamping force

in the horizontal direction, resulting in additional aggregate interlock until cohesive concrete failure and bond failure of the CFRP composite occurs. Based on the currently accepted shear-friction approach, the following equation was used to calculate the shear-friction capacity of the strengthened specimens as

$$v_u = v_c + v_s + v_f \tag{4.5}$$

The individual components of equation (4.5) assume the ultimate shear stress, $v_{u,}$ of a steel reinforced concrete section strengthened with CFRP materials as the sum of the shear-friction capacity of the concrete, $v_{c,}$ a portion of the shear-friction capacity contributed by the steel-concrete interaction, v_s, and that of CFRP-concrete, v_f. The equation therefore can be rewritten in the form

$$v_u = Af_c + B\rho_v f_y + Cc_f \rho_f f_u \tag{4.6}$$

where the first two terms were determined experimentally by Mattock (2001): 1) the concrete shear-friction strength with A as a bond factor (0.117), 2) the second term implies that steel-concrete interaction depends on the yield strength and amount of reinforcement with B as a shear-friction coefficient (0.8) and the final term of equation (4.6) is the equivalent of CFRP-concrete contribution to the overall shear strength of the section, with the C factor determined experimentally on CFRP-strengthened plain concrete specimens by Saenz and Pantelides (2005).

The equation then reads

$$v_u = 0.117f_c + 0.8\rho_v f_y + 0.505c_f \rho_f f_u \tag{4.7}$$

To consider the effects of varying anchorage length, a shear-friction reduction coefficient, c_f, is introduced. Based on the geometry of the specimen and the bond length provided in this experimental study, the coefficients are 0.514 for specimens with 0.8% CFRP ratio and 0.714 for specimens with 1.6% CFRP ratio with short anchorage and 1.0 for all fully wrapped specimens and specimens with long anchorage.

The shear-friction capacity of reinforced concrete push-off specimens strengthened with CFRP bars can be generally expressed using equation (4.8). The first two terms of the equation remain the same with the final term adjusted according to the predicted effective strain levels in the CFRP bars. The capacity of the CFRP-concrete interface depends on the bond strength between the resin and the concrete, limited to 20 MPa, as proposed by

Valerio (2009). The effective tensile strength of the CFRP bars, f_{fe}, is calculated as $\varepsilon_{fe}f_u$, where ε_{fe} is limited to 0.004 (Valerio, 2009). This results in effective strains in CFRP equivalent to those in steel reinforcement.

The equation therefore reads

$$v_u = 0.117f_c + 0.8\rho_v f_y + c_f \rho_f f_{fe} \tag{4.8}$$

The ultimate applied force is calculated as the shear stress, v_u, multiplied by the shear plane area, which was constant throughout the test series and equal to 75000 mm^2. A summary of the predicted and experimental values is presented in Table 4.8.

Table 4.8 – Ultimate shear-friction capacity: predicted versus experimental values.

Specimen	Experimental		Predicted		
	ρ_f [%]	$P_{u\text{-}exp}$ [kN]	c_f [–]	$P_{u\text{-}calc}$ [kN]	$P_{u\text{-}calc}$ / $P_{u\text{-}exp}$
C2	–	411	–	471	1.15
F1S2	0.8	505	0.514	565	1.12
F2S2	1.6	591	0.714	843	1.43
F1L2	0.8	687	1.0	756	1.10
F2L2	1.6	722	1.0	1005	1.39
F1W2	0.8	756	1.0	738	0.98
F2W2	1.6	758	1.0	1005	1.33
D1B2	0.8	705	1.0	720	1.02
PFW2	1.6	510	1.0	633	1.24
C3	–	637	–	482	0.76
F1W3	0.8	796	1.0	744	0.93
F2W3	1.6	807	1.0	1087	1.35
D1B3	0.8	711	1.0	713	1.00
PFW3	1.6	633	1.0	650	1.03

Actual concrete compressive strength obtained on the test date was used for predicted values.

The control specimen C2 prediction is higher than the experimental ultimate load-bearing capacity of the specimen. The predicted ultimate capacity for the control specimen with three shear links, C3, is lower than that obtained experimentally. The equation used for calculation of the predicted shear-friction capacity is based on empirical values derived

from testing on similar pre-cracked specimens (Hofbeck and Mattock, 1962). This suggests that the load sharing between the components might have been different to the one assumed by the conservative approach of the modified shear-friction theory.

The calculated values for the U-wrapped specimens consistently over-predict the ultimate load-bearing capacity, regardless of the anchorage length provided or the CFRP thickness. The calculated values for the specimens fully wrapped with the 'lighter' CFRP fabric, F1W2 and F1W3, however show a good agreement with the experimental results, regardless of the number of internal steel shear links crossing the shear plane. In contrast, the calculated capacity for the specimens strengthened with the 'heavy' FRP fabric, F2W2 and F2W3, is over-predicted by approximately 30% in both cases.

The prediction for the pre-cracked specimens conservatively assumed that the residual strength of the specimens is equal to the yielding steel component, assuming zero residual capacity of the cracked concrete. The CFRP contribution was then added onto this residual strength to obtain the total shear strength of the strengthened pre-cracked specimens. The prediction is in a good agreement with the experimental values for the specimen with three pre-yielded shear links, PF2W3. However, such approach over-predicts the capacity for the specimen with two shear links, PF2W2, by 24%, despite the applied CFRP fabric being identical in both cases. This is possibly due to the assumed residual strength of the specimen, which might have been greater due to some residual shear-friction capacity of the cracked concrete.

The deep embedment specimens both showed a good agreement with the predicted values, confirming the correctness of the assumed bond strength for the CFRP bars (Valerio, 2009). This assumption is supported by the results and findings from the experimental testing, described in detail in Section 4.6.3 and further in Section 4.9.2.

This means that the modified shear-friction theory, which assumes the ultimate shear-friction capacity as the sum of the capacities of the individual components, is wholly inappropriate for the specimens with externally applied CFRP sheets. On the other hand, the contribution of the CFRP bars in the deep embedment specimens is based on effective values of strains, equivalent to yielding steel. Therefore, the additive approach is appropriate for the specimens strengthened with the deep embedded CFRP bars, as these behave similarly to the internal steel shear links.

4.10 Concluding remarks

Following the experimental testing and analysis of results of twelve initially uncracked and two pre-cracked push-off specimens strengthened with CFRP material, the following conclusions can be drawn:

- The anchorage length in externally bonded CFRP U-wraps had a great influence on the ultimate shear capacity of the push-off specimen;
- With increasing anchorage length, the shear-friction capacity of the specimen increased. However, minimum increase was observed in cases where the CFRP sheets were fully wrapped compared to those where the full available bond length was utilized;
- The fully wrapped specimens reached similar values of ultimate shear capacity, regardless of the number of internal steel links or the thickness of the CFRP sheets crossing the shear plane. This finding points to concrete having some limiting shear-friction capacity which was reached and controlled the ultimate shear-friction capacity of the strengthened specimen;
- The specimens strengthened with deep embedded CFRP bars showed similar increase in shear capacity compared with the U-wrapped specimens where the full available bond length was utilized. This in turn means that the deep embedment offers a viable alternative to U-wrap strengthening;
- The investigation of the non-principal stretching of the CFRP sheets showed that with increasing anchorage length the principal angle also increases;
- The investigation on pre-cracked push-off specimens fully wrapped with CFRP sheets showed that a disproportionate amount of increase in shear capacity can be achieved over that of the residual shear capacity of the cracked specimen. The investigation also showed that it is indeed possible to achieve greater shear capacity than that of the underlying unstrengthened control specimen;
- The study on effectiveness of the CFRP materials showed that the CFRP is underutilized. The material utilization for the externally bonded CFRP sheets was between 16% and 27%, for the deep embedment 38% and 48%, and for the pre-cracked specimens at 52% and 57%, where the CFRP was effectively unbonded over the pre-existing discontinuity;
- The debonding of the externally bonded CFRP sheets occurred in all cases

primarily in the concrete substrate through Mode I – crack opening;

- The comparison of experimental values with those calculated using modified shear-friction theory demonstrated that the additive approach to obtaining the ultimate shear capacity is wholly inappropriate for the specimens strengthened with sheets. However, the same study showed that the calculated values for the deep embedment were in a good agreement with the experimental results. Therefore, the additive approach is adequate for the prediction of shear capacity in situations where the CFRP bars behave similarly to traditional steel shear reinforcement in concrete.
- The push-off specimens served as a trial base for the determination of an accurate DIC pattern for the main experimental programme on full-scale T-beams. The results were therefore not presented here as the modified pattern, which was further used for the T-beam specimens, was only used on the pre-cracked push-off specimens. Other patterns were not found successful in accurately tracking the surface strains in the CFRP wraps due to the inadequate size of the speckle pattern.

5 T-BEAM TEST PREPARATION

5.1 Introduction

Two sizes of beam specimens, referred to as large and medium, were fabricated, strengthened and tested under monotonically increasing loading in three-point bending. In total six large and four medium specimens were tested. This Chapter outlines the fabrication and strengthening of the T-beam specimens and their preparation for mechanical testing, including test setup and instrumentation. Traditional physical foil strain gauges were used to monitor strains in the steel and the CFRP materials and their positioning is discussed in detail in this Chapter. The DIC technique was also used to obtain full field displacement and strain measurement in the zone under investigation. The DIC setup is also presented here. Standard material tests were performed on concrete, steel and CFRP sheets and the results are presented in this Chapter altogether with the test matrix.

5.2 Specimen details

5.2.1 Specimen design and construction details

The size and geometry of the two sizes of test T-beam specimens are shown in Figure 5.1 and Figure 5.2.

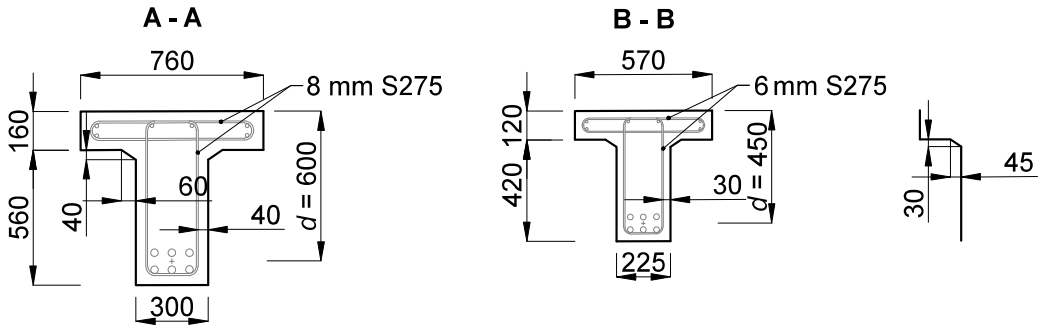

(a) (b)

Figure 5.1 – T-beams reinforcement detail: (a) large T-beam – section through, (b) medium T-beam – section through [mm].

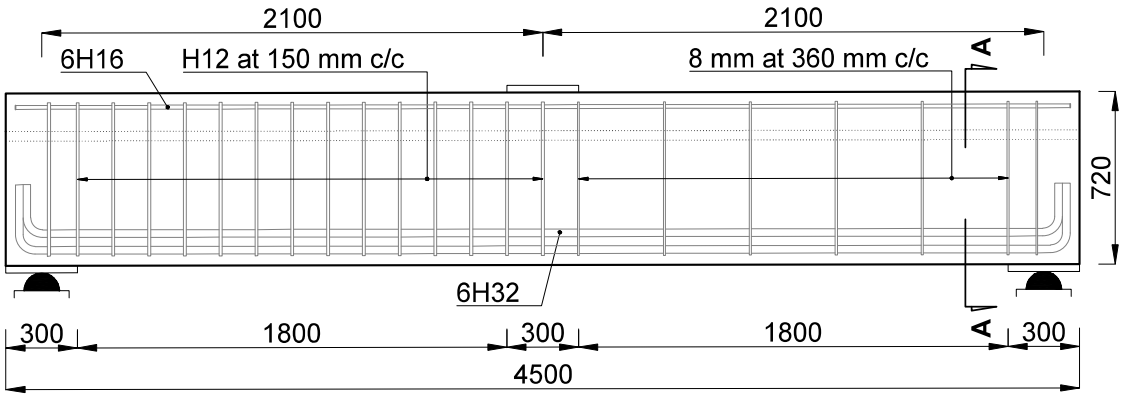

(a)

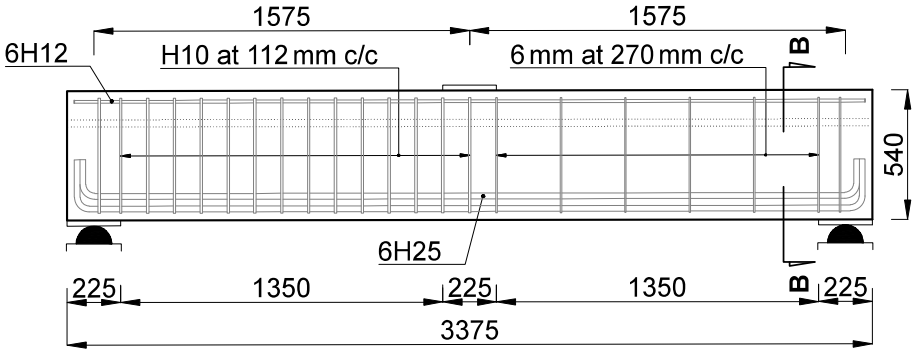

(b)

Figure 5.2 – T-beams – reinforcement detail: (a) large T-beam – long section, (b) medium T-beam – long section. Tested span on the right from the loading plate [mm].

The size and geometry of the large tested beams was based on typical existing reinforced concrete slab-on-beam bridges. The medium-sized beams were a directly scaled down replica of the large beams and therefore with identical but scaled down longitudinal as well as transverse reinforcement ratios. The dimensions of the large beams were 720 mm deep, 760 mm wide and 4.5 m long with width of the web 300 mm. The medium beams were 540 mm deep, 570 mm wide and 3.375 m long with width of the web 225 mm. The length of the beams was selected to purposefully create an *a/d* ratio of 3 between the support and loading plate edges (*a/d* = 3.5 plate centre to plate centre).

The flexural reinforcement in both cases was formed using six bars arranged in two layers. The reinforcement ratio was 2.2% using 32 mm diameter deformed B500C grade bars and

2.4% using 25 mm diameter deformed B500C grade bars for the large and medium beams, respectively. Each bar was bent up at the ends to provide sufficient anchorage extending beyond the support.

To promote shear failure, one half of the beam was designed as deficient in shear. The transverse reinforcement ratio in the tested span was kept constant at 0.1% with steel shear links spaced at 0.6*d*. These two-legged closed loop links with sufficient overlaps were formed using plain mild S275 grade steel, of 8 mm diameter for the large and 6 mm for the medium beams, respectively.

5.2.2 Material properties

The steel properties of the plain mild S275 grade steel used for the shear links and the deformed B500C grade for main reinforcement in the large and medium T-beams are presented in Table 5.1.

Table 5.1 – T-beam specimen steel material properties.

Beam size	d_s [mm]	Grade	Bar type	f_y [MPa]	f_u [MPa]	ε_{sy} [%]
Large	32	B500C	Deformed	510	587	0.32
	16	B500C	Deformed	538	631	0.31
	12	B500C	Deformed	518	586	0.33
	8	S275	Plain	336	438	0.16
Medium	25	B500C	Deformed	554	667	0.38
	12	B500C	Deformed	518	586	0.33
	10	B500C	Deformed	538	625	0.29
	6	S275	Plain	434	536	0.20

Average values from three samples. Tested according to BS 4449:2005 and BS 4482:2005.

The concrete mix used for all specimens was of design strength 60 MPa at 28 days, with maximum allowable aggregate size of diameter 20 mm. Four 100 mm cube control specimens were taken during the casting of each of the test specimens and air dried alongside the beam specimens. Additionally, the precaster sampled three 100 mm cube control specimens, which were wet cured and tested independently on day 7-8 and 28. The air-dried control specimens were tested in compression on the test day of the main test

specimen. The mean compressive strength of all test cubes was 59 MPa and between 54 and 62 MPa. Two 100 mm diameter 200 mm tall cylinders were also cast with each test beam. These were subject to tensile splitting tests on the test day of the main specimen. The average tensile strength was 3.7 MPa.

The concrete mix proportions are presented in Table 5.2.

Table 5.2 – T-beam specimen concrete mix proportions.

Material	Per m^3	Specifications
Stone	975 kg	20 – 6 mm limestone
Sand	800 kg	M-grade grit sand
Cement	350 kg	Portland CEM I 52.5 R
Water	185 l	Water to cement ratio 0.53
Admixture	1312 ml	AdvaCast 554
Admixture	4375 ml	Daraset 580C

Four 100 mm cube control specimens were taken during the casting of each of the test specimens and air dried alongside the beam specimens. Additionally, the precaster sampled three 100 mm cube control specimens, which were wet cured and tested independently on day 7-8 and 28. The air-dried control specimens were tested in compression on the test day of the main test specimen. The mean compressive strength of all test cubes was 59 MPa and between 54 and 62 MPa. Two 100 mm diameter 200 mm tall cylinders were also cast with each test beam. These were subject to tensile splitting tests on the test day of the main specimen. The average tensile strength was 3.7 MPa.

5.2.3 Test specimen fabrication

The beams were precast at a specialist contractor, who also provided timber formwork for the specimens and in-house assembly of the steel cages, shown in Figure 5.3.

The steel links for the tested span were supplied from the same source as for the push-off test programme. The steel links were cut and bent according to the specifications and equipped with strain gauges at the University of Bath and transported to the precaster for use in the specimens. The precaster also sourced the longitudinal reinforcement as well as the shear reinforcement in the non-tested reaction span. Approximately four concrete batches were needed to cast one large test specimen with four standard 100 mm x 100 mm

x 100 mm test cubes and two standard 100 mm x 200 mm cylinders. The concrete was compacted during casting using a vibrating poker. All specimens were cast on a 24-hour cycle and air-cured for a minimum of 28 days.

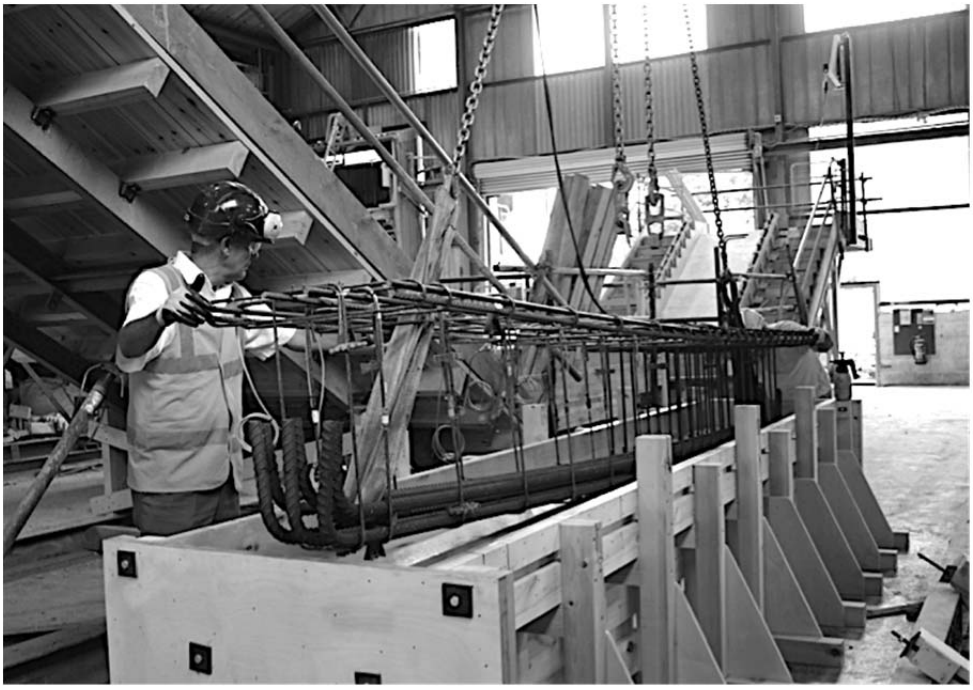

Figure 5.3 – Fabrication of large T-beams.

5.2.4 Test series

In total, ten initially uncracked reinforced concrete T-beams were tested – six large and four medium beams. The tested strengthening schemes included CFRP sheets in a U-wrap configuration, CFRP sheets with a bar-in-slot anchorage system and deep embedment. One specimen within each size group was tested unstrengthened and served as a baseline comparison for the strengthened beams.

For ease of orientation, the designation of the specimens is formed using letters and numbers representing the configuration of the test specimen. The letters **LB** indicate large beams and **MB** the medium beams, respectively. Immediately followed by a letter **C** designates unstrengthened control specimens. In the case of specimens with CFRP sheet strengthening, the number that follows the beam size is indicative of the CFRP material ratio – **1** for the 'lightly' strengthened (0.7% CFRP ratio) and **2** for the 'heavily' strengthened (1.3% CFRP ratio), respectively. The number is followed either by a letter **U** indicating fabric sheets in a U-wrap configuration or by the letters **UA** indicating fabric

sheets in a U-wrap configuration with end anchorage. The deep embedment specimen is designated with letters **DE** following immediately after the letters indicating the beam size. For example, a large beam heavily strengthened with CFRP sheets in a U-wrap configuration with end anchorage is designated LB2UA. The test matrix with details of test specimens is presented in Table 5.3. Details of strengthening specifications were discussed in detail in Chapter 3.

Table 5.3 – Test matrix of T-beam specimens and specimen details.

Specimen	Steel		Concrete		CFRP		
	ρ_l [%]	ρ_v [%]	f_{cu} [a] [MPa]	f_t [b] [MPa]	ρ_f [%]	t_f [mm]	Anchorage bar diameter [mm]
LBC	2.2	0.1	55.0	3.5	–	–	–
LB1U	2.2	0.1	60.3	3.9	0.7	0.5 + 0.5	–
LB1UA	2.2	0.1	55.0	4.1	0.7	0.5 + 0.5	12
LB2U	2.2	0.1	62.0	3.5	1.3	1.0 + 1.0	–
LB2UA	2.2	0.1	54.1	3.4	1.3	1.0 + 1.0	12
LBDE	2.2	0.1	59.0	3.2	0.2	–	–
MBC	2.4	0.1	58.9	4.2	–	–	–
MB2U	2.4	0.1	64.1	3.6	1.3	1.0 + 0.5	–
MB2UA	2.4	0.1	61.1	3.8	1.3	1.0 + 0.5	10
MBDE	2.4	0.1	61.3	4.0	0.2	–	–

[a] Concrete compressive strength on test day according to BS EN 12390-3:2009.

[b] Concrete splitting tensile strength on test day according to BS EN 12390-6:2009.

The sections of the tested strengthening configurations are shown in Figure 5.4.

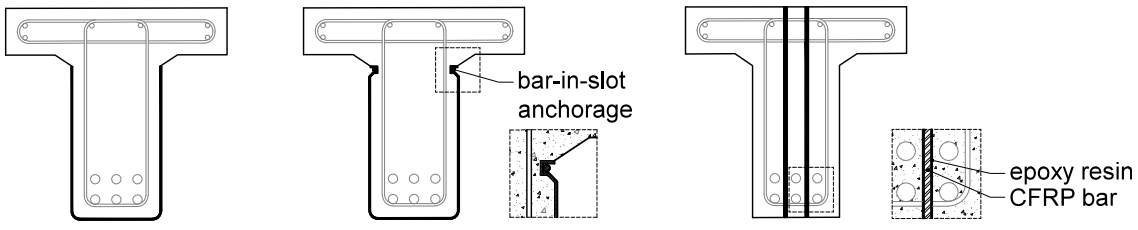

(a) (b) (c)

Figure 5.4 – T-beams – tested strengthening configurations – through sections: (a) U-wrap without end anchorage, (b) U-wrap with bar-in-slot end-anchorage system, and (c) specimen strengthened with deep embedded bars.

Figure 5.5 shows the elevation of the typical specimen strengthened with externally applied CFRP sheets in the U-wrap configuration.

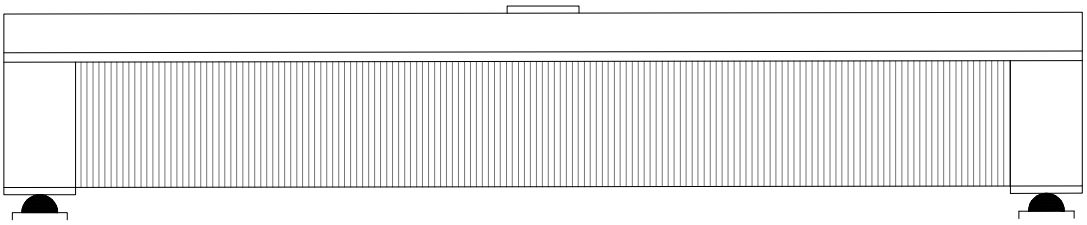

Figure 5.5 – Strengthening configuration with externally bonded CFRP sheets in a U-wrap configuration.

Figure 5.6 shows the positioning of the CFRP bars in the deep embedded specimens.

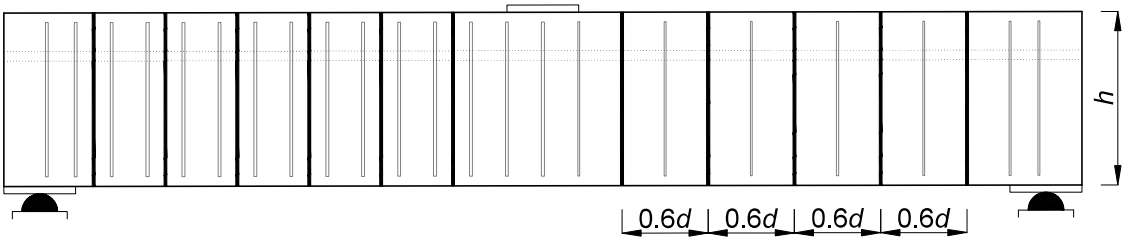

Figure 5.6 – T-beams – schematics of tested strengthening configurations: deep embedment.

5.2.5 Specimen preparation and strengthening

The large specimens were prepared for bonding and strengthened at the precaster's facilities. Four out of six specimens were grit-blasted for external bonding and one specimen was drilled for the application of deep embedded bars. Sponge blasting (dry abrasive grit blasting) was used to remove the top surface concrete layer, see Figure 5.7.

The specimens were turned upside down and rested on their slabs supported on timber for the surface preparation and subsequent strengthening. After the surface layer was removed, pressurized air and wire brushing were used to clean the surfaces from all remaining dust and impurities. A bar-in-slot anchorage system was used for two of the externally strengthened specimens and therefore 25 mm x 25 mm slots were carefully chased along the bottom edge of the haunch underneath the flange; see Figure 5.8 (b) for detail.

Figure 5.7 – On-site preparation of large beams for strengthening: hole drilling for strengthening with deep embedded CFRP bars (front), surface preparation using dry sponge blasting technique for externally bonded CFRP sheets (back).

The sharp edges of the slots were rounded to a minimum 15 mm diameter due to space limitations for tool maneuvering within the slot, shown in Figure 5.8 (b). The slots were then cleaned by wire brushing and with pressurized air.

(a) (b)

Figure 5.8 – Large T-beam preparation for strengthening with externally bonded CFRP sheets: (a) dry sponge blasting, (b) longitudinal channels cut for bar-in-slot anchorage system.

The specimens were kept dry under plastic sheets overnight and cleaned again prior to bonding. Two of the U-wrap specimens were strengthened on the first day of strengthening works and two on the following day. Similarly to the push-off specimens, two weights of fabric were used to vary the CFRP ratios. The CFRP sheets were cut to length and saturated with a thoroughly mixed two-component epoxy adhesive using a roller brush. A thin primer layer of epoxy was also applied to the web of the specimen for bonding. A thickened layer of epoxy was then applied onto the concrete surfaces and the first layer of CFRP sheet was carefully applied to the web. The sheets were 600 mm wide and, to form a continuous sheet, 10 mm overlap was provided. Another thin layer of the thickened epoxy adhesive was applied followed by the second sheet of the CFRP fabric. The full length of the beam was strengthened from the edge of one supporting plate to the other taking care to avoid placing CFRP sheets directly above the support regions, see Figure 5.9 for application detail.

(a) (b)

Figure 5.9 – Large T-beam strengthening with externally bonded CFRP sheets: (a) CFRP sheet application onto primed concrete surfaces, (b) bar-in-slot anchorage application.

Where the CFRP sheets were anchored with the bar-in-slot anchorage system, the CFRP sheets were moulded into the slots primed with epoxy using CFRP bars. Prior to the application into the slot, both the slot and the bar were covered with thickened epoxy, shown in Figure 5.9 (b). The length of each anchorage bar was one third of the length of the beam to provide continuous anchorage across the sheets. Figure 5.9 (b) also shows a detail of the edges of the webs of the specimens, which were cut and rounded to the recommended radius 25 mm (TR55, 2012) to prevent the fabric from premature rupture.

A series of 16 mm diameter holes were drilled according to the schedule through the web

of the deep embedment specimen, shown in Figure 5.6. The beam was then transported with the sheet-strengthened beams to Bath for in-house strengthening. The holes were thoroughly cleaned with a round wire brush and pressurized air prior to the application of the deep embedded CFRP bars. The adhesive used for the deep embedment was identical to the one used for the externally bonded sheets, for consistency throughout the beam test series. Similarly to the sheet-strengthened beams, the beam was turned upside down for the application of the CFRP bars. The surfaces of the holes were primed with a thin layer of the two-component epoxy, and a small amount of the adhesive was poured into the pre-prepared slots. Due to the low viscosity of the adhesive, a stopper was provided at the bottom end of each hole to prevent adhesive from spilling out. A thickened epoxy was also applied to the CFRP bars, while taking care not to damage the strain gauges. The bars were carefully pushed through the holes until the adhesive in the slot appeared at the top end of the hole, suggesting there was no trapped air in the epoxy layer.

The four medium sized specimens were precast separately to the large beams and transported to Bath for curing and subsequent preparation and strengthening. This series comprised of one control specimen, one U-wrapped specimen, one U-wrapped with bar-in-slot anchorage and one deep embedment specimen. The concrete surfaces for the sheet application were prepared using wet grit blasting during the 28-day curing period. The same local contractor was used as in the case of the surface preparation of the push-off specimens. The edges were rounded identically to the large beam series, keeping the radius constant across the beam sizes at 25 mm, detail of which is shown in Figure 5.10.

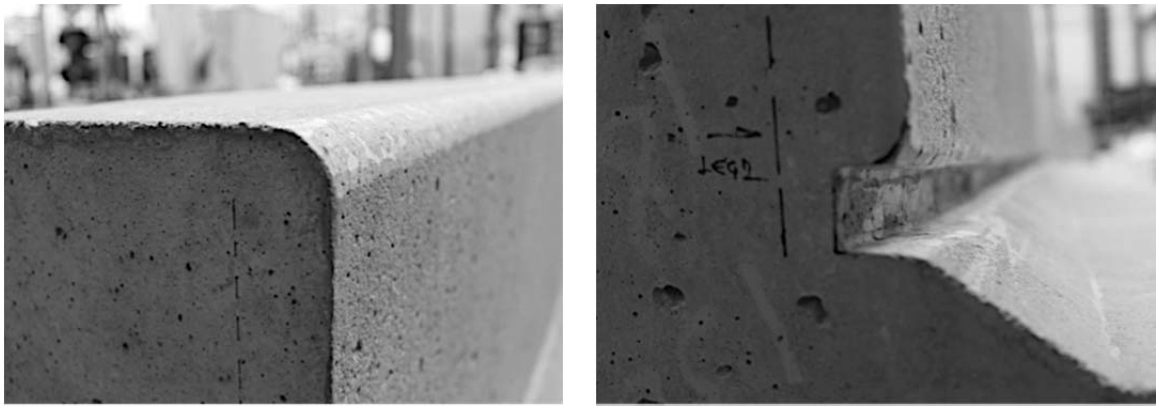

(a) (b)

Figure 5.10 – Medium T-beam preparation for strengthening with externally bonded CFRP sheets: (a) rounded edges and surface after wet grit blasting, (b) anchorage bar channel detail.

The CFRP materials were applied after the specimens were fully cured and dried. The CFRP fabric used for the externally strengthened specimens corresponded to the 'heavily' strengthened scenario (1.3% CFRP) of the large series. To keep the ratio of the CFRP materials and the number of layers constant, one layer of the 'heavy' fabric and one layer of the 'light' fabric was used, as shown in Figure 5.11 (a). In this way, scaling of the CFRP sheets was possible to maintain the ratios throughout the research programme. The heavy fabric was bonded directly onto the concrete to ensure consistency of the CFRP-concrete bond and to obtain comparable data with the large heavily strengthened beams.

CFRP bars of 10 mm diameter were used for the bar-in-slot anchorage in the medium beams strengthened with CFRP sheets with end anchorage. These were of the same type as those used in the large specimens. The bars were moulded into slots 20 mm x 20 mm and the application finished off with a layer of thickened epoxy, as shown in Figure 5.11 (b).

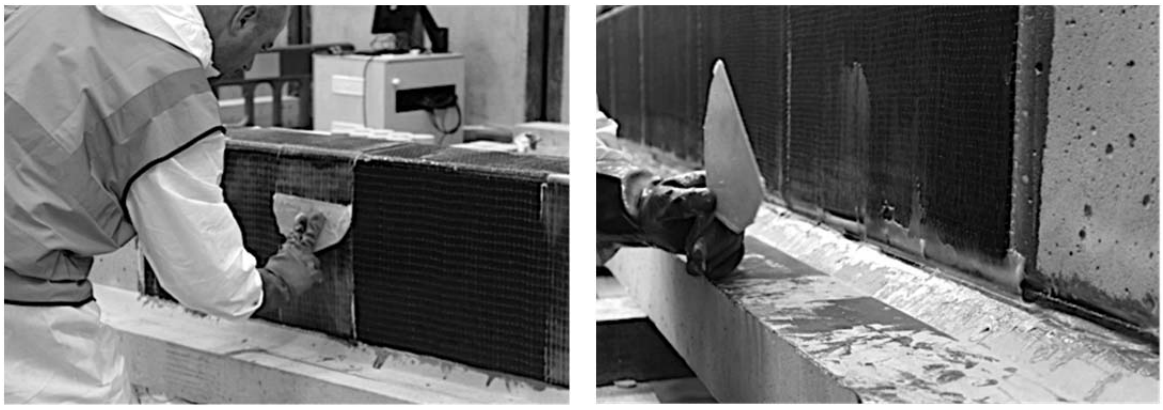

(a) (b)

Figure 5.11 – Medium T-beam strengthening with externally bonded CFRP sheets: (a) CFRP sheet application, (b) bar-in-slot anchorage application.

The deep embedded bars were applied in the same manner as in the large T-beam series, using 10 mm diameter CFRP bars with spacing to maintain ¾ scale, using the same adhesive type. All CFRP bars were sourced from the same batch throughout the entire programme.

5.2.6 Test setup and testing procedure

All beam specimens were tested in three-point bending as a simply supported beam, loaded at a displacement rate of 0.1 mm/minute until failure. The control specimens in both series

were loaded monotonically with the loading paused at pre-determined intervals to mark cracks. The externally strengthened specimens were loaded, completely unloaded and reloaded until failure in stages to observe the beam behaviour under repeated loading. The deep embedment specimens were loaded monotonically without pausing until failure, and cracks marked during testing.

The loading was applied through a plate that was positioned centrally across the entire width of the top flange. The plates were 20 mm thick and 300 mm wide for the large beams and 15 mm thick and 225 mm wide for the medium beams, corresponding to 0.5d of the specimen. The supporting plates were of the same thickness as the loading plate and positioned across the whole width of the web to provide adequate bearing.

The beam was simply supported, positioned on pins at each end of the specimen, with a clear span of 7d between the centres of the supports. The bases were anchored to the strong floor to prevent rocking and potential collapse during testing. The horizontal movement in the support in the tested span was enabled using two layers of lubricated Teflon sheets between two steel plates positioned centrally above the support base at the tested span, see Figure 5.12. The displacement was applied through the top rotary base of the test machine, which was free to rotate to level the loading.

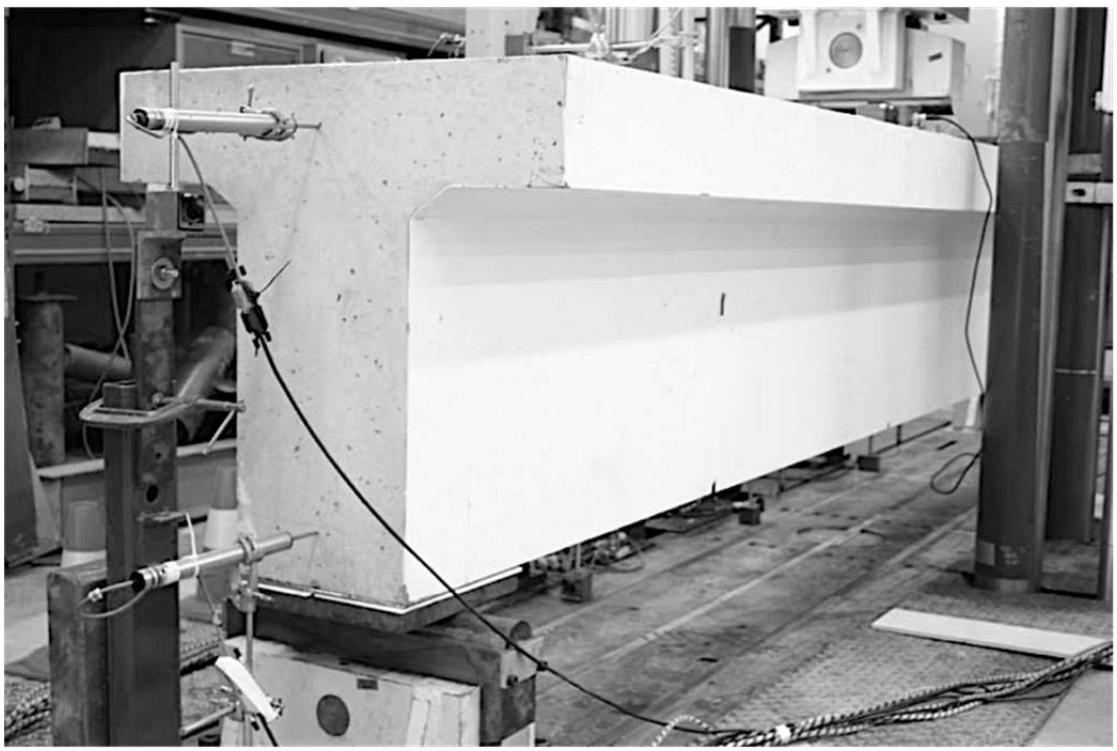

Figure 5.12 – Large T-beam test setup: T-beam in the test rig prior to testing.

5.2.7 Instrumentation

Figure 5.13 shows the schematics of the test arrangement and instrumentation for the beam series.

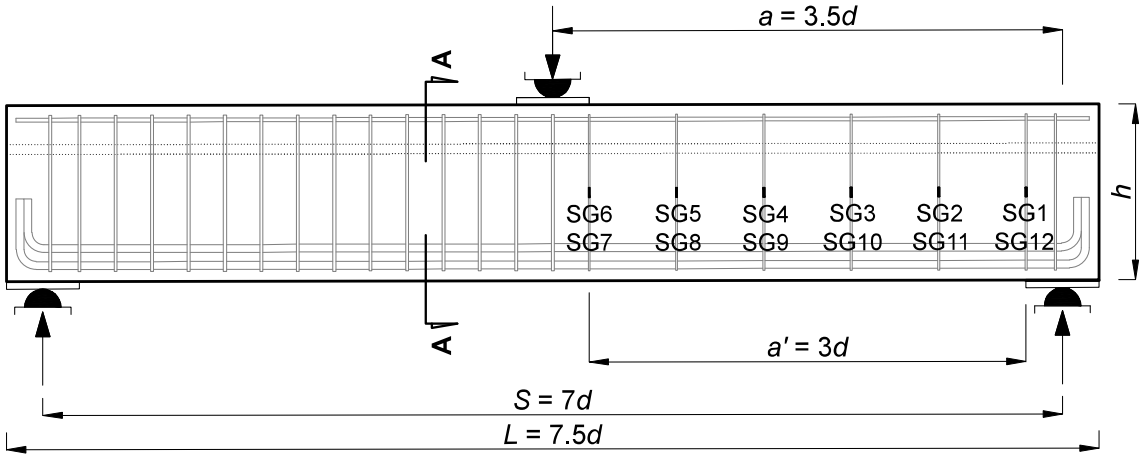

(a)

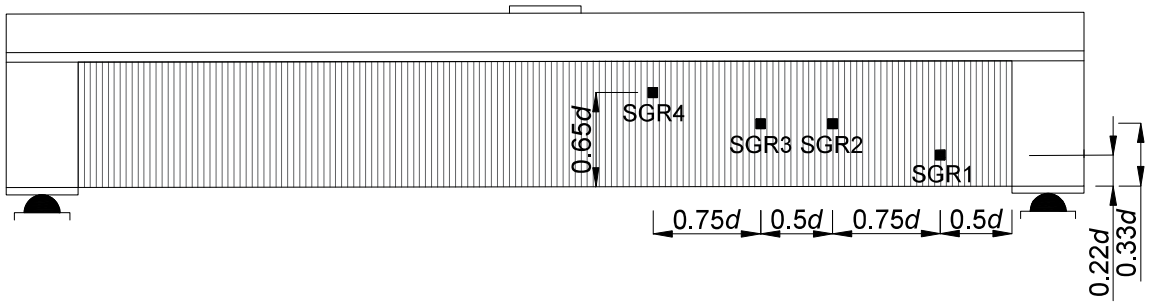

(b)

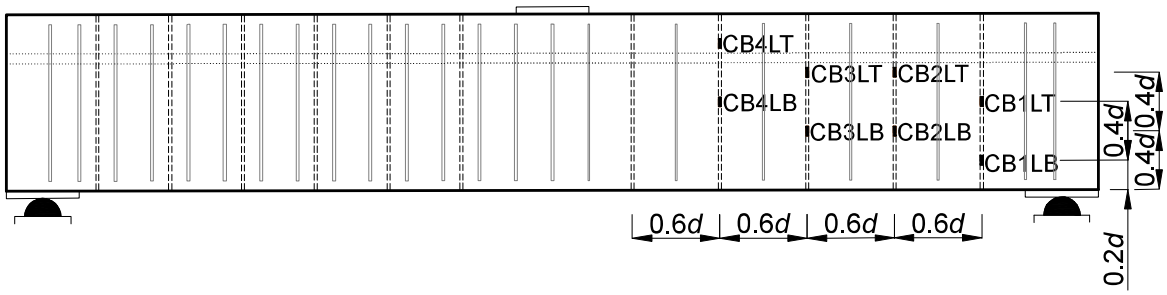

(c)

Figure 5.13 – T-beams test setup and instrumentation: (a) unstrengthened control specimen – long section, (SG1-SG6 rear, SG7-SG12 front), (b) specimen strengthened with externally applied CFRP U-wrap – rear view, and (c) specimen strengthened with deep embedded CFRP bars – long section.

Each specimen had six monitored steel links with two strain gauges each. In total, there were twelve internal strain gauges per specimen for internal steel only. The specimens with externally bonded sheets were equipped with four strain gauge rosettes, resulting in twelve additional channels for data collection per specimen. The strain gauges on the internal steel links were positioned in the centre of each shear leg as shown in Figure 5.13 (a), whereas on the CFRP sheets they were strategically positioned alongside an anticipated shear crack location to capture debonding, see Figure 5.13 (b). Six LVDTs were positioned at midspan and quarter spans at the top and the bottom soffit of the beam.

For the deep embedment specimen, there were eight monitored CFRP bars with two strain gauges each. The location of the strain gauges was also selected to capture debonding of the bars within concrete alongside an anticipated location of the shear crack, similarly to the U-wrapped specimens. During testing of the large unstrengthened control specimen, two additional LVDTs were used to check the horizontal movement of the beam for accuracy of the test setup. Furthermore, the test machine automatically recorded the load and stroke every second. Figure 5.14 shows schematics of loading across the flange and the PTFE layer at support to allow horizontal movement for a simply supported beam.

(a) (b)

Figure 5.14 – T-beams test setup and instrumentation: (a) section through specimen showing internal strain gauge positioning, (b) detail of PTFE layer at support to allow horizontal movement.

To capture the debonding processes and separation of the CFRP sheets in the specimens strengthened with CFRP sheets, a high definition camera was positioned at the edge of the beam. Due to the abruptness with which the CFRP sheets debond, this camera stored images automatically every 5 seconds. To capture the behaviour of the entire beam under

loading, all beams were video-recorded for the duration of each test.

5.2.8 DIC test setup

One DIC camera was carefully aligned with the front face of the specimen for 2D measurements, with images captured automatically every 5 seconds. The details of the DIC setup are shown in Figure 5.15.

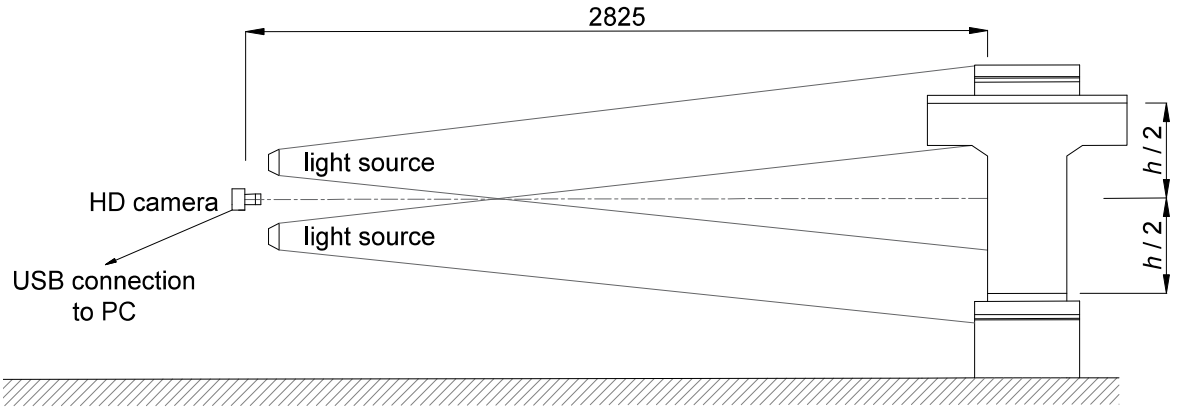

Figure 5.15 – T-beams DIC test setup schematics [mm].

The distance of the camera from the specimen was determined according to the size of the pattern, developed during the testing of the push-off specimens, and the monitored zone to provide accurate measurements. The size of the speckle pattern was determined experimentally prior to testing of the beams, as shown in Figure 5.16 (a).

(a) (b)

Figure 5.16 – DIC pattern and application: (a) determination of speckle size for the large-scale T-beam specimen, (b) application of speckle pattern through a laser-cut stencil using spray paint.

The pattern for the DIC full field displacement and strain mapping was modified during the preliminary tests on the push-off specimens to produce reliable data for such a large monitored area. The modified pattern as well as the application procedure through a custom made laser-cut stencil is shown in Figure 5.16 (b).

5.3 Summary

Ten full-scale reinforced concrete T-beams were designed in two sizes and prefabricated off-site by a certified precaster for further mechanical testing at Bath. The surface preparation and subsequent strengthening was carried out by certified and experienced contractors to ensure bond quality. The beams were equipped with a unique DIC speckle pattern developed in this research programme specifically for the monitoring of the full-scale T-beam specimens. The main objective for the use of the DIC technique was to track surface strains, particularly for the beams with externally strengthened CFRP sheets to detect concrete cracking and debonding. All specimens were equipped with physical strain gauges on the tested steel shear links as well as the CFRP materials used for strengthening. Displacement of the beam was monitored using LVDTs positioned at midspan and at quarter span.

6 T-BEAM TEST RESULTS

6.1 Introduction

This Chapter reports on results and findings obtained from the laboratory testing of the unstrengthened and strengthened large- and medium-scale T-beams. First, a summary of experimental results is presented, followed by results and findings from the tests. For each beam size, the results are divided into categories, based on the strengthening type – unstrengthened control specimen, specimens strengthened with CFRP sheets and deep embedment, and are presented separately.

The outcomes of the experimental investigation for each beam include failure modes, specimen behaviour during and after testing, and internal steel and additional CFRP reinforcement strain profiles. The results from the tests on the beams strengthened with externally bonded CFRP sheets further include strain readings from strain gauge rosettes on the CFRP sheets. Similarly, the deep embedment specimen results include additional strain profiles obtained from the readings on strain gauges on the deep embedded CFRP bars.

The global beam behaviour as well as localized damage and its influence on the beam collapse across both tested sizes are presented in separate sections following the individual beam results for direct comparison. The discussion of the test results follows in Chapter 7.

6.2 Summary of results

All test specimens failed in shear. The ultimate shear force, V_u, was recorded at failure, taken as half the ultimate load, with corresponding midspan displacement, δ_u. V_y represents the shear force at which the internal steel links started to yield, and was determined from strain gauge readings. Midspan displacement corresponding to the shear force at yield of the steel shear links, δ_y, was also determined from the test data.

In the case of both unstrengthened control specimens, LBC and MBC, the shear force recorded when the steel shear links yielded, V_y, was approximately half the ultimate shear force, V_u.

Summary of the test results is presented in Table 6.1.

Table 6.1 – Summary of main experimental results.

Specimen	ρ_v [%]	ρ_f [%]	V_u [kN]	v_u [MPa]	δ_u [mm]	V_y [kN]	δ_y [mm]	Failure mode
LBC	0.1	–	472	2.6	15.6	241	4.8	Shear – brittle
LB1U	0.1	0.7	458	2.5	15.4	409	9.0	Debonding/shear
LB1UA	0.1	0.7	512	2.8	11.8	480	9.5	Debonding/shear
LB2U	0.1	1.3	438	2.4	13.4	396	7.8	Debonding/shear
LB2UA	0.1	1.3	512	2.8	13.7	496	10.7	Debonding/shear
LBDE	0.1	0.2	605	3.4	15.9	443	10.1	Shear
MBC	0.1	–	322	3.2	13.6	163	3.8	Shear – brittle
MB2U	0.1	1.3	306	3.0	9.6	278	6.7	Debonding/shear
MB2UA	0.1	1.3	370	3.7	12.6	305	7.8	Debonding/shear
MBDE	0.1	0.2	482	4.8	17.7	191	4.8	Shear

The U-wrapped specimens in both series showed a decrease in shear capacity of 3% for specimen LB1U, 5% for MB2U and 7% for LB2U, compared with their respective control specimens, regardless of the thickness of the CFRP fabric. The large anchored specimens LB1UA and LB2UA both failed at similar recorded values of ultimate load capacity, regardless of the thickness of the CFRP sheets. The capacity of the unanchored specimen strengthened with the heavier CFRP fabric, specimen LB2U, was 5% lower than that of the specimen strengthened with the lighter CFRP fabric, specimen LB1U. The application of the end-anchorage system for the CFRP U-wraps resulted in 8% increase in shear capacity for the large specimens LB1UA and LB2UA, and 15% for the medium specimen MB2UA. However, if the U-wrap specimens were considered as a baseline for the CFRP-concrete composite beam performance, the bar-in-slot anchorage increased the shear capacity by 12% for LB1UA compared with LB1U and by 17% for LB2UA compared with LB2U. The medium anchored specimen MB2UA showed an increase in shear capacity by 21% compared with its unanchored counterpart specimen MB2U. The values of recorded shear force at steel yield, V_y, in all U-wrapped specimens indicate that the steel had not yielded until the specimen was approaching failure, regardless of the end anchorage.

The deep embedment specimens across both tested sizes showed an increase in shear capacity by 28% (133 kN) and 50% (160 kN) for the large specimen LBDE and the

medium specimen MBDE, respectively. Furthermore, the ultimate load capacity of the medium deep embedment specimen MBDE was comparable to the ultimate capacity reached by the large unstrengthened control specimen LBC.

A summary of strain readings obtained from the strain gauges on CFRP sheets and deep embedded CFRP bars used for strengthening are presented in Table 6.2.

Table 6.2 – Maximum recorded CFRP strains.

Specimen	$\varepsilon_{fe,\ 0\text{-}max}$ [%]	$\varepsilon_{fe,\ 90\text{-}max}$ [%]	$\varepsilon_{fe,\ 45\text{-}max}$ [%]
LB1U	0.15	0.23	-0.37
LB1UA	0.16	0.23	-0.08
LB2U	0.12	0.13	-0.13
LB2UA	0.18	0.20	-0.18
LBDE	–	0.53	–
MB2U	0.22	0.30	-0.43
MB2UA	0.33	0.21	-0.27
MBDE	–	0.73	–

The strains in the CFRP sheets, $\varepsilon_{fe,\ 0\text{-}max}$, $\varepsilon_{fe,\ 90\text{-}max}$ and $\varepsilon_{fe,\ 45\text{-}max}$, are the maximum strains recorded by the 45° strain gauge rosettes in the cross-fibre, the principal fibre and the 45° directions, respectively, obtained from independent strain gauges prior to failure. The CFRP strains recorded on the CFRP bars in the deep embedment specimens LBDE and MBDE correspond with their alignment to strains in the $\varepsilon_{fe,\ 90\text{-}max}$ direction.

The strain values in the U-wrapped specimens across both sizes in the principal fibre direction reached values over 0.20%, apart from specimen LB2U, where the CFRP strains reached 0.13% prior to failure. The strain values reached in the medium U-wrapped specimen MB2U were higher, at 0.30%. The strains in the horizontal cross-fibre direction were lower for all U-wrapped beams, compared with the values recorded in the principal fibre direction, apart from the specimen MB2UA. The strain values in both the principal fibre and the cross-fibre direction were comparable in the case of specimen LB2U. The strains recorded in the 45° direction were relatively high at -0.37% and -0.43% for specimen LB1U and MB2U, respectively. The strain values were particularly low in the case of specimen LB2U.

Strains reached in the CFRP bars in the case of both deep embedment specimens LBDE and MBDE were significantly higher than those in the U-wrapped specimens. The strains recorded were 0.53% and 0.73% for specimen LBDE and specimen MBDE, respectively.

6.3 Specimen LBC

6.3.1 Failure mode

The unstrengthened control specimen failed in diagonal shear. Figure 6.1 shows the shear crack propagation and shear crack at failure.

(a) (b)

Figure 6.1 – Specimen LBC during testing: (a) initial crack inclination, (b) failure.

The critical shear crack initiated at the vicinity of the elastic neutral axis and further propagated as a web shear crack at approximately mid-height of the T-beam, see Figure 6.1 (a). The initial inclination of the crack was much steeper than that of the final crack, at approximately 45°.

The final, shallower shear crack was fully formed at around half the ultimate capacity of the beam, and is also apparent from Figure 6.1 (b). The initial steeper crack remained active until failure as a secondary crack. The inclination of the major shear crack at failure at was approximately 22°.

6.3.2 Observed behaviour

The cracking did not propagate fully to the support region and appeared to have stopped at the level of main reinforcement. A kink was observed in the bottom soffit of the beam

where the shear crack terminated and this is apparent from the difference between Figure 6.1 (a) and Figure 6.1 (b). The critical shear crack fully penetrated the flange at peak load, and is shown in Figure 6.2 (a). The slab failure mode is shown in Figure 6.2 (b).

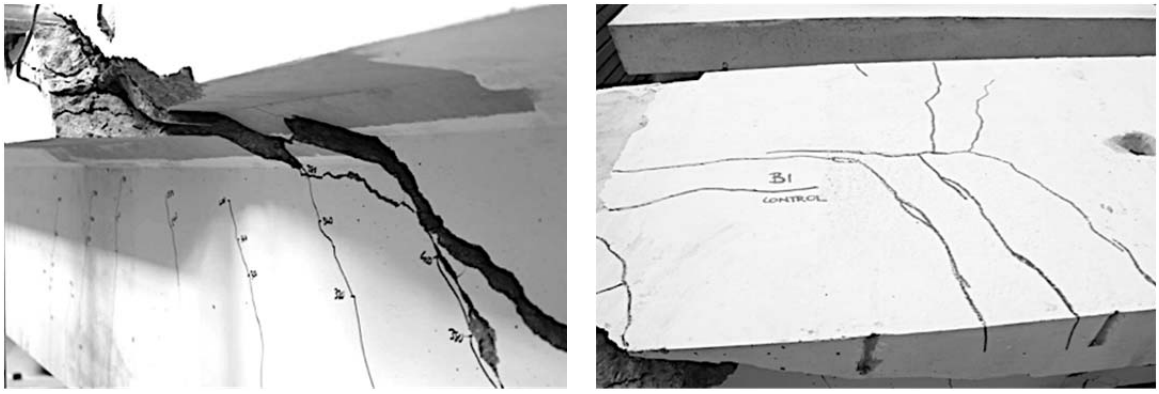

(a) (b)

Figure 6.2 – Specimen LBC after testing: (a) crack penetration into the slab, (b) slab failure mode.

6.3.3 Steel strain profiles

The steel strain profiles obtained from internal strain gauges are presented in Figure 6.3.

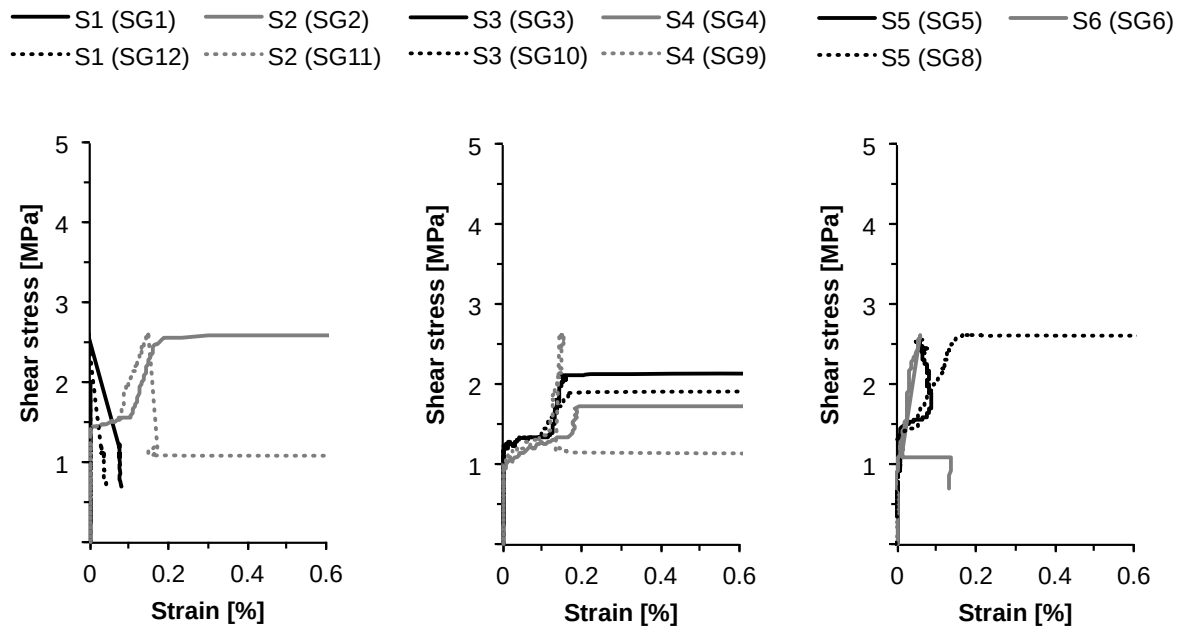

(a) (b) (c)

Figure 6.3 – Specimen LBC – shear stress versus steel strains: (a) support region, (b) middle region and (c) load region.

The readings in the support regions showed very low strains for the shear link closest to the support. However, the neighbouring link reached yield strain levels prior to failure. In the middle region, all the strain gauges reached yield strain prior to and/or at failure. Similarly to the support region, the strain readings in the load region showed that yield strain levels were reached for shear links closer to the middle region whereas the link closest to the load did not register yield.

From the graphs in Figure 6.3 it would appear that some of the strain gauges had failed after the initial cracking in concrete as apparent from Figure 6.3 (b), whereas others seemed to have failed at or immediately after the peak load was reached, see Figure 6.3 (a) and Figure 6.3 (c). The results were not removed from the graphs to observe post-peak readings on the internal strain gauges.

6.4 Specimens LB1U and LB1UA

6.4.1 Failure modes

The failure modes of beams LB1U and LB1U are presented in Figure 6.4.

(a) (b)

Figure 6.4 – Lightly strengthened beam failure modes: (a) specimen LB1U, (b) specimen LB1UA.

Both beams failed in a similar manner, with a web shear crack inclination at approximately 37°. The apparent difference between the anchored LB1UA and unanchored LB1U case is the critical shear crack propagation into the flange. The damage in specimen LB1UA appears more severe, with spalling and apparent deformation of the exposed slab reinforcing bars. A kink formed at the bottom soffit of the LB1UA specimen, which is clearly apparent from both Figure 6.4 (a) and Figure 6.4 (b). The CFRP wraps were

removed after testing for inspection of the extent of the cracking underneath the CFRP sheets as well as the cover layer of concrete. The CFRP from the damaged region separated without difficulties in segments. On the other hand, separation of the CFRP in the undamaged regions where the CFRP-concrete bond was intact was not possible. The separated CFRP sheets were further investigated to determine the locations and amounts of concrete attached to the CFRP surface.

(a) (b)

Figure 6.5 – Separated CFRP U-wraps: (a) specimen LB1U, (b) specimen LB1UA.

Figure 6.5 (a) shows minimum amount of surface concrete attached to the CFRP sheets in the case of specimen LB1U compared to the cover concrete and the surface concrete removed from the slot for LB1UA specimen, see Figure 6.5 (b). The detail shows the extent of concrete cover separation, which corresponded to the full cover concrete to steel stirrups. The region most affected by this separation failure type was near the elastic neutral axis level within the web, which is also apparent from Figure 6.5 (b).

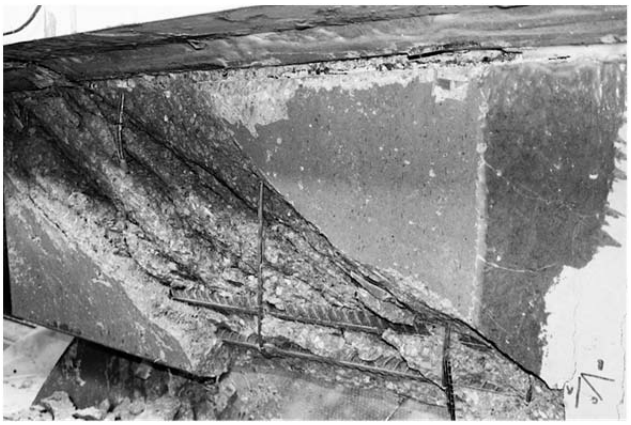

Figure 6.6 – Specimen LB1UA: damage in the shear zone.

Figure 6.6 shows the full extent of the damage after the cracked concrete was probed. The concrete cover was completely removed without using extensive force and the steel reinforcement exposed. Upon closer inspection, steel stirrup S4 in the middle region was bent suggesting that some out of plane movement where concrete was pushed out of the specimen took place.

6.4.2 Observed behaviour

Figure 6.7 shows the load-displacement behaviour of the U-wrapped specimen LB1U and LB1UA in a direct comparison with the unstrengthened control specimen LBC.

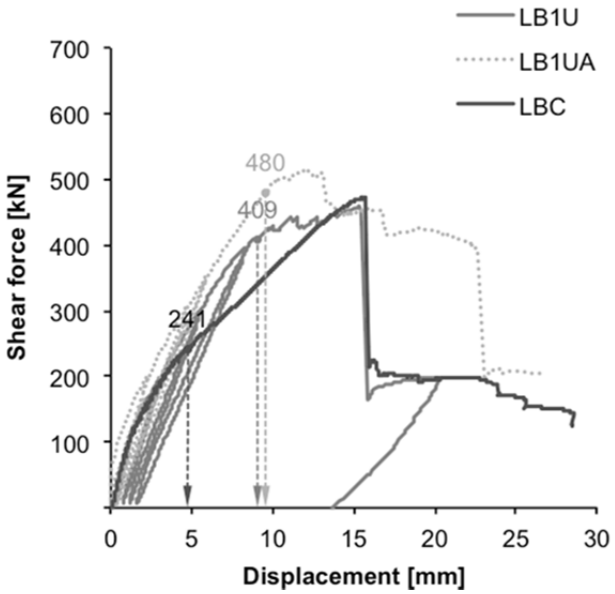

Figure 6.7 – Specimen LB1U and LB1UA: load-displacement curves.

The plots also indicate the shear force at which the internal steel links were registered to start yielding, with corresponding vertical displacement of the beam. The results indicate that the presence of the CFRP U-wrap delayed the yielding of the internal steel links, with yielding at the onset of the CFRP sheets debonding. The strengthened beams loaded and unloaded at certain loads to observe the response of the beams upon reloading.

Figure 6.8 shows critical CFRP debonding stages at which the CFRP started to separate from the concrete surface, when it separated and at the ultimate failure load with corresponding shear force values.

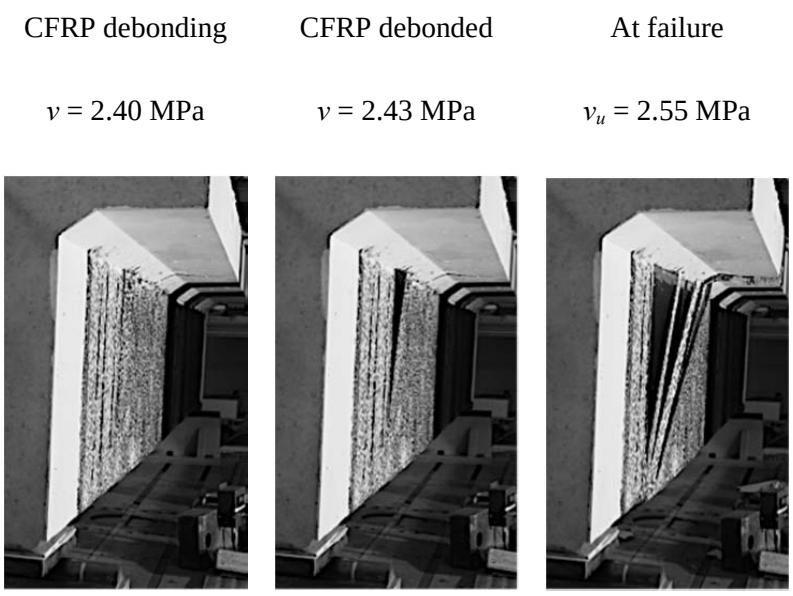

(a)

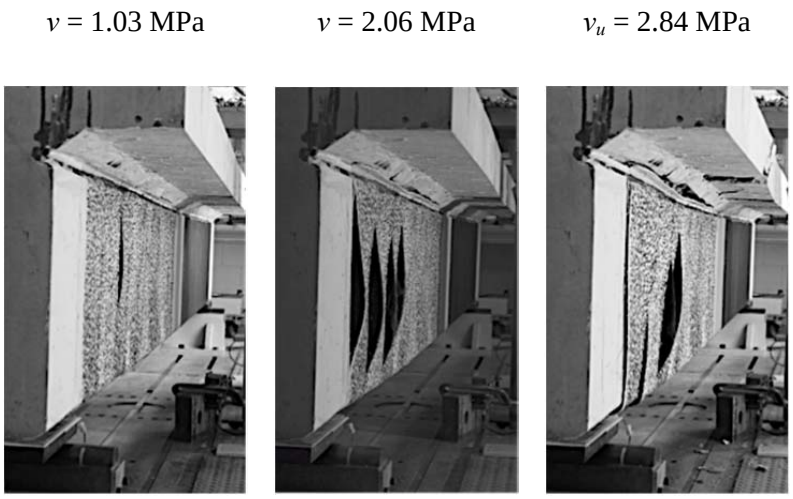

(b)

Figure 6.8 – CFRP U-wrap separation: (a) specimen LB1U, (b) specimen LB1UA.

Figure 6.8 (a) shows debonding processes of the unanchored CFRP sheets in the tested shear span of specimen LB1U. The debonding in the support region was apparent when the shear crack started propagating into the flange. The specimen failed abruptly once the CFRP-concrete bond in the critical shear crack area was damaged through progressive debonding. In the anchored specimen LB1UA, where the debonding at the free edge of the sheets was prevented by the continuous bar-in-slot anchorage system, visible signs of debonding first appeared in approximately the same region as for the unanchored sheets.

However, when the debonding propagated towards the anchored edge of the CFRP sheet, the bar anchoring the sheets was gradually pulled out of the slot. This progressive anchorage failure, shown in Figure 6.8 (b), led to the overall failure of specimen LB1UA. No visual signs of distress were observed until immediately prior to complete CFRP separation. The bar-in-slot anchorage system provided a warning sign through gradual debonding of the bar and led to a marginal increase in shear force resisted before the CFRP sheets fully separated. In neither of the two specimens rupture of the CFRP sheets was observed.

6.4.3 Steel strain profiles

The strain profiles obtained from the strain gauges on internal steel shear links for specimen LB1U are presented in Figure 6.9.

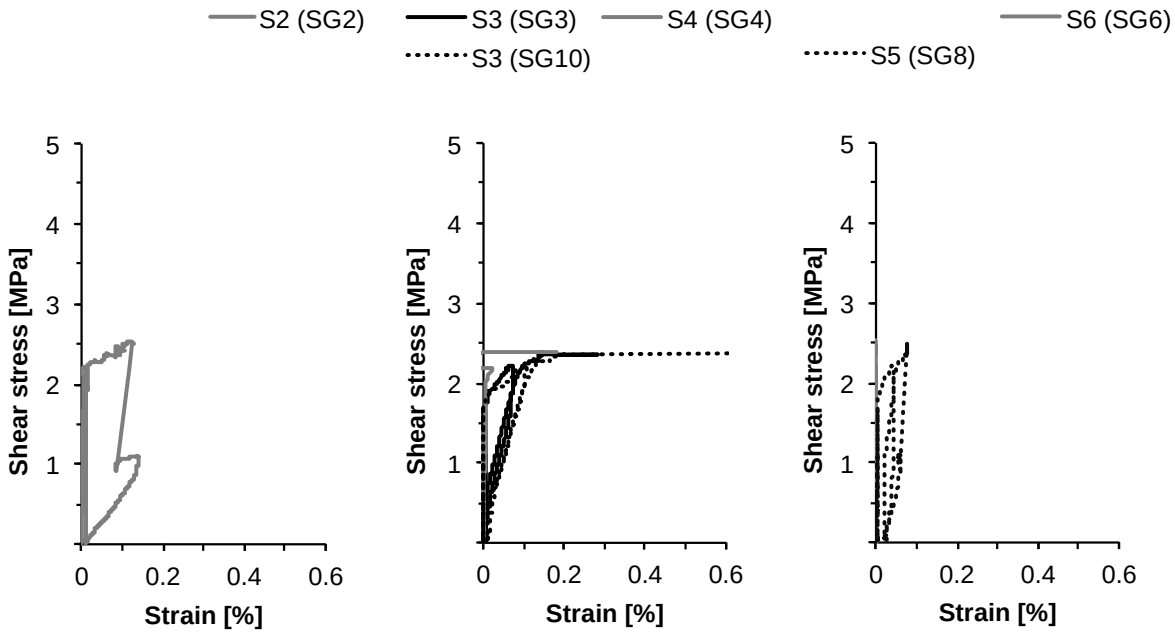

(a) (b) (c)

Figure 6.9 – Specimen LB1U – shear stress versus steel strains: (a) support region, (b) middle region and (c) load region.

The steel links in the support and load region did not reach yield point prior to failure. The strains recorded by strain gauges in the middle region indicated that one of the shear links on the rear face of the specimen was subject to compression prior to reaching yield at

failure. This was initially disregarded as a fluke, however, upon inspection of the U-wrapped test specimens, a possibility exists that the steel links were subject to compression prior to full CFRP separation. This was described in section 6.4.1 and shown in Figure 6.6 for specimen LB1UA.

Similarly to specimen LB1U, the strain gauges located on links in the outermost regions of the tested span of specimen LB1UA registered very low strain levels prior to ultimate load with neither reaching yield point. The second link closest to the support reached yield at ultimate load and only one steel shear link in the middle region yielded prior to failure.

The strain profiles obtained from the strain gauges on internal steel shear links for specimen LB1UA are presented in Figure 6.10.

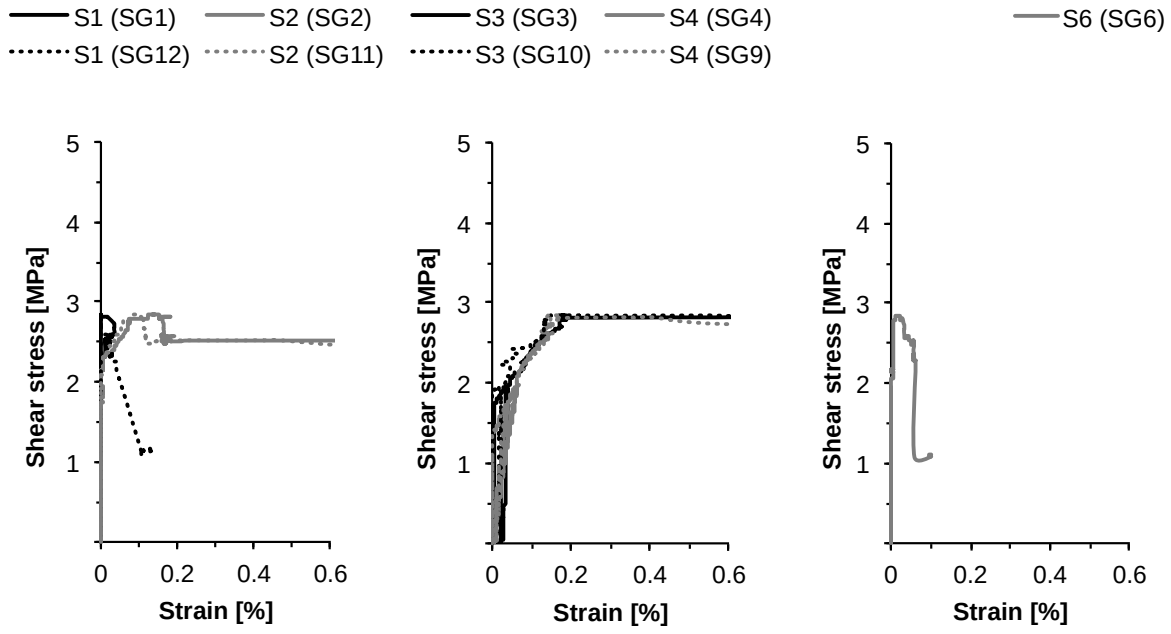

(a) (b) (c)

Figure 6.10 – Specimen LB1UA – shear stress versus steel strains: (a) support region, (b) middle region and (c) load region.

6.4.4 CFRP strain profiles

The CFRP strain profiles in the vertical principal fibre and horizontal cross-fibre direction obtained from the strain gauge rosettes for specimen LB1U and LB1UA are presented in Figure 6.11 and Figure 6.12, respectively.

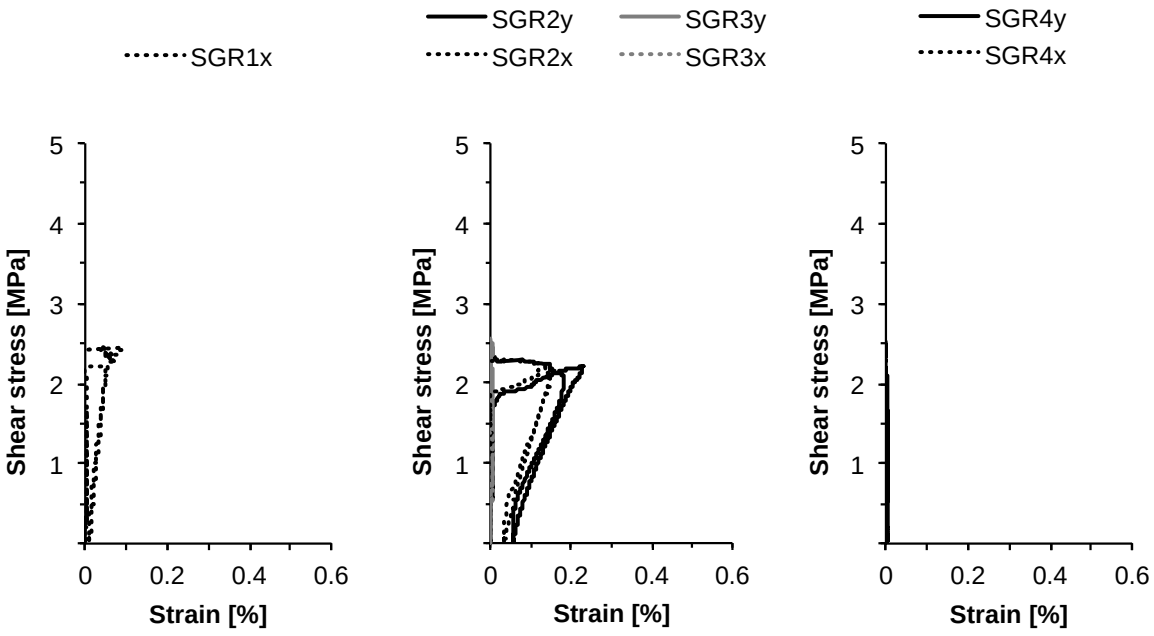

(a) (b) (c)

Figure 6.11 – Specimen LB1U – shear stress versus CFRP strains: (a) support region, (b) middle region and (c) load region.

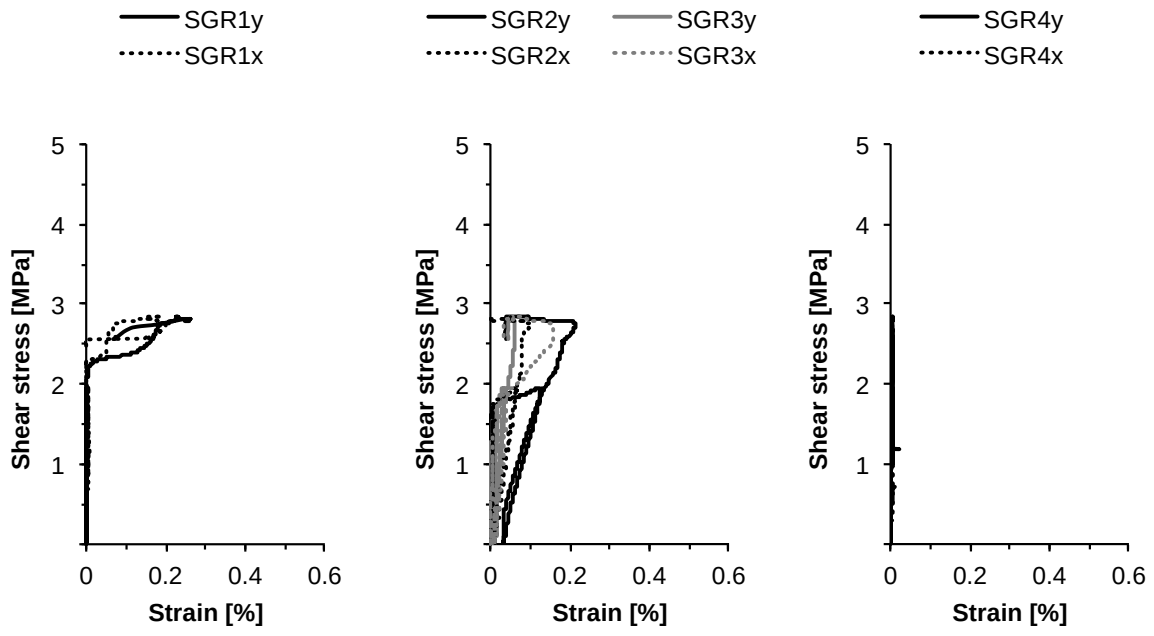

(a) (b) (c)

Figure 6.12 – Specimen LB1UA – shear stress versus CFRP strains: (a) support region, (b) middle region and (c) load region.

Maximum strains in both the vertical and the horizontal direction were recorded in the middle region, with debonding indicated through reversed strains. The strain readings in the outer regions of the tested span remained low under increasing load. The strain readings in the support region showed that debonding of the CFRP sheets occurred in the vertical principal fibre direction.

Specimen LB1UA reached higher strains in the horizontal cross-fibre direction in the support region prior to debonding compared with results from specimen LB1U, suggesting splitting as well as premature debonding may have been prevented by the end-anchorage system. The maximum strains recorded in the middle region were slightly lower than those recorded in specimen LB1U, showing that debonding of the CFRP sheets occurred at lower strain levels. The strains in the load region were consistently low throughout the duration of the test.

6.5 Specimens LB2U and LB2UA

6.5.1 Failure modes

The failure modes of specimen LB2U and LB2UA are presented in Figure 6.13.

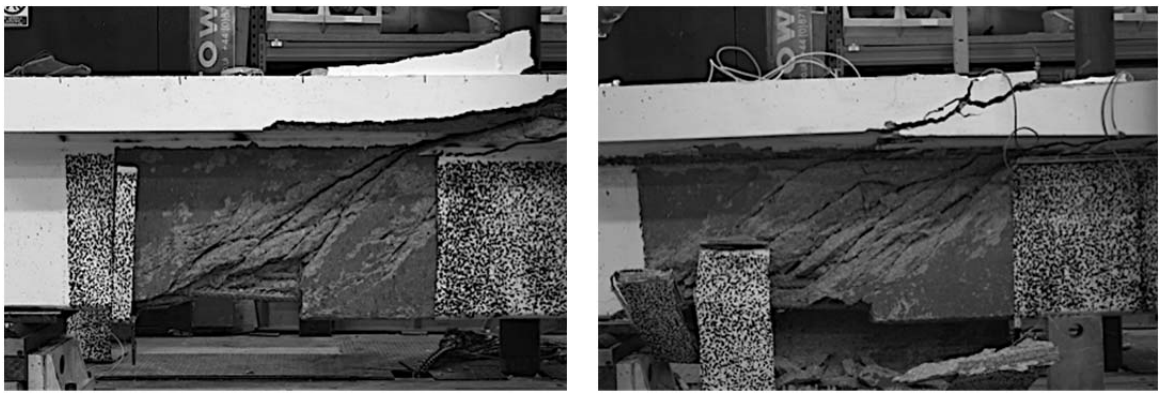

(a) (b)

Figure 6.13 – Heavily strengthened beam failure modes: (a) specimen LB2U, (b) specimen LB2UA.

The major shear crack inclination in both test specimens after the CFRP was removed was approximately 37°. Similarly to the lightly strengthened cases, specimen LB1U and LB1UA, the main difference between the two failure modes was the crack penetration pattern into the flange further away from the load for the specimen with end anchorage,

LB2UA. Furthermore, the damaged area observed in specimen LB2UA is greater than that observed in the unanchored specimen LB2U. In both cases, large amounts of crushed concrete separated from the bottom soffit as well as the sides of the beam upon removal of the separated CFRP. Figure 6.14 shows comparison of the concrete attached to the separated CFRP sheets upon removal after testing obtained from both specimens. The depth of the concrete layer at the critical shear zone locations corresponded to the depth of concrete cover provided to steel stirrups. Marginally larger amount of concrete attached to the CFRP wrap was observed for specimen LB2UA upon inspection.

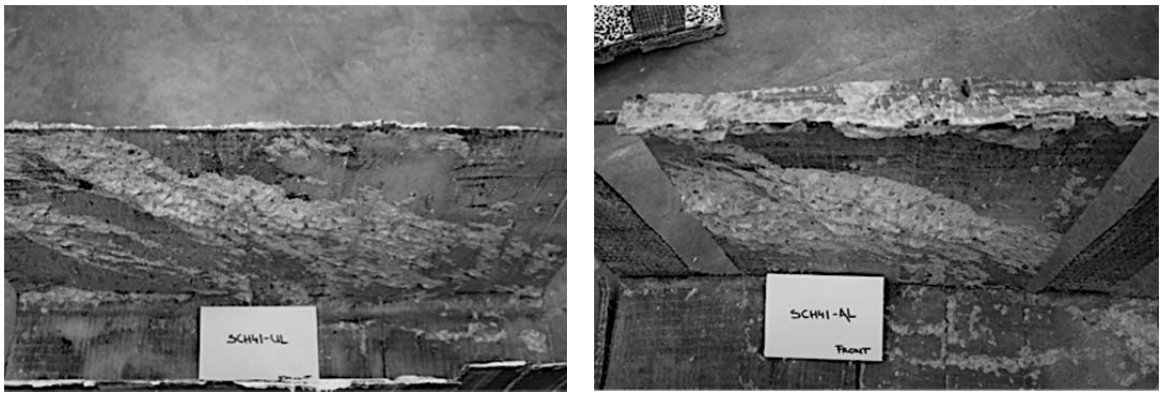

(a) (b)

Figure 6.14 – Separated CFRP U-wraps: (a) specimen LB2U, (b) specimen LB2UA.

Figure 6.15 shows the crack propagation within the slab for the two extremes in strengthening cases, the lightly strengthened LB1U and the heavily strengthened LB2UA, for direct comparison.

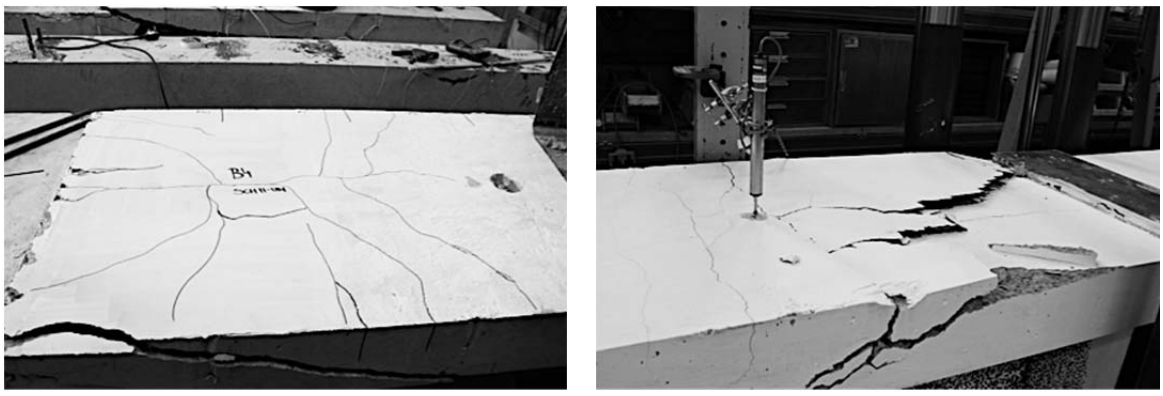

(a) (b)

Figure 6.15 – Slab failure modes in U-wrap systems: (a) specimen LB1U, (b) specimen LB2UA.

The specimen LB2UA exhibited a series of parallel cracks across the full width of the flange at quarter span and cracks perpendicular to these cracks emanating from the location of the loading plate. It is also apparent from Figure 6.15 that the inclination of the crack propagating from the web into the flange is steeper in specimen LB2UA compared with that observed in specimen LB1U.

6.5.2 Observed behaviour

Figure 6.16 shows the load-displacement behaviour of the U-wrapped specimen LB1U and LB1UA in a direct comparison with the unstrengthened control specimen LBC.

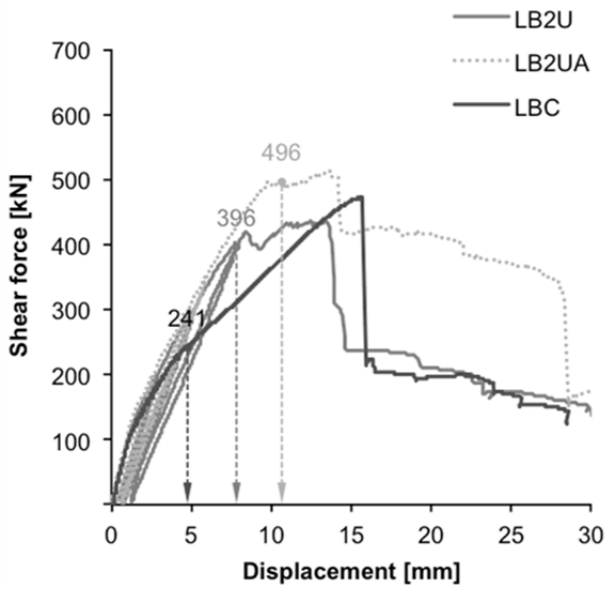

Figure 6.16 – Specimen LB2U and LB2UA: load-displacement curves.

The plots also indicate the shear force at which the internal steel links were registered to start yielding, with corresponding vertical displacement of the beam. The results indicate that the presence of the CFRP U-wrap delayed the yielding of the internal steel links, with yielding at the onset of the CFRP sheets debonding. This corresponds to the similar behaviour of the U-wrapped specimens with the thinner CFRP fabric, specimen LB1U and LB1UA, presented in Figure 6.7.

The debonding processes in both specimens LB2U and LB2UA were captured during testing, similarly to the lightly strengthened cases LB1U and LB1UA, at 5-second intervals. These are presented in Figure 6.17.

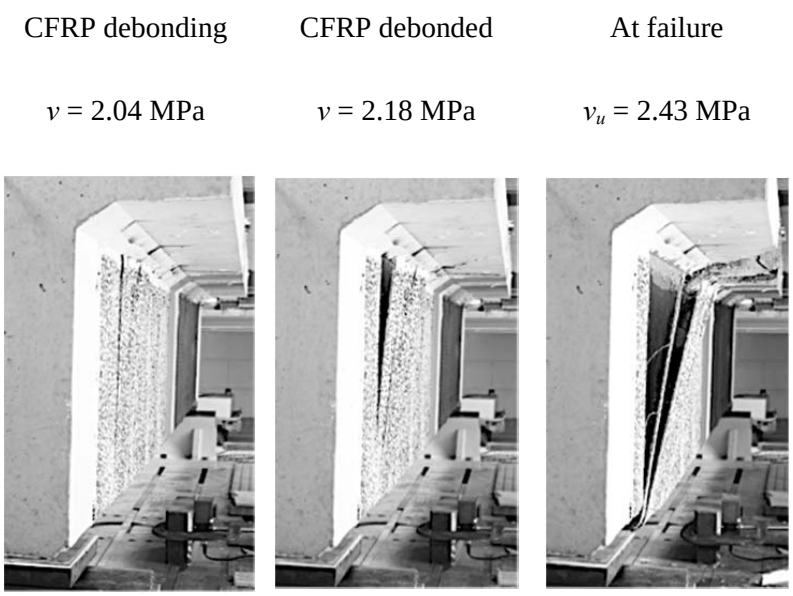

(a)

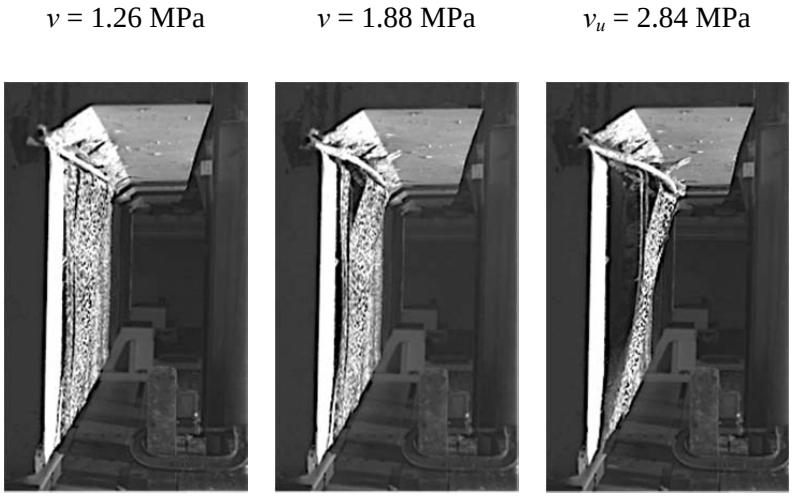

(b)

Figure 6.17 – CFRP U-wrap separation: (a) specimen LB2U, (b) specimen LB2UA.

Figure 6.17 (a) shows the CFRP sheets separating from the specimen LB2U prior to failure. Cracking noises associated with fracturing concrete and the CFRP separation from the concrete surface were noted upon loading to failure, and only upon continued reloading until failure beyond approximately half of the ultimate capacity. Visible signs of debonding were registered shortly before the specimen LB2U failed. The presence of the CFRP bar-in-slot anchorage system in specimen LB2UA only marginally delayed the failure. However, additional visible signs of debonding were observed due to the bar

separating from the slot prior to the failure of the beam. The stages of the progressive sheet debonding behaviour for both specimens with corresponding shear force at each stage are presented in Figure 6.17.

6.5.3 Steel strain profiles

Only the steel links in the middle region reached yield prior to failure whilst the readings in the outer regions remained low throughout testing. In the support region the link closer to the middle region was close to but not yielding at failure.

The steel strain profiles for specimens LB2U and LB2UA are presented in Figure 6.18 and Figure 6.19, respectively. The strain readings across the strain gauges indicate that stirrups in the middle region and those closer to the middle region in both the support and load region either reached yield or were close to yielding prior to failure. Strain gauges on steel links located in the outermost regions of the tested shear span consistently registered lower strains prior to failure.

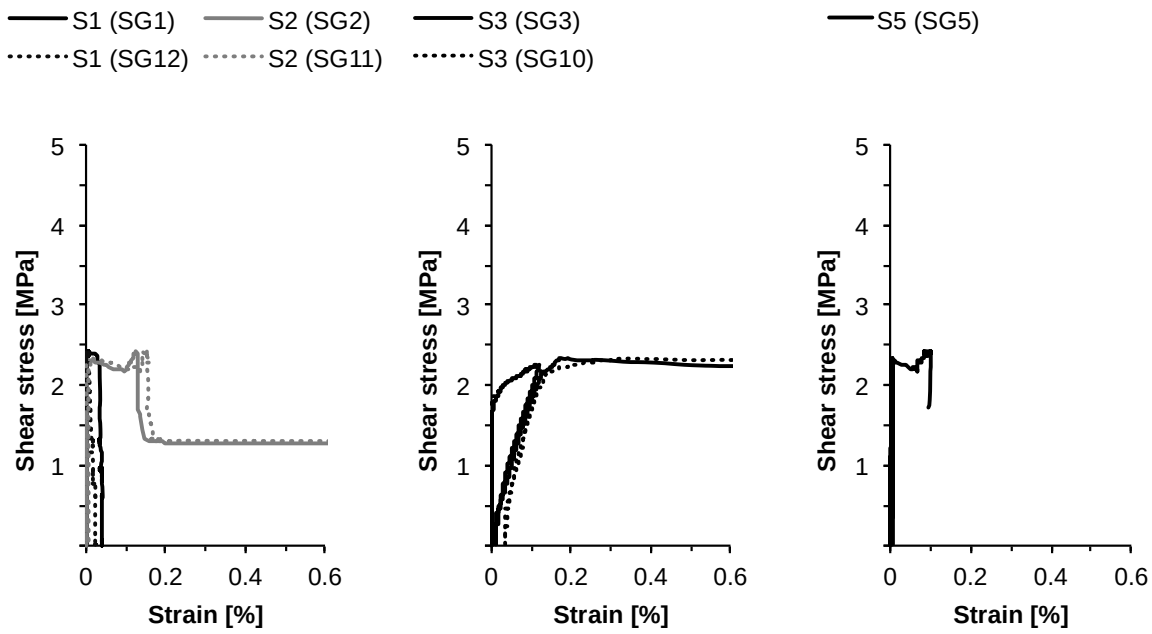

(a) (b) (c)

Figure 6.18 – Specimen LB2U – shear stress versus steel strains: (a) support region, (b) middle region and (c) load region.

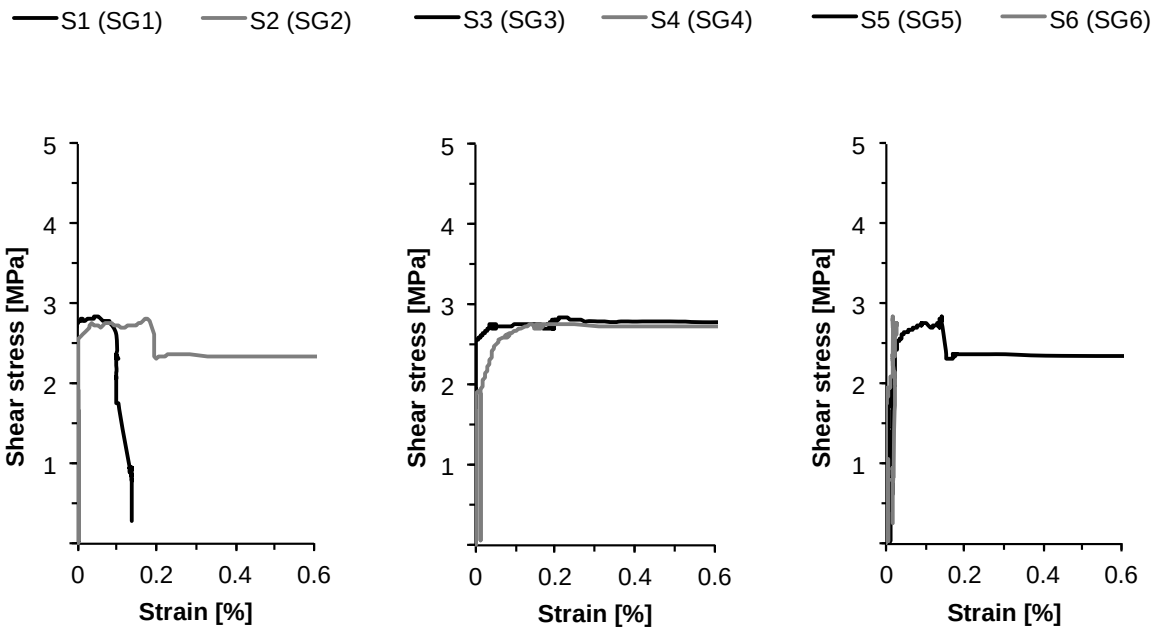

(a) (b) (c)

Figure 6.19 – Specimen LB2UA – shear stress versus steel strains: (a) support region, (b) middle region and (c) load region.

6.5.4 CFRP strain profiles

The CFRP strain profiles for specimen LB2U and LB2UA are presented in Figure 6.20 and Figure 6.21, respectively. The horizontal (cross-fibre) readings from the support region consistently showed low strains prior to failure. In the middle region, strain gauge readings on the steel link closer to the support registered relatively low strains prior to debonding in both the vertical and the horizontal direction. In contrast, readings from steel links further away from the support and closer to the load, exhibited low strains during the entire duration of the test. The strain readings recorded in both the principal fibre and the cross-fibre direction, where both readings were available for comparison, showed comparable strain levels suggesting that stretching of the CFRP sheets was near uniform.

Similarly to the previously discussed specimen LB1U and specimen LB1UA, the CFRP fully debonded prior to failure, indicated by the reversed strains in the graphs. The strains reached in the support and middle region closer to the support were higher for specimen LB2UA than those observed in the same region of specimen LB2U. The strain gauges further away from the support and closer to the location of applied load on the other hand showed very low strains throughout.

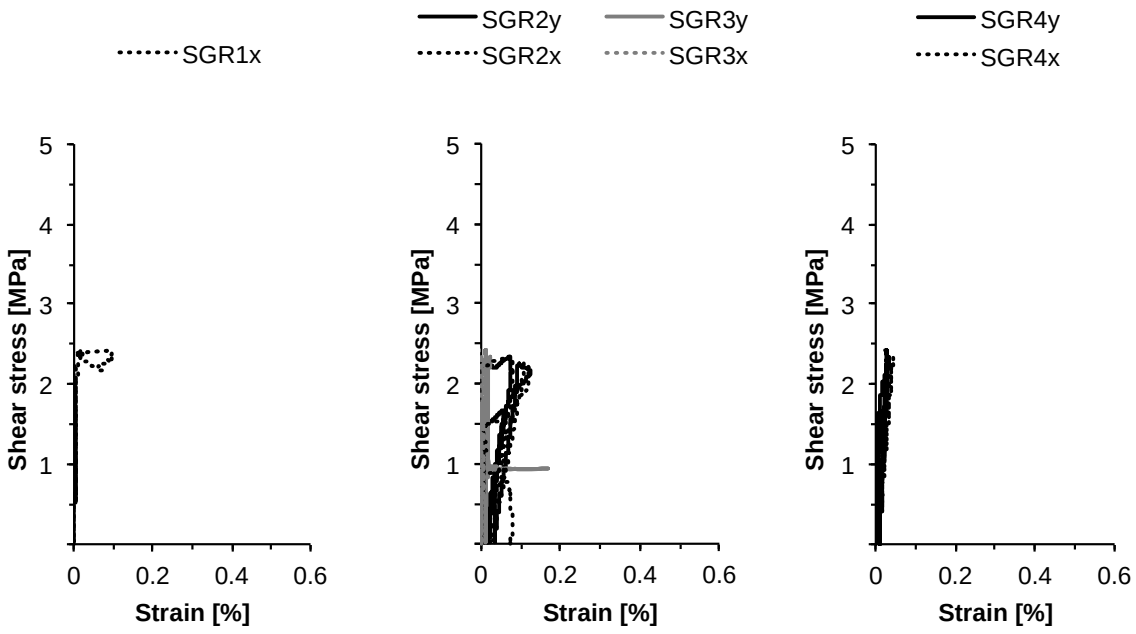

(a) (b) (c)

Figure 6.20 – Specimen LB2U – shear stress versus CFRP strains: (a) support region, (b) middle region and (c) load region.

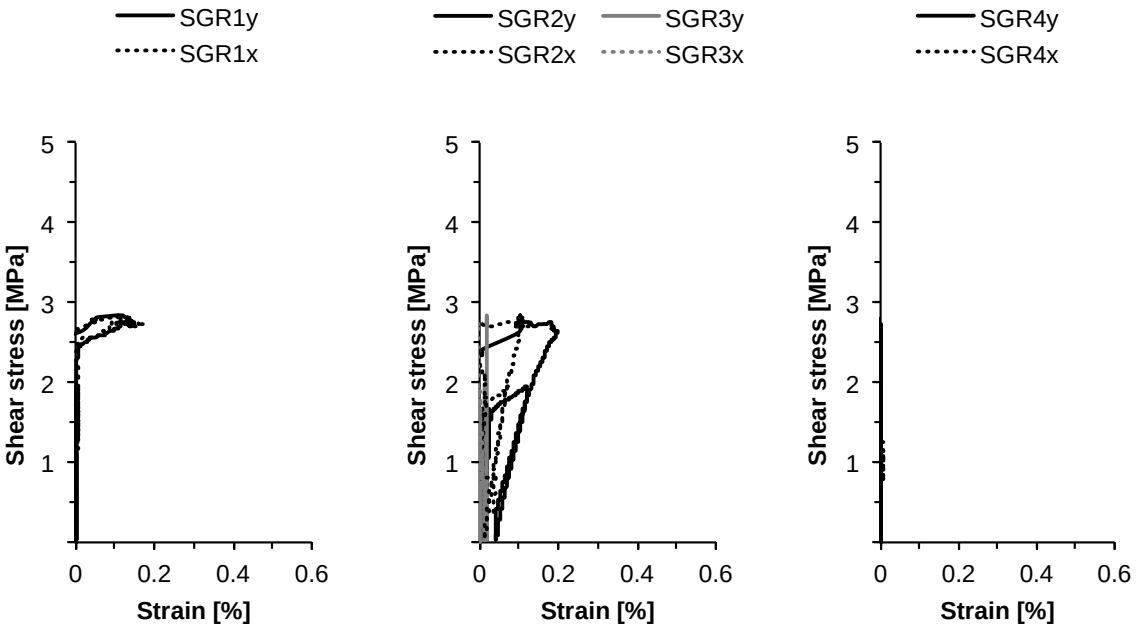

(a) (b) (c)

Figure 6.21 – Specimen LB2UA – shear stress versus CFRP strains: (a) support region, (b) middle region and (c) load region.

6.6 LBDE specimen

6.6.1 Failure mode

The specimen LBDE strengthened with deep embedded bars failed in shear. Figure 6.22 shows the shear crack propagation and shear crack at failure.

(a) (b)

Figure 6.22 – Deep embedment specimen LBDE during testing: (a) initial shear crack inclination, (b) failure mode.

The shear crack inclination was initially approximately 45°, starting and further propagating in a proximity to the location of the elastic neutral axis, see Figure 6.22 (a). Multiple shear cracks were observed parallel to the crack that later developed into the single major shear crack, shown in Figure 6.22 (b).

The crack pattern was dissimilar to that observed in the case of the unstrengthened control specimen LBC as well as that of externally strengthened beams with and without end anchorage. The shear crack upon full opening propagated into the flange and the web under a shallow angle. It can be observed in Figure 6.23 that the cracking in the web propagated along the location of the main reinforcement and had not fully reached the support region. Large amount of spalled concrete separated from the slab at failure, exposing deformed reinforcing bars in the flange.

The damage was inspected post-test, as shown in Figure 6.23. Figure 6.23 (a) shows the shear crack on the rear face of the specimen, altogether with marked cracks during testing. The formation of secondary shear cracks parallel to the major shear crack is apparent from Figure 6.23.

(a) (b)

Figure 6.23 – Specimen LBDE after testing: (a) crack penetration into the slab detail and shear cracking, (b) slab failure mode.

The failure mode of the slab in Figure 6.23 (b) shows a series of cracks perpendicular to the loading plate. These cracks terminated at a crack that crossed the full width of the slab, parallel to the loading plate. Such a fracture pattern, with no cracking observed further away from the loading plate, resembled a punching shear failure. This too was dissimilar to the failure modes observed in the unstrengthened control specimen LBC and all the specimens strengthened with externally applied CFRP sheets where the cracking in the slab was more dispersed.

6.6.2 Observed behaviour

Figure 6.24 shows the load-displacement behaviour of the deep embedment specimen LBDE in a direct comparison with the unstrengthened control specimen LBC. The plots also indicate the shear force at which the internal steel links were registered to start yielding, with corresponding vertical displacement of the beam.

The results indicate that the presence of the deep embedded CFRP bars as additional shear reinforcement also delayed the yielding of the internal steel links, similarly to the specimens strengthened with the CFRP sheets presented in Figure 6.7 and Figure 6.16. The behaviour of the strengthened beam is also stiffer in comparison with the underlying control specimen while achieving similar displacement at peak load. The post-peak behaviour of the strengthened beam indicates that the drop in load occurred due to the debonding of the deep embedded CFRP bars.

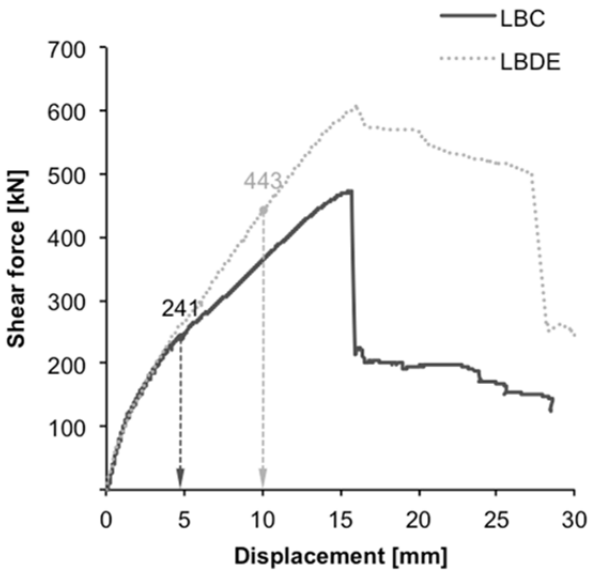

Figure 6.24 – Specimen LBDE: load-displacement curve.

Similarly to the control specimen LBC, the crack propagation was marked during testing on the rear face of the specimen, which was not obstructed by the DIC pattern. A small number of flexural cracks opened in the midspan region, which closed and remained inactive once the shear cracks started to appear and propagate. In the reaction span, only minor cracking was observed close to the load region. No cracking was observed close to or in the support region of the reaction span, see Figure 6.25.

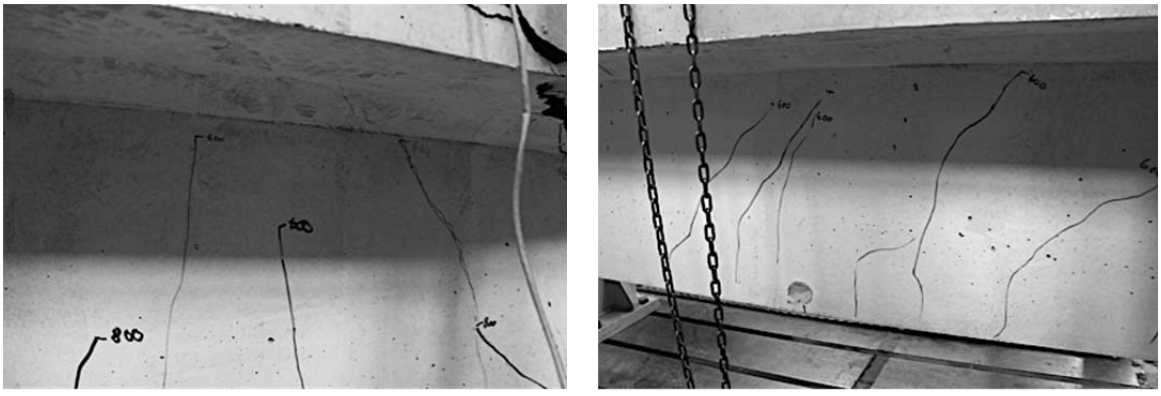

(a) (b)

Figure 6.25 – Cracking in the LBDE specimen: (a) flexural at midspan, (b) reaction span.

6.6.3 Steel strain profiles

The steel strain profiles for specimen LBDE are presented in Figure 6.26.

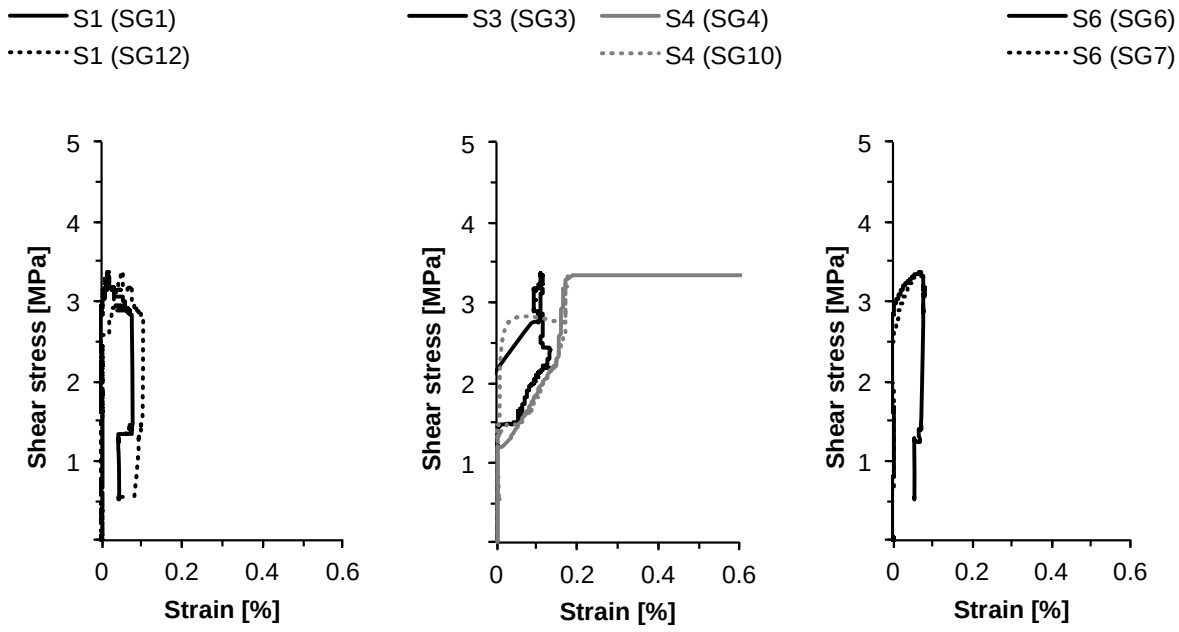

(a) (b) (c)

Figure 6.26 – Specimen LBDE – shear stress versus steel strains: (a) support region, (b) middle region and (c) load region.

The strains recorded in the locations furthest away from the centre of the middle region in the support and load regions, confirm that the steel links have not yielded prior to failure. In the middle region, the strain gauges on the link closer to the load region registered strain levels corresponding to yield strains prior to failure. However, strains registered in the steel link in the same region closer to the support suggested that the steel had not yielded prior to failure. Strains from faulty strain gauges were discarded and are therefore not presented nor are they further used for analysis.

6.6.4 CFRP strain profiles

The CFRP strain profiles obtained from the strain gauges on the deep embedded CFRP bars are presented in Figure 6.27. Similarly to the CFRP strain profiles obtained from the externally bonded sheets, the point where the CFRP fully separated from the concrete surface is apparent from the reversed strains in the graphs.

The strains obtained from strain gauges in the top location of the bars in the region close to the support show strains reaching values in the region close to and over 0.4% at failure,

whereas those in the bottom location show recorded values close to those corresponding to the steel yielding prior to failure. The readings on the CFRP bars in the middle region reached in some cases values over 0.4% prior to failure. The strains measured in the region close to the load were similar to those recorded in the support region, with maximum strains at approximately 0.4%. In all cases of CFRP bars crossing the shear crack, the recorded strains were at or beyond the levels of strains recorded in the steel links, as discussed previously in Section 6.6.3.

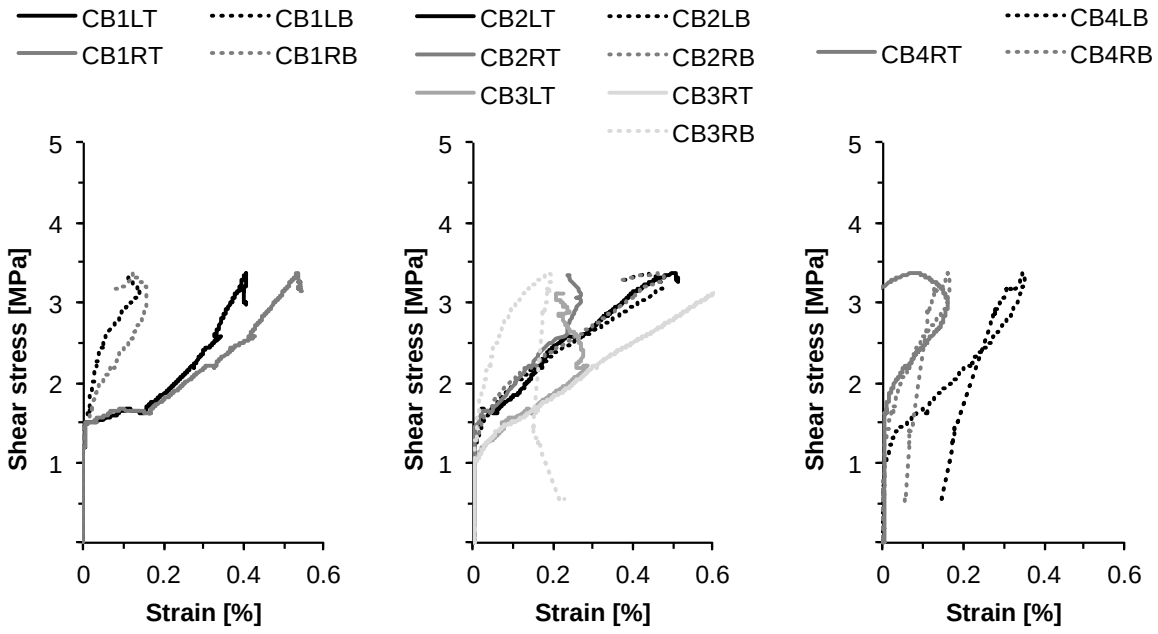

(a) (b) (c)

Figure 6.27 – Specimen LBDE – shear stress versus CFRP strains: (a) support region, (b) middle region and (c) load region.

6.7 MBC specimen

6.7.1 Failure mode

The unstrengthened medium control specimen MBC failed in diagonal shear. The failure mode and the initial crack location are presented in Figure 6.28. From Figure 6.28 (a) it is apparent that the shear crack initiated under an angle of approximately 45° in the web near the location of the elastic neutral axis. This crack further propagated in both directions towards the load and the support. Figure 6.28 (b) shows how the crack further propagated through the web towards the support region and how it penetrated the flange. It is also

apparent from Figure 6.28 (b) that the dispersed cracking in the quarter span region did not reach the support or the region above the support.

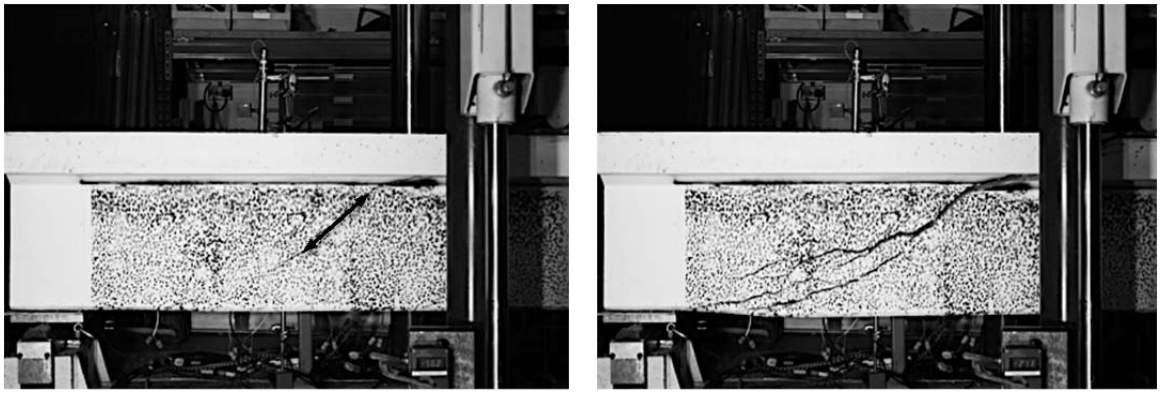

(a) (b)

Figure 6.28 – Medium unstrengthened control specimen MBC during testing: (a) initial shear crack inclination, (b) failure mode.

At failure a kink formed at the bottom soffit of the beam where the crack terminated, apparent from Figure 6.28 (b). The failure mode of the medium control specimen was similar to the large unstrengthened control beam LBC where a shallow major shear crack formed after the initial cracking at approximately 45°, stopping at the level of main reinforcement. However, the kink appeared to be more pronounced in the medium-scale specimen MBC altogether with a more dispersed cracking pattern. The inclination of the major shear crack at failure was approximately 22°, which is also consistent with the observations from specimen LBC discussed in Section 6.3.1.

6.7.2 Observed behaviour

During testing the cracking in the midspan as well as the tested span was monitored and cracks marked on the rear face of the specimen, which was unobstructed by the DIC pattern. Figure 6.29 (a) shows minimum amount of flexural cracking observed under loading. As soon as the shear cracks in the tested span opened, these flexural cracks closed and remained inactive.

The crack pattern in the slab and the final failure mode are shown in Figure 6.29 (b). The cracking was observed in the area between the loading plate and the transportation hook at

quarter span, and appeared to be radiating away from the loading plate towards the edges of the slab.

(a) (b)

Figure 6.29 – Specimen MBC examination after testing: (a) flexural cracking at midspan, (b) slab failure mode.

The flexural cracking at midspan during loading was comparable to that found in the large unstrengthened control specimen. However, the cracking within the slab appeared more dispersed in the case of the medium specimen MBC. The cracking terminated at quarter span similarly to the large control specimen LBC and no evidence was found that the cracking propagated beyond this point. Spalling in the flange where the major shear crack penetrated the slab was observed and is apparent from Figure 6.29 (a).

6.7.3 Steel strain profiles

The strains in the steel shear links during loading were obtained from strain gauges and the strain profiles are presented in Figure 6.30. In the support region the strain readings indicated that while the steel link had yielded on the rear face of the specimen prior to failure, it had not yielded on the front face of the specimen.

In the middle region, the strains obtained from the link closer to the support show that the ultimate capacity of the specimen was reached before the steel yielded. Readings from the link closer to the load in the same region on the other hand indicated that the steel had yielded prior to failure. Neither of the two shear links in the load region had reached yield before the specimen failed. The behaviour of the internal steel links was found similar to that of the large unstrengthened control specimen LBC, presented in Section 6.3.1.

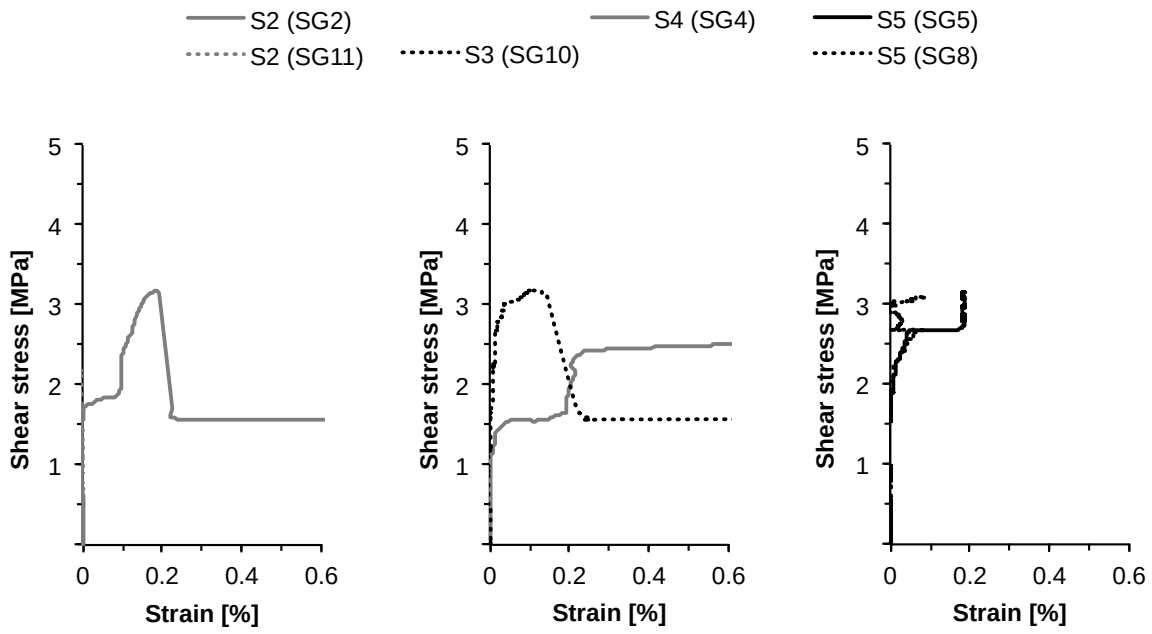

(a) (b) (c)

Figure 6.30 – Specimen MBC – shear stress versus CFRP strains: (a) support region, (b) middle region and (c) load region.

6.8 Specimens MB2U and MB2UA

6.8.1 Failure modes

The failure modes of specimen MB2U and MB2UA are presented in Figure 6.31.

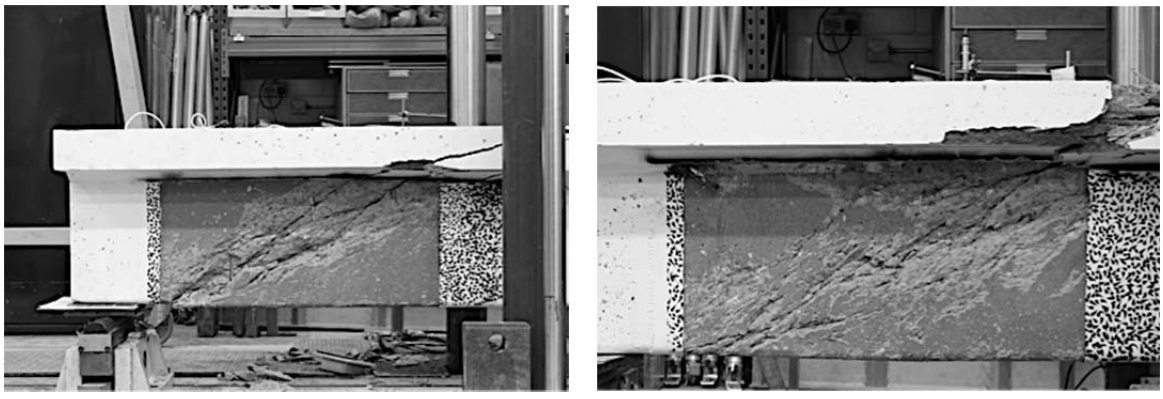

(a) (b)

Figure 6.31 – Failure modes of medium specimens strengthened with CFRP U-wraps: (a) specimen MB2U, (b) specimen MB2UA.

The inclination of the major shear crack was measured after removal of the separated CFRP sheets during inspection and was found to be approximately 37°. The extent of observed cracking in the web was similar for both specimens, regardless of the end anchorage. Furthermore, similar patterns of crack penetration into the flange of the beam to those observed in the corresponding large U-wrapped beams were noted. In the case of specimen MB2UA with the end-anchorage system a steeper crack and spalling in the flange were observed compared to the specimen MB2U without the bar-in-slot anchorage.

Figure 6.32 (a) shows the extent of the damage within the flange at crack penetration from the web of the beam and Figure 6.32 (b) shows the topside view of the flange after testing.

(a) (b)

Figure 6.32 – Anchored U-wrap specimen MB2UA after testing: (a) crack propagation into the slab detail, (b) slab failure mode.

The cracking within the flange appeared very concentrated and emanating from the centre of the loading plate towards the quarter span where the crack propagated towards the edges at an angle of approximately 45°.

6.8.2 Observed behaviour

Figure 6.33 shows the load-displacement behaviour of the medium U-wrapped specimen MB2U and MB2UA in a direct comparison with the unstrengthened control specimen MBC. The plots also indicate the shear force at which the internal steel links were registered to start yielding, with corresponding vertical displacement of the beam.

The results indicate that the presence of the CFRP U-wrap delayed the yielding of the internal steel links, with yielding at the onset of the CFRP sheets debonding. This

corresponds to the similar behaviour of the large U-wrapped specimens presented in Section 6.4 and Section 6.5.

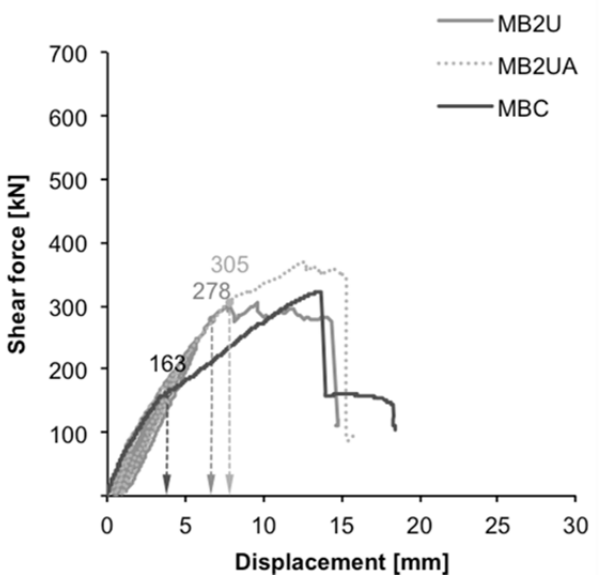

Figure 6.33 – Specimen MB2U and MB2UA: load-displacement curves.

The debonding processes observed and recorded for specimens MB2U and MB2UA are presented in Figure 6.34 (a) and Figure 6.34 (b), respectively.

In both cases no visible signs of debonding or distress were observed until the CFRP sheets started to separate from the concrete surface. In both cases this visible debonding occurred shortly before the specimen failed. The onset of CFRP debonding in specimen MB2UA was delayed by the bar-in-slot anchorage system, compared with the behaviour of the sheets in the unanchored specimen MB2U. This had caused a more abrupt and explosive failure, with nearly no prior warning.

At failure the externally bonded CFRP sheets without the bar-in-slot anchorage in specimen MB2U were visibly separated from the web of the beam. In the case of specimen MB2UA, this was prevented by the end anchorage. Similarly to the large-scale beams with anchorage, the bar debonded along the length of the applied CFRP sheets. However, in the specimen MB2UA the bar did not fully debond at the end support and remained in the slot. As soon as the CFRP fully debonded in the support region, a slip occurred, which resulted in a kink at the bottom soffit, which is apparent from Figure 6.34 (b).

The CFRP sheets removed after testing were further inspected for the amount of surface concrete attached to them. The separated CFRP wraps are shown in Figure 6.35.

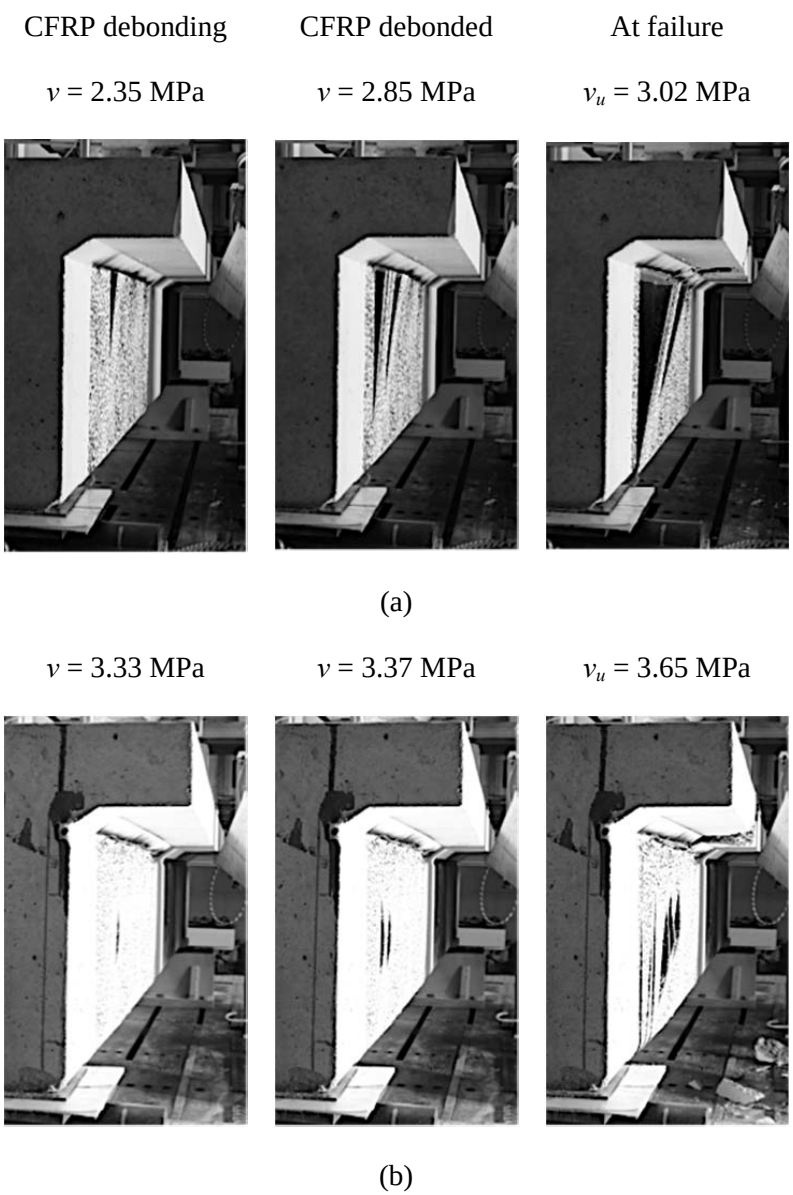

Figure 6.34 – CFRP U-wrap separation: (a) specimen MB2U, (b) specimen MB2UA.

In the case of specimen MB2U, shown in Figure 6.35 (a), the continuous CFRP sheet split in three segments. The segment closest to the support, right in Figure 6.35 (a), was the most affected by splitting of the CFRP between the strands of the unidirectional CFRP fabrics. The middle region remained intact and the portion from the region closest to the load, left in Figure 6.35 (a), was affected by splitting only in the close proximity to the edge of the CFRP wrap. The rest of the CFRP U-wrap remained attached to the specimen and could not be removed. The amount of concrete attached to the inside of the CFRP

wrap was consistent with the amounts found in the corresponding large-scale specimen LB2U. The extent of cracking into the web was approximately the depth of the cover concrete along the location of the major shear crack.

(a) (b)

Figure 6.35 – Separated CFRP U-wraps: (a) specimen MB2U (rear view), (b) specimen MB2UA.

Figure 6.35 (b) shows the inside view of the CFRP wrap removed from specimen MB2UA. The splitting of the CFRP wrap was similar to that found in specimen MB2U. The split strips in the support region were approximately 25 mm wide and attached to the CFRP bar-in-slot anchorage, which was fully attached to the CFRP U-wrap upon removal.

6.8.3 Steel strain profiles

The strains obtained from strain gauges on steel shear links for specimen MB2U and MB2UA are presented in Figure 6.36 and Figure 6.37, respectively.

For specimen MB2U, the strain gauges located on links the furthest away from the middle region consistently showed low readings for the duration of the test. The strain gauges on links in the outer regions closer to the middle region showed that the strain levels in these shear links reached values close to yielding prior to failure.

In the middle region both shear links yielded after the CFRP sheets separated but before the ultimate load was reached. In the specimen MB2UA, the steel links in the middle region yielded prior to failure. The strains in the shear links closest to the outer ends of the support and load regions were consistently low throughout testing. The strains measured in these outer regions on links closer to the middle region showed that while one leg of the link had yielded the other had not reached yield prior to failure.

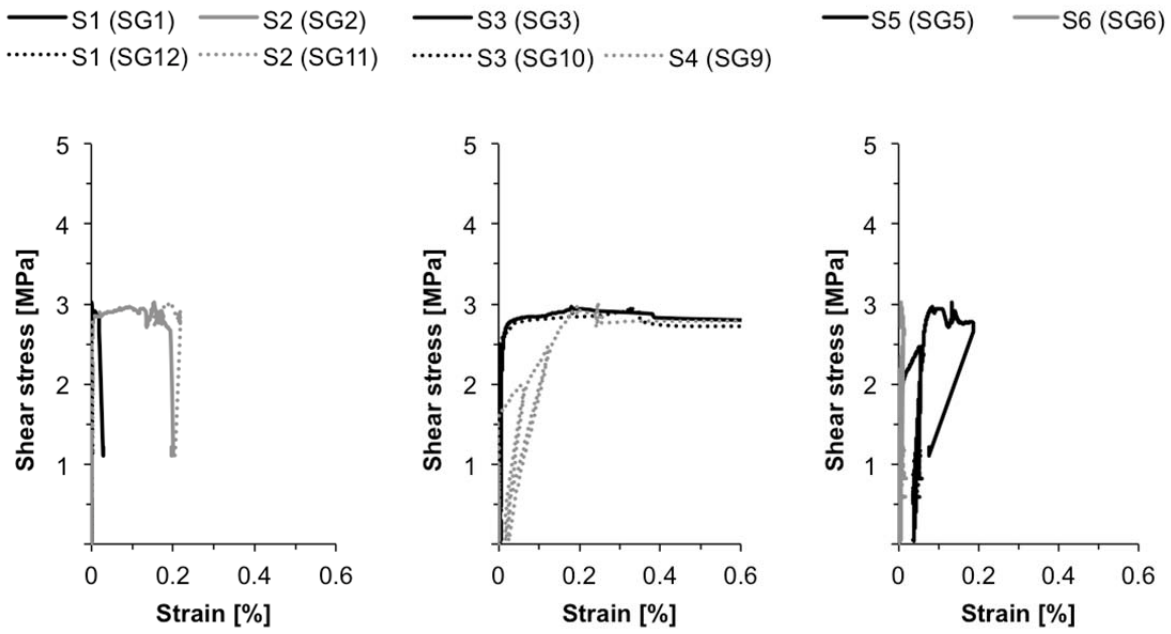

(a) (b) (c)

Figure 6.36 – Specimen MB2U – shear stress versus steel strains: (a) support region, (b) middle region and (c) load region.

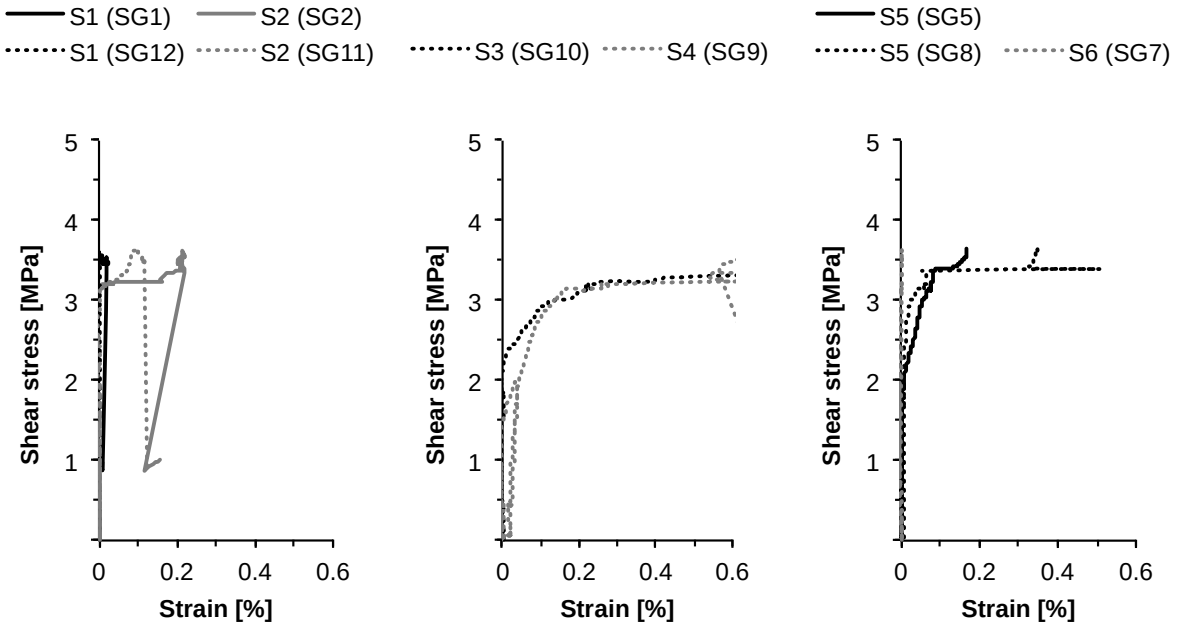

(a) (b) (c)

Figure 6.37 – Specimen MB2UA – shear stress versus steel strains: (a) support region, (b) middle region and (c) load region.

6.8.4 CFRP strain profiles

The CFRP strain profiles for specimen MB2U are presented in Figure 6.38.

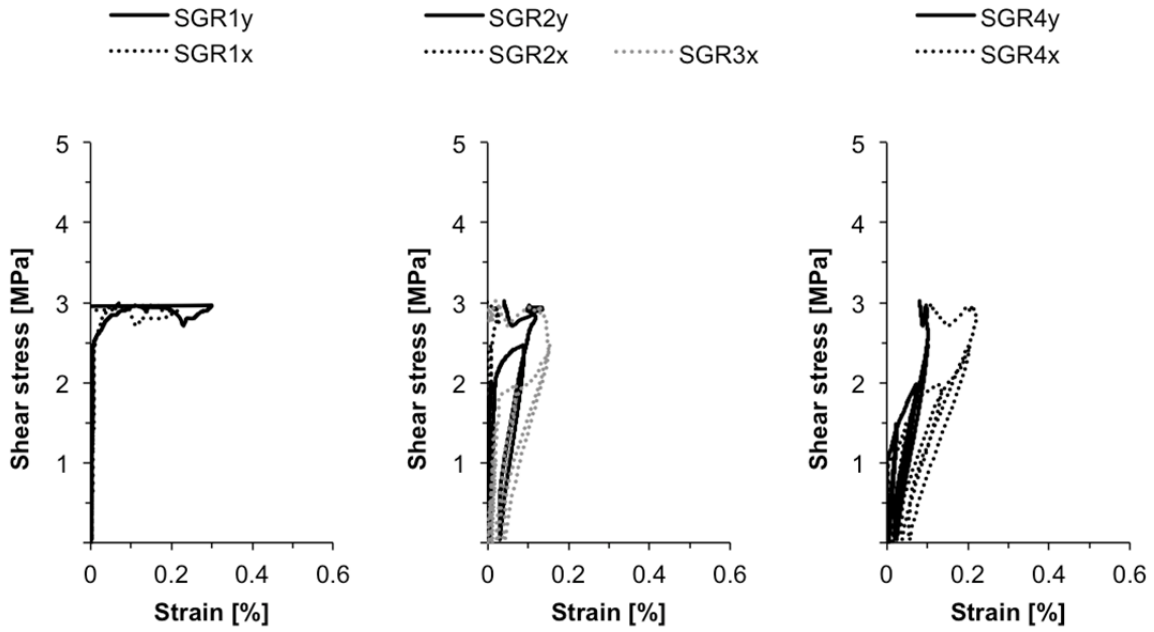

(a) (b) (c)

Figure 6.38 – Specimen MB2U – shear stress versus CFRP strains: (a) support region, (b) middle region and (c) load region.

The highest strains were measured in the vertical principal fibre direction in the support region and the reversed strains indicate that the CFRP fully separated at failure. The strains measured in the middle and load regions were considerably lower. However, in these regions the separation of the CFRP is also indicated through reversed strains, albeit at lower strain levels, suggesting that a premature CFRP separation occurred prior to or close to failure.

The maximum strain levels reached across the applied strain gauges in the principal fibre direction were consistent with the steel stirrup yielding strains, discussed above. Apart from the strain gauge in the middle region closer to the load, all strain gauge readings show higher strains in the horizontal cross-fibre direction, which would suggest that the CFRP stretching was not uniform. In all cases, however, the CFRP fully separated from the concrete surface prior to or at failure. The CFRP strain profiles obtained for the specimen MB2UA are presented in Figure 6.39.

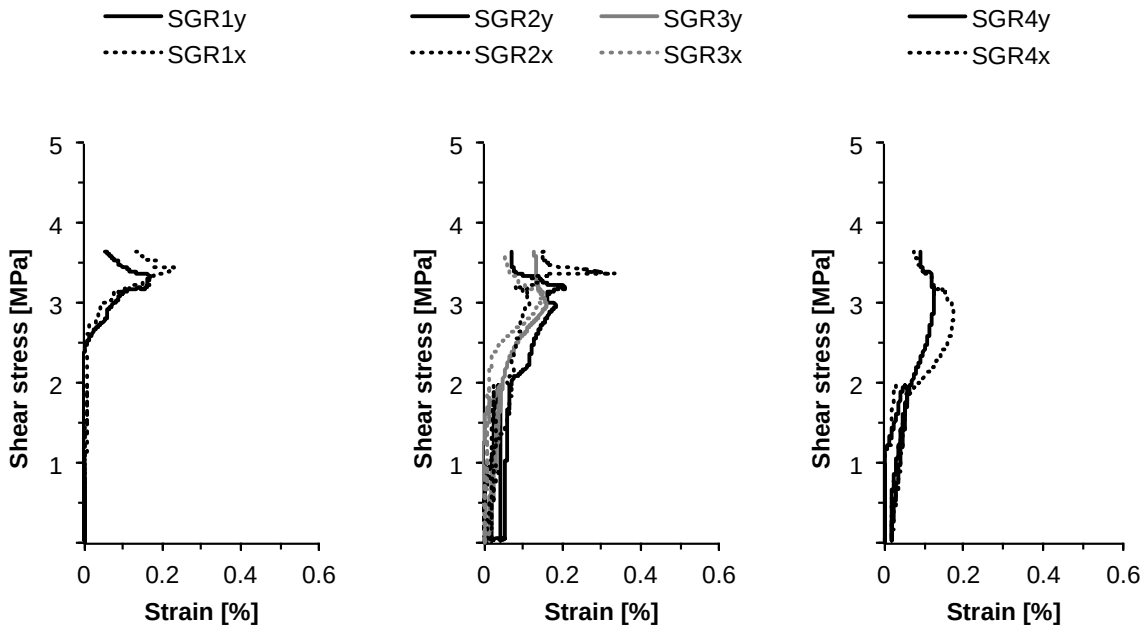

(a) (b) (c)

Figure 6.39 – Specimen MB2UA – shear stress versus CFRP strains: (a) support region, (b) middle region and (c) load region.

6.9 MBDE specimen

6.9.1 Failure mode

The crack pattern and the failure mode of specimen MBDE are shown in Figure 6.40.

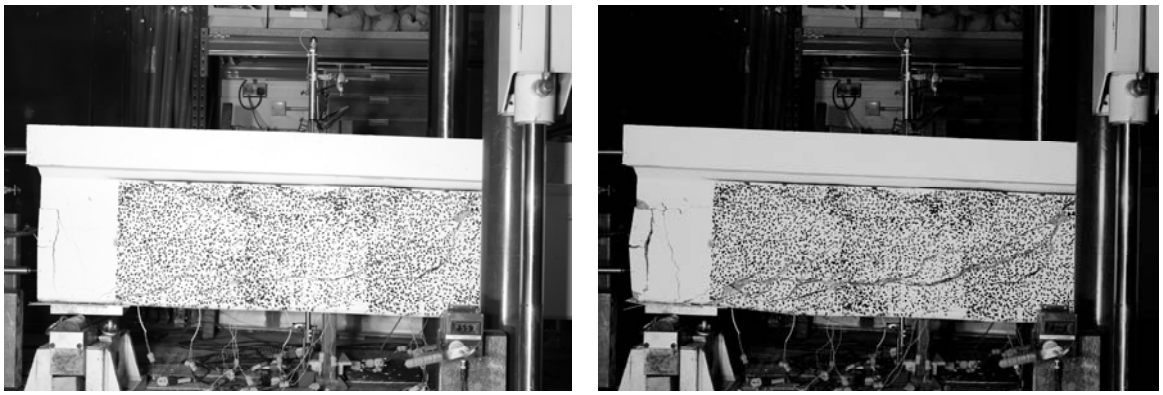

(a) (b)

Figure 6.40 – Specimen MBDE: (a) initial shear crack inclination, (b) failure mode.

The initial inclination of the series of diagonal cracks was at an angle of approximately 45° with subsequent cracking at a much shallower angle. The initial web shear crack further propagated within the web along the main reinforcement. Spalling of the concrete caused by the pulling out of the hooked reinforcing bars at support in the test span was observed shortly after the initial shear crack fully opened. The concrete in the support zone fully separated from the specimen, as is apparent from Figure 6.40 (b).

The specimen was inspected after testing. Detail of the concrete spalling at the main reinforcement anchorage zone is shown in Figure 6.41 (a). The extent of cracking on the rear face of the specimen unobstructed by the DIC pattern shows displacement of the cracked concrete segments along the zone of main reinforcement.

(a) (b)

Figure 6.41 – Specimen MBDE after testing: (a) concrete spalling, (b) slab failure mode.

The slab failure mode is shown in Figure 6.41 (b). Minimum amount of cracking was observed on the topside of the slab with one major crack along the loading plate. This mode of failure resembled that of punching shear failures in slabs.

6.9.2 Observed behaviour

Figure 6.42 shows the load-displacement behaviour of the medium deep embedment specimen MBDE in a direct comparison with the unstrengthened control specimen MBC. The plots also indicate the shear force at which the internal steel links were registered to start yielding, with corresponding vertical displacement of the beam.

The results indicate that the presence of the deep embedded CFRP bars as additional shear reinforcement did not delay the yielding of the internal steel links, unlike in the case of all

strengthened beams described in the previous Sections. The drop in load in the case of the MBDE specimen was less abrupt than in the case of the unstrengthened control specimen MBC. Greater vertical displacement was also observed for the MBDE specimen prior to failure as well as post peak.

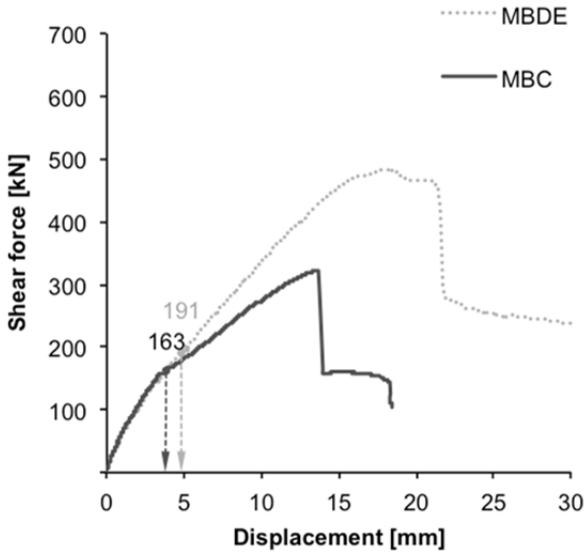

Figure 6.42 – Specimen MBDE: load-displacement curve.

The cracking in the midspan and the reaction span was also monitored during testing on the rear face of the specimen and is shown in Figure 6.43 (a) and Figure 6.43 (b), respectively.

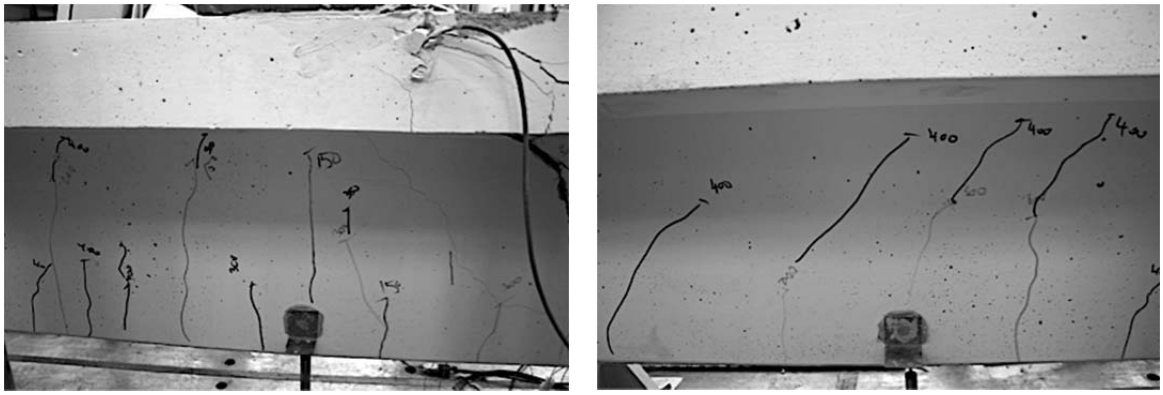

(a) (b)

Figure 6.43 – Cracking in the MBDE specimen: (a) flexural cracking at midspan, (b) shear cracking in the reaction span.

From Figure 6.43 (a) it is apparent that the flexural cracks remained active until large midspan deformations and closed only after the major flexural shear crack had opened. The crack penetrated the flange in a close proximity of the loading plate and propagated from the major shear crack. The shear cracks in the reaction span opened at lower loads at the same time as in the tested span and remained unchanged thereof.

6.9.3 Steel strain profiles

The steel strain measurements for the MBDE specimen are presented in Figure 6.44.

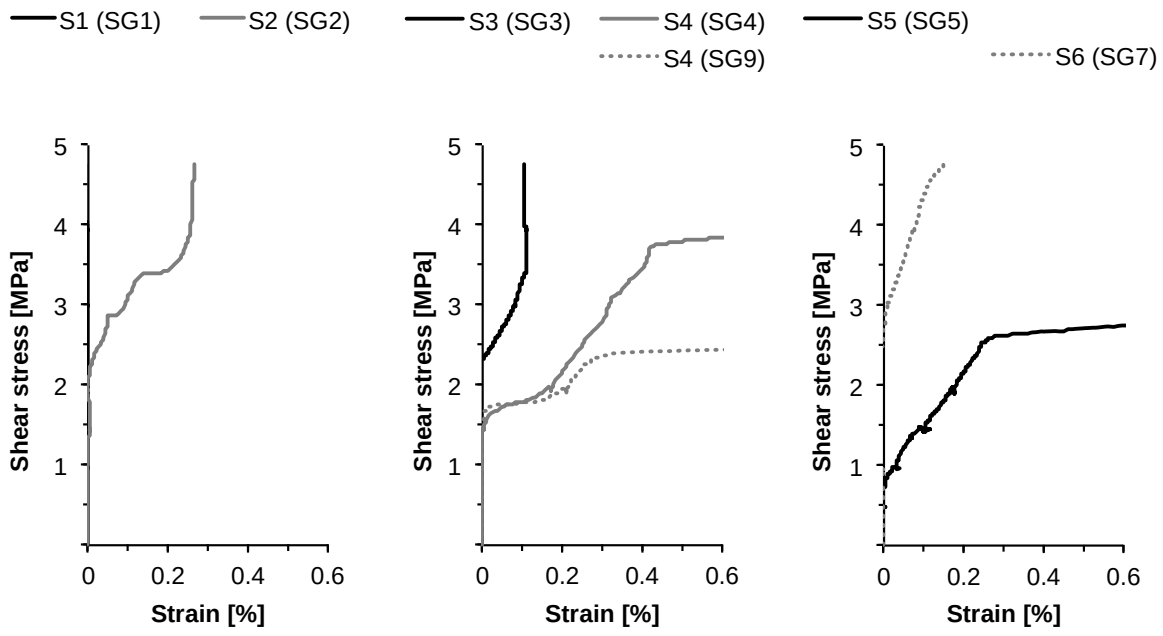

(a) (b) (c)

Figure 6.44 – Specimen MBDE – shear stress versus steel strains: (a) support region, (b) middle region and (c) load region.

In the support region, the strain gauge on the link closest to the support did not register yield and the measurements were very low throughout the duration of the test. However, the readings on the link in the same region further away from the support yielded before the ultimate capacity was reached. In the middle region the link closer to the support had not yielded prior to failure, however, both strain gauges on the link closer to the load recorded yield strains. Similarly to the support region, the strains recorded in the load region showed that while the steel link closer to the middle region had yielded prior to failure, the shear link closer to the load region had not.

6.9.4 CFRP strain profiles

The CFRP strains measured on the deep embedded bars applied for specimen MBDE are presented in Figure 6.45.

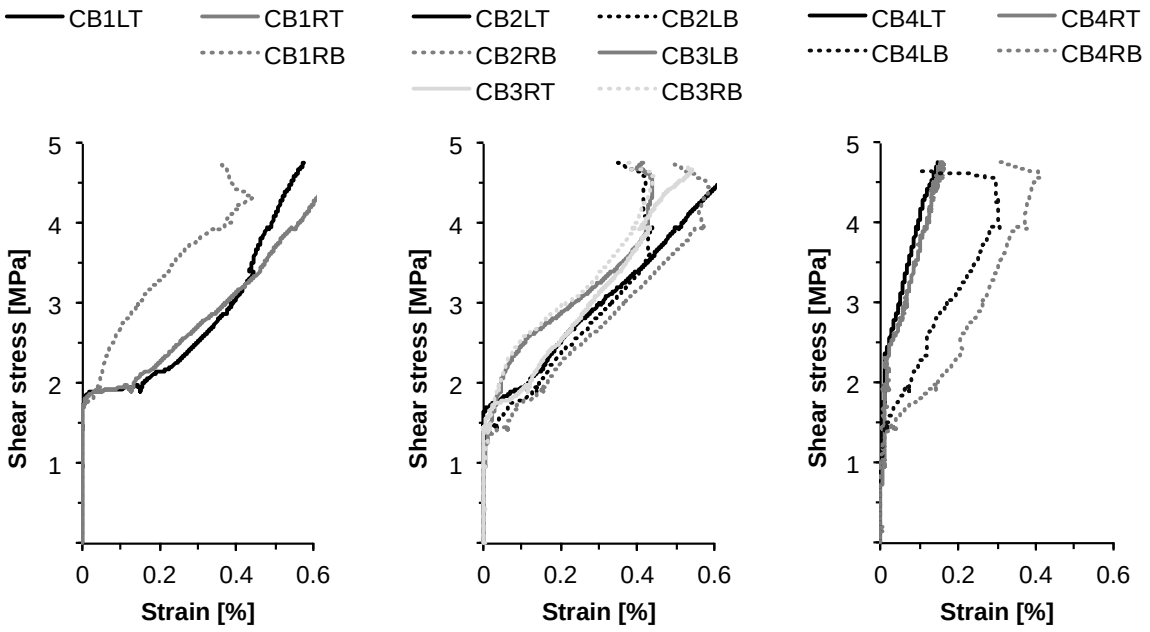

(a) (b) (c)

Figure 6.45 – Specimen MBDE – shear stress versus CFRP strains: (a) support region, (b) middle region and (c) load region.

In the support and middle regions, the strain levels reached up to 0.6%, which is considerably more than the CFRP strain levels observed for the specimens MB2U and MB2UA strengthened with externally bonded CFRP sheets.

The maximum strain readings in all regions overcame the strains at which steel links yield except for the strain gauges at the top location for bars in the load region, where the recorded strains were lower with maximum values of 0.4% at debonding. The readings from the middle region were consistent across all bars and locations with maximum strain values between 0.4% and 0.6%. Furthermore, while all readings from strain gauges located at the bottom of the CFRP bars in the middle region indicated debonding prior to failure, the top strain gauges on CFRP bars in this region did not register debonding.

6.10 Global behaviour of the beams

The shear stress versus shear displacement of the large beams is presented in Figure 6.46 and that obtained for the medium beams in Figure 6.47.

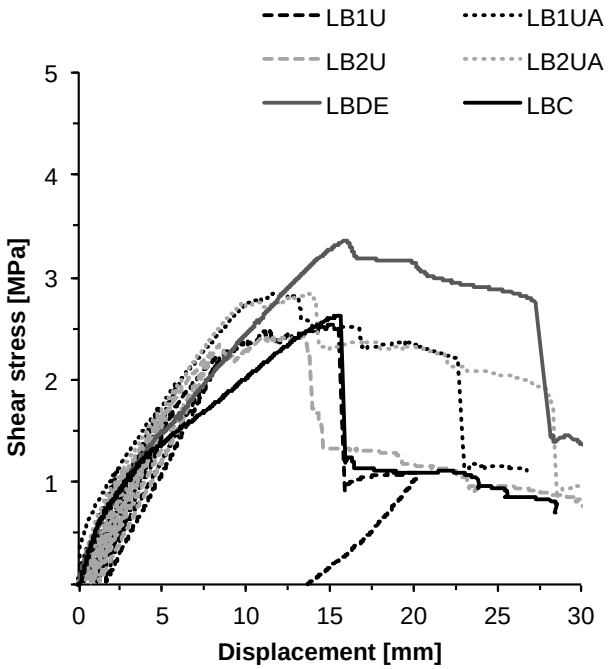

Figure 6.46 – Large beams: shear stress versus displacement.

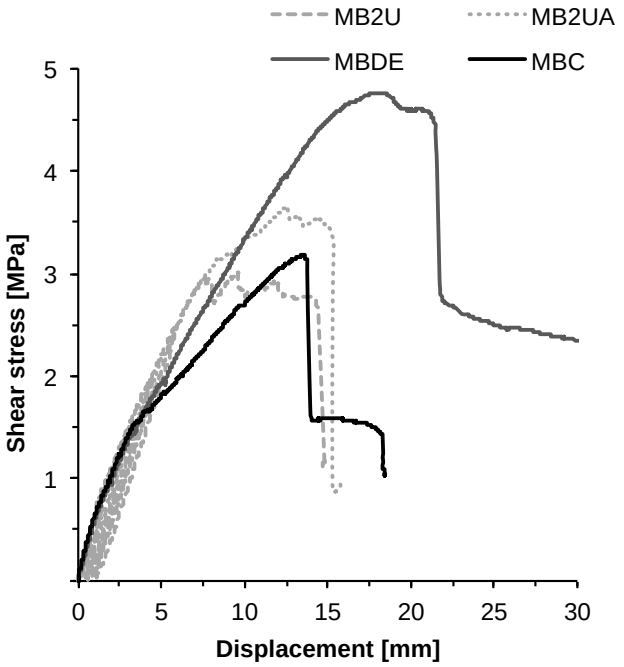

Figure 6.47 – Medium beams: shear stress versus displacement.

The global behaviour of the beams, regardless of their size, highlighted that the beams strengthened with externally bonded CFRP sheets reach similar ultimate capacity at peak, regardless of the amount of CFRP applied. The behaviour until failure is also near identical for all externally strengthened cases, until the CFRP starts debonding. The deep embedment specimen showed a great increase in shear strength for both tested sizes.

6.11 Behaviour of the CFRP sheets

The stretching of the CFRP sheets in the specimens strengthened with externally bonded sheets was investigated through further analysis of strains.

The results are presented in Table 6.3.

Table 6.3 – Strain gauge rosette analysis results.

Specimen	Experimental values				Calculated values			
	Strain gauge	ε_1 [$\mu\varepsilon$]	ε_2 [$\mu\varepsilon$]	ε_3 [$\mu\varepsilon$]	ε_{max} [$\mu\varepsilon$]	ε_{min} [$\mu\varepsilon$]	θ [º]	γ_{max} [$\mu\varepsilon$]
LB1U	SGR1	–	–	–	–	–	–	–
	SGR2	2310	1420	26	3370	360	38	3010
	SGR3	52	-65	-64	50	-70	22	120
	SGR4	36	-38	117	120	-120	54	240
LB1UA	SGR1	2320	1550	-139	3650	220	40	3430
	SGR2	2150	1010	-552	3320	-170	37	3490
	SGR3	608	1520	186	2030	100	59	1930
	SGR4	226	12	-39	260	-20	28	280
LB2U	SGR1	–	–	–	–	–	–	–
	SGR2	1260	1170	-433	2630	-200	44	2830
	SGR3	245	7	59	230	30	15	200
	SGR4	330	426	-186	880	-130	47	1010
LB2UA	SGR1	1510	1140	-37	2460	190	41	2270
	SGR2	1980	1010	-1190	3720	-720	40	4440
	SGR3	203	-153	-226	250	-200	27	450
	SGR4	18	8	-54	70	-40	43	110

Table 6.3. – Strain gauge rosette analysis results (cont'd).

Specimen	Experimental values				Calculated values			
	Strain gauge	ε_1 [$\mu\varepsilon$]	ε_2 [$\mu\varepsilon$]	ε_3 [$\mu\varepsilon$]	ε_{max} [$\mu\varepsilon$]	ε_{min} [$\mu\varepsilon$]	θ [°]	γ_{max} [$\mu\varepsilon$]
MB2U	SGR1	3000	1670	-107	4330	340	37	4000
	SGR2	1360	220	120	1410	170	25	1240
	SGR3	–	–	–	–	–	–	–
	SGR4	1020	2110	-160	3270	-150	54	3420
MB2UA	SGR1	1710	1670	-88	3230	160	45	3070
	SGR2	2100	1130	-843	3640	-410	39	4050
	SGR3	1600	1420	68	2730	290	43	2440
	SGR4	1270	1570	-416	3050	-220	47	3270

The non-principal stretching of the CFRP sheets was of interest. Principal strains ε_{max} and ε_{min} were calculated, as well as the maximum principal strain direction, angle θ, and the maximum engineering shearing strain, $\gamma_{max,}$ according to equations (4.1) through to (4.4) presented in Chapter 4.

The CFRP strains, ε_2, are the maximum-recorded strains in the vertical principal fibre direction prior to failure. The strains ε_2 in the cross-fibre and ε_3 in the 45° directions are corresponding to the maximum strains in the principal fibre direction at the monitored locations. Readings from faulty strain gauges were discarded and not included in the strain analysis.

6.11.1 Large beams

The non-principal stretching of the CFRP sheets was further investigated through plotting the variation of the principal angle with increasing shear stress. The results for the large beams are presented in Figure 6.48 through to Figure 6.51 for comparison.

The strain maps obtained from the DIC monitoring for the large U-wrapped beams are presented in Figure 6.52, with corresponding shear force. The results show that the CFRP sheet stretches to a greater extent in specimens with end-anchorage system that prevents debonding of the CFRP sheets. The values obtained from the DIC strain maps are directly comparable with those obtained from the physical strain gauges.

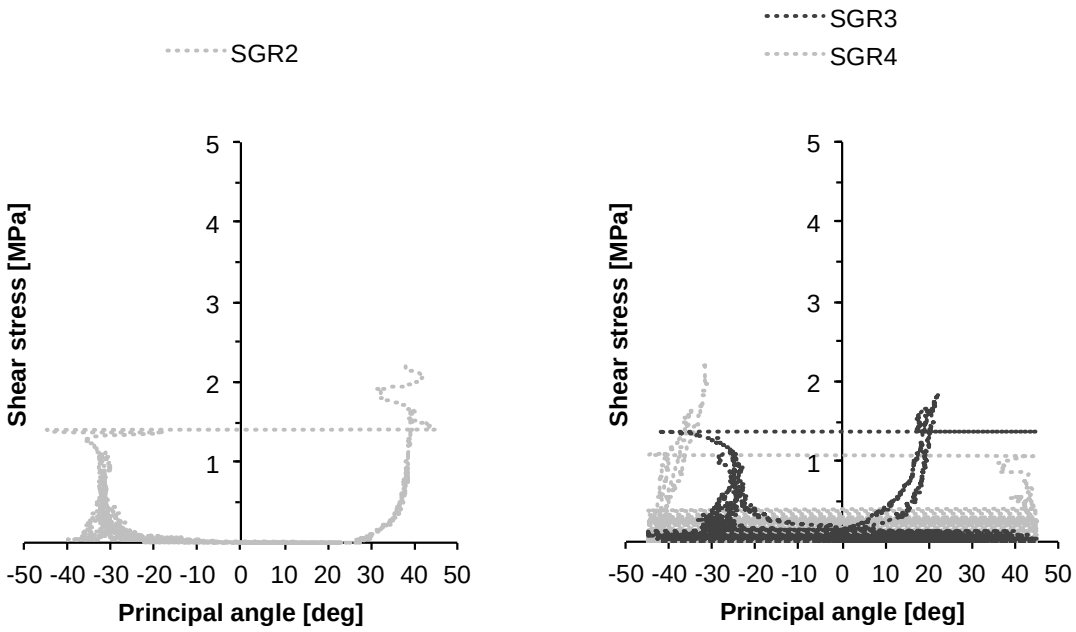

(a) (b)

Figure 6.48 – Specimen LB1U – variation of principal angle with shear stress: (a) near support region, (b) near load region.

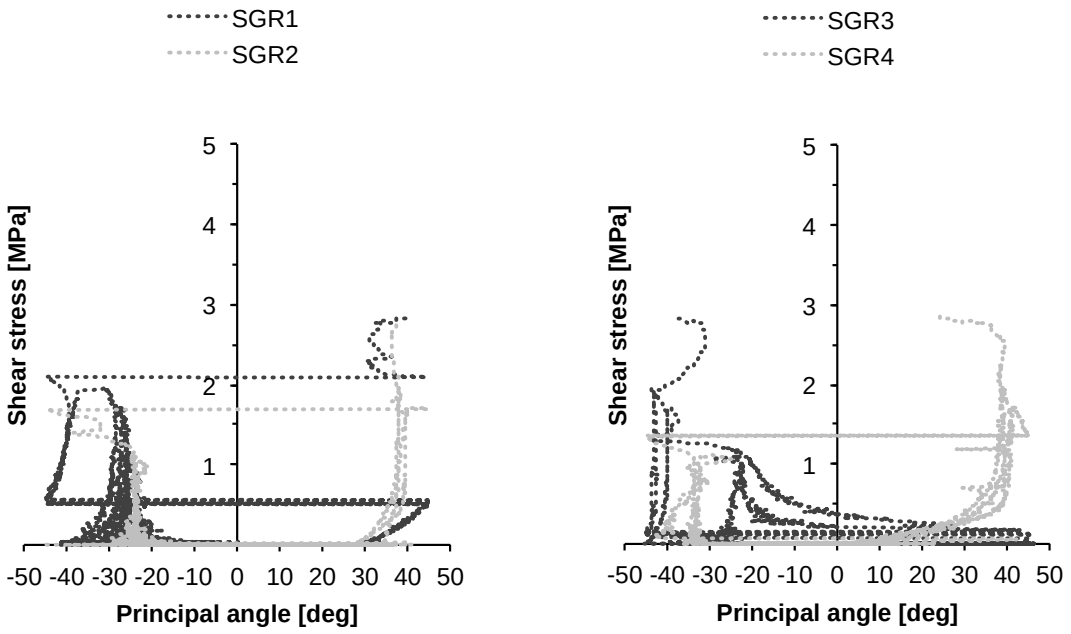

(a) (b)

Figure 6.49 – Specimen LB1UA – variation of principal angle with shear stress: (a) near support region, (b) near load region.

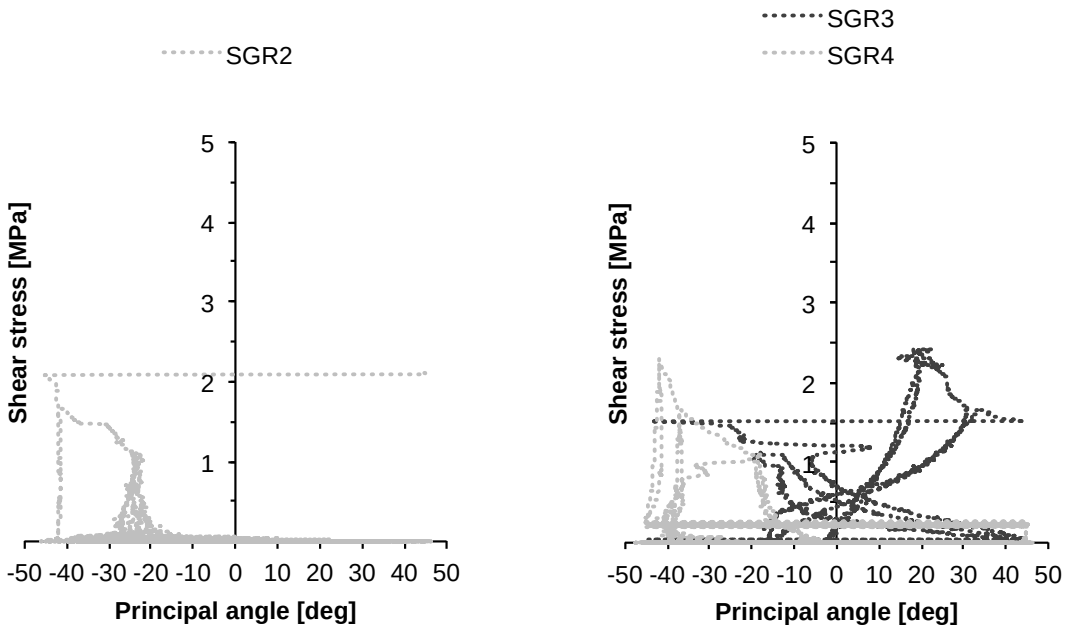

(a) (b)

Figure 6.50 – Specimen LB2U – variation of principal angle with shear stress: (a) near support region, (b) near load region.

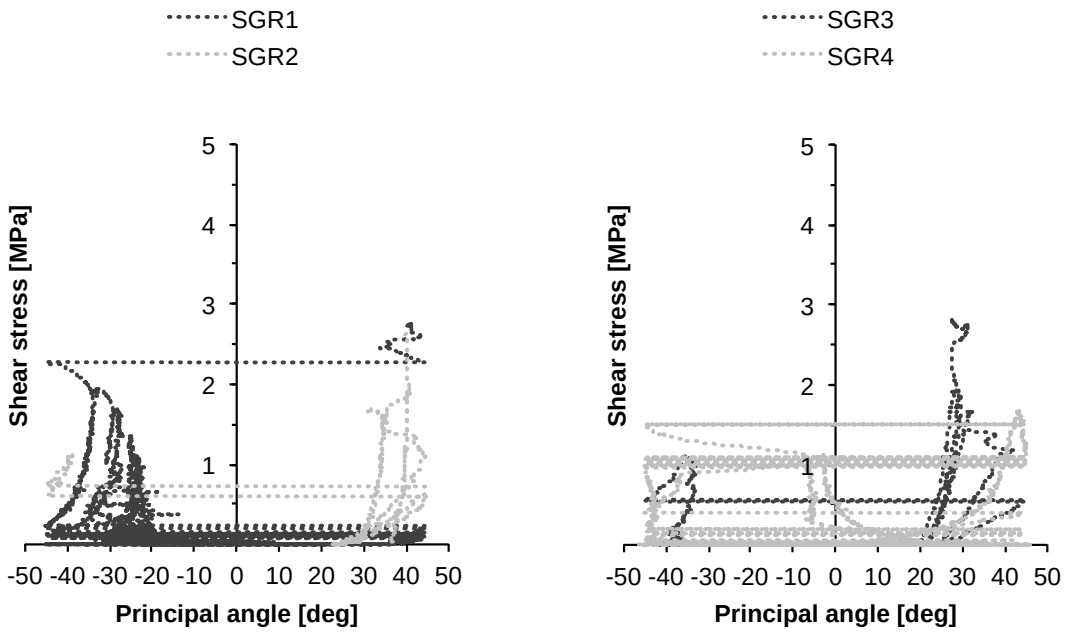

(a) (b)

Figure 6.51 – Specimen LB2UA – variation of principal angle with shear stress: (a) near support region, (b) near load region.

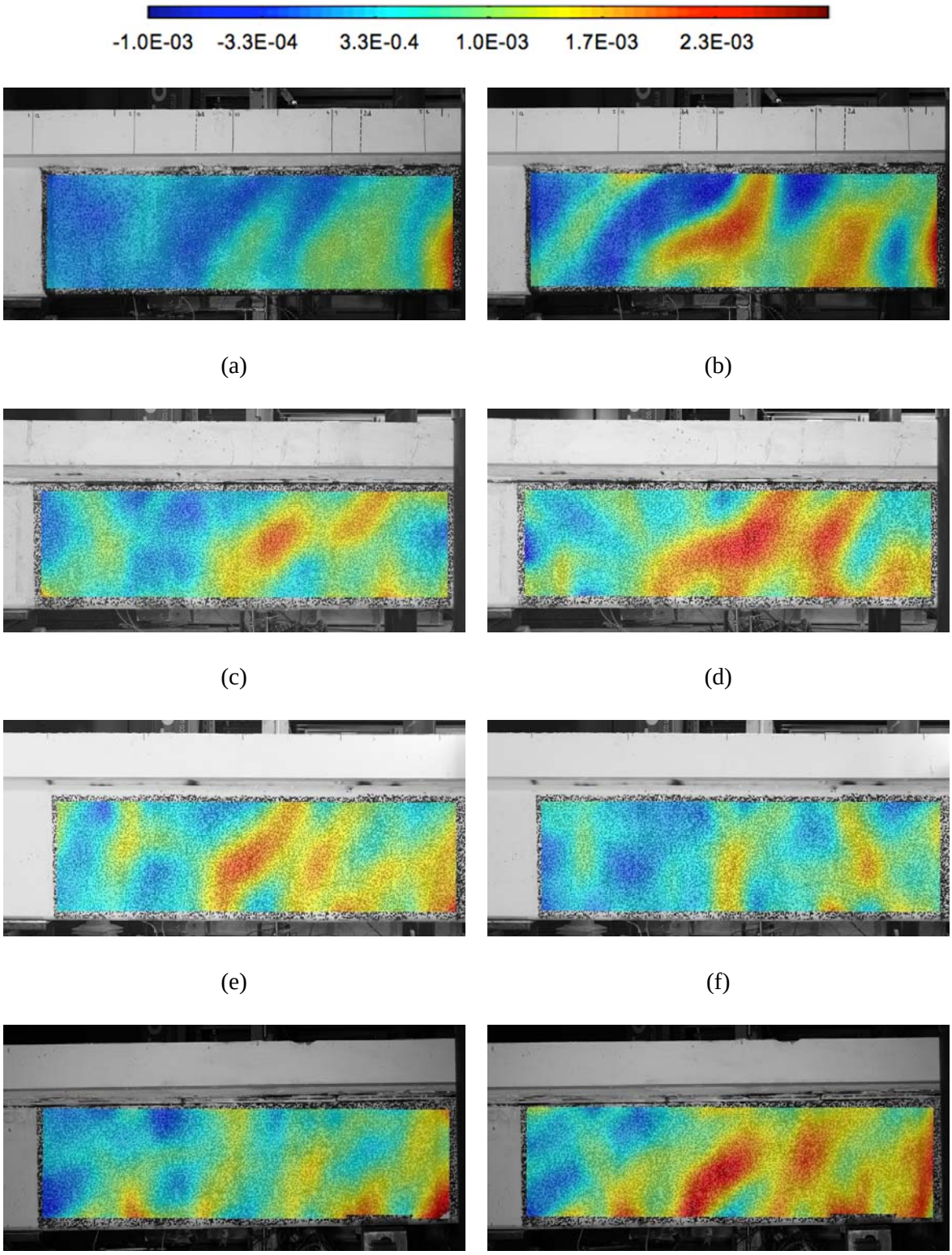

Figure 6.52 – DIC strain maps – principal strains (E1): specimen LB1U (a) at V = 250 kN, (b) at V = 375 kN, and specimen LB1UA (c) at V = 250 kN, (d) at V = 375 kN; specimen LB2UA (e) at V = 250 kN, (f) at V = 375 kN, and specimen LB2UA (g) at V = 250 kN, (h) at V = 375 kN.

6.11.2 Medium beams

Similarly to the large specimens, the readings from the DIC strain maps, presented in Figure 6.53 (d) demonstrated that greater utilization of the CFRP U-wrap is possible using the end-anchorage system.

It should be noted that for specimen MB2U the CFRP sheets were already debonding and moving towards the camera capturing the 2D displacement of the sheets. Therefore the red regions do not necessarily correspond to stretching strains.

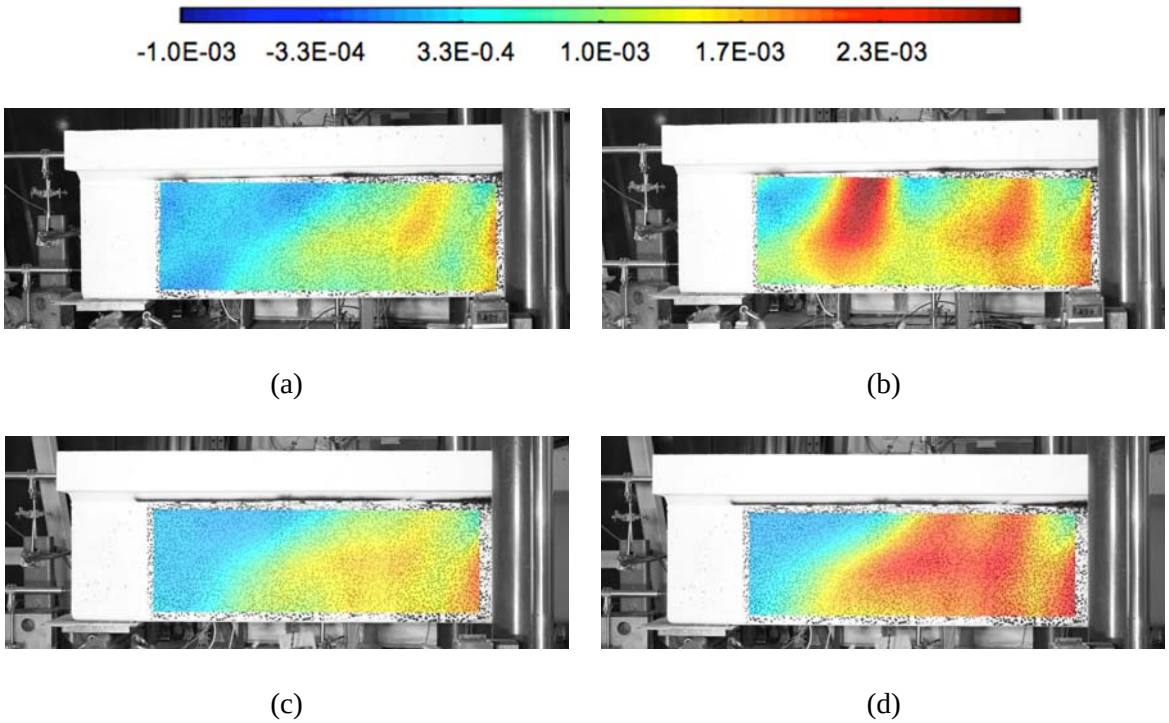

Figure 6.53 – DIC strain maps – principal strains (E1): specimen MB2U (a) at V = 250 kN, (b) at V = 300 kN, and specimen MB2UA (c) at V = 250 kN, (d) at V = 300 kN.

The non-principal stretching of the CFRP sheets was also investigated for the medium specimens strengthened with externally bonded sheets, through plotting the principal angle versus shear stress.

The results for the medium U-wrapped beams are shown in Figure 6.54 and Figure 6.55 for comparison.

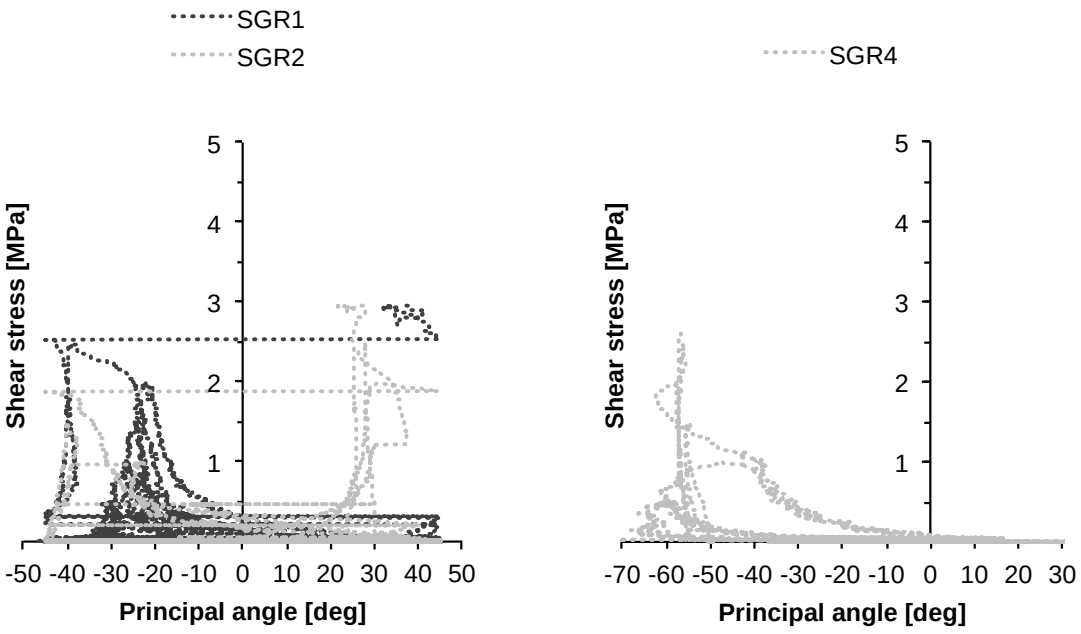

(a) (b)

Figure 6.54 – Specimen MB2U – variation of principal angle with shear stress: (a) near support region, (b) near load region.

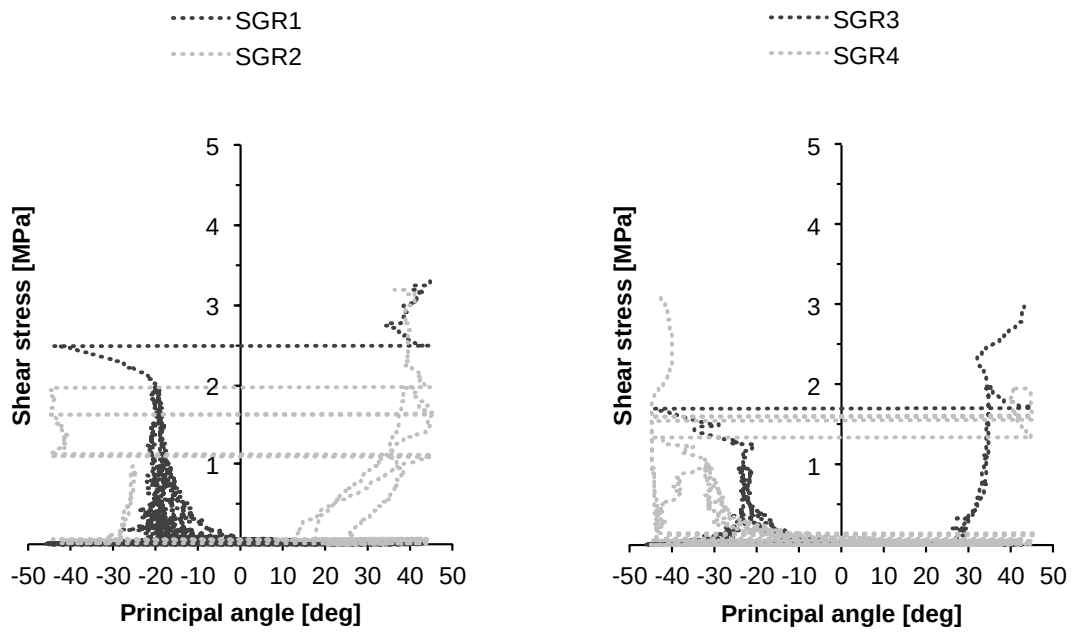

(a) (b)

Figure 6.55 – Specimen MB2UA – variation of principal angle with shear stress: (a) near support region, (b) near load region.

6.12 Concrete bond strength tests

To ascertain the bond strength was adequate in all the tested beams, the bond strength of the surface concrete as well as the CFRP-concrete interface was tested following the beam tests. The tests were carried out using the standard test method for determining the pull-off strength for FRP laminate systems according to ASTM D7522. The test preparation included concrete coring and in the case of the CFRP-concrete interface testing, the CFRP was cut and the underlying concrete cored as coring through the CFRP sheets was not possible. Figure 6.56 (a) shows the tested area on beam after the tester was removed while Figure 6.56 (b) shows the substrate failure in comparison to the possible test outcomes.

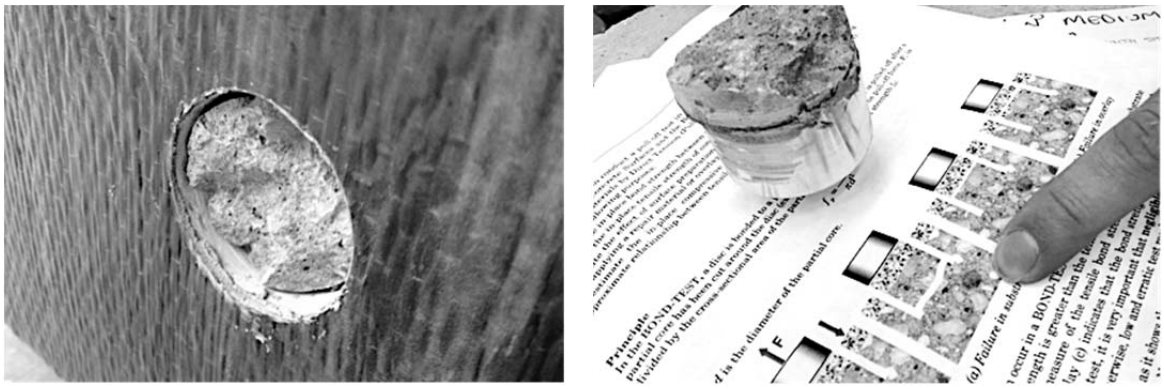

(a) (b)

Figure 6.56 – Bond strength test: (a) separation in the concrete substrate on beam, (b) failure in substrate.

Several locations were tested on all externally strengthened beams in the undamaged web regions for concrete only and CFRP-concrete bond strength to obtain representative data. The mean values of bond strength to the concrete surface, f_b, were 2.6 MPa across both tested sizes of test beams. The recorded bond strengths of the CFRP to the concrete, f_{bf}, were 3.0 MPa and 3.5 MPa for the large and the medium beams, respectively. In all cases where permissible failure according to ASTM D7522 occurred, these values greatly exceeded the 1.4 MPa minimum tension adhesion strength requirements of ACI-440 (2008).

6.13 Summary of main experimental findings

Following the experimental testing and analysis of results of six large and four medium

T-beams strengthened with CFRP materials, the following conclusions can be drawn:

- The shear crack in unstrengthened control specimens initiated at the location of the elastic neutral axis at approximately half the ultimate load and further propagated towards the loading and support plates within the web, regardless of the specimen size;
- Only some of the shear links were activated after concrete cracking in shear – generally in the middle region – and not all the shear links yielded prior to the beam failure;
- Strengthening with externally bonded CFRP U-wraps without end anchorage did not provide any additional increase in shear capacity and only a small increase in shear capacity was observed for U-wraps with bar-in-slot anchorage system;
- The presence of the CFRP U-wraps significantly delayed the onset of steel yielding, regardless of the end anchorage used;
- The thickness of the CFRP U-wraps did not have any influence on the ultimate capacity of the tested specimens as similar values were recorded at failure;
- Debonding of the CFRP sheets initiated in the location of first cracking in the web and further propagated towards the free edge of the CFRP U-wrap, regardless of the anchorage system used;
- The results from the DIC confirmed that the shear crack initiated in the web in all tested cases and that debonding of the externally bonded CFRP sheets started at this location;
- The specimens strengthened with externally bonded CFRP U-wraps failed shortly after the CFRP started to debond often with minimal or no warning;
- The depth of the concrete attached to the CFRP sheets observed upon removal of the wraps post-test found in the location of the elastic neutral axis was equal to the full depth of the concrete cover;
- The test results from the deep embedment specimens showed that a great increase in shear capacity can be achieved with deep embedded CFRP bars as additional shear reinforcement, regardless of the specimen size;
- Low debonding strains were recorded in the CFRP U-wraps compared with the strains recorded in the deep embedded CFRP bars demonstrating that better material utilization is possible through deep embedment.

7 DISCUSSION OF T-BEAM TEST RESULTS

7.1 Introduction

In the previous Chapter the test results and analysis from the experimental programme on unstrengthened and strengthened T-beams were presented. This Chapter presents discussion of the experimental results, findings and their implications considering current design and assessment standards and guidelines. This Chapter also demonstrates how the first two of the objectives of the research as set out in Chapter 1 were met, namely the observation of the size effect and its influence on the behaviour of the tested beams and the applicability of the current codes of practice. The local debonding behaviour of the CFRP sheets and how it affects the overall beam behaviour is also presented here.

7.2 Comparison with shear resistance predictions

7.2.1 Shear resistance according to current design codes

The shear resistance of the unstrengthened specimens was calculated according to Eurocode 2 (EC2), ACI-318 and *fib* Model Code 2010. A summary of the predicted and experimental values is presented in Table 7.1.

Table 7.1 – Unstrengthened control beams: comparison of experimental and predicted values.

Specimen	Experimental		Predicted					
			EC2		ACI-318		*fib* MC10	
	ρ_v [%]	$V_{u\text{-}exp}$ [kN]	V_{EC2} [kN]	$V_{EC2}/V_{u\text{-}exp}$	$V_{ACI\text{-}318}$ [kN]	$V_{ACI\text{-}318}/V_{u\text{-}exp}$	$V_{fibMC10}$ [kN]	$V_{fibMC10}/V_{u\text{-}exp}$
LBC	0.1	472	126	0.27	254	0.54	424	0.89
MBC	0.1	322	93	0.29	157	0.53	264	0.89

The EC2 provides the most conservative predictions, corresponding to approximately one third of the actual ultimate shear force obtained experimentally. The low predicted values of shear force are due to assuming only steel contribution and ignoring the contribution of concrete. This value corresponds to the point where the first shear crack occurred in the

web of the beam but before the steel links yielded. While ACI-318 predicts approximately half of the actual ultimate shear force, it accurately predicts the shear force at which steel links yield in both the large and the medium specimen, as presented in Section 6.3. A large fully open shear crack was observed at this point during experimental testing. The predictions obtained using the *fib* Model Code 2010 on the other hand are the closest to the actual ultimate shear force, with identical ratios of the calculated versus experimental values across both tested sizes.

The predicted shear capacity for the CFRP-strengthened specimens was calculated using TR55, *fib* Bulletin No. 14 and ACI-440. The safety factors, normally present in design and assessment codes, were not used for the predicted values.

The results are presented in Table 7.2.

Table 7.2 – Strengthened beams: comparison of experimental and predicted shear force values according to current design guidelines.

Specimen	Experimental		Predicted					
			TR55		*fib* Bulletin No. 14		ACI-440	
	ρ_f [%]	$V_{u\text{-}exp}$ [kN]	V_{TR55} [kN]	$V_{TR55}/V_{u\text{-}exp}$	V_{fib14} [kN]	$V_{fib14}/V_{u\text{-}exp}$	$V_{ACI\text{-}440}$ [kN]	$V_{ACI\text{-}440}/V_{u\text{-}exp}$
LB1U	0.7	458	322	0.70	494	1.08	563	1.23
LB1UA	0.7	512	351	0.69	481	0.92	536	1.05
LB2U	1.3	438	394	0.90	630	1.44	684	1.57
LB2UA	1.3	512	398	0.78	605	1.18	634	1.24
LBDE	0.2	605	266	0.43	–	–	–	–
MB2U	1.3	306	241	0.79	380	1.24	405	1.32
MB2UA	1.3	370	250	0.68	375	1.01	394	1.06
MBDE	0.2	482	187	0.39	–	–	–	–

The predictions obtained from TR55 and *fib* Bulletin No. 14 use the shear resistance calculated for the underlying reinforced concrete beam, whereas the ACI-440 uses the ACI-318 shear resistance predictions. In the calculations for the U-wrap with the bar-in-slot anchorage system the end anchorage was not considered to enhance the shear capacity and the anchorage length was assumed identical to the U-wrap specimens. In all cases

actual material properties were used for each test specimen, which is reflected in the predicted values.

From the results it is apparent that ACI-440 consistently over-predicts the shear resistance of the strengthened beams. The predicted values obtained from *fib* Bulletin No. 14 are either over-predicted or under-predicted without a clear pattern for either result. While TR55 consistently under-predicts the shear resistance of the strengthened beams, the values it provides are conservative and safe for design of the strengthening systems. The values for the deep embedment specimens are particularly conservative, however, that is due to the assumption that the strains in the FRP bars will remain under the 0.4% level.

Strain predictions for the FRP materials according to the same guidelines in comparison with experimental values are presented in Table 7.3.

Table 7.3 – Maximum recorded CFRP strains in the principal fibre direction: comparison of experimental and predicted values.

Specimen	Experimental		Predicted					
			TR55		*fib* Bulletin No. 14		ACI-440	
	ρ_f [%]	$\varepsilon_{fe0\text{-}exp}$ [%]	$\varepsilon_{fe\text{-}TR55}$ [%]	$\varepsilon_{fe\text{-}TR55}/\varepsilon_{fe0\text{-}exp}$	$\varepsilon_{fe\text{-}fib14}$ [%]	$\varepsilon_{fe\text{-}fib14}/\varepsilon_{fe0\text{-}exp}$	$\varepsilon_{fe\text{-}ACI\text{-}440}$ [%]	$\varepsilon_{fe\text{-}ACI\text{-}440}/\varepsilon_{fe0\text{-}exp}$
LB1U	0.7	0.23	0.27	1.11	0.36	1.56	0.35	1.56
LB1UA	0.7	0.23	0.26	1.11	0.34	1.44	0.33	1.44
LB2U	1.3	0.13	0.19	1.44	0.24	1.89	0.24	1.89
LB2UA	1.3	0.20	0.18	0.90	0.23	1.15	0.22	1.10
LBDE	0.2	0.53	0.40	0.78	–	–	–	–
MB2U	1.3	0.30	0.22	0.73	0.25	0.83	0.28	0.93
MB2UA	1.3	0.21	0.21	1.00	0.24	1.14	0.27	1.22
MBDE	0.2	0.73	0.40	0.56	–	–	–	–

Actual concrete strength as tested and manufacturer provided properties of CFRP were used throughout.

Both ACI-440 and *fib* Bulletin No. 14 over-predict the strains achievable in the CFRP sheets, except for MB2U where the values are under-predicted by both guidelines. TR55 on the other hand provides relatively close values to those obtained from experimental data, except for the specimen LB2U. The actual maximum measured strain values prior to failure for this specimen were particularly low, suggesting premature failure due to

insufficient bond length. This is further elucidated by the difference between the unanchored LB2U specimen and its anchored counterpart LB2UA, where larger strains were recorded. These were in line with the predicted values. However, it should be noted that strain values of 0.19% and 0.26% were recorded for LB2U and LB1UA, respectively, following the failure of the beams, where the CFRP fully debonded from the concrete surface. A possibility exists that the strains recorded at failure were not the maximum strains and not in the location where debonding leading to collapse occurred. The strains obtained from the CFRP bars for both deep embedment specimens are greater than those predicted by TR55. This again demonstrates that TR55 provides a safe and conservative prediction of the maximum shear resistance of the deep embedment T-beam section.

7.3 Effect of size

One of the primary objectives of this experimental study was to determine whether size effect plays an important role in the specimens strengthened with externally bonded CFRP sheets. The damage in the separated CFRP sheets was compared for both sizes of the specimen with and without end anchorage, as shown in Figure 7.1.

(a) (b)

Figure 7.1 – Comparison of separated CFRP U-wraps across the two sizes: (a) LB1U and MB2U, (b) LB2UA and MB2UA.

Figure 7.1 (a) shows the CFRP wraps from the LB1U and MB2U specimens side by side. It is apparent that the splitting of the CFRP laminate in the zone close to support and the amount of concrete attached in the shear crack zone are similar for both sizes. Figure 7.1 (b) shows similar patterns for the wraps obtained from LB2UA and MB2UA. This observation suggests that both specimens failed in a similar manner sustaining near

identical levels of damage underneath the wrap. It should be noted that the concrete attached to the CFRP wrap recovered from specimen LB2UA was approximately of the depth of the cover concrete, whereas that from specimen MB2UA was less than the depth of the cover.

To assess the potential size effect quantitatively rather than qualitatively, it is necessary to provide direct comparison between the two sizes of test specimen. This is achieved through plotting the normalized values of shear stress against midspan displacement normalized by the effective depth *d.* Figure 7.2 shows the behaviour of all specimens strengthened with externally bonded CFRP sheets. It is immediately apparent that the normalized shear stress-deflection behaviour of the large unanchored specimens LB1U and LB2U is strikingly similar and so is that of the anchored specimens LB1UA and LB2UA. From the graph it appears that the strength of the specimen increases as the size decreases. This is true for both the MB2U and MB2UA in direct comparison to their large counterparts.

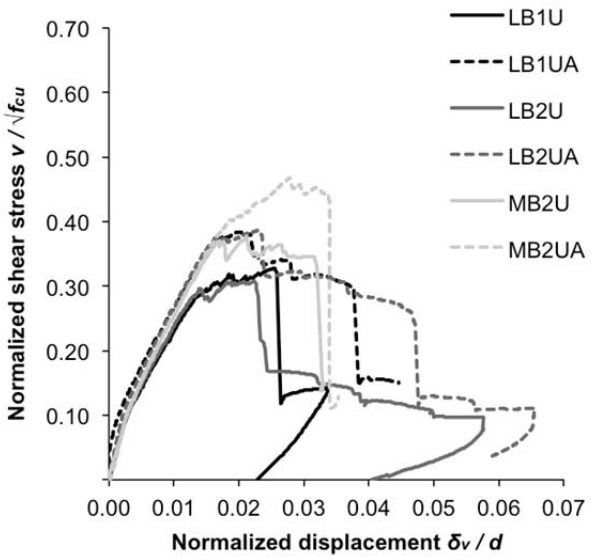

Figure 7.2 – U-wrapped specimens: normalized shear stress plotted against normalized displacement.

In terms of stiffness, the specimens LB1U and LB2U follow the same gradient until debonding of the CFRP sheets occurs. Greater stiffness can be observed for the specimens equipped with end anchorage, LB1UA and LB2UA. The stiffness of the medium beams

lies between these two, with the anchored MB2UA exhibiting a slightly stiffer behaviour to that observed for MB2U.

The size effect was also investigated for the unstrengthened control specimens and the deep embedment specimens. Figure 7.3 shows the normalized shear-deflection behaviour. Size effect can be observed for both the unstrengthened control as well as the deep embedment specimens. The effect of size is more prominent for the deep embedment specimens, where the shear stress dramatically increases with decreasing specimen size.

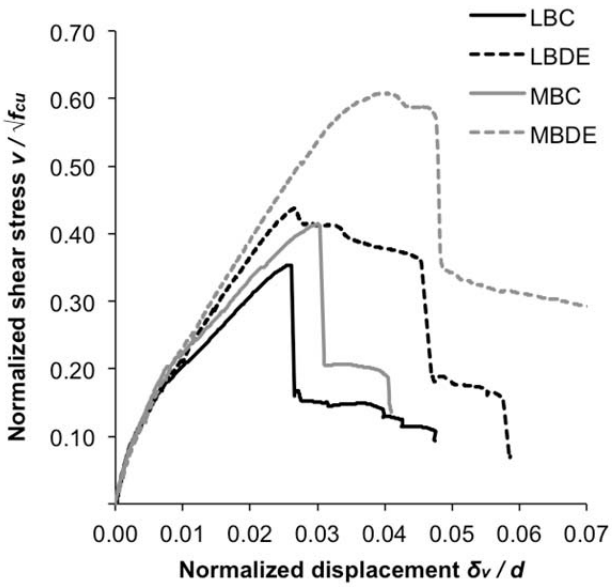

Figure 7.3 – Unstrengthened control beams and deep embedment: normalized shear stress plotted against normalized displacement.

Figure 7.4 shows the results in terms of normalized shear stress against the log of *d*. The dashed line indicates the gradient of the trend predicted by linear fracture mechanics (LEFM) for the size effect on shear in concrete, as proposed by Yu and Bazant (2011). The trends are in good agreement with the LEFM predictions in the case of the unstrengthened control beams and those strengthened with externally bonded CFRP sheets. However, the deep embedment specimens are not following this trend and the shear stress capacity is clearly affected by the size of the specimen.

The fact that the specimens with the externally applied CFRP sheets exhibited similar size effect to that of their unstrengthened counterparts indicates that the overall behaviour may

have been dominated by the behaviour of the underlying reinforced concrete beam. A size effect relating to the effectiveness of the CFRP U-wrap strengthening is not apparent.

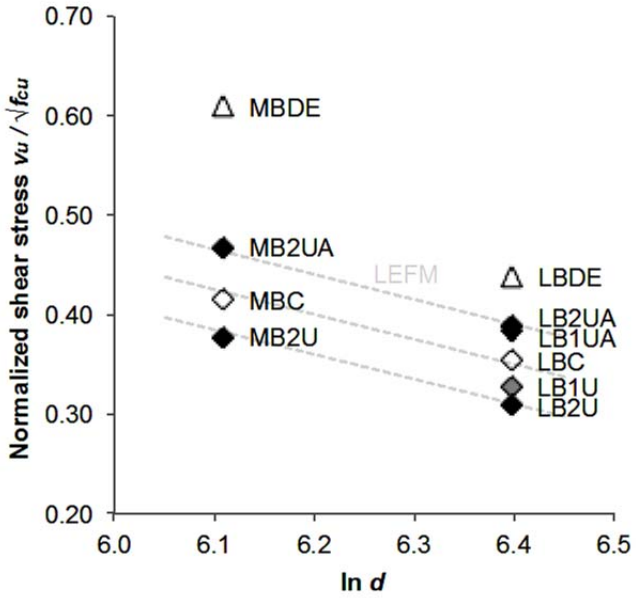

Figure 7.4 – Normalized shear stress plotted against size ln *d* with LEFM predictions.

7.4 CFRP behaviour

The effect of the CFRP thickness and the presence of the end-anchorage system on the overall behaviour and performance of the strengthened beams were of interest. Based on the experimental results, the overall structural performance of the strengthened beams did not appear to be sensitive to the thickness of the CFRP sheets. This trend was also observed in the preliminary testing of the push-off specimens strengthened with externally applied CFRP sheets with varying anchorage length.

According to TR55 (2012), the thickness of the CFRP laminate dictates the minimum required bond length for the debonding strains to develop. This was clearly demonstrated by the premature failure of the specimen LB2U, where particularly low strains were recorded prior to and at failure compared to LB1U. Greater strains were recorded in the anchored case LB2UA; however, those were still lower than those reasonably expected at debonding. Across both tested sizes, greater effective strains were measured in the anchored specimens, confirming that greater effectiveness of the CFRP strengthening system is indeed possible using the bar-in-slot end-anchorage system.

The reliability of the readings obtained from the strain gauges was also scrutinized prior to, during and post-test. Figure 7.5 shows the strain gauge positioning with respect to the cracked zone.

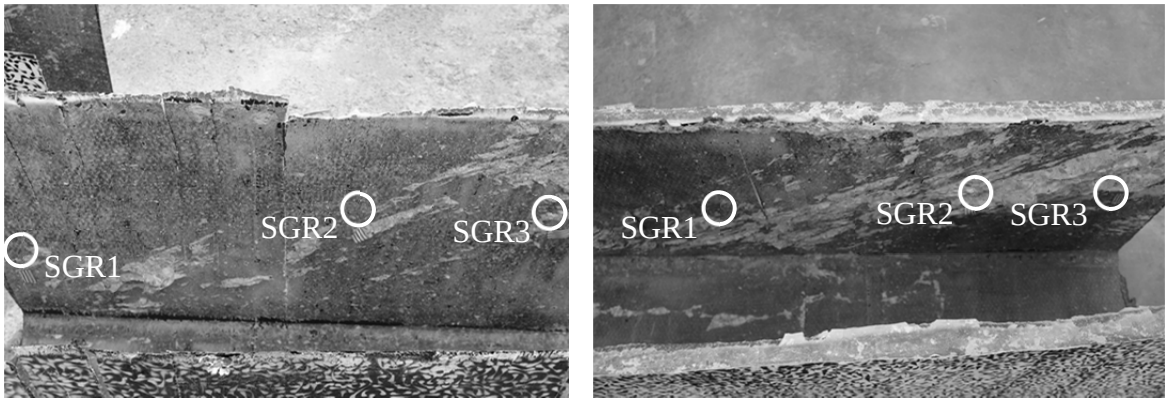

(a) (b)

Figure 7.5 – Positioning of strain gauge rosettes with respect to the shear crack: (a) U-wrap without end anchorage, (b) U-wrap with end anchorage bar-in-slot system.

Even though the strain gauges were positioned along the anticipated main shear crack location, as discussed in Chapter 3 and in Chapter 5, their actual location relative to the discontinuity in concrete is debatable. The strain gauge positioning was traced from the external face of the CFRP wrap onto the internal surface to demonstrate where the strain gauge was in relation to the crack.

As can be seen from Figure 7.5 (a) the strain gauges close to the support region (SGR1 and SGR2) are on or above the crack whereas strain gauges close to the load region (SGR3 pictured on the right) are below the main crack location. This is more apparent from Figure 7.5 (b) where the SGR3 is clearly positioned below the main shear crack location, SGR4 not pictured as this strain gauge remained on the bonded portion of the CFRP wrap. This means that while the strain gauges closer to the support region were more likely to register debonding strains when the CFRP separated above the crack, the CFRP may not have debonded below the crack.

Therefore, it is possible that the strain gauges close to the load region were not picking up on debonding strains. This was more apparent for the large beams as the strains recorded for the medium beams were greater in all monitored locations.

Based on the ultimate capacity values alone and the decrease in shear strength observed in specimens with externally bonded sheets in a U-wrap configuration, specimens LB1U, LB2U and MB2U, the CFRP material appears not to have contributed to the overall capacity. However, upon inspection of the shear stress-displacement graphs as well as the values of strains in the CFRP recorded prior to failure, it is clear, that the CFRP sheets were contributing to the overall capacity of the strengthened beams. The presence of the CFRP sheets alongside the internal steel stirrups prevented the stirrups from yielding until high values of applied load. In a sense the CFRP acted as a clamping force and until fully debonded from the concrete surface the steel was not able to stretch over the discontinuity and yield. This notion was also strengthened by the observation of bent shear links over the crack in the quarter span region suggesting the links underwent compression before being released to act in tension as intended.

The investigation of the non-principal stretching of the CFRP sheets through analysis of the variation of the principal angles with increasing shear force discussed in detail in Section 6.11 revealed that the debonding occurred at angles between 37° and 45°. The results further showed correlation between the failures of the beams strengthened with externally applied CFRP sheets and the principal angle at failure. The more brittle and explosive the failure, the closer the angle value was to 45°.

The CFRP bars in the deep embedment specimens behaved similarly to the internal steel shear links. The predicted values of effective strains for the deep embedded bars were under-predicted by TR55 in both tested cases. This is because the bond strength is approximated and reduced for design, while the bond of the CFRP bars through the bonding agent to the concrete surface is superior to that of concrete-steel, a view supported by extensive experimental evidence obtained by Valerio (2003, 2009). More accurate values of bond strength and subsequently more accurate predictions of shear strength can be obtained using actual tested material properties of bars and adhesives used for strengthening. However, the approach proposed by TR55 is conservative and provides safe design values for shear strengthening with deep embedded CFRP bars as additional shear reinforcement. In terms of effectiveness of the strengthening systems, it is possible to achieve greater shear capacity using the deep embedment technique with a much lower CFRP ratio than in the case of externally bonded CFRP sheets. In this case, similarly to the case of reinforced concrete, the truss analogy may appear to be adequate with appropriate adjustments to the material properties (Valerio, 2009).

7.5 Concluding remarks

Based on the discussion of the results following from the experimental programme on realistically sized unstrengthened and strengthened T-beams, the following conclusions can be drawn:

- The shear capacity predictions by current design and assessment standards under-predict the actual shear capacity of the tested beams, which means that more accurate prediction methods are required for assessment of existing reinforced concrete slab-on-beam structures to better obviate the need for strengthening;
- The shear crack in the tested T-beams with large amount of longitudinal steel reinforcement, representative of existing highway slab-on-beam structures, initiated in the web of the beam and did not propagate from flexural cracks towards the load as is the case of flexural shear failures. This poses a serious issue for the externally bonded CFRP sheets as the anchorage length available beyond the shear crack may be severely reduced and thus the CFRP U-wrap, without the provision of sufficient end anchorage, may not contribute fully to the overall shear capacity of the beam;
- Size effect observed in the specimens strengthened with externally bonded CFRP sheets and that of the unstrengthened control specimens was in a good agreement with the predictions from linear elastic fracture mechanics, suggesting that the size effect may be mitigated by the amount of shear reinforcement;
- Size effect related discrepancies were observed for deep embedment specimens, suggesting a possibility of a different failure mode to direct diagonal shear and opposing the above notion that size effect may be mitigated by the amount of shear reinforcement;
- Strengthening with unanchored CFRP sheets in the U-wrap configuration where the top and the bottom chord of the beam are not fully connected does not present a viable strengthening option for typical slab-on-beam bridges. Limited anchoring into the web using end-anchorage systems provides moderate increase in shear capacity although mainly results in delayed debonding if not anchored into/through the compression zone;
- Insufficient anchorage length of the CFRP sheets in a U-wrap configuration leads to a catastrophic collapse at loads lower than those recorded for their unstrengthened counterparts. This appears to be controlled by the behaviour of the

underlying reinforced concrete beam, a finding which was underpinned by the steeper shear crack at 37° in the case of beams strengthened with CFRP U-wraps compared with 22° in unstrengthened control specimens;

- The presence of the CFRP sheets was found to delay the onset of yielding of the internal steel links, when a sufficient amount of the CFRP debonded from the concrete surface, allowing the steel links to stretch over the concrete discontinuity. This presents a serious concern over the assumption that the concrete, internal steel and any additional CFRP reinforcement contribute at the same time and so the overall shear capacity equals the sum of these individual contributions;
- Comparison of the recorded and predicted effective strain levels according to current design guidelines showed that the values are either greatly over- or under-predicted, with TR55 (2012) consistently providing conservative and safe design predictions for the beams strengthened with externally bonded CFRP sheets as well deep embedded bars;
- Deep embedment presents a reliable and practical strengthening technique for all slab-on-beam structures deficient in shear, including those with high percentage of longitudinal reinforcement, where high gains in shear strength are possible. This can be attributed to the deep embedded bars providing a connection between the top and bottom chord of the T-beam;
- The experimental results from the T-beam programme underpinned by the findings from the push-off test experiments suggest that a practical limit for shear strengthening must exist, where the concrete reaches a certain limit of shear stress up to which it is possible and reasonable to increase the shear capacity through strengthening with CFRP materials.

8 NUMERICAL ANALYSIS

8.1 Introduction

The results presented in the previous Chapter highlighted that the current design codes greatly under-predict the actual capacity of existing reinforced concrete structures. Such conservative assumptions about the shear strength are adequate for design purposes to prevent brittle shear failures and aim to satisfy the minimum requirements to be fulfilled. However, a conservative assessment may lead to unnecessary intervention and potentially result in a lower capacity with catastrophic consequences due to altered failure modes. This was demonstrated experimentally across both sizes of test specimens. This Chapter explores the possibilities of more accurate assessment strategies and investigates the rational limit for repair and strengthening through targeted parametric studies on unstrengthened and strengthened beams using advanced numerical methods.

On the other hand, the design guidelines for strengthening of existing reinforced concrete structures with CFRP composites proved to either over- or under-predict the actual CFRP contribution to the shear capacity of the strengthened beams. The use of these guidelines in combination with predictions of the underlying reinforced concrete beam may lead to inaccurate predictions of the overall capacity of the strengthened beam. Furthermore, it is also necessary to be able to determine where the critical shear crack will likely initiate as this will invariably have a direct impact on the available anchorage length of the externally bonded CFRP sheets beyond the initial crack location. This, in turn, will provide an insight into the limitations for strengthening with continuous externally bonded CFRP sheets and highlight where alternative strengthening with deep embedded bars may be a more appropriate solution.

8.2 Analytical methodology

8.2.1 Rationale for using numerical methods for analysis

Numerical methods offer a significant advantage over codified approaches, presented in Chapter 2 and further discussed in Chapter 7, in obtaining the ultimate capacity of a beam as well as its structural behaviour under load. Non-linear finite element analysis software, which is based on the laws of fracture mechanics, is also capable of predicting the cracking

in concrete within the finite elements. Non-linear fracture mechanics-based software ATENA 2D was therefore used to model the behaviour of unstrengthened and strengthened reinforced concrete beams to determine their ultimate capacity, observe their behaviour and the critical shear crack location. The numerical models and their analysis were limited to 2D and the limitations of the models are discussed. The T-beams tested experimentally were modelled and the results compared with the experimental data and observations. A parametric study on reinforced concrete beams was carried out to determine the key parameters influencing the ultimate capacity of the beam as well as the crack pattern and the failure mode.

8.2.2 Objectives

The objectives for using ATENA 2D to analyze the behaviour of the unstrengthened and strengthened reinforced concrete T-beams was threefold:

1. To realistically model the behaviour of the unstrengthened and strengthened beams to confirm the model can accurately capture size effect;
2. To confirm where the critical shear crack will initiate in unstrengthened and strengthened beams to determine rational limits for strengthening with externally bonded CFRP sheets;
3. To demonstrate the applicability of using ATENA 2D for analysis of existing reinforced concrete slab-on-beam structures.

8.3 FE model preparation

This section describes how the FE model was generated and what parameters were used for the analysis. The modelled configurations include the unstrengthened control specimens LBC and MBC, specimens strengthened with CFRP U-wraps without end anchorage LB2U and MB2U, and the specimens strengthened with deep embedded bars LBDE and MBDE. For the specimens strengthened with the CFRP sheets only the case with extreme strengthening (1.3% CFRP ratio) was selected for a direct comparison between the two modelled sizes of test specimen.

Due to the limitations of the 2D model, the U-wrap cases with end anchorage LB2UA and MB2UA were not modelled as a more complex 3D model would be more appropriate. All

dimensions and material properties for the modelled beams were identical to those presented in Chapter 5 for the tested beams.

8.3.1 Material parameters

The material properties for concrete and steel used for the models were identical with the properties in the tested beams presented in Chapter 5. The concrete compressive strength remained constant throughout at 60 MPa and the concrete tensile strength 3.8 MPa, to correspond with the design values used in the experimental programme. The concrete material model used for the ATENA 2D analyses was the concrete model *Sbeta*. This model is suitable for plane stress 2D analysis and employs an orthotropic smeared crack model.

The model calculates all parameters for concrete based on the input of concrete compressive strength alone. It is however possible to manually specify the parameters, such as concrete tensile strength, fracture energy and crack opening law. The default setting was used for all analyses, apart from specifying the values for actual concrete tensile strength, as the fracture energy and the crack opening law were not determined experimentally. A fictitious crack width is therefore assumed according to the default model.

The specific details of the concrete material model are presented in Figure 8.1 through to Figure 8.4.

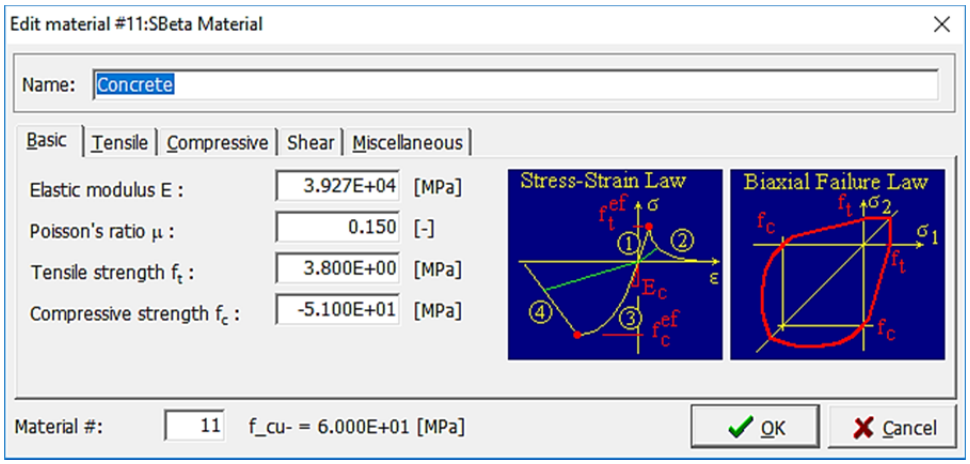

Figure 8.1 – Concrete material model – basic information.

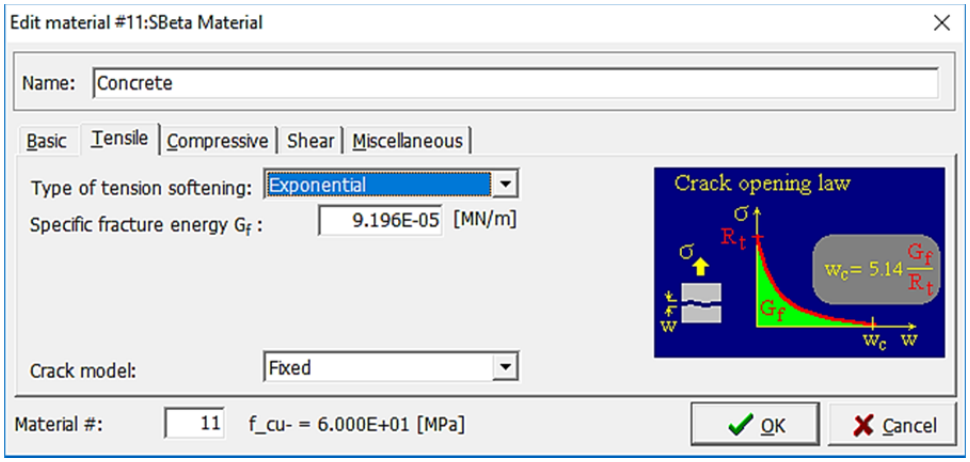

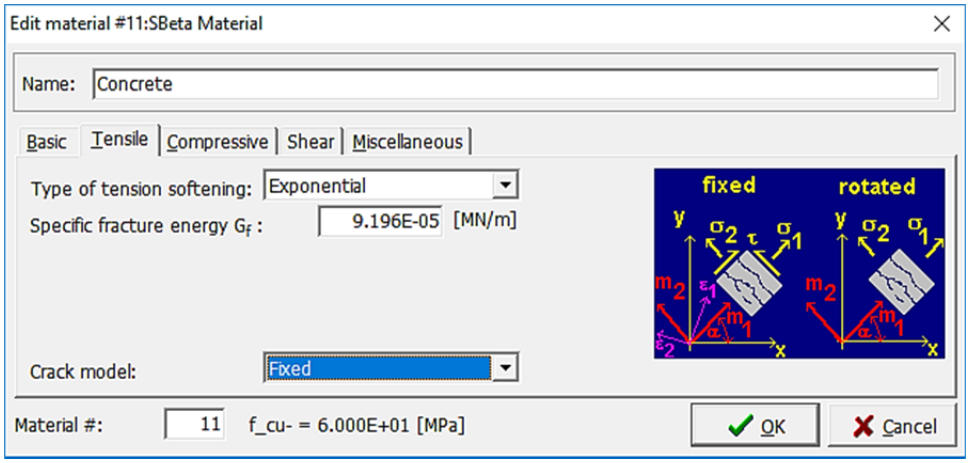

Figure 8.2 – Concrete material model – tensile properties.

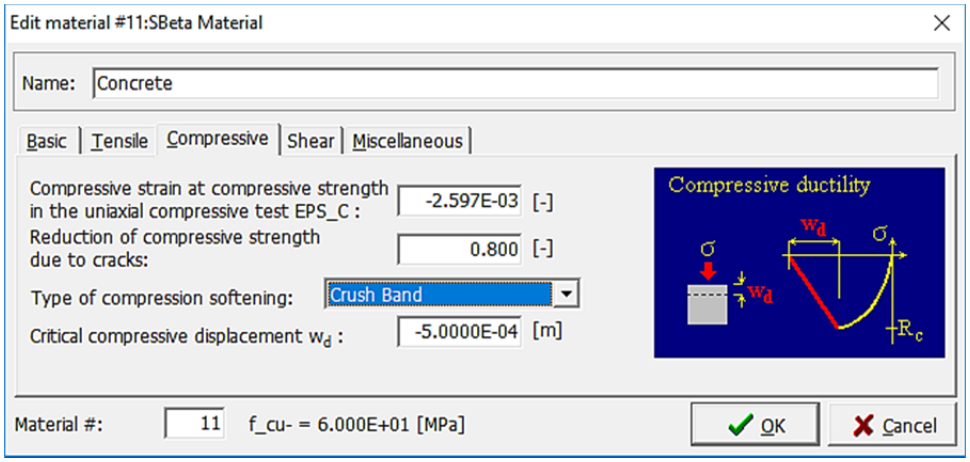

Figure 8.3 – Concrete material model – compressive properties.

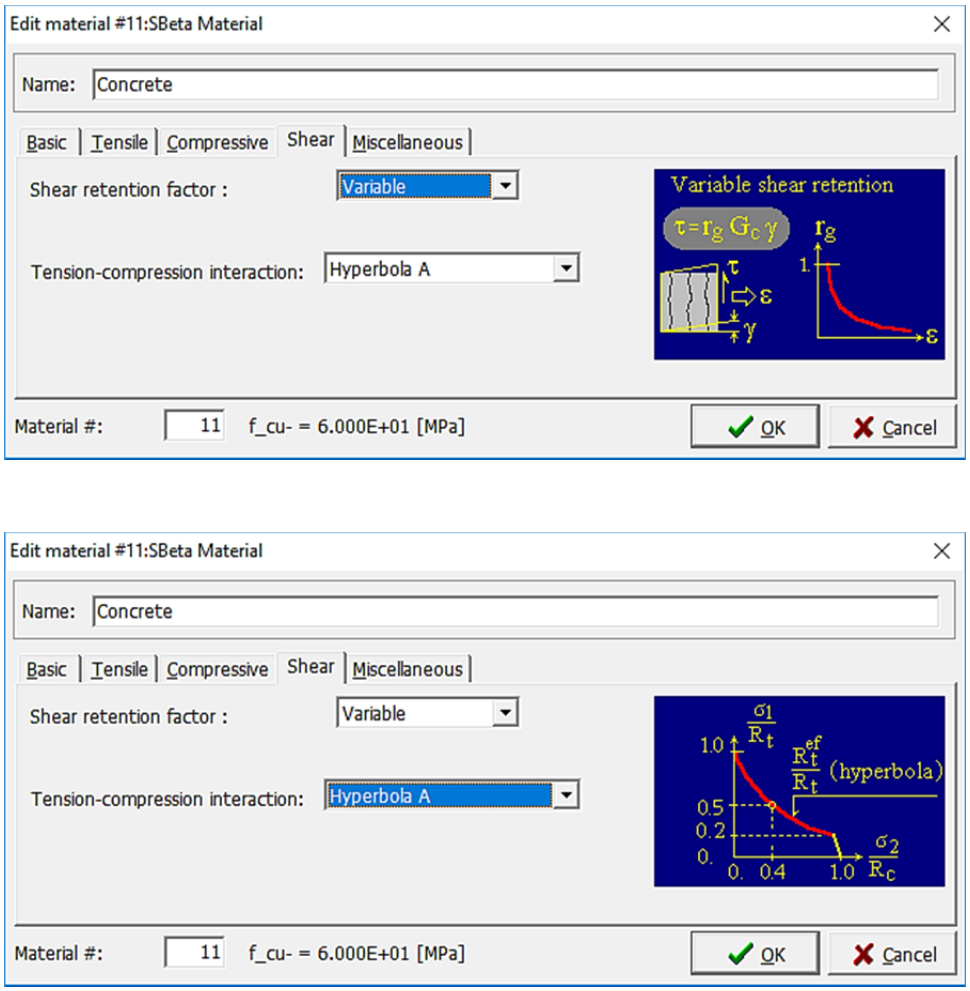

Figure 8.4 – Concrete material model – shear properties.

The material properties for the support and loading plates were specified within the material *Steel*, with parameters as shown in Figure 8.5.

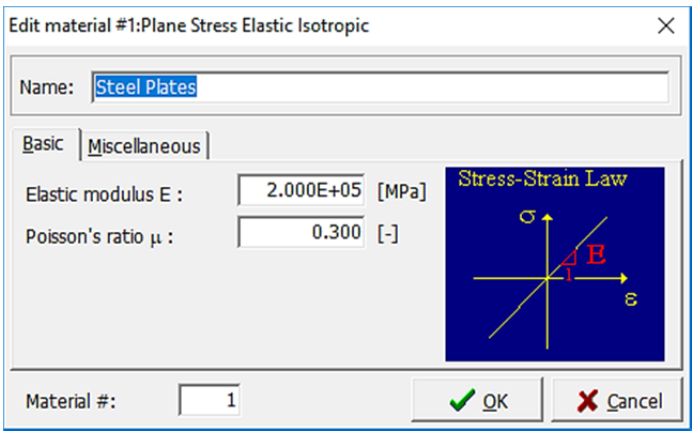

Figure 8.5 – Steel material model – support and loading plates.

Reinforcement material properties for discrete bars are included in the package in the

material *Reinforcement*. A uni-axial law for stress-strain relationship is offered by this model with three types available – linear, bi-linear and multi-linear. The model operates on a complete symmetric form for tension and compression, and therefore only the tension part of the law is required to be defined. Bi-linear law with hardening was used to model the steel reinforcing bars, as shown in Figure 8.6.

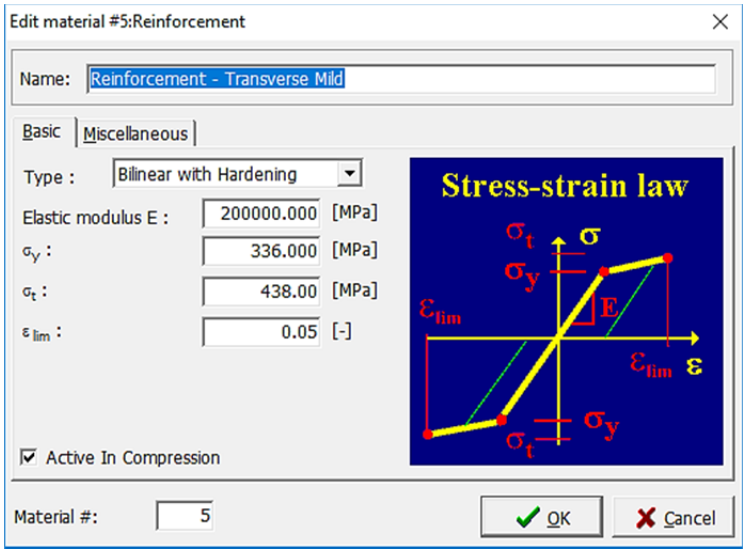

Figure 8.6 – Reinforcement material model with bi-linear hardening for mild steel links.

The material properties for the externally bonded CFRP sheets and bars were specified within the *Reinforcement* material model. The linear model was used, and only the Elastic Modulus was specified for each material type, see Figure 8.7 and Figure 8.8 for the CFRP sheets and bars, respectively.

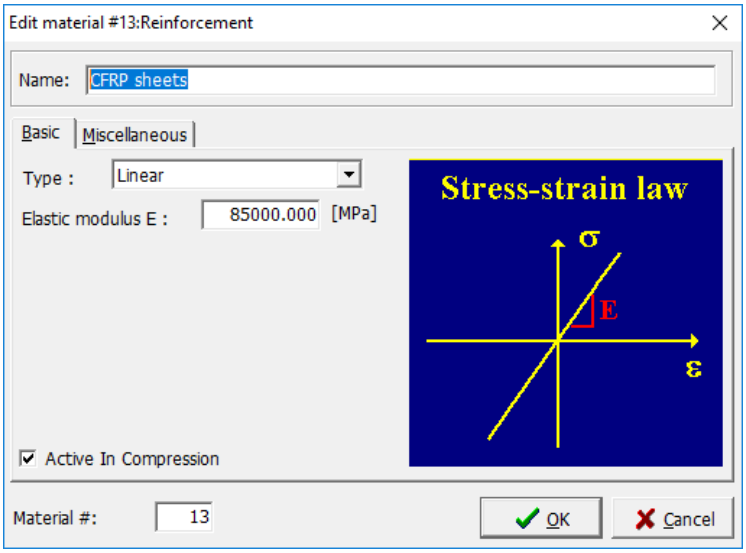

Figure 8.7 – CFRP sheets material model – linear.

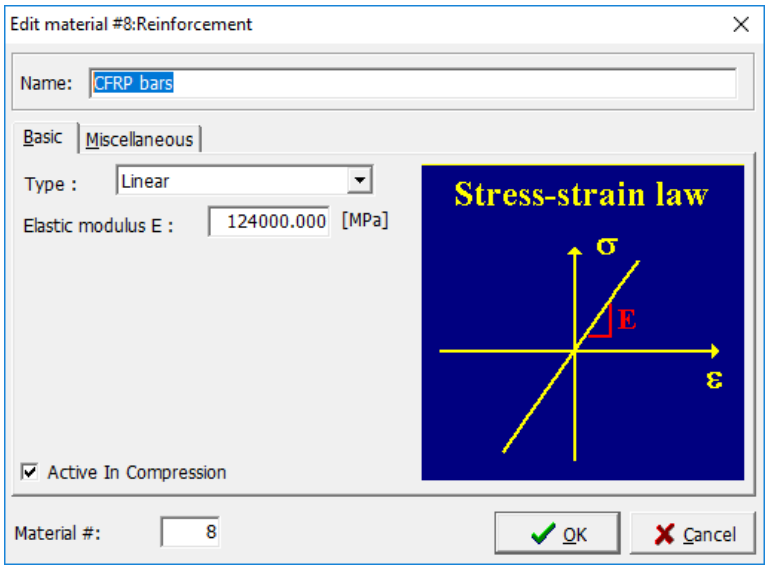

Figure 8.8 – CFRP bars material model – linear.

The slip between the reinforcement and the concrete can be defined within the model using material *Bond for reinforcement.* The relationship between the bond stress and the slip between the bar and the surrounding concrete is defined by default according to CEB-FIB Model Code 1990 (ATENA Manual, 2016, ATENA Theory, 2016), see Figure 8.9.

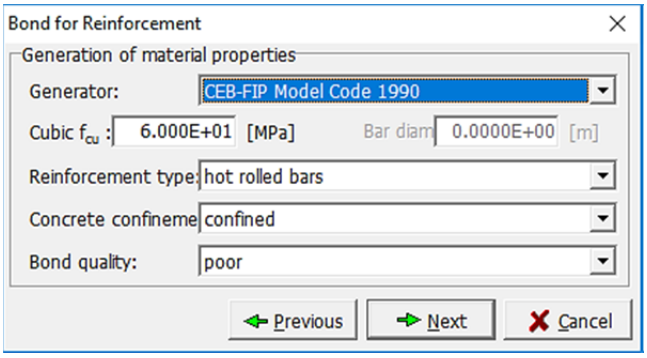

Figure 8.9 – CEB FIP Model Code 1990 material model – bond for reinforcement.

This default model was used for modelling of the bond for the mild steel shear links in the tested span as slip was likely to occur due to the links being of smooth mild steel, see Figure 8.10. For all other cases, perfect connection until fracture of the CFRP was assumed.

The bond for the CFRP sheets was manually specified within the model. A tri-linear bond model, simplified from the work of Dai et al. (2013), was used with values of bond stress and slip as shown in Figure 8.11.

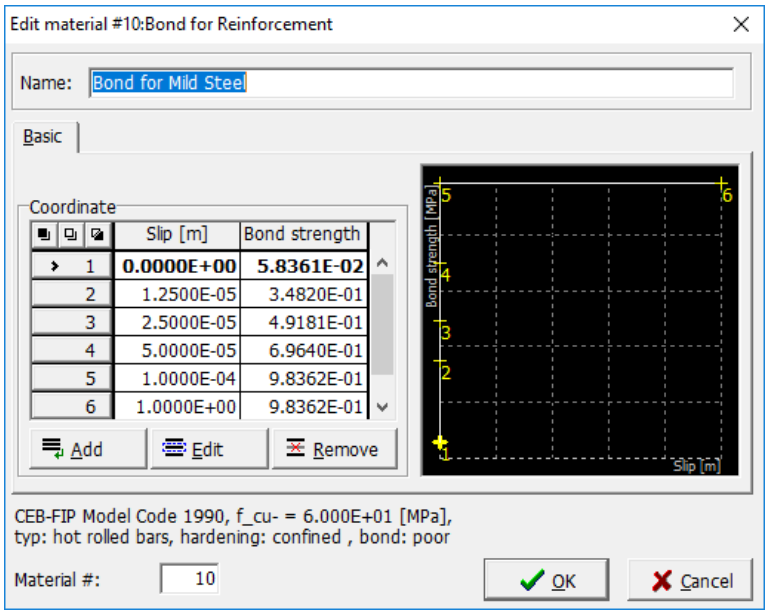

Figure 8.10 – Bond slip law for mild steel shear links.

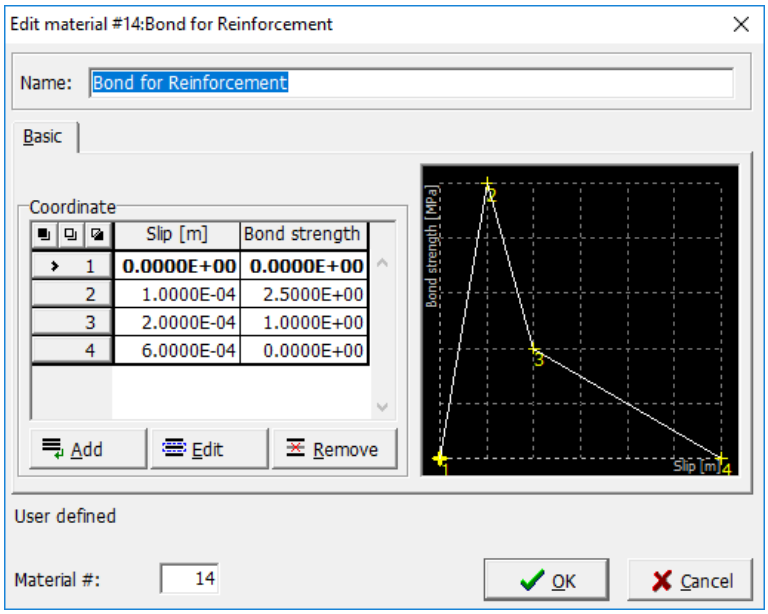

Figure 8.11 – Bond slip law for CFRP sheets – tri-linear.

The bond for the CFRP bars for the deep embedment specimens was assumed as perfect bond.

8.3.2 Geometrical model and mesh generation

The beams were modelled in 2D as simply supported on steel support plates and loaded through a loading plate, as was the case in the experimental test setup presented in Chapter

5. The entire beam was modelled in each case as symmetry does not apply due to the differing shear reinforcement within the tested and the reaction spans. The model generation in ATENA 2D is through input of joints and lines and specification of macro-elements within the boundaries of these lines; see Figure 8.12 and Figure 8.13. The depth of the macro-elements is specified as *thickness* of the macro-elements, to model the 3D nature of the reinforced concrete T-beam and the support and loading plates in a 2D environment.

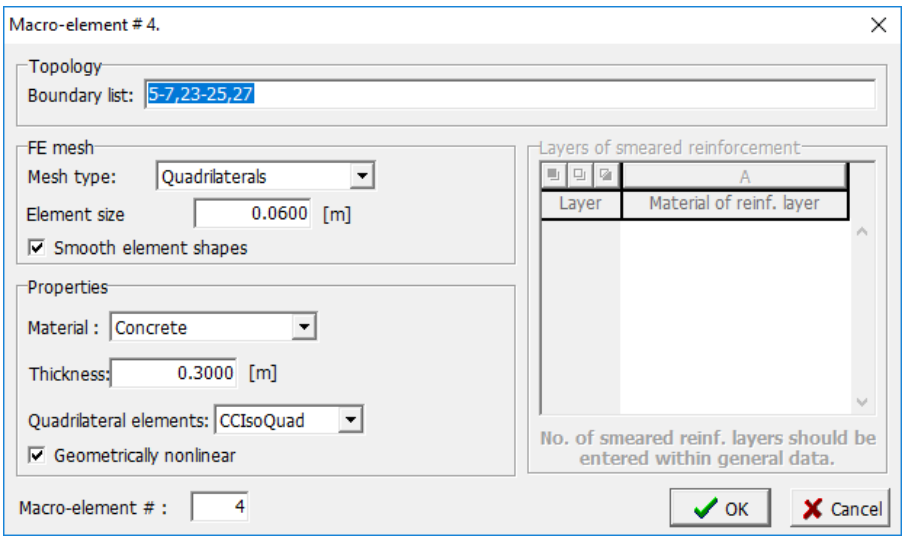

Figure 8.12 – Macro-elements for concrete.

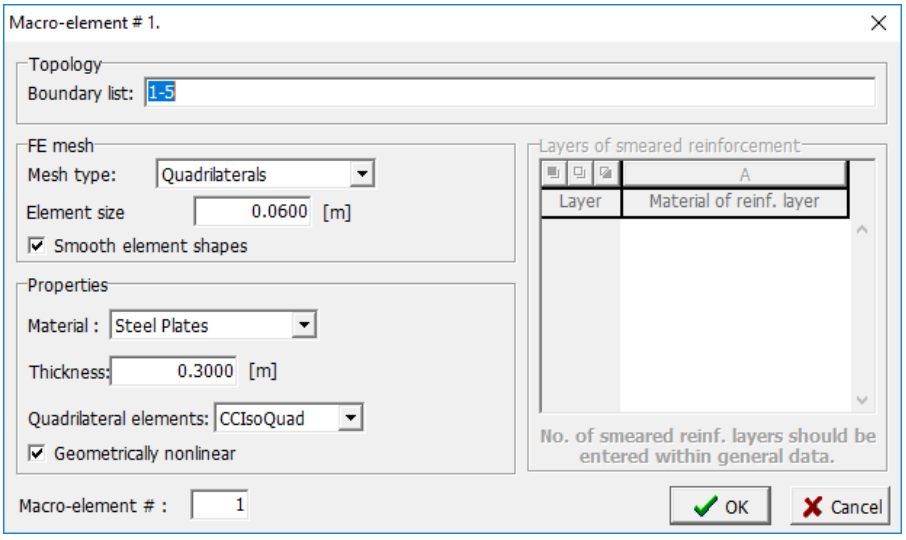

Figure 8.13 – Macro-elements for steel plates.

The element size specified for each macro-element determines the finite element mesh size. The finite element mesh was generated using the default recommended *quadrilateral*

elements, with element size of 60 mm and 40 mm for the large LBC FEM and the medium MBC FEM, respectively. This mesh size was initially selected so that there are at least 12 finite elements across the depth of the beam with no fewer than 2 within the flange. The minimum recommended mesh size for ATENA 2D to return at least qualitative results is 4 to 6 elements over the height of the modelled element (ATENA Manual, 2016).

8.3.3 Reinforcement

The reinforcement in ATENA 2D is modelled as discrete bars with their diameter and perimeter for the application of bond models with the option of disabling the top and the bottom of the bars against slip. The reinforcement detail was identical to that for the tested beams, with mild steel shear links within the tested span, and deformed bars as per specimen design. The top and the bottom of the shear links was disabled against slip as the links were formed from closed loops. ATENA only models the legs of the links and not the entire loop and therefore disabling the slip is appropriate. Figure 8.14 shows the complete models LBC FEM and MBC FEM corresponding to the tested specimens LBC and MBC.

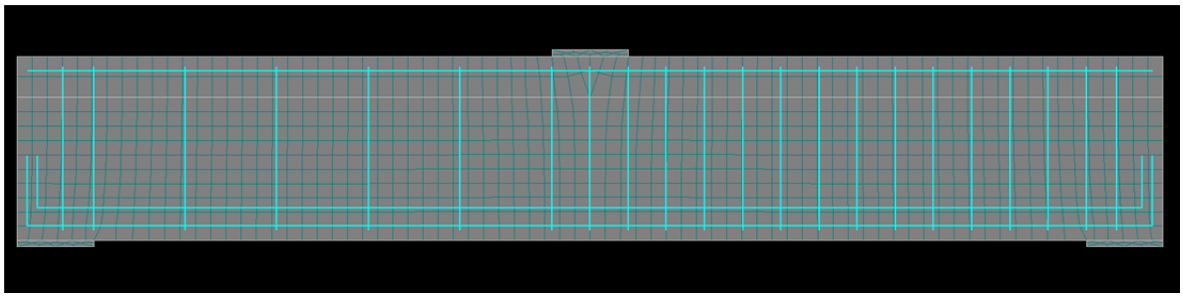

(a)

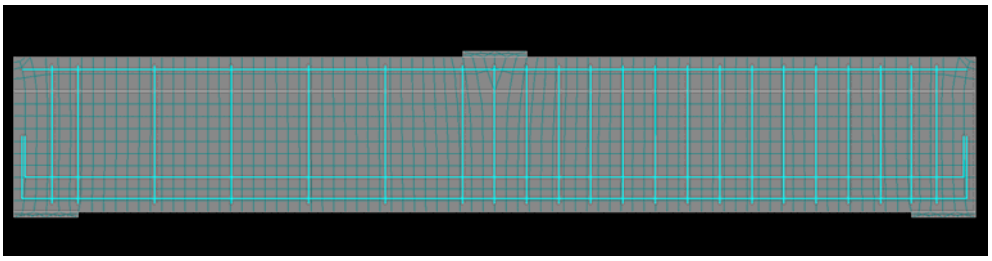

(b)

Figure 8.14 – Finite element models for (a) LBC FEM, (b) MBC FEM.

Due to the limitations of the model, the externally bonded CFRP reinforcement was also modelled as discrete reinforcing bars, where the area and the perimeter of the bar was determined from the material density of the CFRP fabric (Tyfo strengthening systems, 2012, 2014). The amount of CFRP reinforcement for the model assumed two discrete CFRP bars of a fixed area and perimeter per location; see parameters in Table 8.1 for models LB2U FEM and MB2U FEM.

Table 8.1 – Geometric and material properties for modelling of bonded CFRP sheets.

Model	A_b [mm^2]	P_b [mm]	Spacing [mm]	Bond model for bar slip	$E_{f,d}$ [GPa]	FRP material model
LB2U FEM	3.73	3.95	13.3	Tri-linear	85	Linear
MB2U FEM	2.80	2.97	10.0	Tri-linear	85	Linear

The parametric model used for specifying the bond is shown in Figure 8.15.

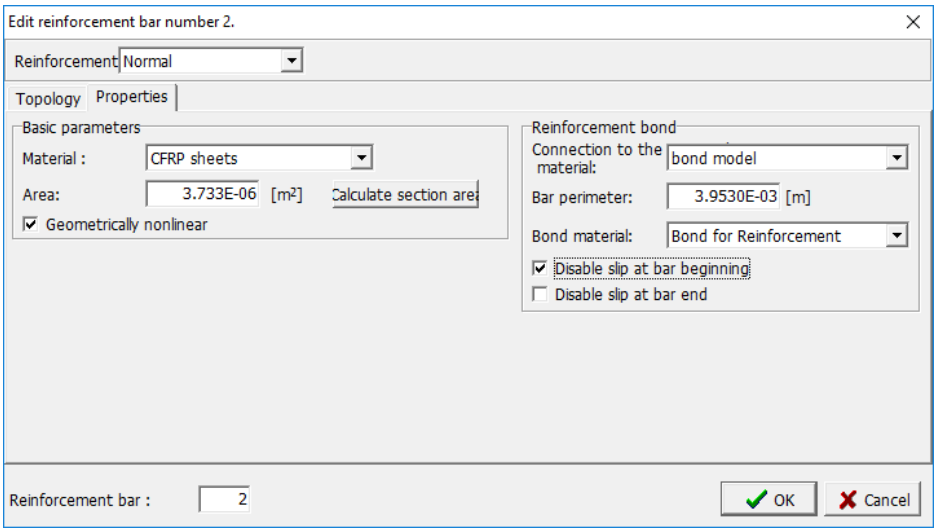

Figure 8.15 – Defining bond model parameter for CFRP sheets.

The models LB2U FEM and MB2U FEM corresponding to the tested cases LB2U and MB2U, respectively, are presented in Figure 8.16.

Similarly to the reinforced concrete specimens, the specimens strengthened with deep embedded CFRP bars were modelled in the same way as the unstrengthened beams with steel shear reinforcement. The CFRP reinforcement was modelled as discrete bars of diameter equivalent to that used in the experimental programme. Material properties given

by the manufacturer presented in Chapter 5 were used. The models LBDE FEM and MBDE FEM corresponding to the tested specimens LBDE and MBDE, respectively, are presented in Figure 8.17.

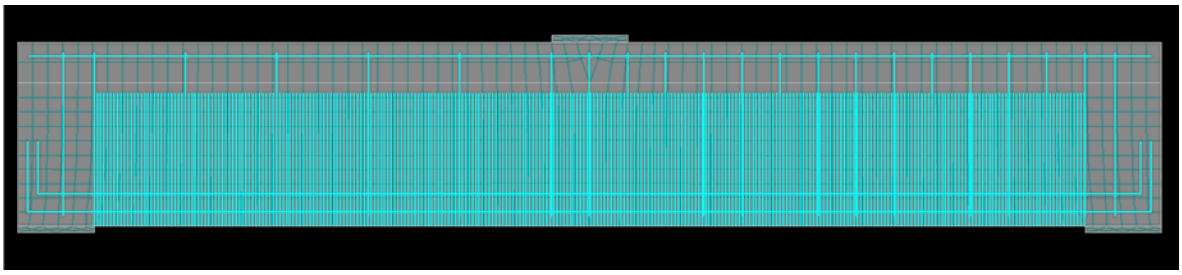

(a)

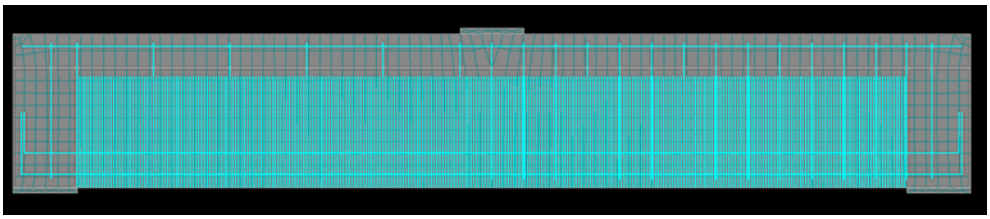

(b)

Figure 8.16 – Finite element models for (a) LB2U FEM, (b) MB2U FEM.

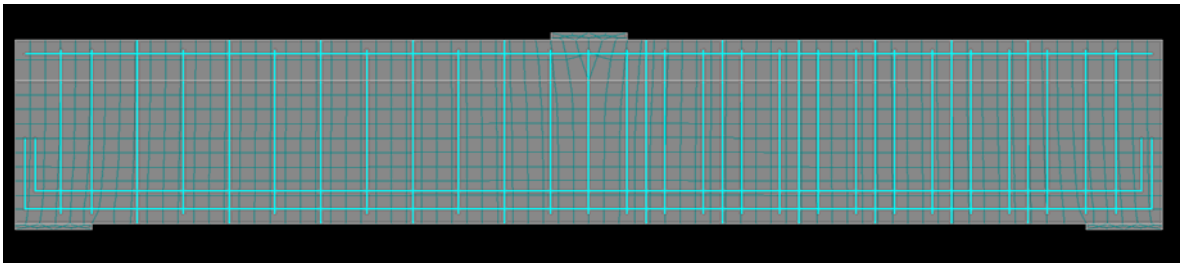

(a)

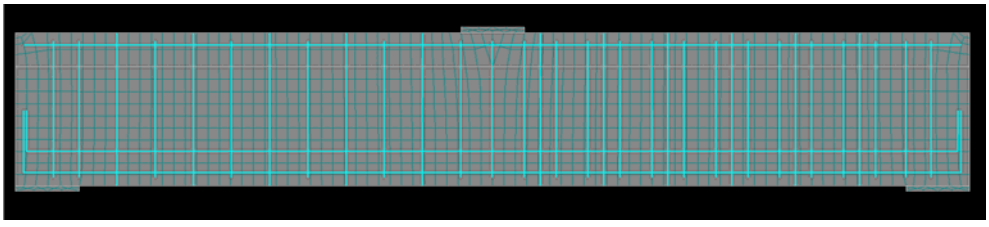

(b)

Figure 8.17 – Finite element models for (a) LBDE FEM, (b) MBDE FEM.

8.3.4 Supports and actions

Two load cases were created in ATENA 2D – *Load case with supports* and *Load case with actions*. Figure 8.18 (a) shows the support conditions and Figure 8.18 (b) shows the applied displacement at midspan and the monitoring points. Two monitoring points were used to – *Monitor 1* at the centre of the loading plate to track the corresponding load and *Monitor 2* at the bottom soffit at midspan tracking vertical displacement of the beam, shown in Figure 8.18 (a).

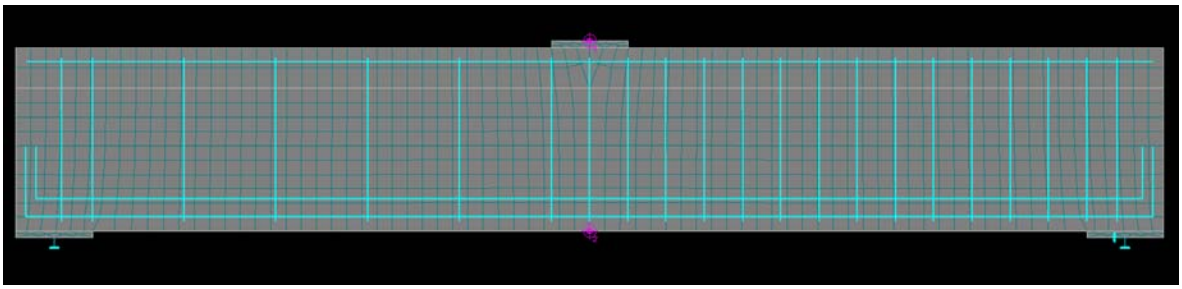

(a)

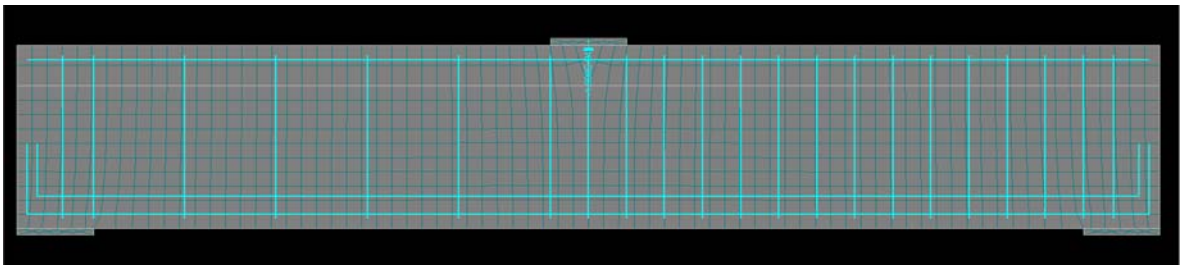

(b)

Figure 8.18 – Finite element model showing (a) simply supported condition and monitoring points, (b) applied displacement at loading plate.

8.3.5 Loading history and solution parameters

The dead load of the modelled beam is applied in ATENA 2D automatically through the material model for concrete and steel as material density is defined for each material model. The applied load was modelled as a *Prescribed deformation* at the centre of the loading plate in increments of 0.1 mm until failure. The loading history was created using a step multiplier of 0.5, which was further reduced to 0.25 after cracking initiated. Such an approach was identified as appropriate after several initial runs to determine whether the

loading within each step size was sufficiently small for the solution to converge. The analysis was performed using the standard *Solution Parameters* within the package with number of iteration of 60 per analysis step and the results were stored after each step of the analysis, see Figure 8.19. All other parameters remained as per default settings.

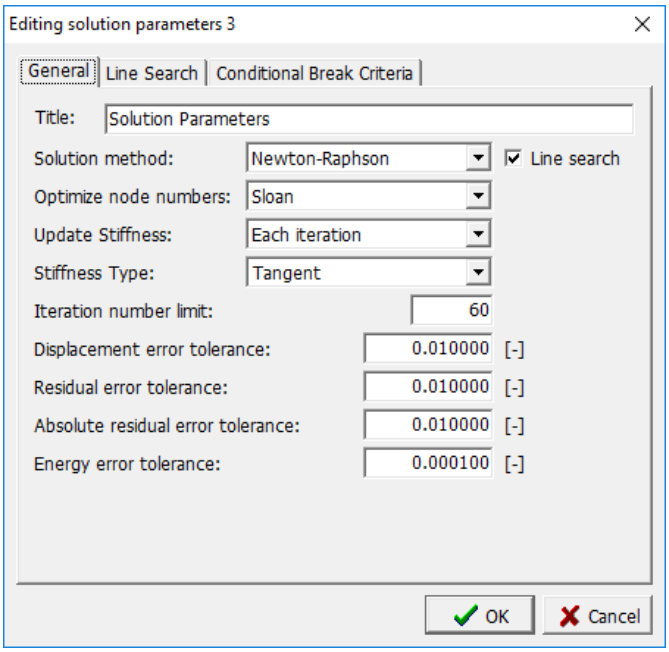

Figure 8.19 – Solution parameters – all other tabs remained in default settings.

8.4 FE non-linear analysis

8.4.1 Mesh sensitivity

Mesh sensitivity was carried out to confirm that using a coarser mesh was adequate for the modelled cases. The large unstrengthened control beam LBC FEM was modelled with a reduced mesh element size of 45 mm and the medium beam MBC FEM with element mesh size of 30 mm while keeping the analysis parameters constant.

The shear stress versus displacement curves for models of both mesh sizes for LBC FEM and MBC FEM are presented in Figure 8.20. The results from both mesh sizes for both modelled beam sizes returned similar results, including the load-displacement behaviour, confirming that the coarser mesh is adequate for this type of analysis. The coarser mesh was therefore selected for all analysis purposes due to the accuracy of the predicted ultimate capacity within the analysis parameters used and for a greater computational efficiency of the model.

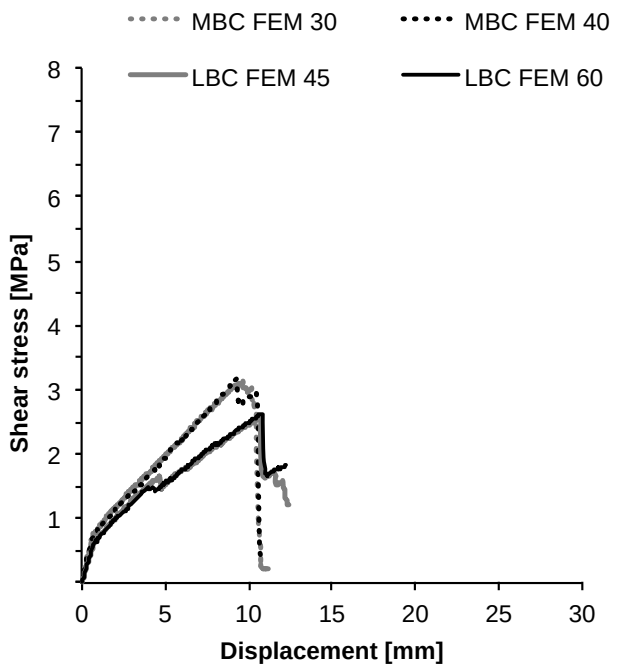

Figure 8.20 – Mesh sensitivity for configurations LBC FEM and MBC FEM – shear stress versus displacement.

8.4.2 Summary of results

The summary of numerically obtained results is presented in Table 8.2.

Table 8.2 – Summary of numerical results in comparison with experimental values.

Model	Experimental				Predicted	
					ATENA FEM	
	ρ_l [%]	ρ_v [%]	ρ_f [%]	$V_{u\text{-}exp}$ [kN]	$V_{u\text{-}ATENA}$ [kN]	$V_{u\text{-}ATENA}/V_{u\text{-}exp}$
LBC	2.2	0.1	–	472	472	1.00
LB2U	2.2	0.1	1.3	438	458	1.05
LB2UA	2.2	0.1	1.3	512	458	0.88
LBDE	2.2	0.1	0.2	605	551	0.92
MBC	2.4	0.1	–	322	321	1.00
MB2U	2.4	0.1	1.3	306	329	1.08
MB2UA	2.4	0.1	1.3	370	329	0.89
MBDE	2.4	0.1	0.2	482	455	0.94

The ultimate shear force, $V_{u\text{-}ATENA}$, recorded at failure corresponds to the peak shear force, obtained from the FE model and was compared with the experimentally obtained values, $V_{u\text{-}exp}$. The results obtained from the FE model are in good agreement with the experimental data for the unstrengthened control specimens LBC and MBC. However, the model over-predicts the capacity of the beams strengthened with CFRP U-wrap by 5% and 8% for the large LB2U and the medium MB2U specimens, respectively. Using the LB2U and MB2U models without end anchorage to predict the lower-bound capacity of the specimens with end anchorage, LB2UA and MB2UA, would provide a safe prediction of ultimate capacity.

This will be discussed further in detail in Section 8.3.3. Furthermore, the model under-predicts the capacity of the specimens strengthened with deep embedded CFRP bars by 8% for the large specimen LBDE and by 6% for the medium MBDE specimen. However, this would also provide a safe design prediction for the strengthened beams.

8.4.3 Unstrengthened control specimens

The results from the experimental testing of the unstrengthened control specimens LBC and MBC were compared with the results obtained from the FE model and are presented in Figure 8.21.

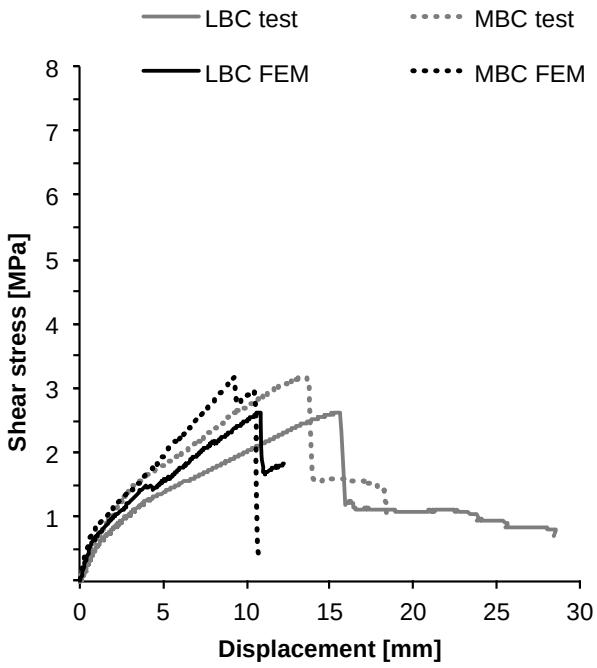

Figure 8.21 – Unstrengthened control specimens: shear-stress versus displacement.

The crack patterns at first cracking and at ultimate for both modelled specimens LBC FEM and MBC FEM were obtained from the FE model. The crack widths for the large unstrengthened control specimen LBC FEM at crack initiation and at failure are presented in Figure 8.22 (a) and Figure 8.22 (b).

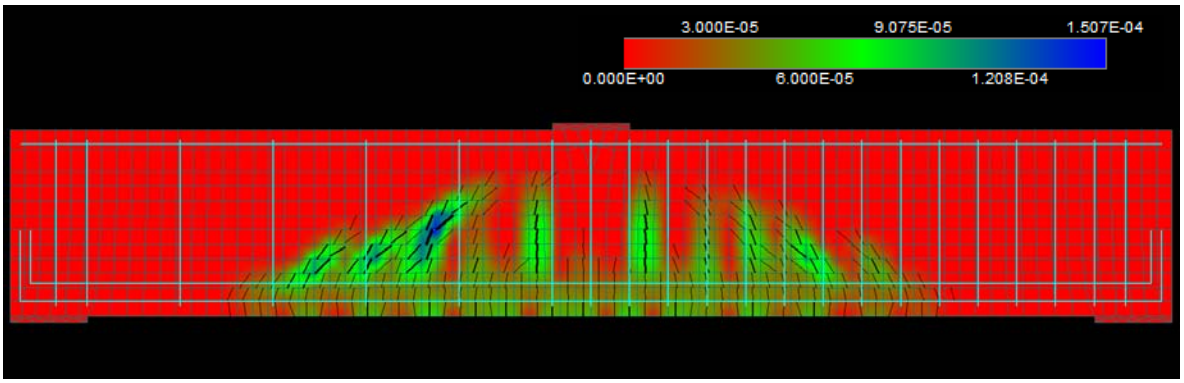

(a)

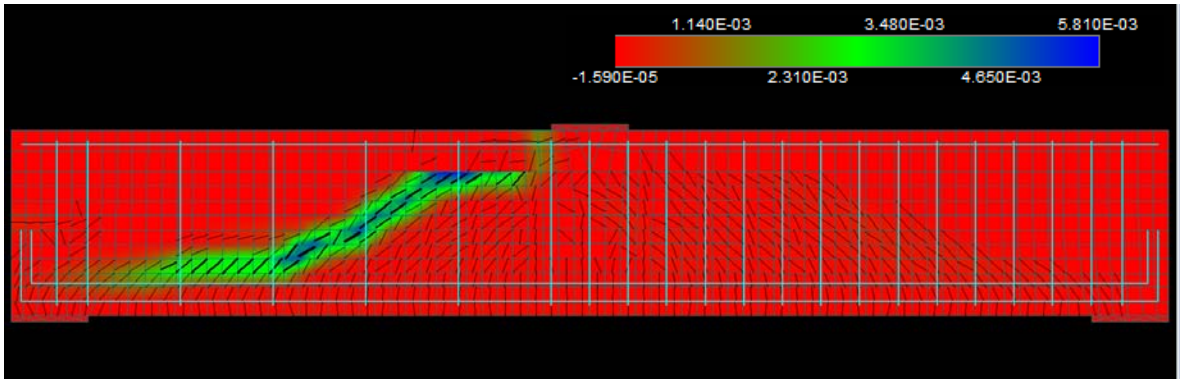

(b)

Figure 8.22 – Configuration LBC FEM – crack patterns: (a) web shear crack initiation, (b) shear crack prior to failure [m].

The cracking initially starts as moderate flexural cracking, with shear cracks at the location of the elastic neutral axis at an angle of approximately 45°, as shown in Figure 8.22 (a). These cracks further propagated into a fully developed shear crack in the web, terminating at the level of the longitudinal reinforcing bars, apparent from Figure 8.22 (b).

The crack patterns with corresponding crack widths for the medium unstrengthened control specimen MBC FEM at crack initiation and at failure are presented in Figure 8.23. Initially, the beam cracked in flexure, similarly to the large specimen LBC FEM, with

shear cracks initiating at the level of the elastic neutral axis at an angle of approximately 45°, as shown in Figure 8.23 (a). These further propagated into a fully developed diagonal shear crack; see Figure 8.23 (b).

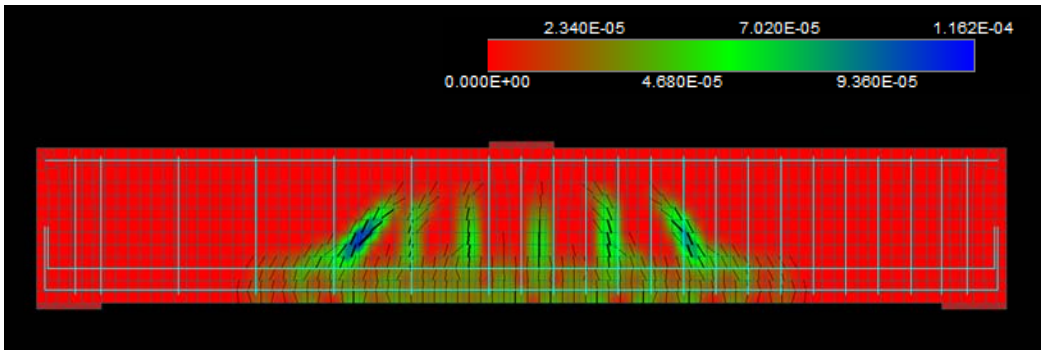

(a)

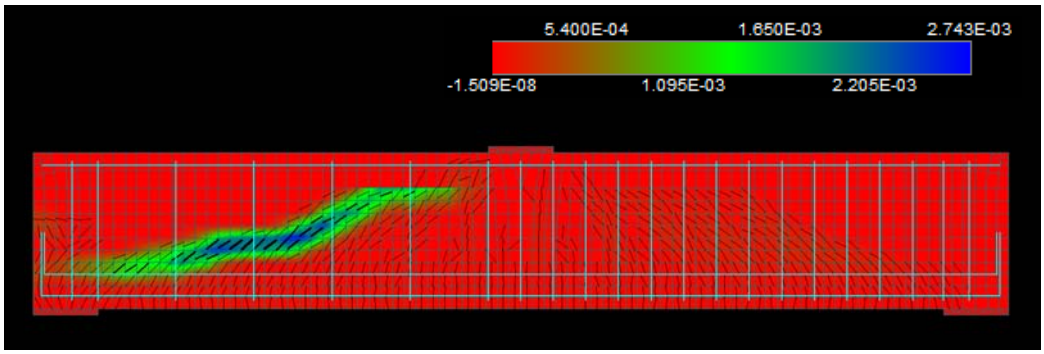

(b)

Figure 8.23 – Configuration MBC FEM – crack patterns: (a) web shear crack initiation, (b) shear crack prior to failure [m].

Comparison of the crack patterns obtained from the numerical models with DIC images from experimental testing is presented in Figure 8.24.

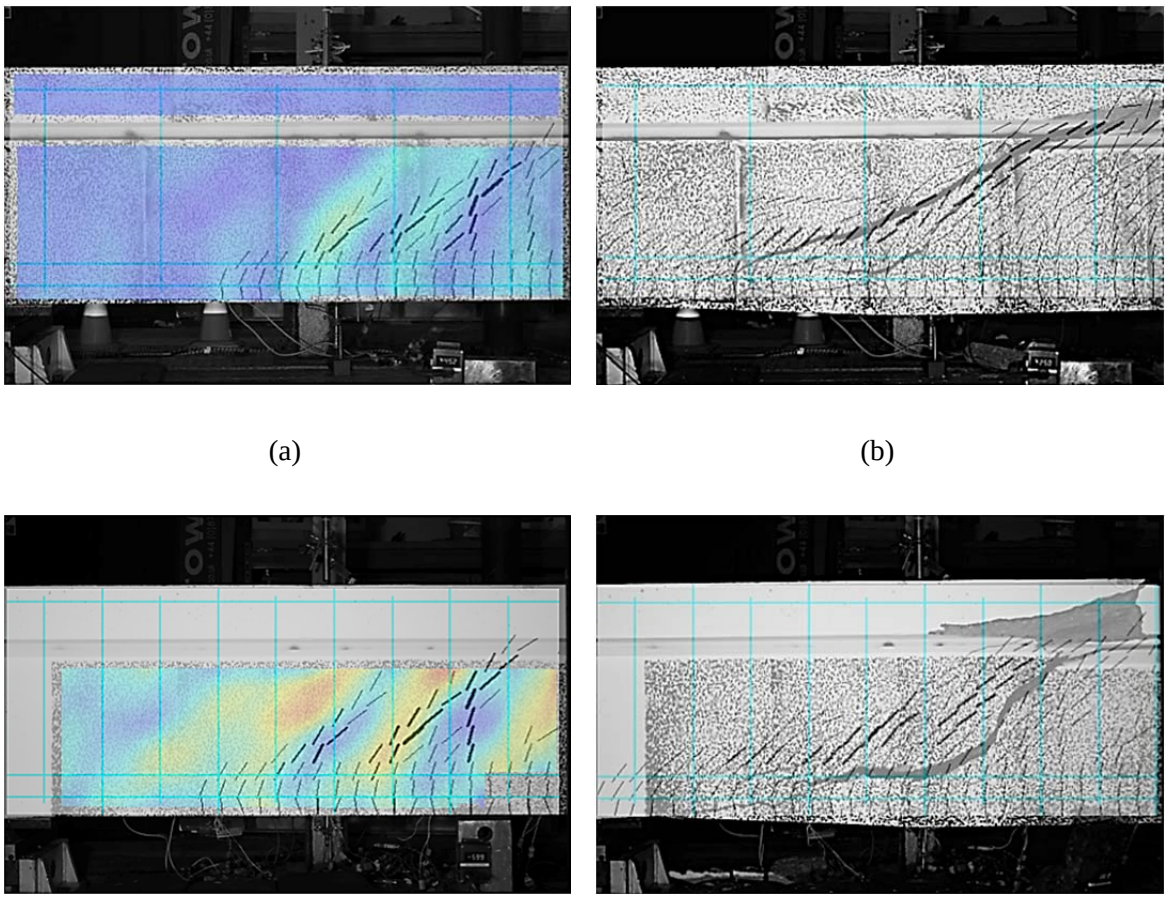

(a) (b)

(c) (d)

Figure 8.24 – Comparison of experimentally observed crack patterns for configuration LBC (a) at crack initiation, (b) at failure, and for MBC (c) at crack initiation, (d) at failure.

8.4.4 Specimens strengthened with externally bonded CFRP sheets

The results obtained experimentally for specimen strengthened with 1.3% CFRP LB2U and LB2UA and the results obtained numerically for LB2U FEM are presented in Figure 8.25 for comparison. The results obtained experimentally for the medium-sized specimens MB2U and MB2UA are compared with those obtained numerically for the modelled case MB2U FEM in Figure 8.26.

The comparison indicated that the *Sbeta* material parameter for concrete is adequate for beams strengthened with CFRP sheets, where the crack opening is constrained by the external CFRP sheets. This is due to the assumption of the fictitious crack width for the crack opening law, as prescribed by the default material model.

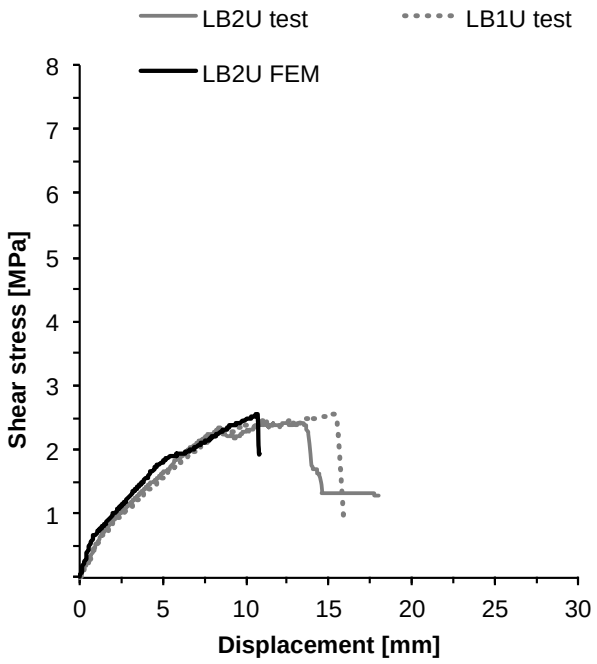

Figure 8.25 – Large beams with externally bonded CFRP U-wraps: shear stress versus displacement.

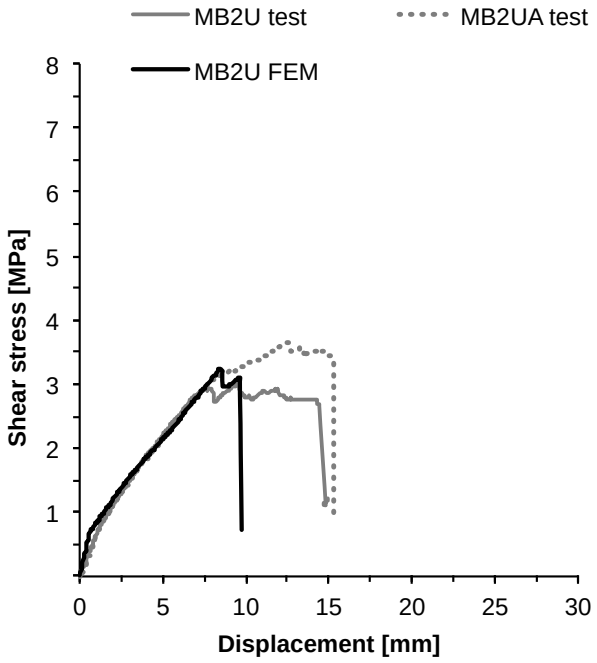

Figure 8.26 – Medium beams with externally bonded CFRP U-wraps: shear stress versus displacement.

The crack patterns with corresponding crack widths for the modelled LB2U FEM at shear crack initiation and at failure are presented in Figure 8.27.

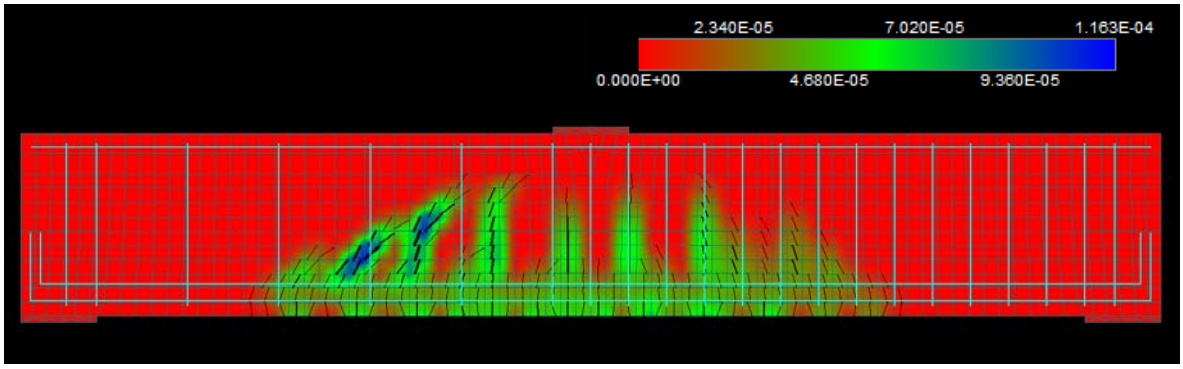

(a)

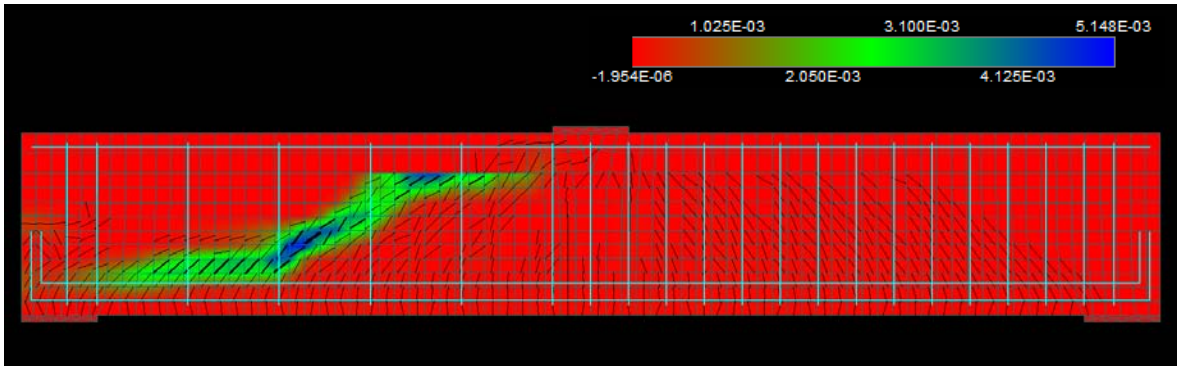

(b)

Figure 8.27 – Configuration LB2U FEM – crack patterns: (a) web shear crack initiation, (b) shear crack prior to failure [m].

The crack patterns with corresponding crack widths for the modelled MB2U FEM at shear crack initiation and at failure are presented in Figure 8.28.

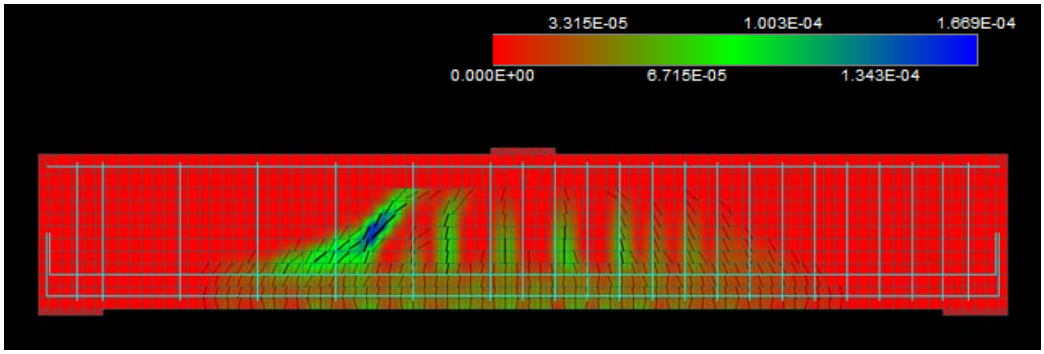

(a)

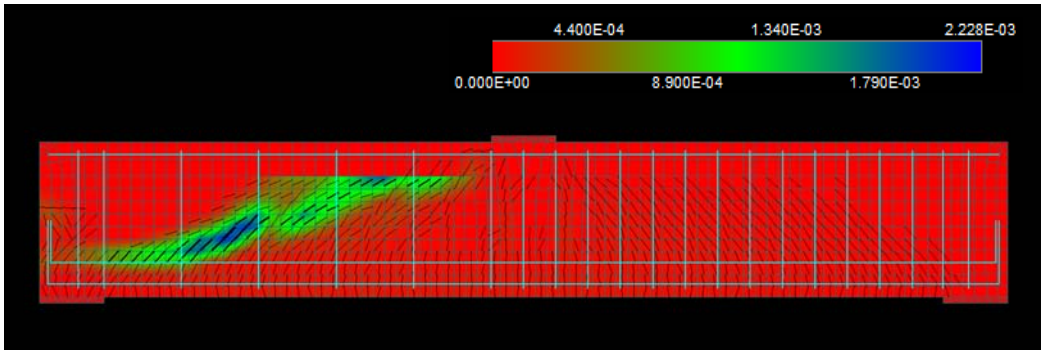

(b)

Figure 8.28 – Configuration MB2U FEM – crack patterns: (a) web shear crack initiation, (b) shear crack prior to failure [m].

Comparison of the crack patterns obtained from the numerical models with DIC images from experimental testing is presented in Figure 8.29.

From the comparison with the experimental results it is evident that the critical shear crack initiates in the web and further propagates within the web, causing premature debonding of the CFRP sheets.

The results obtained from the numerical model are in good agreement with those obtained experimentally, confirming that it is sufficiently appropriate to model the continuous CFRP sheet reinforcement as discrete bars in 2D.

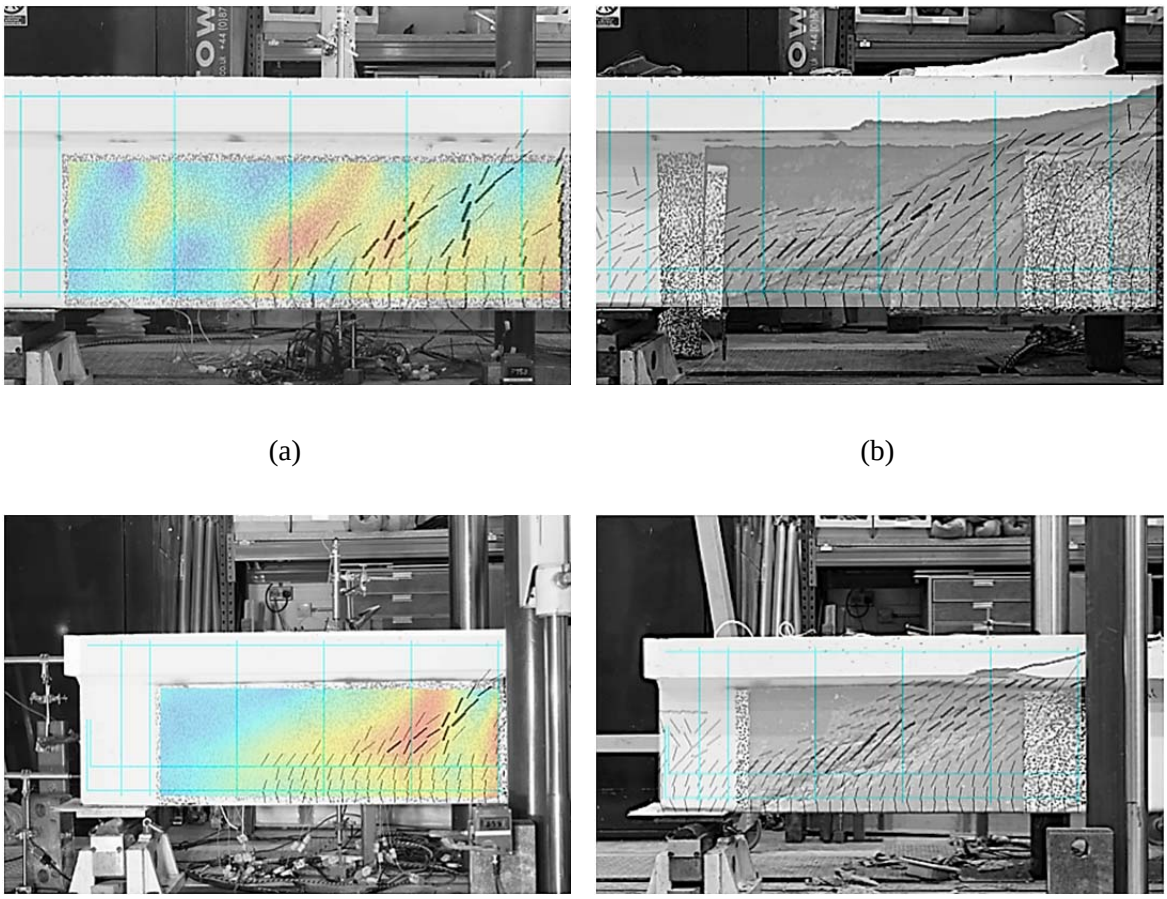

(a) (b)

(c) (d)

Figure 8.29 – Comparison of experimentally observed crack patterns for configuration LB2U (a) at crack initiation, (b) at failure, and for MB2U (c) at crack initiation, (d) at failure.

8.4.5 Specimens strengthened with deep embedded CFRP bars

Figure 8.30 shows the shear stress versus displacement graphs obtained for the modelled strengthened configuration LBDE FEM and MBDE FEM in comparison with the experimental data obtained from the tested specimens LBDE and MBDE, respectively.

The shear stress versus displacement graph indicated, that similarly to the unstrengthened reinforced concrete beams investigated in Section 8.4.2, the theoretical crack widths assumed by the default concrete model resulted in stiffer behaviour of the modelled beam.

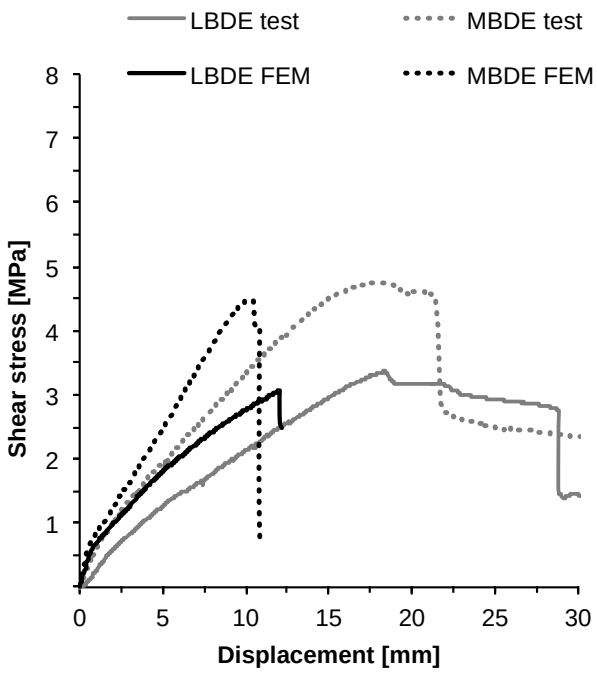

Figure 8.30 – Configuration deep embedment: shear stress versus displacement.

The crack patterns with corresponding crack widths for the modelled LBDE FEM configuration showing the crack initiation and further propagation of shear cracking are presented in Figure 8.31 (a) and Figure 8.31 (b), respectively. The crack patterns for the modelled MBDE FEM configuration showing the crack initiation and further propagation of shear cracking are presented in Figure 8.32 (a) and Figure 8.32 (b), respectively.

In this case, the flexural cracks at midspan did not close after the shear cracks developed in the web and remained active until failure, as shown in Figure 8.32 (b). Also, a more dispersed crack pattern across the shear links can be observed, suggesting that the amount of shear cracking is controlled by the transverse steel and the additional CFRP reinforcement.

Comparison of the crack patterns obtained from the numerical models with DIC images from experimental testing is presented in Figure 8.33.

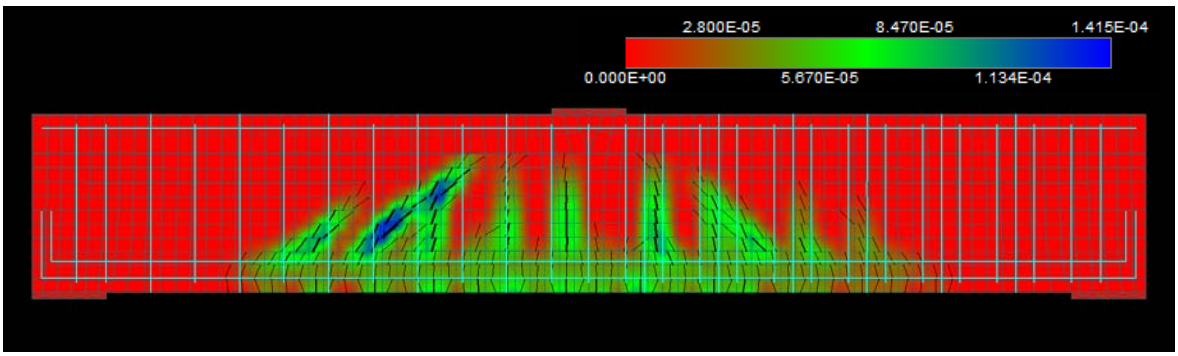

(a)

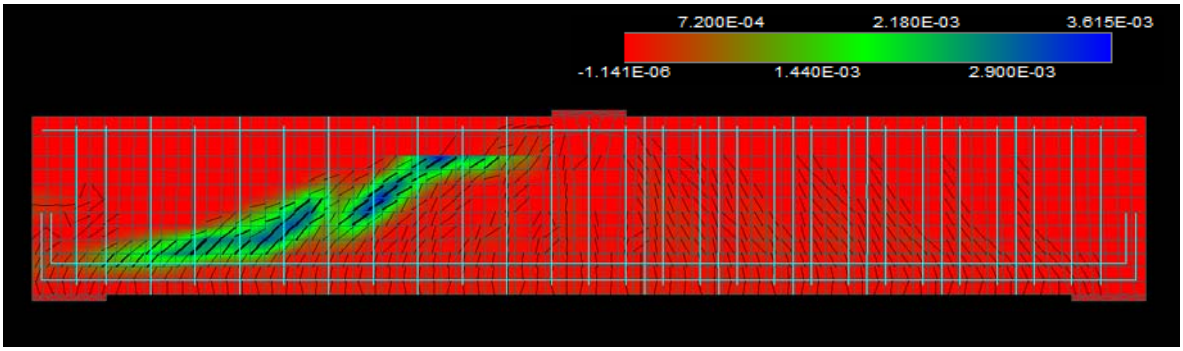

(b)

Figure 8.31 – Configuration LBDE FEM – crack patterns: (a) web shear crack initiation, (b) shear crack prior to failure [m].

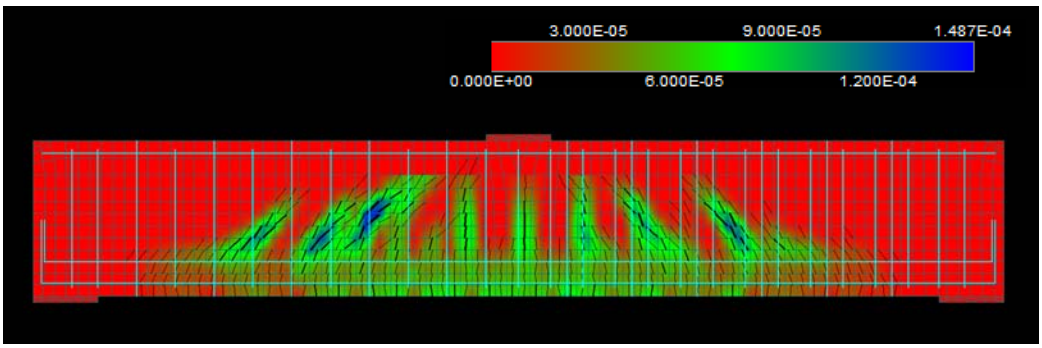

(a)

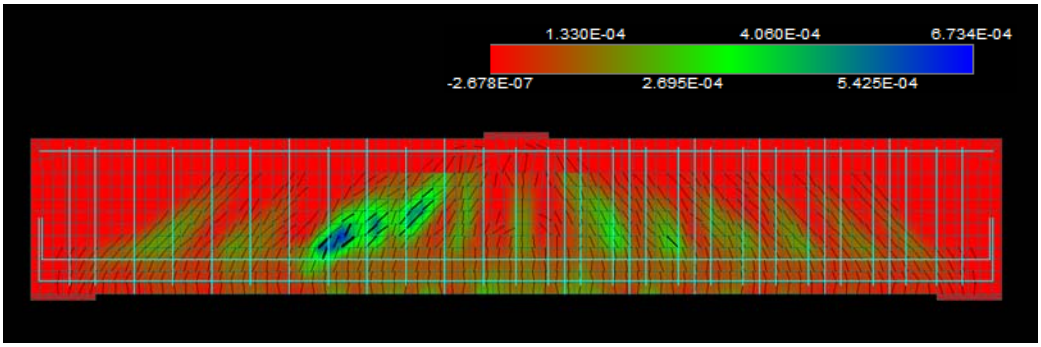

(b)

Figure 8.32 – Configuration MBDE FEM – crack patterns: (a) web shear crack initiation, (b) shear crack prior to failure [m].

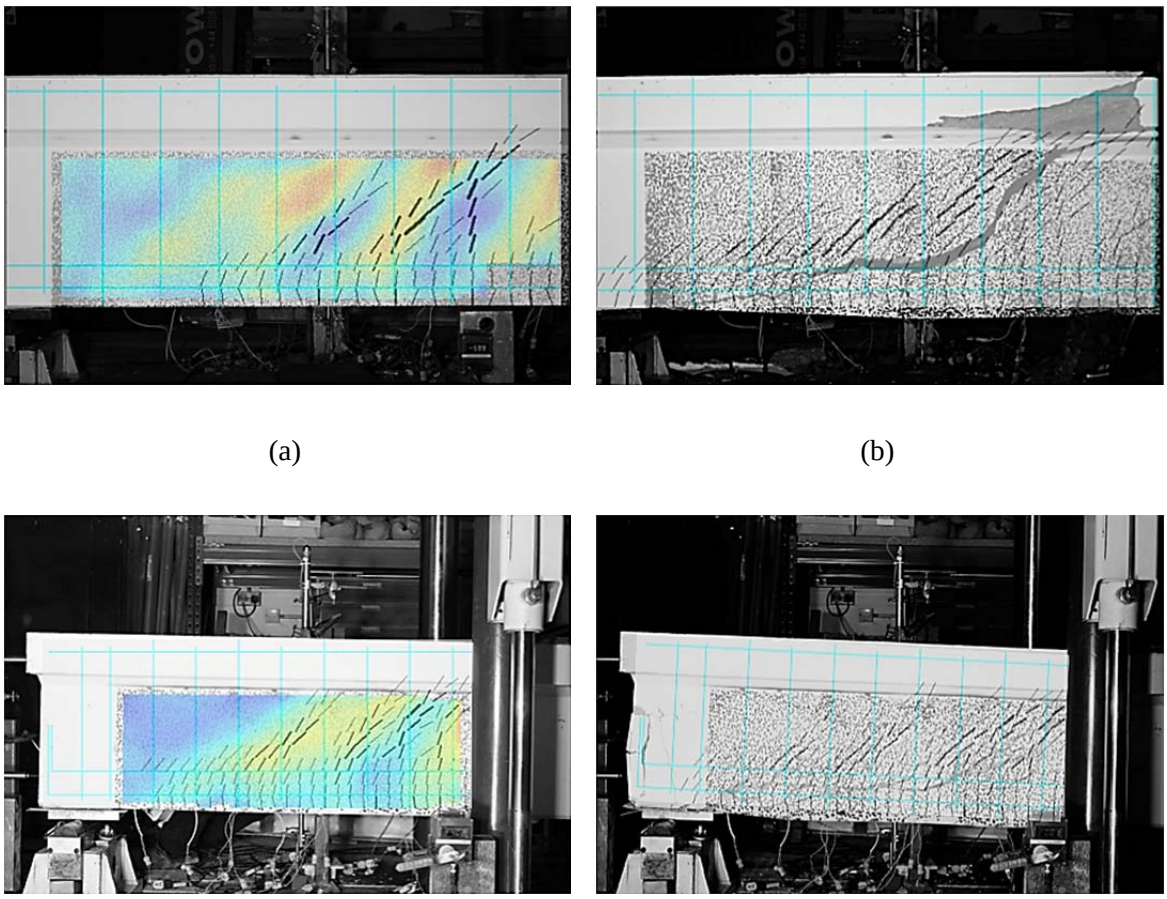

(a) (b)

(c) (d)

Figure 8.33 – Comparison of experimentally observed crack patterns for configuration LB2U (a) at crack initiation, (b) at failure, and for MB2U (c) at crack initiation, (d) at failure.

8.5 Parametric study on reinforced concrete T-beams

To better understand the interlinked behaviour of the individual components of reinforced concrete beams on the overall structural behaviour, a parametric study was carried out.

The main objective of this study was to identify the key parameters that would render the strengthening with CFRP U-wraps ineffective due to the location of the critical shear crack within the web, causing premature debonding. The medium beam geometry as presented in Chapter 5 was selected and used throughout for reasons of numerical efficiency, as the package was demonstrated to capture size effect in reinforced concrete beams. In this targeted study, the overall geometry of the concrete only section remains the same with one parameter studied at a time to prevent multiple parameter variation using ATENA 2D. The following parameters and their influence on the ultimate shear capacity and initial

shear crack location were investigated: concrete compressive strength, longitudinal steel ratio, shear reinforcement ratio, beam geometry and shear span.

8.5.1 Concrete strength

In this parametric study, the compressive concrete strength varied from 20 MPa to 60 MPa in 10 MPa increments. Such an approach was selected to model realistic scenarios of concrete strengths typically assumed for assessment of existing reinforced concrete structures due to lack of as-built information.

The designation of the modelled specimens follows the format of MBC-concrete grade for ease of orientation. The ratio of the longitudinal and shear reinforcement remained unchanged as per test specimen design. The results from this parametric study are presented in Table 8.3, alongside material properties for the modelled configurations.

Table 8.3 – Influence of concrete compressive strength on ultimate shear capacity.

Model	Steel		Concrete		FEM Results		
	ρ_l [%]	ρ_v [%]	f'_c [a] [MPa]	f_t [b] [MPa]	V_u [kN]	v_u [MPa]	Failure mode
MBC-20	2.4	0.1	17.0	1.77	171	1.69	Shear
MBC-30	2.4	0.1	25.5	2.32	196	1.94	Shear
MBC-40	2.4	0.1	34.0	2.81	210	2.07	Shear
MBC-50	2.4	0.1	42.5	3.26	241	2.38	Shear
MBC-60*	2.4	0.1	51.0	3.80	321	3.17	Shear

[a] Concrete compressive strength determined by FE package ATENA 2D.

[b] Concrete tensile strength determined by FE package ATENA 2D apart from MBC-60.

* Corresponds to the tested specimen MBC FEM.

The relationship between the concrete compressive strength, represented as concrete grade in MPa, and the shear stress is shown in Figure 8.34. The results revealed that the increase in shear capacity with increasing concrete compressive strength was near linear. Increasing concrete compressive strength, f'_c, from 17 MPa (MBC-20) to 51 MPa (MBC-60) resulted in 41% increase in shear capacity.

Figure 8.35 shows the shear stress versus displacement graphs obtained for the modelled cases, where MBC-60 corresponds to the tested unstrengthened control specimen MBC for

direct comparison with the theoretical scenarios.

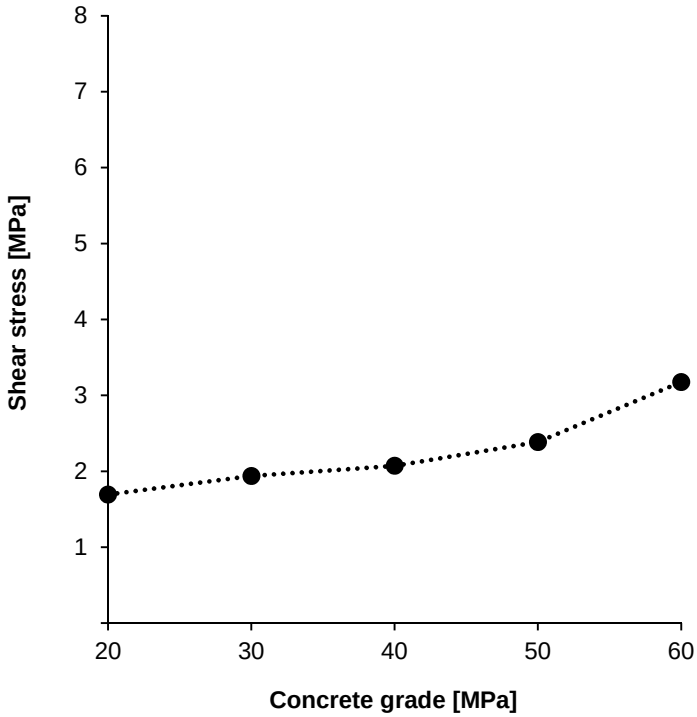

Figure 8.34 – Concrete compressive strength versus shear stress.

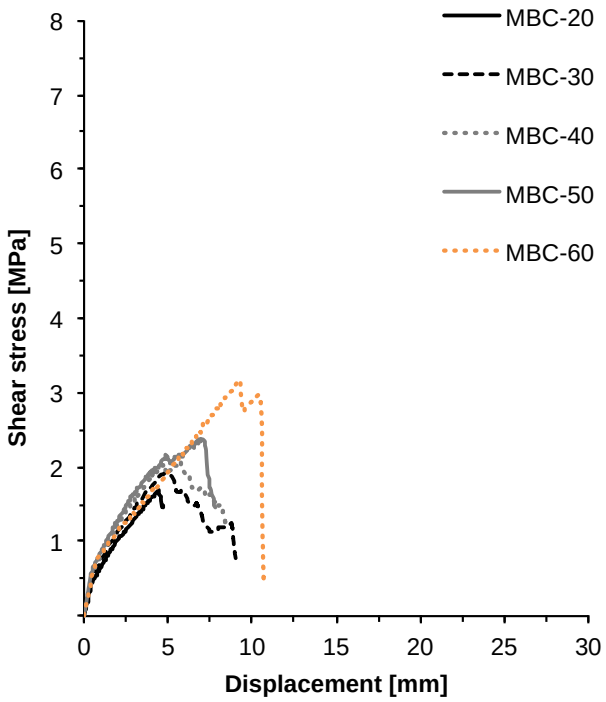

Figure 8.35 – MBC concrete compressive strength: shear stress versus displacement.

The shear stress versus displacement curves revealed that the modelled beams all failed in shear with configurations MBC-20 and MBC-60 exhibiting a particularly brittle failure mode, evident through the presence of the abrupt post-peak slip. The results also indicated that there is a great increase in shear strength with increase in concrete compressive strength for MBC-60, compared with MBC-50.

It should be noted that the default values for concrete tensile strength were used for the modelled cases apart from MBC-60 where actual tested values were used. All other values remained in the default setting.

The crack patterns at crack initiation and at failure for the MBC-20 and MBC-60 were obtained from their respective numerical models and are presented in Figure 8.36.

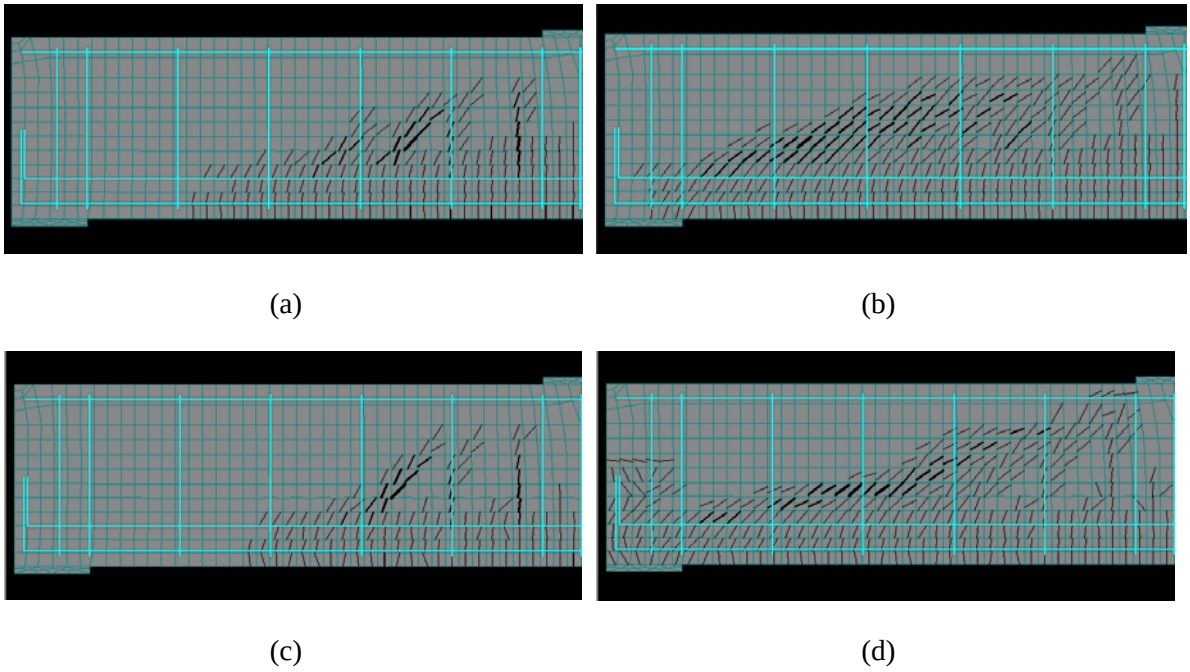

(a) (b)

(c) (d)

Figure 8.36 – MBC concrete compressive strength – shear crack patterns: (a) MBC-20 at shear crack initiation, (b) MBC-20 at failure, (c) MBC-60 at shear crack initiation, (d) MBC-60 at failure.

The comparison of the two selected cases demonstrated that the shear crack initiates at the same location for both the configuration MBC-20 and MBC-60, as shown in Figure 8.36 (a) and Figure 8.36 (c), respectively. The diagonal shear crack that further developed in the modelled beam MBC-20 exhibited more dispersed cracking in the shear zone, while more localized cracking was observed for the MBC-60 configuration. This is likely due to the

low tensile strength of the concrete in the case of MBC-20 and the predetermined crack opening law.

It should be noted that these are fictitious crack patterns that would not occur in a real life situation, as the beam would fail due to a localized shear crack. The crack patterns for the remaining modelled cases MBC-30 to MBC-50 generally displayed identical behaviour at first shear cracking, with a diagonal shear crack at ultimate within the bounds of the two extreme cases presented above.

The results therefore demonstrated that while the shear capacity was influenced by the concrete compressive strength, the failure modes of the modelled cases were not dependent on the concrete grade.

8.5.2 Longitudinal steel ratio

In this parametric study, the variable was the amount of longitudinal reinforcement provided for the MBC tested configuration. To model realistic scenarios that are considered representative of existing reinforced concrete slab-on-beam structures, the longitudinal steel ratio varied from 0.81% (typical for buildings) to 2.65% (typical for bridges). The reinforcing bars were either arranged in one or two rows, as would be typical for under-reinforced, balanced and over-reinforced sections.

In all modelled configurations, the concrete compressive strength remained constant at 60 MPa throughout the entire parametric study, as well as the amount of shear reinforcement, which remained as per test specimen MBC design, presented in Chapter 5. The designation of the modelled specimens follows format MBC-number of bars followed by R for reinforcing steel and ends with the bar diameter for ease of orientation.

The modelled configuration MBC-2R25 failed in flexure, whereas all other modelled configurations failed in shear. The results revealed that the amount of longitudinal steel reinforcement affects the ultimate load capacity as well as the failure mode. It should be noted that the modelled case MBC-2R35 with 1.58% reinforcement ratio (one layer of reinforcement) failed at a slightly higher ultimate capacity compared with MBC-4R25 with 1.62% reinforcement ratio (two layers of reinforcement). The crack patterns with corresponding crack widths at crack initiation for these two cases are presented in Figure 8.37.

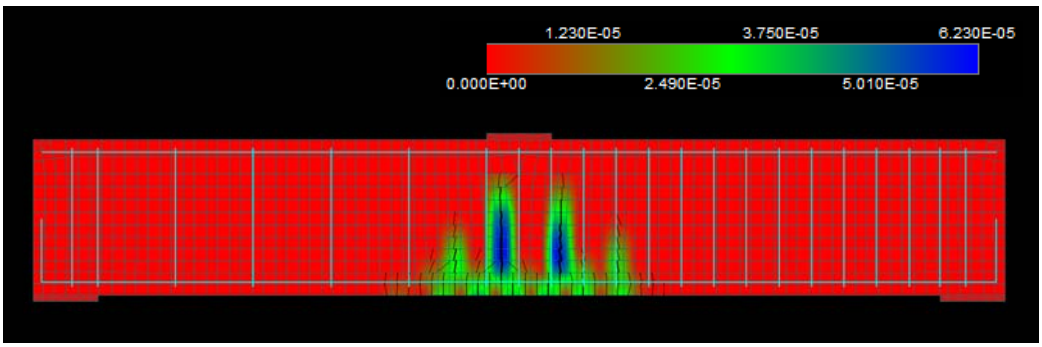

(a)

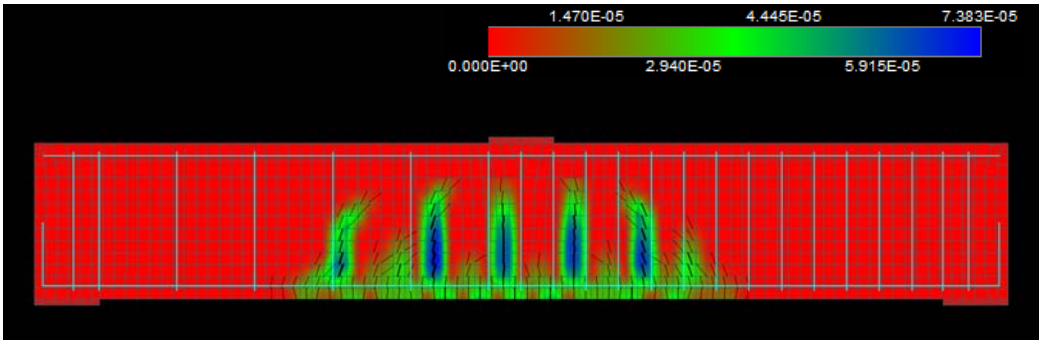

(b)

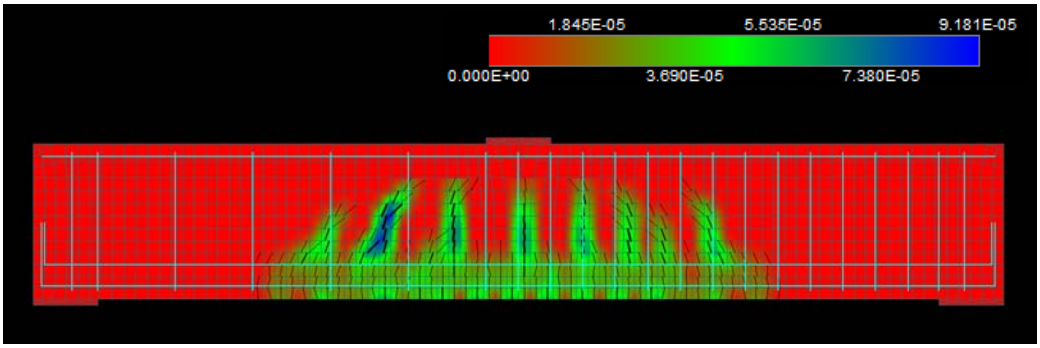

(c)

Figure 8.37 – MBC longitudinal steel reinforcement ratio – crack initiation: (a) MBC-2R25, (b) MBC-2R35, (c) MBC-4R25 [m].

The crack patterns at failure for the modelled beams MBC-2R25, MBC-2R35 and MBC-42R25 are presented in Figure 8.38. The initial flexural cracking observed in model MBC-2R25 further developed into flexural cracks with no shear cracking. The shear crack in model MBC-2R35 developed from the initial flexural shear cracks, with cracking propagating from the bottom soffit of the beam. The cracking also developed along the position of the main reinforcing bars, moving towards the support. In contrast to this, the beam MBC-4R25 initially developed flexural cracks, which then closed upon formation of

a web shear crack near midspan. The failure of the model MBC-4R25 was also more brittle compared with the MBC-2R35, which exhibited a more ductile shear stress versus displacement response.

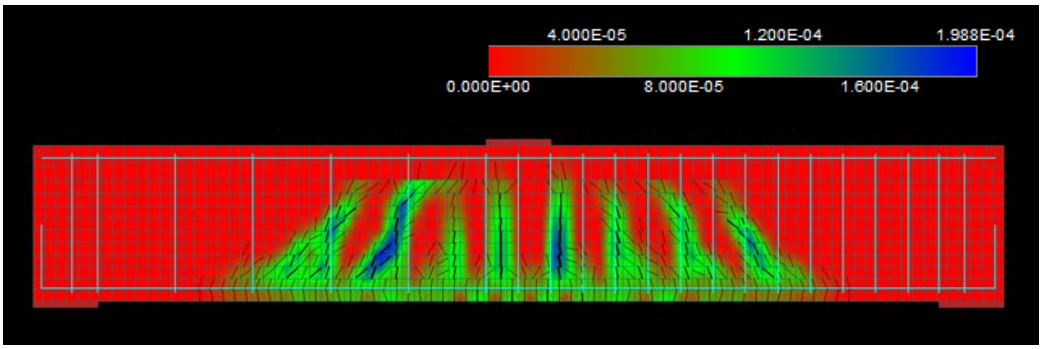

(a)

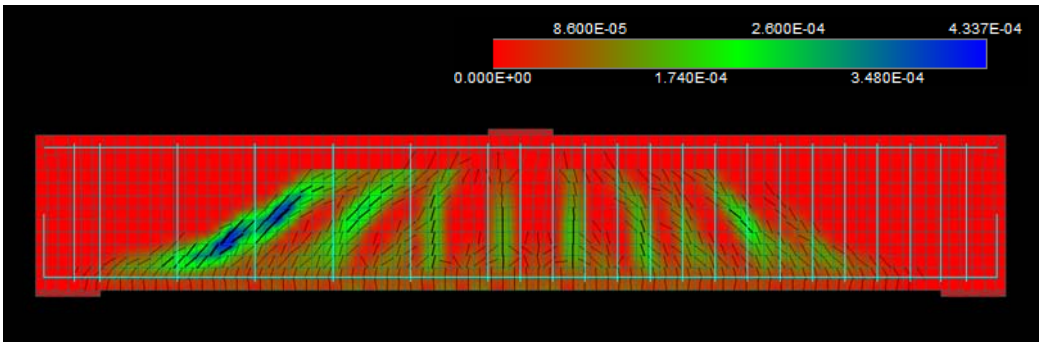

(b)

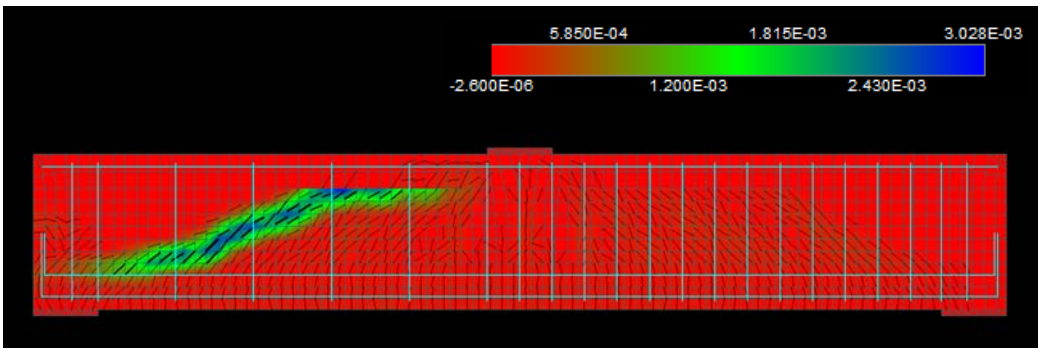

(c)

Figure 8.38 – MBC longitudinal steel reinforcement ratio – crack pattern prior to failure: (a) MBC-2R25, (b) MBC-2R35, (c) MBC-4R25 [m].

The results of this numerical parametric study as well as the details of the modelled configurations are presented in Table 8.4.

Table 8.4 – Influence of longitudinal steel ratio on ultimate shear capacity: results and modelled configurations.

Model	Steel		Concrete		FEM Results		
	ρ_l [%]	ρ_v [%]	f'_c [MPa]	f_t [a] [MPa]	V_u [kN]	v_u [MPa]	Failure Mode
MBC-2R25	0.81	0.1	51.0	3.80	177	1.75	Flexure
MBC-3R25	1.21	0.1	51.0	3.80	260	2.56	Shear
MBC-2R32	1.32	0.1	51.0	3.80	282	2.78	Shear
MBC-2R35	1.58	0.1	51.0	3.80	304	3.00	Shear
MBC-4R25	1.62	0.1	51.0	3.80	294	2.90	Shear
MBC-5R25	2.02	0.1	51.0	3.80	315	3.11	Shear
MBC-6R25*	2.42	0.1	51.0	3.80	321	3.17	Shear
MBC-4R32	2.65	0.1	51.0	3.80	327	3.23	Shear

[a] Concrete tensile strength as tested for specimen MBC.

* Corresponds to the tested specimen MBC FEM.

The shear-stress versus displacement graphs for all modelled cases are presented in Figure 8.39.

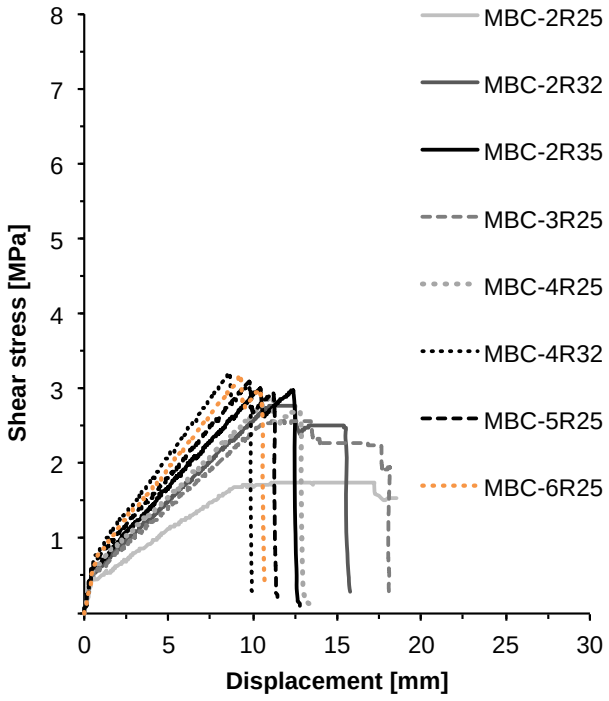

Figure 8.39 – MBC longitudinal steel ratio: shear stress versus displacement.

The relationship between the longitudinal steel ratio, represented as a percentage of the reinforced concrete section, and the shear stress is shown in Figure 8.40.

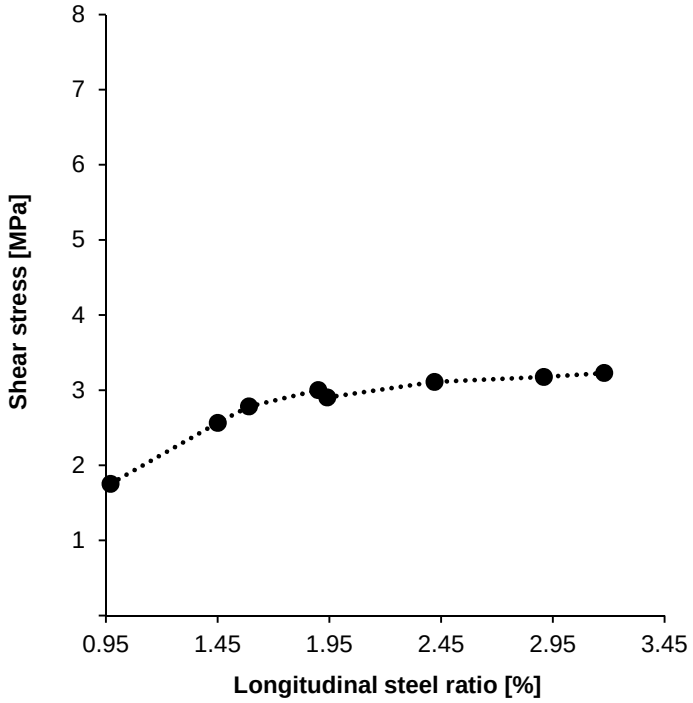

Figure 8.40 – Longitudinal steel ratio versus shear stress.

The results revealed that the amount of longitudinal reinforcement as well as the reinforcing bar arrangement significantly affects the ultimate load-carrying capacity as well as the beam behaviour prior to and at failure. It was demonstrated that flanged beams with identical longitudinal reinforcement ratios but with differing reinforcement detail exhibit different failure modes.

For the modelled beams in this study, the results clearly identified the 1.60% reinforcement ratio as a threshold value at which the beam fails either in flexure-shear or web shear, depending on the bar arrangement. The results further indicated that a limit must exist at which adding more longitudinal reinforcement will not result in increased ultimate capacity.

8.5.3 Shear reinforcement ratio

The shear reinforcement ratio varied from 0% for sections without transverse reinforcement to 0.22% with steel stirrups closely spaced at 0.25*d*. The diameter of the

shear links remained unchanged at 6 mm. The concrete compressive strength remained constant at 60 MPa throughout the study.

The designation of the modelled specimens with shear links followed format MBC-spacing of shear links for ease of orientation. The results as well as the details of the modelled configurations are presented in Table 8.5.

Table 8.5 – Influence of shear reinforcement ratio on ultimate shear capacity.

Model	Steel		Concrete		Results		
	ρ_l [%]	ρ_v [%]	f'_c [MPa]	f_t [a] [MPa]	V_u [kN]	v_u [MPa]	Failure mode
MBC-0	2.4	–	51.0	3.80	281	2.77	Shear
MBC-1*d*	2.4	0.05	51.0	3.80	300	2.97	Shear
MBC-0.75*d*	2.4	0.07	51.0	3.80	319	3.15	Shear
MBC-0.60*d**	2.4	0.09	51.0	3.80	321	3.17	Shear
MBC-0.50*d*	2.4	0.11	51.0	3.80	331	3.26	Shear
MBC-0.30*d*	2.4	0.19	51.0	3.80	364	3.59	Shear
MBC-0.25*d*	2.4	0.22	51.0	3.80	373	3.68	Shear

[a] Concrete tensile strength as tested for specimen MBC.

* Corresponds to the tested specimen MBC FEM.

The results from this study showed that with increasing amount of shear reinforcement and with closer spacing of shear links the shear capacity also increases near linearly. The increase in shear capacity from a model with no links (MBC-0) to that of a model with 0.22% of shear reinforcement ratio (MBC-0.25d) was approximately by 32%, see Figure 8.41. Figure 8.42 shows the shear stress versus displacement graphs obtained for the modelled cases, where MBC-0.60d corresponds to the tested unstrengthened control specimen MBC for direct comparison with the theoretical scenarios.

All modelled configurations failed in web shear and therefore it was concluded that the shear reinforcement ratio in the range of 0.05% to 0.22% would not be sufficient to change the failure mode for flanged beams of the modelled geometry with large amount of longitudinal reinforcement. The crack patterns at initiation and failure for the modelled configurations MBC-0 and MBC-0.25*d* are presented in Figure 8.43.

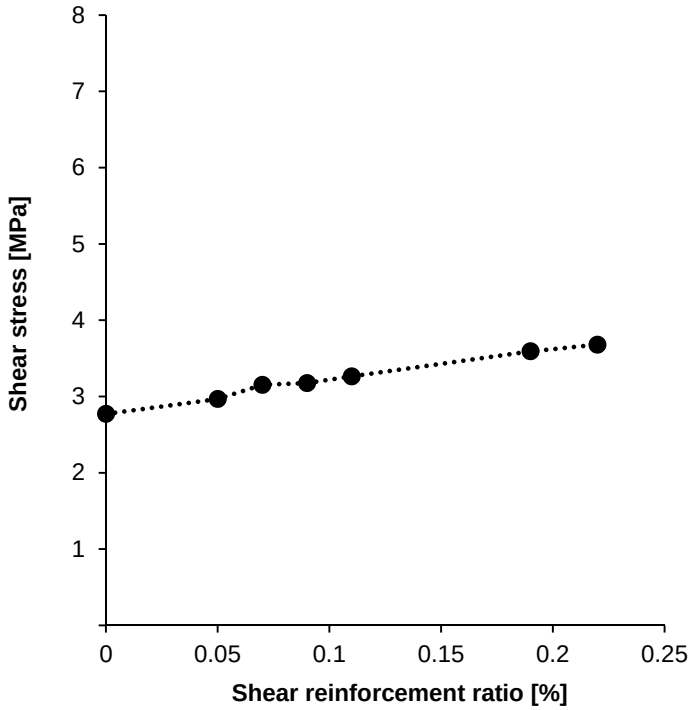

Figure 8.41 – Shear reinforcement ratio versus shear stress.

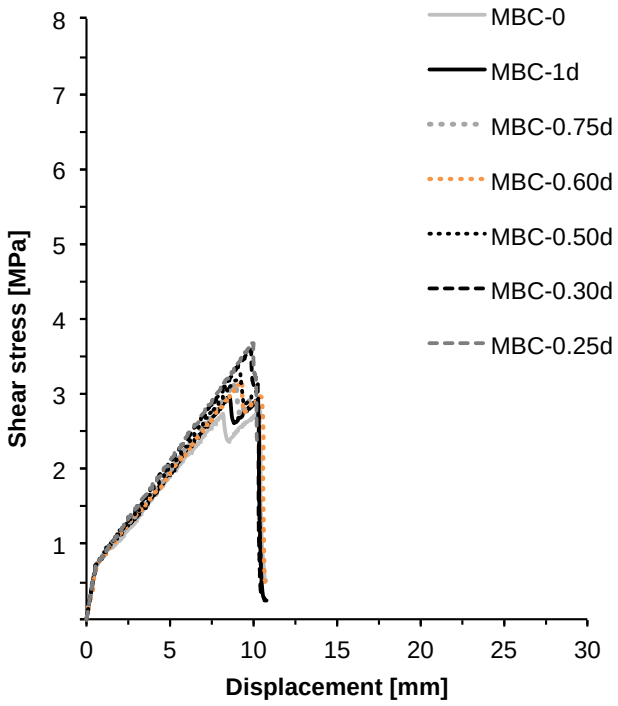

Figure 8.42 – MBC shear reinforcement ratio: shear stress versus displacement.

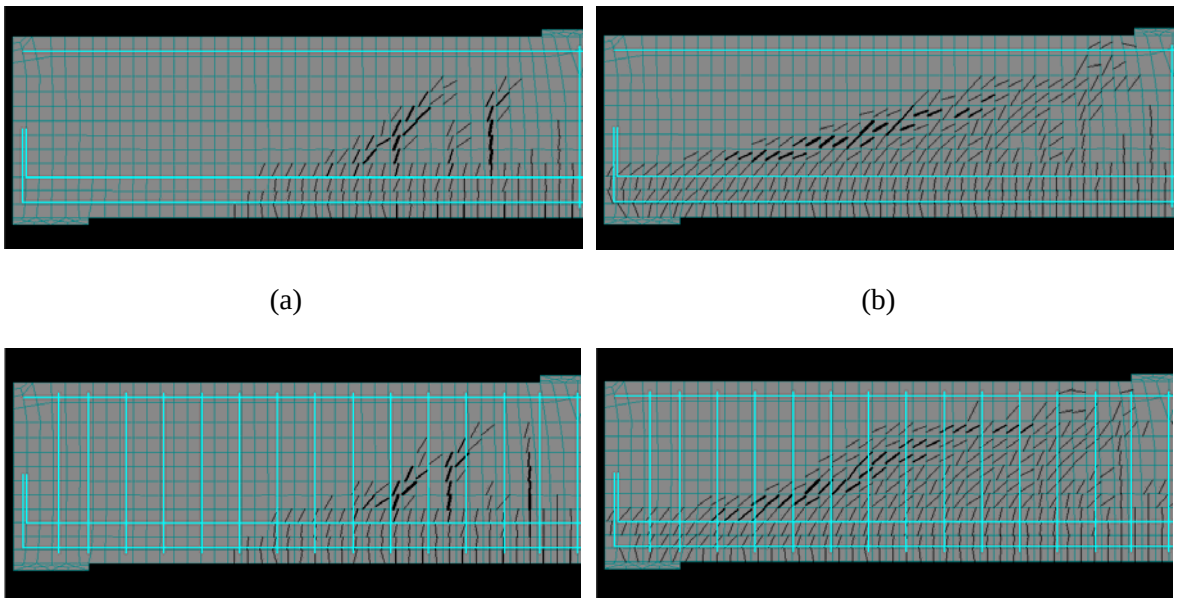

(a) (b)

(c) (d)

Figure 8.43 – MBC ratio of shear reinforcement: (a) MBC-0 at shear crack initiation, (b) MBC-0 at failure, (c) MBC-0.25*d* at shear crack formation, (d) MBC-0.25*d* at failure.

The crack patterns from the two modelled extreme cases presented above show that the initial cracking differs as well as the crack pattern at ultimate for MBC-0 and MBC-0.25d. However, the crack initiates within the web, regardless of the number of shear links crossing the web. Therefore, the amount of shear reinforcement does have influence on the overall shear capacity of the beam but does not have influence on the location of the critical shear crack for the modelled cases of flanged beams.

8.5.4 Beam geometry

In this parametric study, the geometry of the beam varied to model the influence of the shape and size of the flange on the overall behaviour of the beam. The overall shape of the beam in this study was varied from rectangular with no slab to a flanged section with effective flange width of 1.5 m to vary the geometry dramatically. The slab thickness varied according to typical slab thicknesses of existing slab-on-beam structures.

The designation of the modelled specimens follows the geometry of the beam in a format MBC-flange thickness/flange width for ease of orientation. The reinforcement detail remained unchanged throughout the parametric study and was identical to that of the tested medium-sized T-beam. The dimensions of the modelled beams are presented in Table 8.6.

Table 8.6 – Geometry of modelled reinforced concrete beams.

Designation	b_w [mm]	h_b [mm]	b_s [mm]	h_s [mm]	A_c [mm^2]
MBC-0/570	225	540	–	–	121500
MBC-80/570	225	540	570	80	149100
MBC-120/570*	225	540	570	120	162900
MBC-120/1000	225	540	1000	120	214500
MBC-120/1500	225	540	1500	120	301380

* Corresponds to the tested specimen MBC FEM.

Figure 8.44 shows the overall dimensions of the T-beam as tested and the modified cross-section of the modelled T-beams.

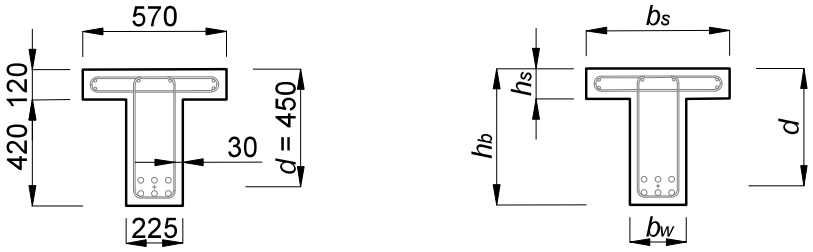

(a) (b)

Figure 8.44 – Modelled T-beam geometry – through section: (a) as tested, (b) schematics of modified T-beam geometry [mm].

The results revealed that all modelled configurations failed in shear. The greatest shear capacity was obtained for MBC-120/1500 where the slab thickness was 120 mm (as tested) and the effective width of the flanged section 1.5 m as would be typical in a slab-on-beam bridge structure (scaled in proportion to a full bridge size for the medium-sized model).

The lowest capacity on the other hand was recorded for configuration MBC-0/570 where the beam was modelled as rectangular with beam width of 225 mm and height of 540 mm (as tested without slab). Increasing the slab thickness resulted in increased shear capacity. However, this increase was not as dramatic as that achieved through increasing the effective width of the flange.

The summary of results as well as material properties of the modelled configurations is presented in Table 8.7.

Table 8.7 – Influence of section geometry on ultimate shear capacity.

Model	Steel		Concrete		Results		
	ρ_l [%]	ρ_v [%]	f'_c [MPa]	f_t [a] [MPa]	V_u [kN]	v_u [MPa]	Failure mode
MBC-0/570	2.4	0.1	51.0	3.80	213	2.10	Shear
MBC-80/570	2.4	0.1	51.0	3.80	290	2.86	Shear
MBC-120/570	2.4	0.1	51.0	3.80	321	3.17	Shear
MBC-120/1000	2.4	0.1	51.0	3.80	440	4.35	Shear
MBC-120/1500	2.4	0.1	51.0	3.80	479	4.73	Shear

[a] Concrete tensile strength as tested for specimen MBC.

$v_u = V_u / (b_w\, d)$

Figure 8.45 shows the shear stress versus displacement graphs for the modelled cases.

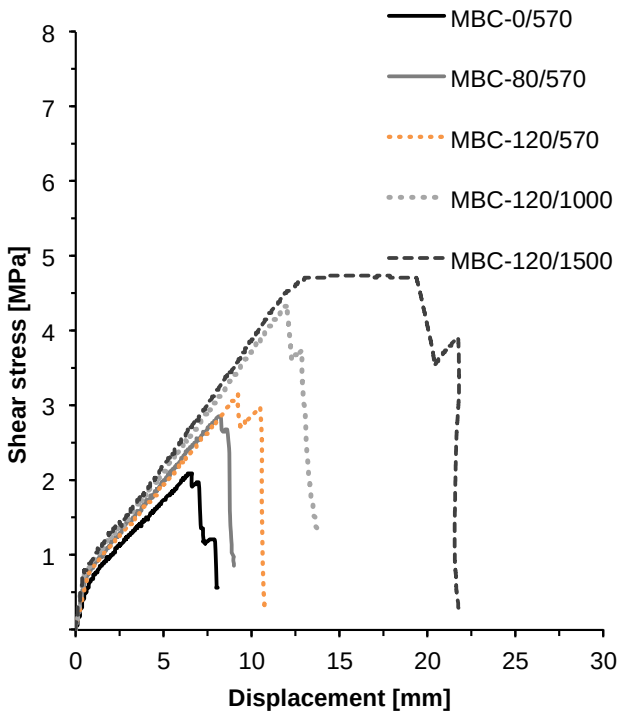

Figure 8.45 – MBC beam geometry: shear stress versus displacement.

The crack patterns with corresponding crack widths at the shear crack initiation obtained for the modelled case without flange, MBC-0/570, and the case with a realistic flange width, MBC-120/1500, are presented in Figure 8.46.

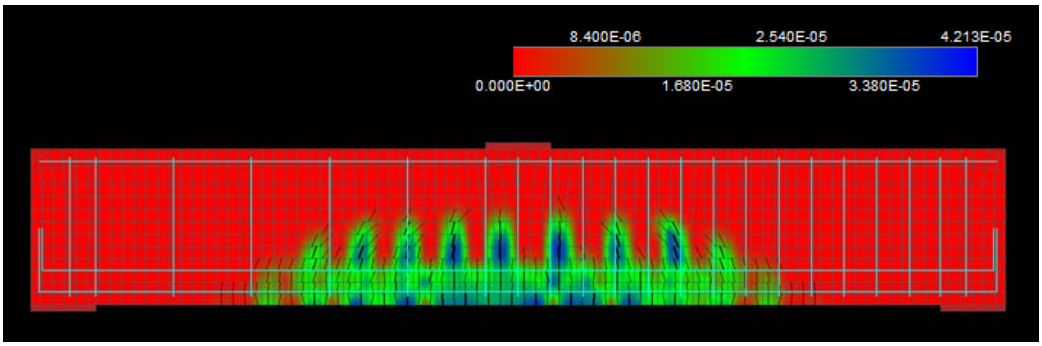

(a)

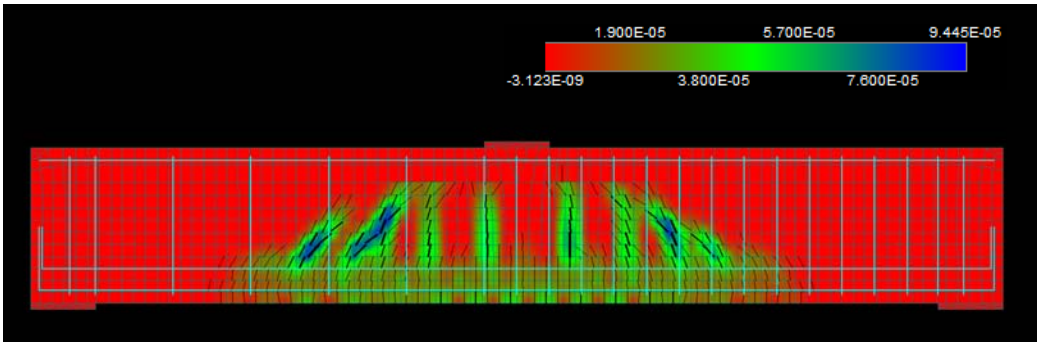

(b)

Figure 8.46 – MBC slab geometry – crack initiation: (a) MBC-0/570, (b) MBC-120/1500 [m].

The shear crack observed in model MBC-0/570 initiated in the web and further propagated within the web towards the load and the support plate, similarly to the tested specimen MBC. The cracking observed in model MBC-120/1500 initiated through flexural cracking and then further propagated along the main reinforcing bars.

The crack patterns at failure for MBC-0/570 and MBC-120/1500 are shown in Figure 8.47.

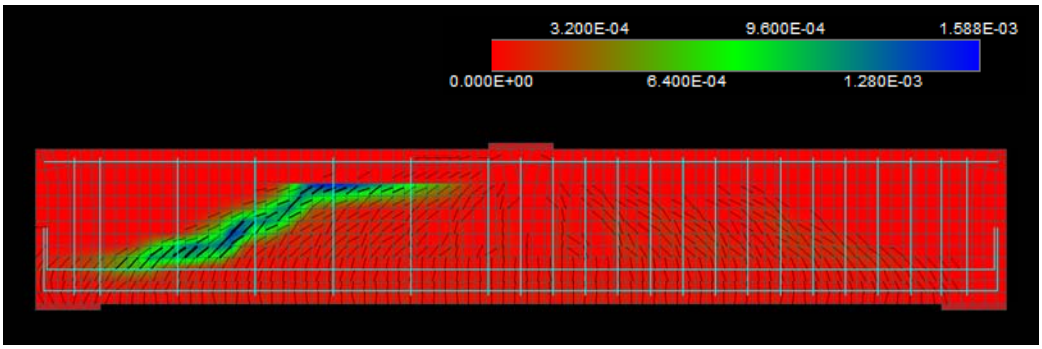

(a)

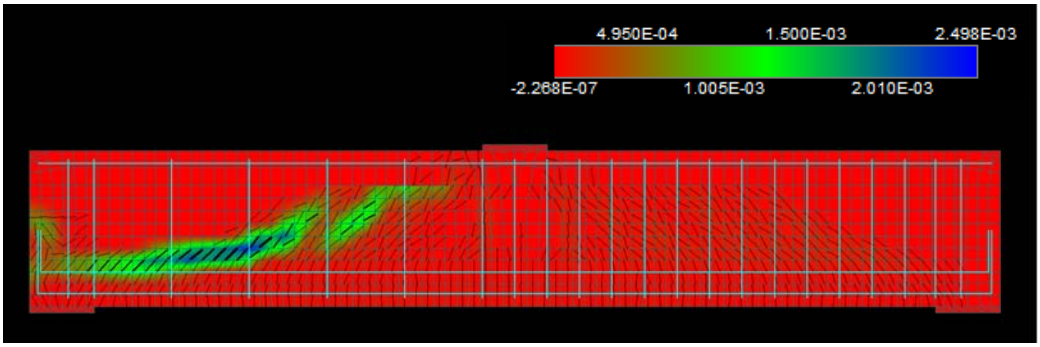

(b)

Figure 8.47 – MBC slab geometry – crack pattern prior to failure: (a) MBC-0/570, (b) MBC-120/1500 [m].

8.5.5 Shear span

In this study, the shear span varied from 1*d* to 3.5*d* in increments presented in Table 8.8 on a model of a specimen as per test specimen design to investigate the influence of load positioning on the behaviour of the beam as well as the values of shear stress at failure.

The designation of the modelled cases follows in the format of MBC-shear span for ease of orientation. The concrete and steel properties and the geometry of the beam remained constant throughout the study.

The results as well as the details of the modelled configurations are presented in Table 8.8.

Table 8.8 – Influence of shear span length on ultimate shear capacity.

Model	Steel		Concrete		Results		
	ρ_l [%]	ρ_v [%]	f'_c [MPa]	f_t [a] [MPa]	V_u [kN]	v_u [MPa]	Failure Mode
MBC-1d	2.4	0.1	51.0	3.80	775	7.65	Shear
MBC-1.5d	2.4	0.1	51.0	3.80	537	5.30	Shear
MBC-2.5d	2.4	0.1	51.0	3.80	422	4.17	Shear
MBC-3.5d*	2.4	0.1	51.0	3.80	321	3.17	Shear

[a] Concrete tensile strength as tested for specimen MBC.

* Corresponds to the tested specimen MBC FEM.

The influence of the shear span on the ultimate shear stress is shown in Figure 8.48.

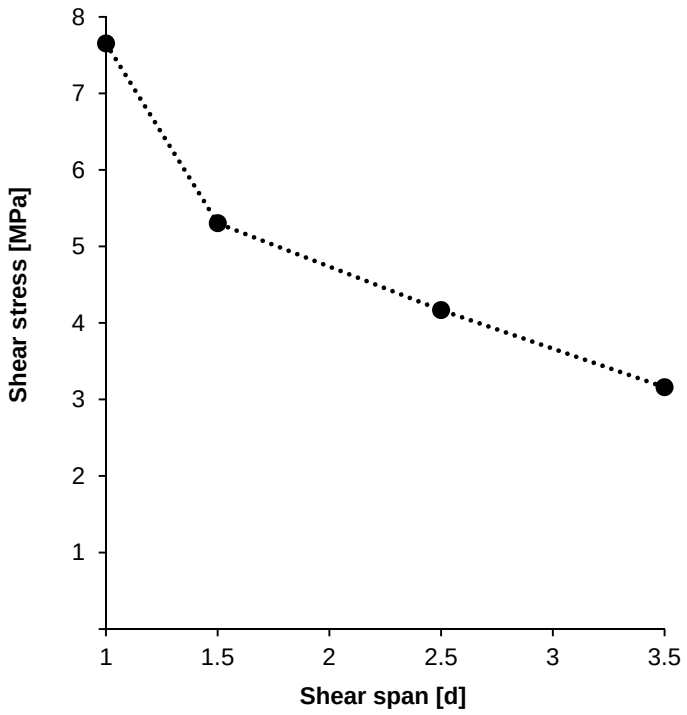

Figure 8.48 – Shear span versus shear stress.

The results from this study demonstrated that the shear capacity reduces dramatically with increasing shear span length. In other words, the closer the load is positioned to the support, the greater the shear capacity.

The crack patterns for all the modelled configurations showing diagonal web shear crack at ultimate load are presented in Figure 8.49.

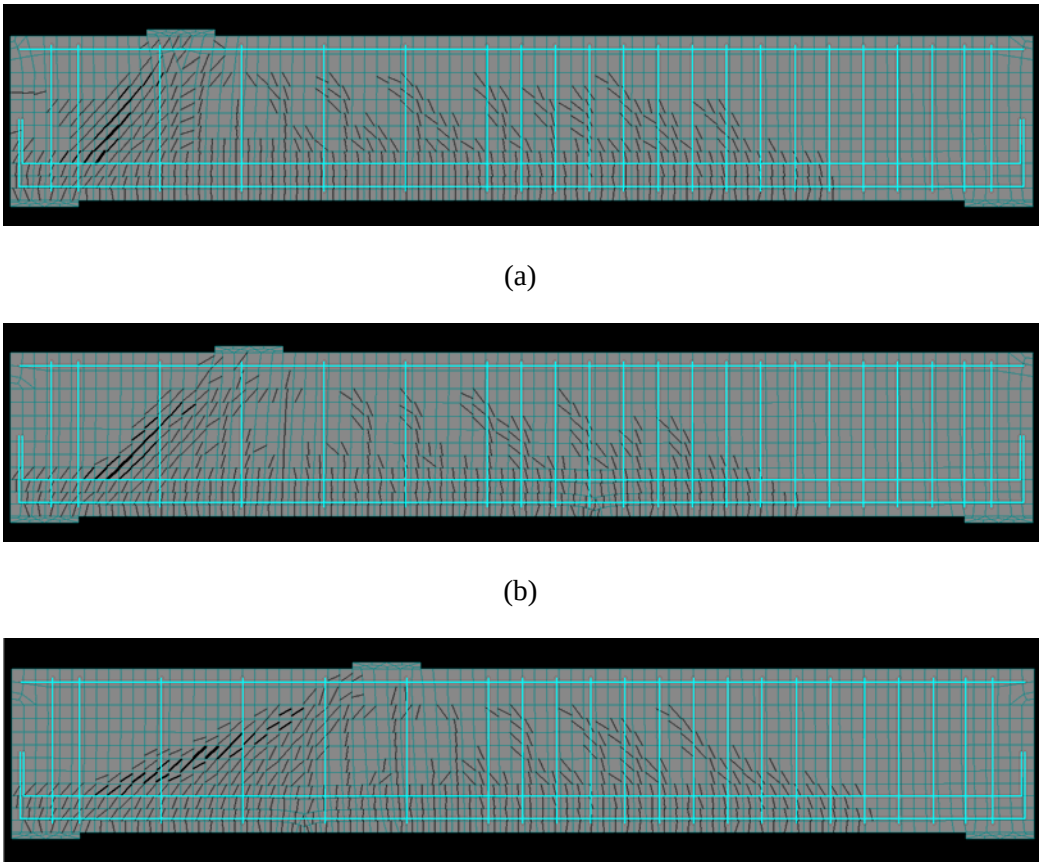

(a)

(b)

(c)

Figure 8.49 – MBC shear span: (a) configuration MBC-1*d*, (b) configuration MBC-1.5*d* and (c) configuration MBC-2.5*d* prior to failure.

8.6 Discussion

8.6.1 Applicability of numerical models for analysis of reinforced concrete

The study presented in this Chapter demonstrated that advanced numerical approaches could be beneficial in assessing the capacity of existing reinforced concrete structures. The non-linear finite element fracture mechanics-based package ATENA proved to be a suitable tool for analysis of unstrengthened reinforced concrete beams in 2D as well as strengthened beams within given limitations. The theoretical crack widths assumed by the FE model for reinforced concrete beams caused stiffer behaviour of the model, suggesting

that a more refined material model taking into account rather large localized deformations would be more appropriate.

However, the model used in the presented analyses proved adequate for modelling beams strengthened with externally bonded CFRP sheets within the elastic range. The assumption regarding crack widths appeared to be suitable to model the behaviour of the beams strengthened with externally bonded CFRP sheets accurately to the point of debonding. The predicted capacity for both unstrengthened control specimens discussed in Chapter 6 was in good agreement for both the critical cracking load as well as the ultimate capacity at failure. The crack patterns for the unstrengthened as well as the strengthened beams were in good agreement with the experimental data presented in Chapter 6.

8.6.2 Modelling of strengthened reinforced concrete beams

The model used to simulate the behaviour of the beam strengthened with externally bonded CFRP sheets with assumed perfect bond between the concrete surface and the CFRP proved adequate to the point of first debonding. The model did not assume any bond-slip behaviour and therefore only an elastic range check was performed to confirm where the cracking initiates and how the crack further propagates within the web. The behaviour of the model was in good agreement with the experimental data.

The deep embedment configuration also showed good agreement with the experimental data, albeit the ultimate capacity of the tested specimen was marginally greater than that reached by the model. However, the model behaved in a similar manner to that of unstrengthened reinforced concrete configurations, suggesting that larger crack widths and material softening due to extensive cracking were present in the actual tested specimen.

8.6.3 Effect of size on shear capacity

The model accurately captures size effect in both the unstrengthened and strengthened T-beams. This is shown in the normalized shear stress versus normalized shear displacement presented in Figure 8.50 and Figure 8.51.

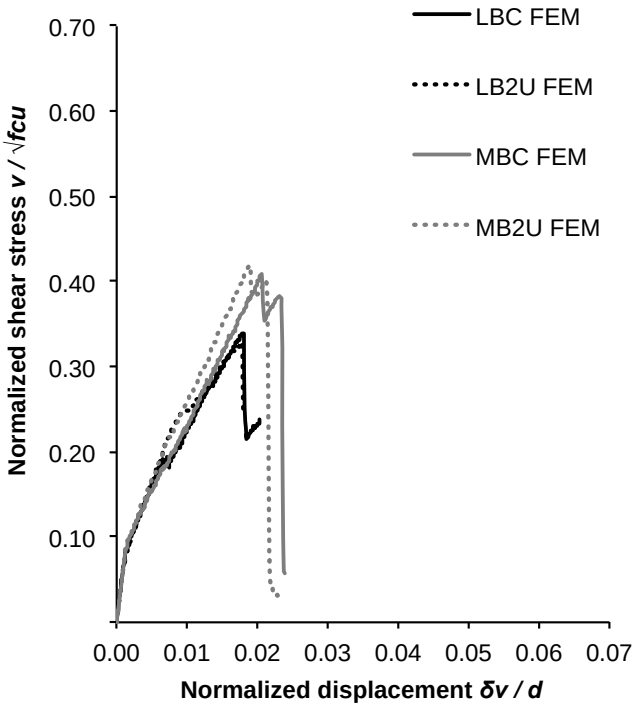

Figure 8.50 – Normalized shear stress versus normalized displacement: U-wrap cases.

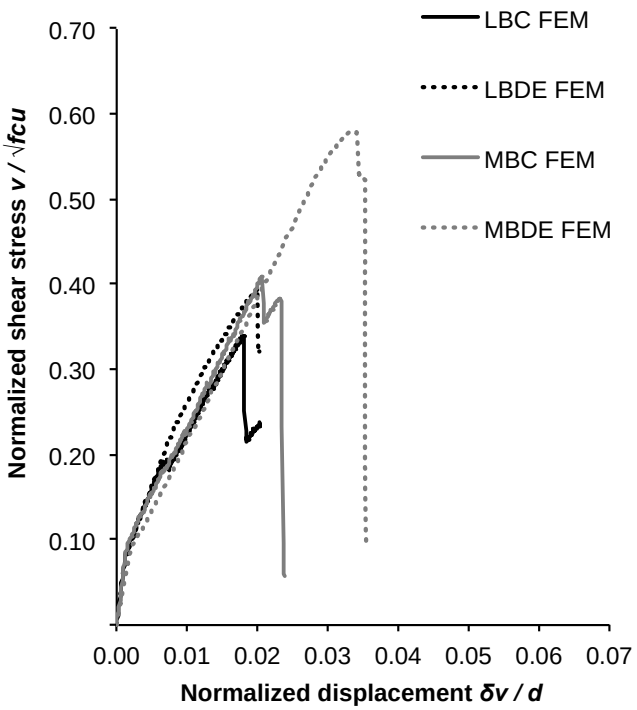

Figure 8.51 – Normalized shear stress versus normalized displacement: deep embedment cases.

8.6.4 Other parameters affecting shear capacity

The results of the targeted parametric study revealed that the parameters dramatically affecting the shear capacity are the longitudinal reinforcement, the beam geometry and the shear span. It was demonstrated that not only the longitudinal reinforcement ratio but also the reinforcement layout influence the load-carrying capacity of the beam as well as the crack patterns and ultimately the failure mode. For the modelled cases, the configurations with the longitudinal reinforcing bars arranged in two rows consistently failed in web shear, whereas those with one layer of reinforcing bars failed in flexure or flexure-shear.

The shear capacity of the modelled beams with varying geometry was greatly affected by the dimensions of the slab. Although the results showed that the depth of the slab had minimal effect on the overall shear capacity, increasing the effective width resulted in a significant increase in shear capacity as well as altered failure mode. In particular, increasing the slab width from 0.57 m to 1.5 m resulted in an increase in shear strength capacity by approximately 33%. Furthermore, the difference in shear capacity between a rectangular section (assuming identical overall beam height) and that with 1.5 m wide slab was 55%. This result illustrates, that flanged sections have a significantly greater shear capacity than those of identical rectangular sections. Practically that means, that the shear capacity of flanged beams to current design and assessment codes is conservative, completely ignoring the contribution of the slab to the overall capacity of the beam.

The position of the load with respect to the support within the tested shear span had a great impact on the overall shear capacity of the modelled beams. The shear capacity reduced to less than a half at a distance 3.5d away from the support compared with that at 1d. A significant drop in shear capacity was observed for the modelled configuration with load positioned at 1.5d, where the capacity reduced by approximately 31% compared with that at 1d. In all modelled cases, a single shear crack initiated and further propagated within the web between the load plate and the support plate.

The parametric study where the influence of the concrete compressive strength on the overall shear capacity of the beam revealed that with increasing concrete compressive strength the shear strength of the beam also increases. A dramatic increase in shear strength was observed for a modelled configuration with concrete strength of 60 MPa compared with that of a beam with concrete strength of 50 MPa. The concrete compressive strength did not alter the failure mode; however, the crack pattern differed for the modelled

beams. The lower the concrete compressive strength, the more localized the shear crack within the web.

Increasing the amount of shear links within the 3.5*d* shear span resulted in near-linear increase in shear capacity. The results revealed that within the investigated shear reinforcement ratios of 0.05% and 0.22% the failure mode remained unchanged and all beams failed in web shear. However, more dispersed cracking covering more of the web and propagating further into the flange as well as the zone of longitudinal reinforcement was observed in the case of no shear links. On the other hand, more controlled cracking was observed in the extreme case with closely spaced shear links, located in the central portion of the web and not propagating further into the flange or the zone of longitudinal reinforcement.

8.7 Conclusions

Following the numerical analysis of tested specimens and parametric study on unstrengthened reinforced concrete medium beams, the following conclusions can be drawn:

- The models accurately predicted the cracking load and the ultimate load-carrying capacity of the tested specimens;
- The fracture mechanics-based models enabled to determine where the crack will initiate and so if it is feasible to strengthen with externally bonded CFRP sheets;
- The validation exercise revealed limitations of the material model for concrete in 2D and issues with accurately predicting the beam behaviour in reinforced concrete beams with large localized deformations;
- The modelled configurations based on the tested specimens demonstrated that size effect is more prominent in beams with internal shear reinforcement compared with those strengthened with externally applied CFRP sheets. This was confirmed experimentally and discussed in Chapter 6 and Chapter 7;
- The parametric study on unstrengthened medium-sized reinforced concrete beams showed that the parameters dramatically affecting the shear capacity are the amount and the layout of longitudinal reinforcement, the beam geometry and the shear span;
- The nature and location of the shear crack (web shear crack versus flexural shear

crack) was found to be affected by the arrangement of the longitudinal reinforcement and varying slab dimensions within the beam geometry study;

- Conversely, parameters not affecting the web shear crack formation were the concrete compressive strength within the modelled region of 20 to 60 MPa, the shear span varied from 1*d* up to 3.5*d* and the amount of shear reinforcement in the range of 0.05% to 0.22%.

9 SHEAR ASSESSMENT AND STRENGTHENING EXAMPLE

9.1 Introduction

To demonstrate the practical applicability of the proposed strengthening solution using deep embedded CFRP bars to a real slab-on-beam structure, a shear assessment and strengthening example is presented in this Chapter. The shear capacity of the beams from a typical bridge deck, which formed the basis for the experimental testing, was assessed according to current assessment codes rather than design standards, as discussed in Chapter 7. Following this assessment, the bridge deck was considered for structural strengthening using deep embedment, demonstrating potential increase in shear capacity due to the application of deep embedded CFRP bars as additional shear reinforcement.

9.2 Bridge assessment

9.2.1 Assessment methods

The slab-on-beam bridge deck was assessed according to BD 21/01 and BD 44/15 for 40 Tonnes vehicle live loading, assuming High traffic and poor (Hp) surfacing conditions. The deck was divided into notional lanes per carriageway in accordance with cl. 5.6 of BD 21/01. Assessment Live Loading (ALL) of 40 Tonnes was applied and considered cl. 5.8 of BD 21/01 HA UDL with Knife Edge Load (KEL). Single Axle Load and Single Wheel Load were not considered, as HA UDL with KEL produced the most onerous effect on the span under consideration. The beams underneath the footway were checked for Accidental Wheel Loading using real vehicles according to Annex D of BD 21/01, as the footways are not protected from the effects of errant vehicles. Pedestrian loading on the footways was not considered in this assessment as the footway beams were checked for 40 Tonnes Accidental Wheel Loading (AWL) and therefore, a check for 5 kN/m^2 loading from pedestrian traffic was not necessary.

The section properties were calculated according to BD 44/15. The shear capacity of the carriageway and footway beams was checked at the support, and at a distance d, $2d$, $3d$ and $3.5\,d$ (quarter span) away from the support. The structure was found to be of

inadequate shear capacity to support the 40 Tonnes Assessment Live and Accidental Wheel Loading, and therefore a suitable mitigation strategy was proposed as part of this assessment.

9.2.2 Structure information

The structure consists of a single span slab-on-beam deck with footways either side of the carriageway with an overall beam length of 8.7 m and the skew angle of 0°. The bridge deck comprises six 0.56 m deep reinforced concrete beams with 0.16 m deep slab, spaced at 1.4 m centre-to-centre with overall height of the beam at 0.72 m. The bridge deck geometry is presented in Figure 9.1 and the beam cross-section in Figure 9.2.

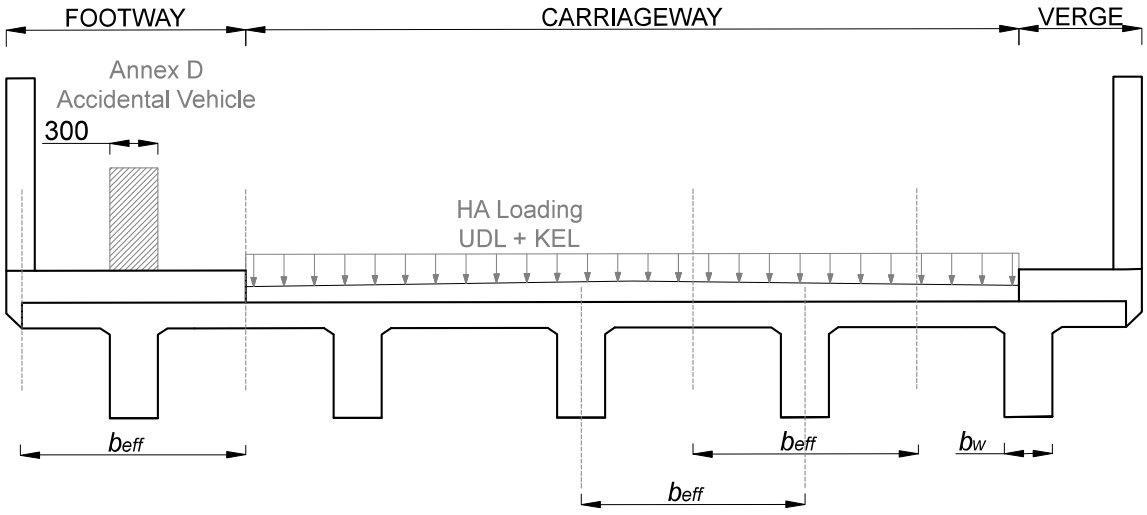

Figure 9.1 – Bridge section showing applied loading and effective width for load application [mm].

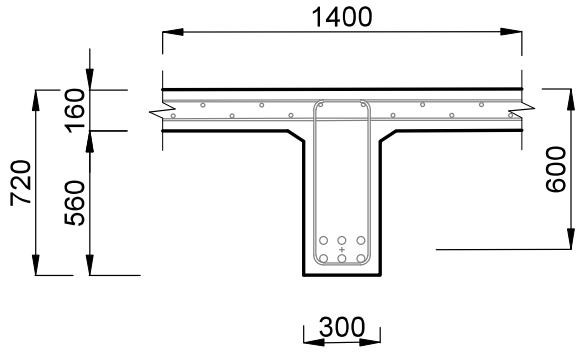

Figure 9.2 – T-beam dimensions with reinforcement detail identical to tested beams [mm].

The beams bear onto steel bearing plates at the abutments and are therefore considered as simply supported. The concrete and steel material properties and the section geometry are identical to those of the tested beams discussed in detail in Chapter 5. The edge beams carry footways and parapets, and the inner beams support the carriageway. The parapet and cill are constructed of reinforced concrete.

The bridge is in good condition and the substructure was assessed as adequate to sustain current live loading demands at 40 Tonnes to the requirements of BD 21/01. This does not form part of this assessment example.

9.2.3 Permanent loading

The permanent load effects on the bridge deck are dead load and the superimposed dead load. The total area of the beam considered in this assessment is 0.394 m^2. The effective span was calculated as 8.4 m, assuming bearing pads of 0.3 m x 0.3 m, and the effective width was determined as 1.4 m.

The depth of road surfacing was assumed as 0.1 m and the depth of the fill was also assumed as 0.1 m, which is considered representative of highway bridges. The depth of the pavement was assumed as 0.2 m and the width 0.7 m. The depth of the concrete parapet was assumed as 0.18 m and the height as 1.1 m.

The nominal and factored dead and superimposed dead load for the carriageway are presented in Table 9.1.

Table 9.1 – Dead and superimposed dead load on a carriageway beam.

Carriageway beam	Unit weight [kN/m^3]	Nominal [kN/m]	Factor γ_{fL}	Factor γ_{f3}	Factored [kN/m]
Beam self-weight	24.0	9.47	1.15	1.1	12.0
Road surfacing	24.0	3.36	1.75	1.1	6.47
Fill	23.0	3.22	1.20	1.1	4.25
Total per beam	–	16.1	–	–	22.7

The nominal and factored dead and superimposed dead load for the footway beams are presented in Table 9.2.

Table 9.2 – Dead and superimposed dead load on a footway beam.

Footway beam	Unit weight [kN/m^3]	Nominal [kN/m]	Factor γ_{fL}	Factor γ_{f3}	Factored [kN/m]
Beam self-weight	24.0	9.47	1.15	1.1	12.0
Fill	23.0	3.22	1.20	1.1	4.25
Pavement and cill	24.0	3.65	1.20	1.1	4.82
Parapet	24.0	4.75	1.20	1.1	6.27
Total per beam	–	21.1	–	–	27.3

The material factor, γ_{fL}, was applied in accordance with BD 21/01 Table 3.1 and the contingency factor, γ_{f3}, was applied to all dead and superimposed dead loads throughout the assessment to consider inaccuracies in the assessment calculations according to BD 21/01 cl. 3.10. The values of these factors are presented in Table 9.2.

9.2.4 Assessment live loading

The Assessment Live Loading effects applied on the carriageway portion of the bridge deck are summarized in Table 9.3.

Table 9.3 – Applied live load on carriageway – per beam.

Type	Applied Load		K	Nominal	Factor γ_{fL}	Factor γ_{f3}	Factored
HA UDL	80.74	kN/m/lane	0.91	28.18	1.5	1.1	46.50
HA KEL	120	kN	0.91	41.89	1.5	1.1	69.12

The HA UDL loading was calculated according to cl. 5.18 as

$$\text{HA UDL} = 336\left(\frac{1}{L}\right)^{0.67} \quad (9.1)$$

HA KEL was applied as a patch load of 120 kN above the support and then at each critical location. The HA UDL and KEL loading are distributed over a single lane of width 2.5 m and the adjustment factor for spans of less than 20 m equals 1.46. The reduction factor K considers the surfacing conditions for the 40 Tonnes Assessment Live Loading, in this case

High traffic and poor surfacing (Hp), determined from Figure 5.2 of BD 21/01. The nominal values of Live Loading, LL_{nom}, were then calculated according to the following equation

$$LL_{nom} = \frac{\text{Applied load} \times K \times \text{loaded width}}{\text{lane width} \times \text{adjustment factor}} \quad (9.2)$$

For the Accidental Wheel Load, the heaviest axle load was factored using an Impact Factor of 1.8, in accordance with Annex D of BD 21/01. Only Axle Loads W1, W2 and W3 were used to obtain the most onerous shear load case, as only these axles would physically fit onto the effective span between the two bearing centres. Axle Loads W2 and W3 were reversed to produce the worst shear effect on the span due to the 40 Tonnes vehicle load, according to Table D1 of BD 21/01. It was conservatively assumed that the full wheel load would bear directly onto the footway beam without dispersal.

The Accidental Wheel Loading effects applied on the footway beams are summarized in Table 9.4.

Table 9.4 – Applied live load on footway – per beam.

Applied Axle Load	Nominal Axle Load [Tonnes]	Axle Spacing [a] [m]	Factor γ_{fL}	Impact Factor	Factor γ_{f3}	Factored Wheel Load [kN]
W1	6.00	2.80	1.5	–	1.1	48.6
W2	11.5	1.30	1.5	1.8	1.1	168
W3	6.50	5.28	1.5	–	1.1	105

[a] Spacing between Axle Load W1 and W2, W2 and W3, W3 and W4, respectively

The schematics of the applied loading for the carriageway and footway beams, considering moving loads along the length of the beam, are shown in Figure 9.3 and Figure 9.4, respectively.

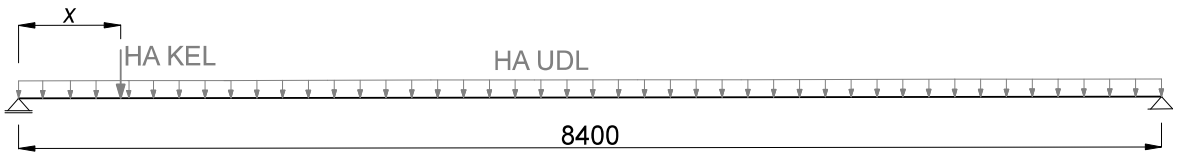

Figure 9.3 – Schematics of live loading on carriageway beams: HA UDL and HA KEL [mm].

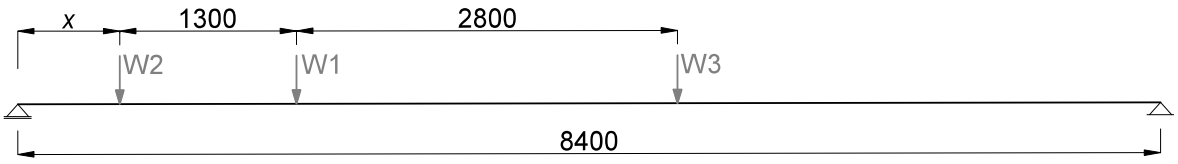

Figure 9.4 – Schematics of live loading on footway beams: Annex D loading [mm].

9.2.5 Resistance of section

The shear capacity was calculated using BD 44/15. Note that the current code does not impose limitations on the maximum concrete compressive strength, f_{cu}, to be used with this equation based on experimental evidence, cl. 5.3.3.2A of BD 44/15. Therefore, the concrete compressive strength of 60 MPa was used in line with the most up-to-date assessment code. In contrast to this, the maximum allowable concrete compressive strength according to BD 44/97 was 40 MPa, producing conservative shear capacity predictions.

The ultimate shear capacity of the section was calculated as the sum of the shear capacity of the uncracked concrete and the shear capacity of the internal steel links as follows

$$V_u = V_c + V_s \tag{9.3}$$

The individual shear capacities of the concrete and steel reinforcement were calculated from the following equations

$$V_c = \xi_s \nu_c b_w d \tag{9.4}$$

$$\xi_s = \left(\frac{500}{d}\right)^{\frac{1}{4}} \tag{9.5}$$

$$\nu_c = \frac{0.24}{\gamma_{mv}} \left(\frac{100 A_s}{b_w d}\right)^{\frac{1}{3}} (f_{cu})^{\frac{1}{3}} \tag{9.6}$$

$$V_s = \frac{f_{yv}}{\gamma_{ms}} \frac{d}{s_v} A_{sv} \tag{9.7}$$

The factors γ_{mv} and γ_{ms} used in the above equations were 1.25 and 1.15, respectively. The total shear resistance of the section, V_u, calculated according to equation (9.3) is presented in Table 9.4.

BD 44/15 considers enhancement in shear capacity in regions close to supports by means of increased concrete contribution with reduction due to the contribution of the anchorage of main reinforcing bars, as discussed in detail in Chapter 2. An initial sensitivity study was performed on the minimum anchorage length that would result in equal or lower capacity compared with that provided by the section without consideration of the enhancement from supports. This was found to be 200 mm taken from the face of the support. Provision of such a short anchorage length does not comply with the requirements for the inclusion of the enhancement close to support in the distance less than 3*d* and therefore, the shear capacity will be assumed constant for the entire length of the beam. Such a scenario was selected for this illustrative example to demonstrate the worst-case scenario in shear deficiency leading to subsequent strengthening.

The worst-case scenario with short anchorage length for the main reinforcing bars considered in this example is presented in Figure 9.5.

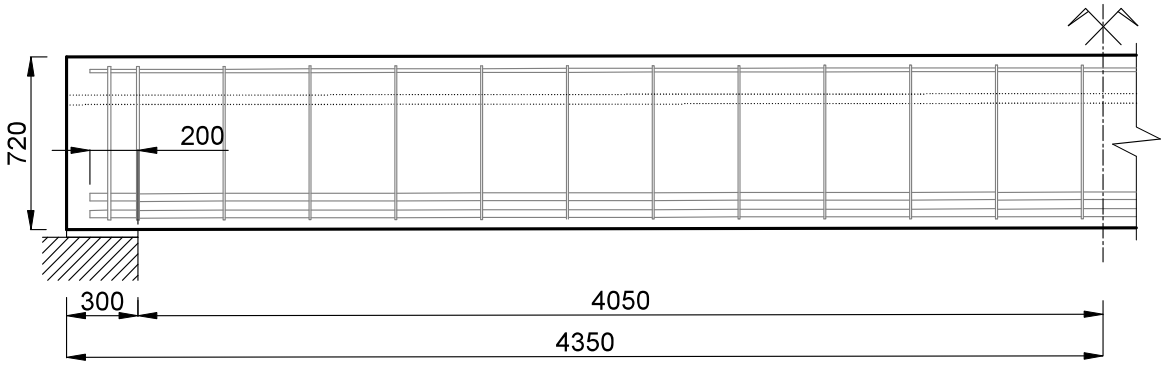

Figure 9.5 – T-beam reinforcement detail – long section (symmetry applies): beam with short end anchorage length for main reinforcement bars [mm].

9.2.6 Assessment results

The comparison of the applied permanent and live load with the resistance of the section at various locations along the beam length is presented in Table 9.5.

Table 9.5 – Comparison of applied permanent and live load with the section resistance.

Element	Distance from support		Due to load V_{load}	Resistance V_u	V_{load} / V_u	Increase required
	$[d]$	[m]	[kN]	[kN]		[kN]
Carriageway beam	0	0	325	240	1.35	85
	1	0.6	284	240	1.18	44
	2	1.2	242	240	1.01	2
	3	1.8	201	240	0.84	0
	3.5	2.1	180	240	0.75	0
Footway beam	0	0	378	240	1.58	138
	1	0.6	338	240	1.41	98
	2	1.2	299	240	1.25	59
	3	1.8	259	240	1.08	19
	3.5	2.1	240	240	1.00	0

The results revealed that the carriageway beams have insufficient shear capacity to carry 40 Tonnes Assessment Live Load at the support and up to the distance of $2d$ away from the support. The footway beams were found inadequate to support 40 Tonnes Accidental Wheel Load in the region from the support up to $3.5d$ (quarter span).

9.2.7 Summary

The assessment of the bridge deck revealed that the carriageway beams fail the assessment for 40 Tonnes Assessment Live Loading and the footway beams are inadequate to carry 40 Tonnes Accidental Wheel Load. This structure is required to reach 40 Tonnes live loading capacity and therefore a further option study is required to determine the most suitable management strategy for the bridge.

9.3 Shear strengthening

9.3.1 Justification for strengthening

The assessment results indicated that 18% and 41% increase in shear capacity is required to achieve 40 Tonnes Assessment Live Load and 40 Tonnes Accidental Wheel Load (Annex D Vehicle Loading) for the carriageway and the footway beams, respectively,

considered at d away from the support. The assessment standard BD 44/15 does not require checking shear at support up to the distance of d away from the support. However, it was included in this assessment to demonstrate what shear forces can be reasonably expected to be acting at the support and for completeness of the assessment example. If the beams were required to withstand the shear force acting at the face of the support this would mean a further increase in shear capacity beyond that at d away from the support was necessary. This shear force, as presented in Table 9.5, was taken as equal to the reaction at support where the heaviest factored axle was applied.

The assessment standard BD 44/15 requires a check to be performed at a location where the most onerous loading to BD 21/01 will occur. It is however anticipated that this shear force will be transferred directly into the support and therefore is considered overly conservative. In most practical assessment cases this check is performed nevertheless. From the results it is apparent that strengthening of the carriageway beams is required up to $2d$ away from the support to achieve 40 Tonnes capacity.

Consideration was given to protecting the footway beams from the effects of Accidental Wheel Loading by means of effective edge protection. However, implementation of edge protection such as trief kerbs or bollards would result in increased dead load over the footways. Furthermore, due to the narrow footways, edge protection would not be feasible and therefore strengthening would offer a better long-term alternative to increase the shear capacity of the beams to 40 Tonnes capacity.

9.3.2 Proposed strengthening solution

The results from the mechanical testing presented in Chapter 6 and further discussed and analyzed in Chapter 7 and Chapter 8 demonstrated that deep embedment offers a reliable strengthening solution where great increase in shear capacity is required and indeed possible.

Therefore, strengthening with deep embedded CFRP bars is proposed, as it was demonstrated experimentally and numerically that the CFRP U-wrap was not suitable for the type of shear failure that was observed and can realistically be expected to occur in this bridge.

9.3.3 Strengthened T-beam section properties

The strengthening solution proposed here is identical to that used for the tested beams presented in Chapter 5. The spacing of the 12 mm diameter CFRP bars is identical to that of the internal steel links at $0.6d$ (0.36 m). The material properties and the geometry of the strengthened beams are identical to those tested and presented in Chapter 5.

9.3.4 Resistance of strengthened section

The shear capacity due to strengthening, V_f, was calculated from the following equations given in TR55, which were presented and discussed in detail in Chapter 2

$$V_f = \frac{\varepsilon_{fe} E_{fd} A_f}{s_b} w_{eff} \quad (9.8)$$

$$w_{eff} = h - 2l_{b,max} \quad (9.9)$$

$$l_{b,max} = \frac{\varepsilon_{fse} E_{fd} A_f}{\pi d_b \tau_b / \gamma_A} \quad (9.10)$$

The overall ultimate shear capacity of the strengthened section is therefore

$$V_{u,DE} = V_u + V_f \quad (9.11)$$

determined as the sum of the ultimate shear capacity of the unstrengthened section, V_u, calculated in Section 9.2.5, and the shear capacity due to the presence of the CFRP bars, V_f as calculated above.

9.3.5 Summary of results

The comparison of the applied permanent and live load with the resistance of the section at the critical locations along the beam length determined in Section 9.2.6 is presented in Table 9.6.

Table 9.6 – Comparison of applied permanent and live loads with strengthened section resistance.

Element	Distance from support		Due to load V_{load}	Resistance $V_{u,DE}$	V_{load} / $V_{u,DE}$	Outcome
	$[d]$	[m]	[kN]	[kN]		
Carriageway beam	0	0	325	423	0.77	PASS
	1	0.6	284	423	0.67	PASS
	2	1.2	242	423	0.57	PASS
	3	1.8	201	423	0.48	PASS
	3.5	2.1	180	–	–	PASS
Footway beam	0	0	378	423	0.89	PASS
	1	0.6	338	423	0.80	PASS
	2	1.2	299	423	0.71	PASS
	3	1.8	259	423	0.61	PASS
	3.5	2.1	240	–	–	PASS

The results revealed that the strengthening solution with deep embedded CFRP bars provides adequate shear capacity to withstand the applied permanent and 40 Tonnes live load for both the carriageway and the footway beams.

The comparison of the shear force due to load, V_{load}, and the ultimate capacity of the strengthened section, $V_{u,DE}$, showed that there is a considerable shear capacity reserve. At this point the bending capacity Ultimate Limit State (ULS) check should be performed to confirm failure mode.

9.4 Recommendations for further assessment

This example clearly demonstrated that strengthening using deep embedded CFRP bars as additional shear reinforcement provides adequate increase in shear capacity beyond that required for the structure to safely carry the 40 Tonnes ALL and 40 Tonnes AWL. It is therefore recommended that this strengthening solution be accepted as a suitable mitigation strategy for this substandard structure.

Furthermore, it was showed that the TR55 approach for calculating the increase in shear strength due to the application of the CFRP bars is compatible with the assessment philosophy of BD 44/15. This is because the deep embedded CFRP bars function in the

same way as the internal steel links and therefore the additive approach of shear resistances of the individual components in this instance is wholly appropriate.

However, considering the actual capacity of the tested beams and the numerically obtained resistance of the section being much higher than the shear capacity obtained using BD 44/15, further increase in strength may be possible through assessment using more advanced methods. The shear capacity obtained from ATENA 2D, which was in good agreement with the experimental results, was greater than that achieved by using BD 44/15 in combination with deep embedment strengthening according to TR55.

The tested beam of the same geometry but with a reduced flange size due to laboratory space constraints failed due to shear force of 472 kN. This would provide a conservative shear capacity, ignoring the contribution of the wider flange in this assessment example. The capacity of the strengthened beam in this example is 423 kN. Furthermore, the shear capacity of the unstrengthened beam using *fib* Model Code (2010) was determined as 424 kN, which would be sufficient for the applied live load.

Strengthening would therefore not be required if either of those two methods was used for assessment of the existing reinforced concrete beam. It should be noted that BD 44/15 gives comparable shear capacity predictions to those obtained using ACI-318, as presented in Chapter 7.

It would be therefore recommended to either use the Level III shear capacity prediction model of *fib* Model Code (2010) or alternatively perform further assessment using non-linear FE analysis using ATENA or similar, to more accurately determine the shear capacity of the existing reinforced concrete beam.

9.5 Outline of proposed methodology

The limitations of the design as well as the assessment codes may result in under-predicted capacity for the existing reinforced concrete structure and therefore lead to unnecessary strengthening or removal of a substandard structure.

To prevent such a costly intervention, which may not be required, and to accurately assess the capacity of the existing structure, a reviewed assessment methodology was proposed, see Figure 9.6.

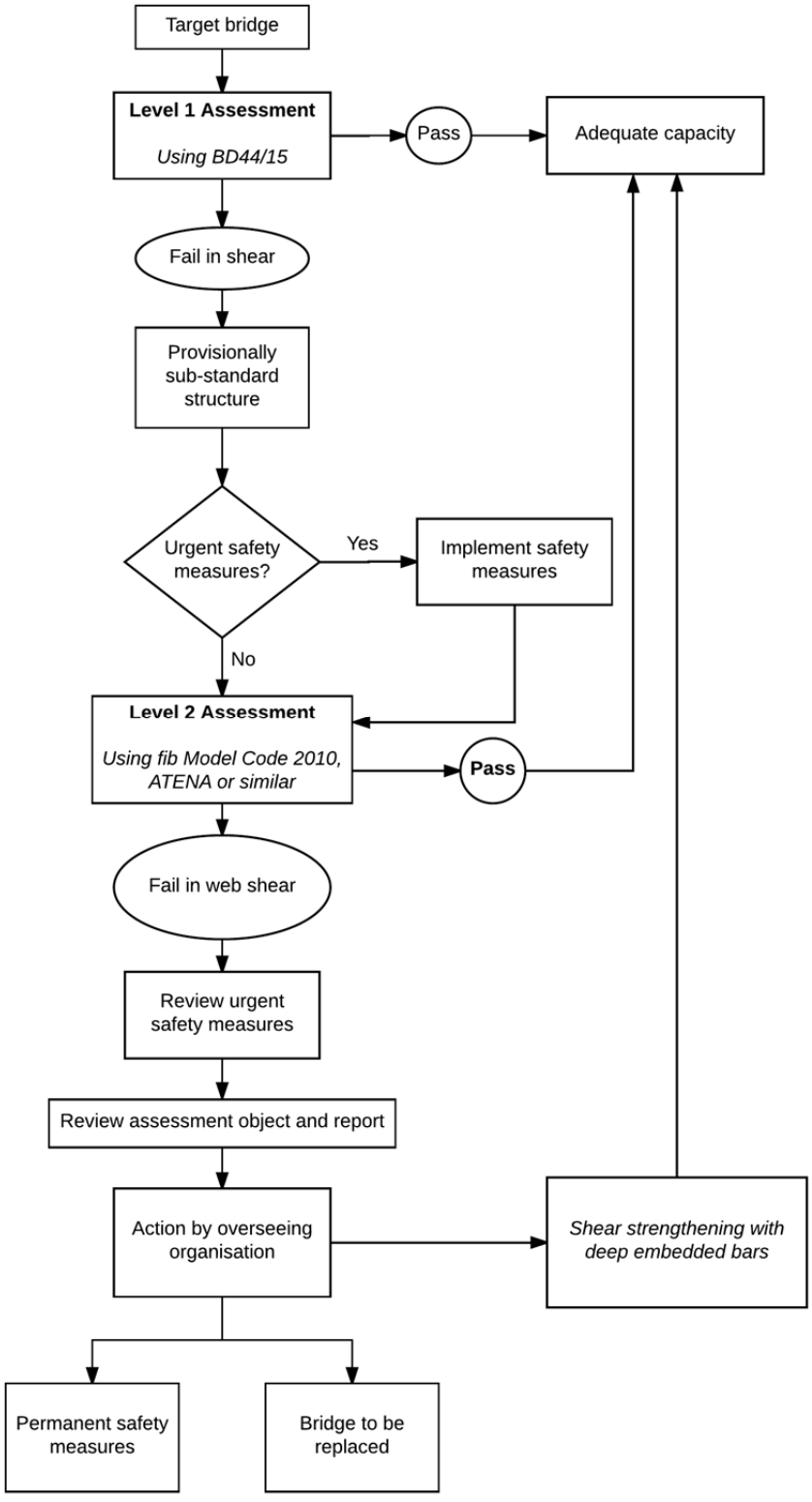

Figure 9.6 – Outlined proposed methodology for shear assessment and strengthening of reinforced concrete bridges.

10 CONCLUSIONS AND RECOMMENDATIONS

10.1 Conclusions

One of the primary objectives of the presented research was to determine the influence of size on the behaviour and ultimate load-bearing capacity of CFRP-strengthened reinforced concrete T-beams subject to shear. A targeted experimental study conducted on ten realistically sized and shaped T-beams confirmed that size effect is indeed present in the strengthened beams as well as in the unstrengthened control specimens. The behaviour and the ultimate shear capacity of the beams strengthened with deep embedded CFRP bars and those without CFRP reinforcement were clearly identified as being heavily influenced by the effect of size of the tested specimen.

A size effect was also observed in the specimens strengthened with externally bonded CFRP sheets, both with and without end anchorage. The size effect in the fabric-strengthened beams appears to be directly associated with the behaviour of the underlying reinforced concrete beam, which is broadly compatible with the general trends predicted by fracture mechanics. This is possibly caused by the CFRP sheets, anchored and unanchored, bridging the shear crack and therefore controlling the crack propagation.

The deep embedment specimens, however, showed a greater increase in shear capacity for the smaller of the two specimens, inconsistent with the predictions of fracture mechanics. The general behaviour of this beam also highlighted the possibility that the failure mode was altered from direct shear due to the higher internal shear reinforcement ratio. Therefore, it may be concluded that the size effect in T-beams with high amount of longitudinal reinforcement subject to shear is influenced by the amount of shear reinforcement, both internal steel and additional CFRP.

The U-wrapped specimens failed consistently at lower loads than their unstrengthened counterparts, regardless of their size and thickness of the applied CFRP fabric. The observed variation in the shear capacity of the unstrengthened control beams was significant in comparison with the magnitude of the shear capacity enhancement expected from the additional CFRP reinforcement. The relatively small enhancement achieved by

the T-beams with anchored CFRP U-wrap compared with the unstrengthened control specimens indicates that the potential of the bar-in-slot anchorage system to increase the effectiveness of the CFRP wrap is rather limited. The increase achieved in the beams with end anchorage appears to be attributed to a greater effective width of the CFRP sheet contributing to the overall shear capacity rather than the development of increased strains in the CFRP. This notion is further reinforced by the fact that the results were near identical regardless of the thickness of the CFRP fabric applied across both sizes of test specimen.

The experimental results also highlighted that the effectiveness of the CFRP U-wrap may be influenced by the location of the shear crack initiation. The implication of this observation is that in cases where the crack initiates within the web rather than at the soffit, the available bond length may be dramatically reduced, increasing the potential for a premature failure due to debonding. This finding is underpinned by the observations from the initial experimental study conducted on push-off specimens with varying anchorage lengths of the CFRP sheets.

Inclinations of the critical diagonal web crack in unstrengthened control beams were observed at 22º for both sizes of test specimen. The beams strengthened with CFRP U-wraps consistently developed shear cracks with an inclination of approximately 37º. Higher shear capacities can reasonably be expected from reinforced concrete beams with flatter critical diagonal web cracking angles, and therefore the higher capacity of the unstrengthened control specimens is justified. The observed shear-deflection behaviour indicated that the presence of the CFRP U-wrap delayed the onset of the diagonal cracking in all U-wrapped beams, regardless of the end anchorage. Therefore it appears that the reduction in shear capacity in the strengthened beams was caused by higher shear stresses in the underlying concrete due to the presence of the CFRP wrap. This is also corroborated by the steeper angle of the shear crack observed in the fabric-strengthened beams and the consistent shear capacities recorded for the beams, regardless of the thickness of the CFRP sheets. Furthermore, the experimental results showed that the presence of the CFRP U-wrap delayed the strain development in the internal shear reinforcement, suggesting that the steel had not fully yielded until after the CFRP had separated. Based on the observations from the experimental testing and the analysis of strains in the CFRP sheets it may be concluded that in the case of a unidirectional CFRP fabric the stretching in the non-principal direction is not critical. Moreover, it would appear that the performance of

the CFRP wrap, and so the extent to which it contributes to the overall shear capacity, is dependent on the bond strength between the CFRP and the concrete surface.

The deep embedment specimens, on the other hand, showed a great increase in shear strength compared with both the U-wrapped specimens and the unstrengthened control specimens. The behaviour of the beams was consistent with that of reinforced concrete beams with internal steel reinforcement, indicating that the additional CFRP bars behave similarly to the internal steel reinforcement. This finding was also underpinned by the results from the tests on push-off specimens strengthened with deep embedded CFRP bars. In both cases, the strains measured on the CFRP bars were consistent with those measured on the internal steel at the onset of concrete cracking, showing that both the steel and the CFRP contributed at the same time.

The experimental results indicated that the capacity of full-scale reinforced concrete T-beams with large amount of longitudinal reinforcement and minimal shear reinforcement is greatly underpredicted according to modern standards. The EC2 only accounts of up to 30% of the actual shear capacity, which would inevitably lead to unnecessary strengthening. The assessment standard BD 44/15, which relaxes some of the constraints as well as allows for enhancement from support derived from experimental testing, achieves up to 50% of the actual shear capacity. This is comparable with the predictions of ACI-318. More accurate predictions are possible through the use of more sophisticated assessment codes, such as the *fib* Model Code 2010 where up to 90% accurate predictions are possible at the highest level of approximation.

However, the most accurate capacity predictions are only possible using non-linear finite element methods based on fracture mechanics, as was demonstrated in this work using a commercial package ATENA. In this case not only was the shear capacity correctly determined but the location of the shear crack initiation as well as further propagation was identified. Furthermore, the software also successfully picked up on the size effect, which was not the case in any of the design and assessment standards. The only drawback of the software is the stiffer shear-displacement behaviour of the modelled beams compared with the experimental data. This appears to be caused by the uncertainty about the shear parameters, such as the crack opening law, which was not determined experimentally and therefore the default values were used.

Comparison of measured versus predicted effective strain levels according to current design guidelines for FRP fabric-strengthened reinforced concrete beams showed that the values might be over- or underpredicted. For the beams with unanchored CFRP U-wraps, the peak CFRP strains were only observed to occur over a relatively narrow width of the CFRP at peak load. This width may be less than the effective width of the CFRP assumed to be mobilized by the 45º truss model of TR55, *fib* Bulletin No. 14 and ACI-440. Contrary to this, the comparison of the strains measured on the deep embedded CFRP bars with the values predicted by TR55 showed that while the predicted values may be conservative, they offer a safe design capacity. The truss model analogy offered by the design codes and their combination therefore appears to be appropriate for T-beams strengthened with deep embedded bars, while wholly inappropriate for T-beams strengthened with externally bonded CFRP U-wraps.

The numerical modelling of the strengthened beams showed that the software ATENA 2D might be successfully used for the design of strengthening with CFRP materials. The nature of the 2D environment appears sufficient for the capacity predictions of the T-beams strengthened with deep embedded CFRP bars. However, the modelling of the CFRP sheets may require a full 3D analysis. The 2D analysis of the CFRP U-wraps where the sheets are approximated as discrete bars may be appropriate at the initial design stages. However, there are uncertainties in such approximations, which might be overcome by a more appropriate 3D analysis where the use of shell elements to model the CFRP-concrete interaction is possible. It was also observed that the shear-displacement behaviour of the modelled U-wrapped beams was consistent with that of the tested beams, suggesting that the default crack opening law is appropriate for beams where the shear crack is bridged by the CFRP sheets.

10.2 Recommendations

The recommended strategy for assessment of existing reinforced concrete slab-on-beam structures was outlined in this work. Should the structure fail the initial assessment to either the design codes or the assessment code BD 44/15, it is recommended to assess the structure using more advanced empirical or numerical methods. The capability of the empirical models in the current codes and standards was found to be increasing in accuracy with increase in complexity of the empirical model. This was from approximately 30% accuracy for Eurocode 2, 50% for the ACI-318 standard, which was comparable with the

assessment standard BD 44/15 and 90% for the Level III model of *fib* Model Code (2010). If the structure initially passes the assessment using the simpler and more conservative methods for shear capacity predictions, the structure has adequate capacity and further assessment is therefore not required.

Should the structure fail the initial assessment either to the design or the assessment codes, further assessment using appropriate finite element methods is recommended. It was demonstrated in this work that 100% accurate predictions of ultimate capacity for flanged beams regardless of their size is possible using advanced fracture mechanics-based FE package ATENA in 2D. Should the structure fail the assessment using these advanced methods, the likely failure mode should be investigated and the most appropriate strengthening solution devised. For reinforced concrete beams that are prone to exhibiting web shear cracking, strengthening with deep embedded bars is recommended for a safe and reliable increase in shear capacity. The model in ATENA 2D used for the assessment of the existing structure can then be modified to analyze the shear strengthening solution with deep embedded bars.

10.3 Future work

Non-linear finite element modelling of reinforced concrete beams in ATENA 2D proved sufficiently accurate to predict the ultimate capacity of the tested reinforced concrete beams within the default model parameters for concrete in shear. However, improvements can be made to accurately capture the load-displacement behaviour with a more refined material model for concrete, which is appropriate for modelling of reinforced concrete structures in ATENA 3D. The improved material models would benefit from further experimental investigation of shear crack opening laws and fracture energy appropriate for beams exhibiting large localized deformations may be required.

The limitations of the ATENA 2D model to accurately simulate the behaviour of strengthened beams with externally bonded CFRP sheets highlighted that a more complex 3D model would be more suitable for this task. It would therefore be beneficial to further model the tested beams strengthened with CFRP U-wraps in ATENA 3D to capture debonding using shell elements and bond model applied over a surface area rather than discrete bars. The 3D environment would also enable to model the numerically complex

continuous bar-in-slot anchorage system with bond properties applied to the interface between the anchored sheet and the concrete within the slot.

For the development of analytical models that could be included within design and assessments standards for reinforced concrete structures, further modelling work is required to simulate the behaviour of large beams and compare with the modelled medium beams in the parametric study presented in Chapter 8. However, these analytical models would only be applicable for T-beams of the geometry and reinforcement detail investigated within this research programme, and therefore, their application would be limited to these specific cases.

REFERENCES

ACI-318. (2014). Building Code Requirements for Structural Concrete. (No. ACI 318-14) Farmington Hills (Michigan): American Concrete Institute.

ACI-440. (2008). Guide for the Design and Construction of Externally Bonded FRP Systems for Strengthening Concrete Structures. (No. ACI 440.2R-08) Farmington Hills (Michigan): American Concrete Institute.

Ahmad, S. H., Khaloo, A. R., and Poveda, A. (1986). Shear Capacity of Reinforced High-Strength Concrete Beams, ACI Structural Journal, 83(2): 97-305.

Al-Bayati, G. and Al-Mahaidi, R. (2014). Effective bond length of modified cement-based adhesive for FRP-NSM strengthening systems. 23rd Australasian Conference on the Mechanics of Structures and Materials (ACMSM23), 1-12 December 2014, Southern Cross University, Lismore: 389-396.

Al-Mahaidi, R. and Kalfat, R. (2011). Investigation into CFRP plate end anchorage utilizing uni-directional fabric wrap. Composite Structures, 93(2): 821-830.

ASCE-ACI Committee 426 on Shear and Diagonal Tension. (1973). The shear strength of reinforced concrete members. Journal of the Structural Division, 99(6): 1091-1187.

ASCE-ACI Committee 445 on Shear and Torsion. (1998). Recent approaches to shear design of structural concrete. Journal of Structural Engineering, 124(12): 1375-1417.

ASCE-ACI Task Committee 426. (1974). The shear strength of reinforced concrete members - slabs. Journal of the Structural Division, 100(8): 1543-1591.

ASTM D7522. (2015). Standard Test Method for Pull-Off Strength for FRP Laminate Systems Bonded to Concrete Substrate, ASTM International, West Conshohocken, Pennsylvania, US.

ATENA Manual. (2017). User's Manual for ATENA 2D. Cervenka Consulting s.r.o.: http://www.cervenka.cz/products/atena/documentation/ last accessed 2 October 2016.

ATENA Strengthening. (2016). ATENA documentation – Tutorial for ATENA Science Gid Strengthening. Cervenka Consulting Ltd: http://www.cervenka.cz/products/atena/documentation/ last accessed 2 October 2016.

ATENA Theory. (2016). ATENA documentation. Cervenka Consulting s.r.o.: http://www.cervenka.cz/products/atena/documentation/ last accessed 2 October 2016.

ATENA Troubleshooting. (2015). ATENA documentation. Cervenka Consulting s.r.o.: http://www.cervenka.cz/products/atena/documentation/ last accessed 2 October 2016.

Bae, S. and Belarbi, A. (2013). Behavior of various anchorage systems used for shear strengthening of concrete structures with externally bonded FRP sheets. Journal of Bridge Engineering, 18(9): 837-847.

Barros, J. A. O. and Dias, S. J. E. (2005). Near surface mounted CFRP laminates for shear strengthening of concrete beams. Cement Concrete Composites, 28: 289-94.

Bazant, P., Kim, J. K. (1968). Size Effect in Shear Failure of Longitudinally Reinforced Beams. ACI Structural Journal, (81): 456-468.

Bazant, Z. P., Kazemi, M. T. (1991). Size effect on Diagonal Shear Failure of Beams without Stirrups. ACI Structural Journal, 88(3): 268-276.

Bazant, Z. P., Kim, J. K. (1984). Size Effect in Shear Failure of Longitudinally Reinforced Beams. ACI Structural Journal, 81(5): 456-468.

Bazant, Z. P., Yu, Q., Gerstle, W., Hanson, J. and JU, J. W. (2007). Justification of ACI 446 proposal for updating ACI code provisions for shear design of reinforced concrete beams. ACI Structural Journal, 104(5): 601-610.

BD 21/01. (2001). The assessment of highway bridges and structures (DMRB 3.4.3). The Highways Agency, HMSO, London.

BD 44/15. (2015). The assessment of concrete highway bridges and structures (DMRB 3.4.14). The Highways Agency, HMSO, London.

BD 44/95. (1995). The assessment of concrete highway bridges and structures (DMRB 3.4.14). The Highways Agency, HMSO, London.

Belarbi, A. and Acun, B. (2013). FRP Systems in shear strengthening of reinforced concrete structures. Proceedings of the 11th International Conference on Modern Building Materials, Structures and Techniques, May 2013, Vilnius. 57:2-8. doi:10.1016/j.proeng.2013.04.004.

Belletti, B., Damoni, C., den Uijl, J. A., Hendriks, M. A. N. and Walraven, J. C. (2013). Shear resistance evaluation of prestressed concrete bridge beams: fib Model Code 2010 guidelines for level IV approximations. Structural Concrete, 14: 242–249. doi:10.1002/suco.201200046.

Bousselham, A. and Chaallal, O. (2004). Shear strengthening of reinforced concrete beams with fiber-reinforced polymer: Assessment of influencing parameters and required research. ACI Structural Journal, 101(2): 219-227.

Bousselham, A. and Chaallal, O. (2006). Behavior of reinforced concrete T-beams strengthened in shear with carbon fiber-reinforced polymer – An experimental study. ACI Structural Journal, 103(3): 339-347.

Bousselham, A. and Chaallal, O. (2008). Mechanisms of shear resistance of concrete beams strengthened in shear with externally bonded FRP. ASCE Journal of Composites for Construction, 12(5): 499-512.

Brown, M. D., Bayrak, O. and Jirsa, J. O. (2006). Design for shear based on loading conditions. ACI Structural Journal, 103(4): 541-550.

BS 4449: 2005. (2005). Steel for the reinforcement of concrete weldable reinforcing steel, bar, coil and decoiled product. British Standard Institution, London.

BS 4482:2005. (2005). Steel wire for the reinforcement of concrete products. Specification. British Standard Institution, London.

BS 5400-4. (1990). Steel, concrete and composite bridges. Part 4: Code of practice for design of concrete bridges. British Standard Institution, London.

BS 8110-1. (1997). Structural use of concrete. Part 1: Code of practice for design and construction. British Standard Institution, London.

BS EN 12390-3:2009. (2009).Testing hardened concrete. Compressive strength of test specimens. British Standard Institution, London.

BS EN 12390-6:2009. (2009).Testing hardened concrete. Tensile splitting strength of test specimens. British Standard Institution, London.

BS EN 1992-1-1. (2004). Eurocode 2: Design of Concrete Structures: General Rules and Rules for Buildings. British Standard Institution, London.

BS EN ISO 527-5:2009. (2009). Plastics. Determination of tensile properties. Test conditions for unidirectional fibre-reinforced plastic composites. British Standard Institution, London.

Bukhari, I. A., Vollum, R. L., Ahmad, S., Sagaseta, J. (2010). Shear strengthening of reinforced concrete beams with CFRP. Magazine of Concrete Research, 62(1): 65-77.

Carolin, A. and Taljsten, B. (2005). Theoretical study of strengthening for increased shear bearing capacity. ASCE Journal of Composites for Construction, 9(6): 497-506.

CEB-FIP MODEL CODE. (2010). International recommendations for the design and construction of concrete structures. Comité Euro-International du Béton, Thomas Telford, London.

Chaallal, O., Mofidi, A., Benmokrane, B. and Neale, K. (2011). Embedded Through-Section FRP Rod Method for Shear Strengthening of RC Beams: Performance and Comparison with Existing Techniques. ASCE Journal of Composites for Construction, 15(3): 374-383.

Chen, G. M., Teng, J. G., Chen, J. F. (2010). RC beams shear-strengthened with FRP: shear resistance contributed by FRP. Magazine of Concrete Research, 62(4): 301-311.

Chen, G. M., Teng, J. G., Chen, J. F. (2013). Shear strength model for FRP-strengthened RC beams with adverse FRP-steel interaction. ASCE Journal of Composites for Construction, 17(12): 50-66.

Chen, G. M., Teng, J. G., Chen, J. F., Rosenboom, O. A. (2010). Interaction between steel stirrups and shear-strengthening FRP strips in RC beams. ASCE Journal of Composites for Construction, 14(5): 498-509.

Chen, G., Teng, J., Chen, J. (2012). Process of debonding in RC beams shear-strengthened with FRP U-strips or side strips. International Journal of Solids and Structures, 49(10): 1266-1282.

Chen, J. and Teng, J. (2003a). Shear capacity of FRP-strengthened RC beams: FRP debonding. Construction and Building Materials, 17(1): 27-41.

Chen, J. and Teng, J. (2003b). Shear capacity of fiber-reinforced polymer-strengthened reinforced concrete beams: fiber reinforced polymer rupture. Journal of Structural Engineering, 129(5): 615-625.

CNR-DT 200/2004. (2004). Guide for the Design and Construction of Externally Bonded FRP Systems for Strengthening Existing Structures. Rome, Italy.

Colalillo, M. A. and Sheikh, S. A. (2014). Behavior of shear-critical reinforced concrete beams strengthened with fiber-reinforced polymer – Analytical method. ACI Structural Journal, 111(6): 1385-1396.

Collins, M. and Kuchma, D. (1999). How Safe are our Large, Lightly Reinforced Concrete Beams, Slabs, and Footings? ACI Structural Journal, 96(4): 482-490.

Collins, M. P., Bentz, E. C. and Sherwood, E. G. (2008). Where is Shear Reinforcement Required? Review of Research Results and Design Procedures, ACI Structural Journal, 105(5).

Concrete Society TR55. (2012). Design guidance for strengthening concrete structures using fibre composite materials. Second edition. Technical Report, The Concrete Society, Camberley, UK, 102.

CP114. (1969). British Standards Institution, Code of Practice CP 114:1969: The Structural Use of Reinforced Concrete in Buildings. British Standards Institution, London.

Dadvar, B. (2014). Design and Modeling of Slender and Deep Beams with Linear Finite Element Method. MSc Thesis. Delft University of Technology, Delft, The Netherlands.

Dai, J. G., Gao, W. Y. and Teng, J. G. (2013). Bond-slip Model for FRP Laminates Externally Bonded to Concrete at Elevated Temperature. ASCE Journal of Composites for Construction, 17(2).

Deifalla, A. and Ghobarah, A. (2010). Strengthening of RC T-beams subjected to combined torsion and shear using FRP fabrics: experimental study. ASCE Journal of Composites for Construction, 14(3): 301-311.

Denton, S. R., Shave, J. D. and Porter, A. D. (2004), Shear Strengthening of Reinforced Concrete Structures Using FRP Composites, ACIC 2004, Editors Hollaway, Chryssanthopoulos and Moy: 134-143.

Elzanaty, A. H., Nilson, A. H., Slate, F. O. (1986). Shear Capacity of Reinforced Concrete Beams Using High-Strength Concrete. ACI Structural Journal, 83(2): 290-296.

Fernandez Ruiz, M., Vaz Rodrigues, R., Muttoni, A. (2009). Dimensionnement et verification des dalles de roulement des ponts routiers. Ecole Polytechnique Federale de Lausanne, Laboratoire de Construction en Beton, 53.

fib-TG9.3. (2001). Design and use of externally bonded fibre-reinforced polymer reinforcement (FRP EBR) for reinforced concrete structures. Technical Report Prepared by Task Group 9.3, Bulletin 14, Lausanne, Switzerland.

Foster, R., Brindley, M., Lees, J., Ibell, T., Morley, C., Darby, A., Evernden, M. (2016). Experimental investigation of reinforced concrete T-beams strengthened in shear with externally bonded FRP sheets: ASCE Journal of Composites for Construction, 21(2): https://dx.doi.org/10.1061/(ASCE)CC.1945-5614.0000743.

Grande, E., Imbimbo, M., Rasulo, A. (2007). Experimental behaviour of RC beams strengthened in shear by FRP sheets. Proceedings of the 8th International Symposium on Fiber-Reinforced Polymer Reinforcement for Concrete Structures, July 2007, Patrasso, Greece.

Grelle, S. V. and Sneed, L. H. (2013). Review of anchorage systems for externally bonded FRP laminates. International Journal of Concrete Structures and Materials, 17(1): 17-33.

Hassan Dirar, S. M. O., Morley, C. T., and Lees, J. M. (2007). Effect of Effective Depth and Longitudinal Steel Ratio on the Behaviour of Precracked RC T-beams Strengthened in Shear with CFRP Fabrics FRPRCS-8, Greece: 5-8.

Highways Agency. (2003). A Review of Bridge Assessment Failures on the Motorway and Trunk Road Network, Final Project Report.

Hofbeck, J. A., Ibrahim, I. O., Mattock, A. H. (1969). Shear Transfer in Reinforced Concrete. ACI Structural Journal, 66(2): 119-128.

Hughes Brothers, Inc. (2008). Aslan 100 GFRP rebar / Aslan 200 CFRP rebar. Technical Data Sheet. Online at http://www.hughesbros.com/Aslan_FRP.html, last accessed 15 September 2008.

Hughes Brothers, Inc. (2011). Carbon fiber reinforced polymer (CFRP) Bar — Aslan 200 series with approved Hilti Hit-RE 500 V3 adhesive, Seward, NE.

Ibell, T. J., Darby, A. P. and Denton, S. R. (2007). The use of FRP to strengthen structures: A UK perspective. (CD-ROM) Proceedings of the 4th Structural Engineering Mechanics Conference. Cape Town.

Jayaprakash, J., Samad, A. A., Abbasvoch, A. A., Ali, A. A. (2007). Externally bonded bi-directional CFRP shear reinforcement for reinforced concrete T-beams with steel reinforcement. Proceedings of the 8th International Symposium on FiberReinforced Polymer Reinforcement for Concrete Structures, July 2007, Patrasso, Greece.

Jayaprakash, J., Samad, A. Z. A., Abdasvoch, A. A. (2009). Experimental Investigation on Shear Capacity of Reinforced concrete Precracked Push-off Specimens with Externally Bonded Bi-Directional Carbon Fibre Polymer Fabrics: Journal of Modern Applied Science, (3)7: 86-98.

Jeemaa, Y., Jones, C., Dirar, S. (2015). Deep embedment strengthening of full scale shear deficient reinforced concrete beams: The 12th International Symposium on Fiber Reinforced Polymers for Reinforced Concrete Structures (FRPRCS-12) and The 5th Asia-Pacific Conference on Fiber Reinforced Polymers in Structures (APFIS-2015) Joint Conference, 14-16 December 2015, Nanjing, China.

Jinno, Y., Tsukagoshi, H., Yabe, Y. (2001). RC beams with slabs strengthened by CF sheets and bundles of CF strands. Proceedings of the 5th International Conference on Fibre-Reinforced Plastics for Reinforced Concrete Structures, July 2001, Cambridge, UK: 981-998.

Kani, G. N. J. (1964). The Riddle of Shear Failure and Its Solution. ACI Structural Journal, 61(4): 441-467.

Kani, G. N. J. (1966). Basic Facts Concerning Shear Failure. ACI Structural Journal, 63(6): 675-692.

Kani, G. N. J. (1967). How safe are our large reinforced concrete beams? ACI Structural Journal, 64(3): 128-141.

Kani, G. N. J., Huggins, M. W., Wittkopp, R. R. (1979). Kani on Shear in Reinforced Concrete, University of Toronto, Department of Civil Engineering, Toronto, 225.

Khalifa, A. and Nanni, A. (2000). Improving shear capacity of existing RC T-section beams using CFRP composites. Cement and Concrete Composites, 22(3): 165-174.

Khalifa, A. and Nanni, A. (2002). Rehabilitation of rectangular simply supported RC beams with shear deficiencies using CFRP composites. Construction and Building Materials, 16(3): 135-146.

Khalifa, A., Alkhrdaji, T., Nanni, A., Lansburg, S. (1999). Anchorage of surface mounted FRP reinforcement. Concrete International: Design and Construction, 21(10): 49-54.

Khalifa, A., Gold, W. J., Nanni, A., Aziz, A. (1998). Contribution of externally bonded FRP to shear capacity of RC flexural members. ASCE Journal of Composites for Construction, 2(4): 195-202.

Khene, A., Chikh, N. E., Mesbah, H. A. (2016). Numerical Modelling of Reinforced Concrete Beams Strengthened by NSM-CFRP Technique. International Journal of Research in Chemical, Metallurgical and Civil Engineering (IJRCMCE), 3(2): 226-230.

Kotes, P., Kotula, P. (2007). Modeling and strengthening of RC bridges by means of CFRP. Proceedings of the 6th international conference on fracture mechanics of concrete and concrete structures, 17-22 June 2007, Catania, Italy: 1139-1147.

Kotsovos, M. D. (1984). Behaviour of Reinforced Concrete Beams with a Shear Span to Depth Ratio Between 1.0 and 2.5. ACI Structural Journal, 81(3): 279-286.

Kotsovos, M. D. (1987). Shear failure of reinforced concrete beams. Engineering Structures, 9(1):3 2–38.

Koutas, L. and Triantafillou, T. C. (2013). Use of anchors in shear strengthening of reinforced concrete T-beams with FRP. ASCE Journal of Composites for Construction, 17(1): 101-107.

Lees, J. M. (2001). Fibre-reinforced Polymers in Reinforced and Prestressed Concrete Applications: Moving Forward, Progress in Structural Engineering and Materials, 3(2): 122-131.

Lopez-Gonzalez, C., J., Fernandez-Gomez, J., González-Valle, E. (2012). Effect of adhesive thickness and concrete strength on FRP-concrete bonds. ASCE Journal of Composites for Construction, 16: 705-711.

Lu, X., Chen, J., Ye, L., Teng, J., Rotter, J. (2009). RC beams shear-strengthened with FRP: stress distributions in the FRP reinforcement. Construction and Building Materials, 23: 1544-1554.

Mattock, A. H. (2001). Shear friction and high-strength concrete. ACI Structural Journal, 98(1): 50-59.

Mofidi, A. and Chaallal, O. (2011). Shear strengthening of RC beams with EB FRP: influencing factors and conceptual debonding model. ASCE Journal of Composites for Construction, 15(1): 62-74.

Mofidi, A., Chaallal, O., Benmokrane, B., Neale, K. (2012). Performance of end-anchorage systems for RC beams strengthened in shear with epoxy-bonded FRP. ASCE Journal of Composites for Construction, 16(3): 322-331.

Moody, K. G., Viest, I. M., Elstner, R. C. and Hognestad, E. (1954). Shear Strength of Reinforced Concrete Beams Part 1– Tests of Simple Beams, ACI Structural Journal, 26(4): 317-332.

Morsch, E. (1909). Concrete-steel construction (English translation of Der Eisenbetonbau). McGraw-Hill, New York.

Mphonde, A. G., and Frantz, G. C. (1984). Shear Strength of High Strength Reinforced Concrete Beams (Report CE 84-157), Civil Engineering Department, University of Connecticut, Storrs, CT. 260.

NCHRP Report 678. (2011). Design of FRP systems for strengthening concrete girders in shear. Transportation Research Board. Washington DC, US.

Neubauer, U. and Rostasy, F. S. (1997). Design Aspects of Concrete Structures Strengthened with Externally Bonded CFRP Plates, Proceedings of the 7th International Conference on Structural Faults and Repair, 2: 109-118.

Ortega, C. A., Belarbi, A., Bae, S. W. (2009). End anchorage of externally bonded FRP sheets for the case of shear strengthening of concrete girders. Proceedings of the 9th International Symposium on Fiber-Reinforced Polymer Reinforcement for Concrete Structures, July 2009, Sydney, Australia.

Pillai, S. U. and Menon, D. (2003). Reinforced Concrete Design. New Delhi: Tata McGraw-Hill Publishing Company Limited.

Qapo, M., Dirar, S. and Jemaa, Y. (2013). Finite element parametric study on reinforced concrete beams shear-strengthened with embedded FRP bars: Composite Structures, 149: 93-105.

Qin, S., Dirar, S., Yang, J., Chan, A. H. C., Elshafie, M. (2014). CFRP Shear Strengthening of Reinforced Concrete T-beams with Corroded Shear Links. ASCE Journal of Composites for Construction, 19 (5.04014081): https://doi.org/10.1061/(ASCE)CC.1943-5614.0000548.

Raicic, V., Ibell, T., Darby, A., Evernden, M. and Orr, J. (2016). Deep embedment shear strengthening of continuous reinforced concrete T-beams: The 11th fib International PhD Symposium in Civil Engineering, 29-31 August 2016, University of Tokyo, Japan.

REF3b. (2014). Prolonging the Life of our Concrete Infrastructure (Case study, REF2014), University of Bath, Bath, UK.

Sabol, P. and Priganc, S. (2013). Shear Strength of Concrete Members Using NSM Method. Procedia Engineering, 65: 364-369.

Saenz, N. and Pantelides, C. P. (2005). Shear Friction Capacity of Concrete with External Carbon FRP Strips. ASCE Journal of Structural Engineering, 131(12): 1911-1919.

Sas, G., Carolin, A. and Täljsten, B. (2008). A model for predicting the shear bearing capacity of FRP strengthened beams. Mechanics of Composite Materials, 44(3): 245-256.

Sas, G., Täljsten, B., Barros, J., Lima, J., Carolin, A. (2009). Are available models reliable for predicting the FRP contribution to the shear resistance of RC beams? ASCE Journal of Composites for Construction, 13(6): 514-534.

Schnerch, A. (2001). Shear behavior of large-scale concrete beams strengthened with fibre reinforced polymer (FRP) sheets. MSc Thesis, Department of Civil Engineering, University of Manitoba, Winnipeg, Manitoba.

Smith, S. and Kim, S. (2008). Shear strength and behaviour of FRP spike anchors in FRP to concrete joint assemblies. Proceedings of the 5th International Conference on Advanced Composite Materials in Bridges and Structures, September 2008, Winnipeg, Manitoba.

Sucharda, O. and Brozovsky, J. (2014). Numerical modelling of reinforced concrete beams with fracture plastic material. Conference proceedings of Frattura ed Integrita Strutturale – Fracture and Structural Integrity Related Issues, 30(2014): 375-382. DOI: 10.3221/IGF-ESIS.30.45.

Taljsten, B. (1999b). Strengthening of existing concrete structures with carbon fibre fabrics or laminates. Design, material and execution. Extract from Swedish National Railroad and Road Codes.

Teng, J. G. and Chen, J. F. (2009). Mechanics of debonding in FRP-plated RC beams. Structures and Buildings, 162(5): 335-345.

Teng, J. G., Chen, G. M., Chen, J. F., Rosenboom, O. A. Lam, L. (2009). Behavior of RC beams shear strengthened with bonded or unbonded FRP wraps. ASCE Journal of Composites for Construction, 13(5): 394-404.

Thun, H., Ohlsson, U., and Elfgren, L. (2006). Concrete strength in old Swedish concrete bridges. Nordic Concrete Research Journal, 35(1-2): 47-60.

Triantafillou, T. (1998). Shear strengthening of reinforced concrete beams using epoxy-bonded FRP composites. ACI Structural Journal, 95(2): 107-115.

Triantfillou, T. C. and Antonopoulos, C. P. (2000). Design of concrete flexural members strengthened in shear with FRP. ASCE Journal of Composites for Construction, 4(4): 198-205.

Tyfo Fibrwrap Systems. (2012). Tyfo SCH-11UP composite using Tyfo S Epoxy. 1/12 SCH-11UP.

Tyfo Fibrwrap Systems. (2014). Tyfo SCH-41 composite using Tyfo S Epoxy. 1/14 SCH-41.

Valerio, P. (2009). Realistic shear assessment and novel strengthening of existing reinforced concrete bridges. PhD Thesis, University of Bath, Bath, UK.

Valerio, P. and Ibell, T. J. (2003). Shear strengthening of existing concrete bridges. Proceedings of the Institution of Civil Engineers, Structures and Buildings, 156(1):75-84.

Valerio, P., Ibell, T. J. and Darby, A. P. (2009). Deep embedment of FRP for concrete shear strengthening. Proceedings of Institution of Civil Engineers: Structures and Buildings, 162(5): 311-321.

Walraven, J. C. (1980). Aggregate interlock: a theoretical and experimental analysis. PhD Thesis, Delft University of Technology, Delft, The Netherlands, 197.

Wen, X. (2009). Size effect in FRP shear strengthening of concrete structures. MPhil dissertation, University of Bath, Bath, UK.

Whitehead, P. A. (2002). Shear strength of concrete containing fibre reinforced-plastic reinforcement. PhD Thesis, Department of Architecture and Civil Engineering, University of Bath, Bath, UK.

Yu, Q., Bazant, Z. P. (2011). Can Stirrups Suppress Size Effect on Shear Strength of RC Beams? ASCE Journal of Structural Engineering, 137(5): 607-617.

Zhang, Z., Tzu, C., Hsu, T. (2005). Shear strengthening of reinforced concrete beams using carbon-fiber-reinforced polymer laminates. ASCE Journal of Composites for Construction, 9(2): 158-169.

Zsutty, T. C. (1971). Shear strength prediction for separate categories of simple beam test. Proceeding of the ACI Journal, 68(2): 138-143.